Exhibit 1

FEBS 23144

p38pc, p38de

FEBS Letters 465 (2000) 23–27

The role of p38 mitogen-activated protein kinase in IL-6 and IL-8 production from the TNF-α- or IL-1β-stimulated rheumatoid synovial fibroblasts

Masaki Suzuki[a,b], Toshifumi Tetsuka[a], Shinichi Yoshida[a,b], Nobuyuki Watanabe[a,b], Masaaki Kobayashi[b], Nobuo Matsui[b], Takashi Okamoto[a,*]

[a] *Department of Molecular Genetics, Nagoya City University Medical School, 1 Kawasumi, Mizuho-cho, Mizuho-ku, Nagoya 467-8601, Japan*
[b] *Department of Orthopaedic Surgery, Nagoya City University Medical School, 1 Kawasumi, Mizuho-cho, Mizuho-ku, Nagoya 467-8601, Japan*

Received 1 October 1999; received in revised form 2 December 1999

Edited by Shozo Yamamoto

Abstract We examined the role of p38 mitogen-activated protein (MAP) kinase in the tumor necrosis factor α (TNF-α)- or interleukin-1β (IL-1β)-induced production of interleukin-6 (IL-6) and interleukin-8 (IL-8) in fresh rheumatoid synovial fibroblast (RSF) cultures concomitantly with the induction of p38 MAP kinase activity. Pretreatment of RSF with a specific p38 MAP kinase inhibitor, SB203580, blocked the induction of IL-6 and IL-8 without affecting nuclear translocation of nuclear factor κB (NF-κB) or IL-6 and IL-8 mRNA levels. These findings suggest that p38 MAP kinase inhibitor may have synergistic, rather than additive, effect for the treatment of rheumatoid arthritis.

Key words: Rheumatoid arthritis; p38 MAP kinase; Inflammatory cytokine; NF-κB

1. Introduction

Rheumatoid arthritis (RA) is characterized as chronic and progressive inflammatory processes of the affected joints with systemic immunological abnormalities leading to synovial hyperplasia and joint destruction. Cytokines that are abundantly produced in the inflamed rheumatoid synovial fluid, such as tumor necrosis factor α (TNF-α), interleukin-1β (IL-1β), interleukin-6 (IL-6), and interleukin-8 (IL-8) play crucial roles in the pathophysiology of RA. Among these cytokines, TNF-α and IL-1β are considered indispensable for RA pathogenesis since they are known to induce IL-6, IL-8, and themselves through activation of a cellular transcription factor nuclear factor κB (NF-κB) [1]. On the other hand, TNF-α and IL-1β induced a rapid increase in p38 mitogen-activated protein kinase (p38 MAP kinase) phosphorylation and the subsequent activation of its enzyme activity [2–4]. Thus, we determined the roles of p38 MAP kinase in IL-6 and IL-8 production using a specific inhibitor SB203580 [5]. In this study we demonstrate that SB203580 inhibits IL-6 and IL-8 production without affecting the steady-state mRNA levels of IL-6 and IL-8 or blocking NF-κB activation as viewed by its nuclear translocation.

2. Materials and methods

2.1. Reagents

Recombinant human TNF-α (TNF-α) and recombinant human IL-1β (IL-1β) were purchased from Roche Diagnostics. Anti-p38 MAP kinase polyclonal antibody and GST-ATF-2 (1–96) were from Santa Cruz Biotechnology. The specific antibodies to the phosphorylated form of p38 MAP kinase at threonine 180 and tyrosine 182 and to the phosphorylated ATF-2 (phosph-ATF-2) were from New England Biolabs. Protein A Sepharose CL-4B was purchased from Amersham Pharmacia Biotech. Rabbit polyclonal antibodies to human NF-κB subunits, p65 and p50, were from Santa Cruz Biotechnology. The specific inhibitor for p38 MAP kinase SB203580, a pyridinyl imidazole compound, was purchased from Calbiochem and was dissolved in DMSO.

2.2. Cells

Rheumatoid synovial fibroblasts (RSF) were isolated as previously reported [6–8] from the fresh synovial tissue biopsy samples from active three RA patients at total arthro-replacement or arthroscopic synovectomy, as defined by the clinical criteria of the American Rheumatism Association [9]. Written informed consent was obtained from each patient. The data obtained using RSF are presented in this paper, since the same results were obtained qualitatively using RSF derived from RA patients. Briefly, the tissue samples were minced into small pieces and treated with 1 mg/ml collagenase/dispase (Roche Diagnostics) for 10–20 min at 37°C. The cells obtained were cultured in F-12 (Hams) (Life Technologies) supplemented with 10% fetal calf serum, 100 U/ml of penicillin, 100 μg/ml of streptomycin and 0.5 mM 2-mercaptoethanol. The culture medium was changed every 3–5 days and non-adherent lymphoid cells were removed. Adherent cell subcultures were maintained in the same medium and harvested by trypsinization (trypsin/EDTA, Life Technologies) every 7–10 days before they reached cellular confluency. All the experiments described here were conducted using the RSF during the fifth to the tenth passage to characterize the phenotype of adherent cells.

2.3. Western blot analysis

RSF cultures at approximately 80% confluency in 60 mm dishes in F-12 with various treatment were harvested and the total cell extract was prepared according to the method previously described [8]. Briefly, treated cells were washed twice with cold PBS and suspended in 0.2 ml ice-cold total cell extract (TOTEX) buffer (20 mM HEPES-KOH (pH 7.9), 350 mM NaCl, 1.0 mM $MgCl_2$, 20% glycerol, 1.0% NP-40, 0.5 mM EDTA, 0.1 mM EGTA, 1.0 mM DTT, 0.5 mM PMSF, 20 mM β-glycerophosphate, 0.1 mM Na_3VO_4, and 1.0 μg/ml each of aprotinin, pepstatin, leupeptin) with scraping. The solubilized cell homogenate was harvested and centrifuged at 10000×g for

*Corresponding author. Fax: (81)-52-859 1235.
E-mail: tokamoto@med.nagoya-cu.ac.jp

Abbreviations: RA, rheumatoid arthritis; RSF, rheumatoid synovial fibroblasts; p38 MAP kinase, p38 mitogen-activated protein kinase; TNF-α, tumor necrosis factor α; IL-1β, interleukin-1β; IL-6, interleukin-6; IL-8, interleukin-8; RT-PCR, reverse transcription-polymerase chain reaction; NF-κB, nuclear factor κB

PII: S0014-5793(99)01717-2

30 min at 4°C, and the resultant supernatant was used for further analysis. Protein contents were determined with the DC Protein Assay kit (Bio-Rad). Equal amounts of protein were loaded on 10% SDS polyacrylamide gel. Proteins were separated electrophoretically and transferred to nitrocellulose membrane (Hybond-C Super: Amersham Pharmacia Biotech). The protein-blotted membranes were blocked with 5% (w/v) fat-free dry milk in phosphate-buffered saline with 0.05% Tween 20 (PBS-T) for over-night at 4°C. They were then incubated for 1 h at room temperature with anti-phospho p38 MAP kinase antibody at 1:500 dilution in PBS-T containing 1% bovine serum albumin. After washing three times for 5 min with PBS-T solution, blots were further incubated for 1 h at room temperature with donkey anti-rabbit IgG antibody coupled to horseradish peroxidase (Amersham Pharmacia Biotech) at 1:2000 dilution in 5% skim milk in PBS-T and washed three times in PBS-T before visualization. The phosphorylated p38 MAP kinase was detected by anti-phospho-specific p38 MAP kinase antibody by Western blot analysis and detected by SuperSignal Substrate Western Blotting (Pierce) for enhanced chemiluminescence.

2.4. Immune complex kinase assay for p38 MAP kinase activity

The p38 MAP kinase activity in RSF cultures was examined according to the method of Livingstone et al. [4]. Briefly, the soluble proteins in the cell lysate were immunoprecipitated with anti-p38 MAP kinase antibody for overnight at 4°C and further incubated with protein A Sepharose beads for 1 h. The beads were washed three times with 500 μl of ice-cold wash buffer (20 mM HEPES (pH 7.7), 50 mM NaCl, 2.5 mM $MgCl_2$, 0.1 mM EDTA, 0.05% Triton X). The immune complex kinase assay was then performed using GST-ATF-2 (as a substrate) for 30 min at 30°C in 300 μl of kinase reaction buffer (5 μg/ml of GST-ATF-2, 20 mM HEPES (pH 7.6), 20 mM $MgCl_2$, 20 mM β-glycerophosphate, 2.0 mM DTT) containing 200 μM ATP. The reaction was terminated with Laemmli SDS-PAGE loading buffer and the proteins were boiled for 5 min. Equal amounts of protein samples were loaded on 10% SDS-PAGE. The gel was blotted on a nitrocellulose membrane (Hybond-C super). After membranes were blocked with 5% (w/v) fat-free dry milk in PBS-T for overnight at 4°C, they were incubated at room temperature for 1 h with phospho-ATF-2 antibody at 1:1000 dilution. Then, after washing for three times with PBS-T, they were reacted with the secondary antibody, donkey anti-rabbit IgG antibody coupled to horseradish peroxidase, at 1:2000 dilution. Blots were washed three times in PBS-T before visualization using SuperSignal Substrate Western Blotting.

2.5. Cytotoxicity assay

In order to examine the cytotoxicity of SB203580, the cell viability of RSF upon treatment with SB203580 at various concentrations of this compound was determined using WST-1 (Roche Diagnostics) according to the manufacturer's protocol. RSF cultures were incubated with SB203580 in a 96 well plate, incubated for 4 h in the presence of WST-1, and the dissolved formazan was measured at 450 nm by spectrophotometry.

2.6. Cytokine assays

The cytokine concentrations in RSF culture supernatant under various conditions were determined using cytokine-specific ELISA kits for IL-6, IL-8 and VEGF (Biotrak human ELISA kits: Amersham Pharmacia Biotech). All the procedures were carried out as recommended by the manufacturer. Triplicates were used for each test condition in the three independent cultures. The statistical significances of difference in the mean cytokine production were evaluated by the *t*-test.

2.7. Immunofluorescence

In order to determine subcellular localization of NF-κB, RSF were cultured in four well LabTek chamber slides (Nalge Nunc International) and allowed to adhere for 72 h. Cells were then stimulated with 10 ng/ml TNF-α or 20 ng/ml IL-1β with or without pretreatment for 1 h with 30 μM SB203580. Indirect immunofluorescence staining using specific anti-NF-κB antibodies was performed as reported [6–8]. Briefly, the cells were fixed in PBS containing 4.5% paraformaldehyde for 10 min at room temperature and then permeabilized by 0.5% Triton X-100 in PBS for 20 min at room temperature. They were then incubated with rabbit polyclonal antibody against p65 or p50 NF-κB subunits (Santa Cruz Biotech) for 45 min at 37°C. After washing with PBS, the cells were incubated with FITC-conjugated goat anti-rabbit (whole IgG) antibody (Cappel Organon Teknika, Durham, NC, USA) for 20 min at 37°C. Subcellular localization was determined using a fluorescent microscope.

2.8. Semi-quantitation of IL-6 and IL-8 mRNA by reverse transcription-polymerase chain reaction (RT-PCR)

Total cellular RNA was prepared from RSF with TRIzol reagent (Life Technologies) according to the manufacturer's instructions. Amplification of IL-6, IL-8, and β-actin mRNA was performed using a commercial RT-PCR system (Titan® One Tube RT-PCR System: Roche Diagnostics). Gene specific oligonucleotide primers to human IL-6, IL-8 and human β-actin were purchased from CLP. PCR reactions were performed according to the manufacturer's protocol and the products were analyzed following 5, 10, 15, 20, or 30 cycles of amplification and were resolved on a 1.5% agarose gel, stained by ethidium bromide and visualized under an ultraviolet (UV) light.

3. Results

3.1. Activation of p38 MAP kinase by TNF-α during induction of IL-6 and IL-8

TNF-α and IL-1β are known to induce production of various cytokines including IL-6 and IL-8 in fibroblasts [6–8]. In order to examine the involvement of p38 MAP kinase in induction of IL-6 and IL-8 by TNF-α or IL-1β, we have examined if p38 MAP kinase is activated in RSF cultures. In Fig. 1A, RSF were treated with TNF-α (10 ng/ml) and the p38 MAP kinase activity was measured by immune complex kinase assay using recombinant GST-ATF2 protein as a substrate. The increase of p38 MAP kinase activity was observed

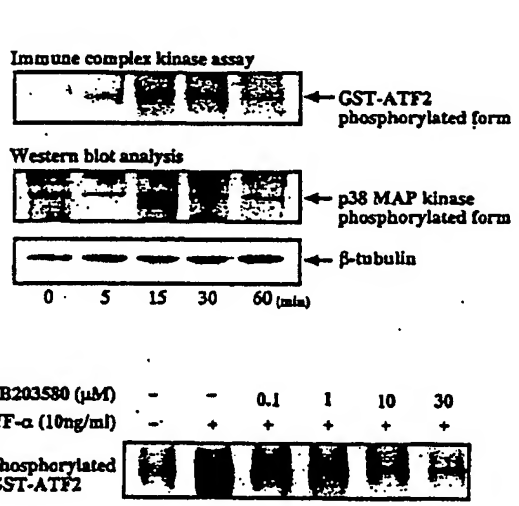

Fig. 1. Activation of p38 MAP kinase in the fresh RSF cultures and the effect of a p38 MAP kinase inhibitor SB203580. A: In vitro activation of p38 MAP kinase. RSF were treated with 10 ng/ml of TNF-α and p38 MAP kinase activity was measured by immune complex kinase assay using recombinant GST-ATF2 protein as a substrate (upper panel). The phosphorylated form of p38 MAP kinase at Thr-180 and Tyr-182 was demonstrated by Western blot analysis using a specific antibody against the phosphorylated form of p38 MAP kinase (lower panel). The same protein samples were probed with antibody to β-tubulin as an internal control. B: Effects of SB203580 on p38 MAP kinase activity detected by immune complex kinase assay. RSF were pretreated for 1 h with various concentrations (0.1, 1, 10, 30 μM) of SB203580 and were stimulated with 10 ng/ml of TNF-α for 30 min. The cell lysate was immunoprecipitated with anti-p38 MAP kinase antibody and the p38 MAP kinase activity was measured with purified recombinant GST-ATF2 as described in Section 2.

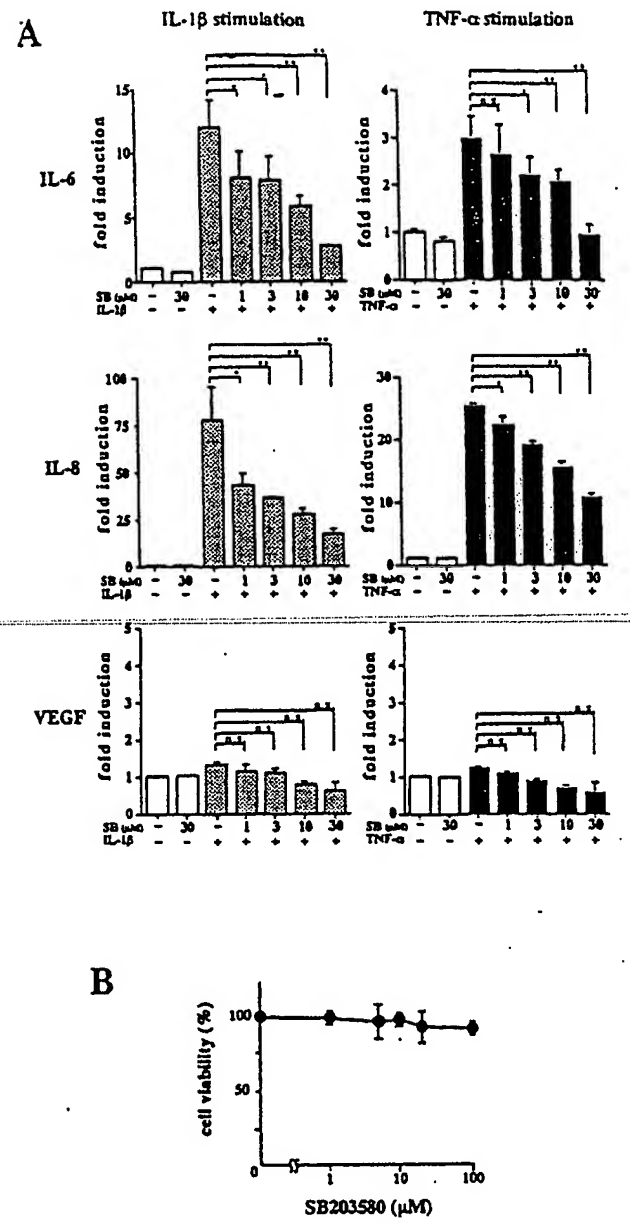

Fig. 2. Effects of a SB203580 on the induced production of IL-6 and IL-8 in RSF. The levels of IL-6 and IL-8 were measured by ELISA systems. At least three independent RSF cultures were examined and the representative results are shown. The experiments were performed in triplicates and the results represent the mean ± S.D. A: SB203580 (SB) inhibited IL-6 and IL-8 production in a dose-dependent manner. Cells were treated with SB203580 for 1 h prior to stimulation with IL-1β (20 ng/ml) (□) or TNF-α (10 ng/ml) (■) for 12 h. (□) means no treatment with TNF-α or IL-1β. Statistical significance: *, $P<0.05$; **, $P<0.01$; n.s., not significant. B: Cytotoxicity of SB203580 in RSF cultures.

as fast as 15 min of stimulation and reached its maximum after 30 min by TNF-α treatment (about six fold increase by densitometric measurement). Moreover, we demonstrated, in the lower panel of Fig. 1A, that the amount of phosphorylation form of p38 MAP kinase at Thr-180 and Tyr-182 was readily increased as demonstrated by Western blot analysis using a specific antibody against the phosphorylated form of p38 MAP kinase (at Thr-180 and Tyr-182). These phosphorylations on p38 MAP kinase, indicating its activation, became detectable after 15 min of TNF-α stimulation and disappeared after 60 min, which was consistent with the results of immune complex kinase assay (upper panel). Similar results were obtained when RSF were stimulated with IL-1β (data not shown).

These results establish that the p38 MAP kinase pathway is rapidly activated in RSF by the actions of proinflammatory cytokine as previously reported with various cell lines [3,10].

In Fig. 1B, RSF were pretreated for 1 h with SB203580 and stimulated with 10 ng/ml of TNF-α for 30 min. Cell lysates were prepared and subjected to the immune complex kinase assay using GST-ATF2 as a substrate. The TNF-α treatment stimulated p38 MAP kinase activity. However, pretreatment with SB203580 prevented this increase of p38 MAP kinase activity in a dose-dependent manner. At 30 μM SB203580, p38 MAP kinase activity was inhibited almost to the basal level.

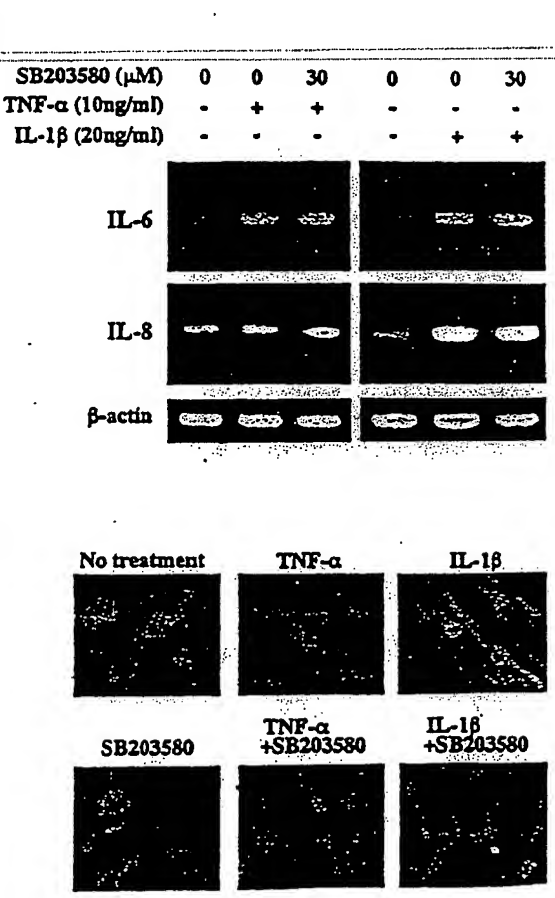

Fig. 3. Transcription of IL-6 or IL-8 was not affected by the p38 MAP kinase inhibitor SB203580. A: The effect of SB203580 on the steady-state level of IL-6 and IL-8 mRNA. RSF were pretreated for 1 h with 30 μM of SB203580 and stimulated for 12 h with 10 ng/ml of TNF-α (left) or 20 ng/ml of IL-1β (right). The steady-state mRNA levels for IL-6 and IL-8 were examined by RT-PCR. B: The effect of SB203580 on the nuclear translocation of NF-κB that was induced by TNF-α or IL-1β. Indirect immunofluorescence was carried out with rabbit polyclonal antibody against NF-κB subunit p65. The cells were similarly treated with SB203580 and TNF-α or IL-1β as in (A).

3.2. Suppression of the IL-6 and IL-8 induction by a p38 MAP kinase inhibitor SB203580

In order to evaluate the effect of p38 MAP kinase on the induction of IL-6/IL-8 production by TNF-α or IL-1β, the effect of SB203580, a p38 MAP kinase inhibitor, was examined. As shown in Fig. 2, RSF cultures were stimulated with TNF-α (10 ng/ml) or IL-1β (20 ng/ml), and concentrations of IL-6 and IL-8 in the cell culture supernatant were measured after 12 h of stimulation. After 12 h of stimulation by TNF-α (10 ng/ml), the extents of augmentation were 3 and 26 fold for IL-6 and IL-8, respectively. Similarly, after 12 h of stimulation by of IL-1β (20 ng/ml), IL-6 and IL-8 production were augmented by 12 and 75 fold, respectively. When the RSF was pretreated with various concentrations of SB203580 (up to 30μM) for 1 h before the treatment with TNF-α or IL-1β, the extents of induction of IL-6 and IL-8 by either TNF-α or IL-1β were significantly reduced by SB203580 in a dose-dependent manner. Similar profiles of suppression were observed with RSF cultures from other RA patients (data not shown). The basal levels of IL-6 and IL-8 production, without TNF-α or IL-1β treatment, were not significantly affected. For example, at 10 μM SB203580 the IL-1β-stimulated IL-6 and IL-8 production were inhibited by 50.8% and 53%, respectively (both statistically significant, $P < 0.01$). Similarly, the TNF-α-mediated inductions were inhibited by 30.7% and 38.5% for IL-6 and IL-8, respectively ($P < 0.01$). In contrast, the concentration of VEGF, known not to be under the control of NF-κB, in the supernatant of RSF cultures stimulated by TNF-α or IL-1β were not significantly reduced. Moreover, SB203580 at these concentrations did not show significant cytotoxicity (Fig. 2B). These findings indicate that a p38 MAP kinase inhibitor SB203580 suppressed the levels of IL-6 and IL-8 that were induced by TNF-α or IL-1β at non-cytotoxic concentrations. Thus, the effect of p38 MAP kinase on IL-6 and IL-8 production appeared to be specific.

3.3. The lack of evidence that p38 MAP kinase inhibitor acts on IL-6 and IL-8 transcription

Since it was reported previously that p38 MAP kinase is involved in gene expression at the post-transcriptional level [11,12], we examined the effect of SB203580 on the steady-state level of IL-6 and IL-8 mRNA. RSF was pretreated for 1 h with 30 μM of SB203580, and then TNF-α (10 ng/ml) or IL-1β (20 ng/ml) was added for a further 12 h. Total RNA samples were prepared from these cells and the steady-state mRNA levels for IL-6 and IL-8 were examined by RT-PCR. A series of PCR reactions were monitored for amplification of IL-6 and IL-8 mRNA at 5, 10, 15, 20 and 30 cycles of PCR. At PCR cycles over 20, there was no difference in intensity of the gene-specific bands. Thus, the results shown in Fig. 3A represent the amplified band for IL-6 and IL-8 mRNA detected at 15 cycles of the RT-PCR. As demonstrated in Fig. 3A, SB203580 even at the highest concentration (30 μM) did not significantly inhibit the induction of IL-6 and IL-8 mRNA. Since NF-κB is known to play a crucial role in IL-6 and IL-8 induction as a positive transcriptional regulator, we examined whether SB203580 could affect the nuclear translocation of NF-κB, as an indication of its signal-induced activation, stimulated by TNF-α or IL-1β. To determine the subcellular distribution of NF-κB, indirect immunofluorescence was performed with rabbit polyclonal antibody against NF-κB subunit p65. As shown in Fig. 3B, p65 was localized in the cytoplasm of unstimulated RSF. When the cells were stimulated with 10 ng/ml of TNF-α or 20 ng/ml of IL-1β, p65 was translocated to the nucleus within 30 min as we previously reported [6–8,13]. We further examined whether this nuclear translocation could be blocked by SB203580. When RSF were pretreated for 1 h with SB203580 (30μM), at which concentration the induction of IL-6 and IL-8 production was remarkably suppressed (Fig. 3A), the nuclear translocation of NF-κB was not blocked.

4. Discussion

Accumulating evidences have incriminated various cytokines and their interactions in pathophysiology of RA [8]. Among these cytokines, TNF-α and IL-1β are considered to play crucial roles [6–8]. These notions have been confirmed by demonstration of clinical efficacies of antibodies against TNF-α [14,15], IL-6 [16] and IL-1 antagonists [17] in the treatment of RA synovitis. Induction of IL-6 and IL-8 by IL-1β or TNF-α is mediated by intracellular signal transduction cascades involving a number of protein kinases. In addition to a common kinase pathway involving IκB kinases that lead to NF-κB activation [1,18,19], both IL-1β and TNF-α signaling cascades include three distinct types of MAP kinases (p42/p44, p54/JNK, and p38) [10,20].

We were particularly interested in p38 MAP kinase since SB203580 had been initially identified as a potent inhibitor of inflammatory cytokine production from THP-1 cells by random screening and p38 MAP kinase was identified as the specific target molecule [5]. In fact, previous reports have demonstrated that p38 MAP kinase is involved in the induction of inflammatory cytokines [5,10,21,22].

In this paper we confirmed that in the fresh RSF cultures prepared from RA patients either TNF-α or IL-1β could induce phosphorylation (and activation) of p38 MAP kinase within 15 min followed by augmented production of IL-6 and IL-8 (Fig. 1A). As expected, SB203580 could block p38 MAP kinase activity and cytokines (IL-6 and IL-8) induction in RSF (Figs. 1B and 2). Although earlier studies reported that p38 MAP kinase appeared to be involved in the nuclear translocation (signal-induced activation) of NF-κB and transcriptional initiation of the genes under the control of NF-κB [23,24], we did not see any effect of SB203580 on the NF-κB nuclear translocation nor steady-state levels of IL-6 and IL-8 mRNA even at the highest concentration of SB203580 (Fig. 3), which was consistent with recent studies by others using fibroblast cell lines.

There are a number of reports regarding the mechanism of SB203580 in blocking the induced production of inflammatory cytokines such as IL-6 and IL-8 by stimulation with proinflammatory cytokines, TNF-α or IL-1β [6,25]. However, the mechanism of its action is still controversial. For example, Beyaert et al. [3] reported that the NF-κB-dependent gene expression was inhibited by SB203580 in a mouse fibrosarcoma cell line L929 stably transfected with a NF-κB-dependent chloramphenicol acetyl transferase (CAT) plasmid. Yet, SB203580 did not affect the TNF-induced DNA-binding of NF-κB or phosphorylation of NF-κB or IκB. In contrast, Miyazawa et al. [26] showed that SB203580 did not block transient expression of luciferase gene under the control of IL-6 promoter in a transient assay with synovial fibroblasts. They claimed that the effect of SB203580 might be post-trun-

scriptional since the transcriptional initiation of the TNF-induced IL-6 mRNA level was not suppressed at all by SB203580 in a nuclear run-on assay using the isolated nuclei of the TNF-stimulated synovial fibroblasts. Similarly to our observations, Caivano [11] and Pietersma et al. [12] reported that SB203580 blocked production of inducible nitric oxide synthetase and intercellular cell adhesion molecule 1, respectively, without affecting the mRNA levels as observed by RT-PCR.

Our findings together with others demonstrated clearly that p38 MAP kinase is involved in the TNF-α- or IL-1β-induced production of inflammatory cytokines independently from the NF-κB cascade. Many of anti-rheumatic drugs currently used for the treatment of RA patients are known to block the NF-κB pathway at various steps, such as inhibition of IκB kinases by aspirin [27,28] and Sulindac [29] and inhibition of NF-κB DNA-binding by gold [7,30]. Thus, use of p38 MAP kinase inhibitors such as SB203580 and its derivatives should have synergistic, rather than additive, effects in combination with conventional anti-rheumatic drugs in blocking the production of inflammatory cytokines, cell adhesion molecules and inducible nitric oxide synthetase that participate in the maintenance and expansion of rheumatoid inflammation. It may also circumvent side effects of conventional anti-rheumatic therapy without losing therapeutic efficacies.

Acknowledgements: This work was supported by grants-in-aid from the Ministry of Health and Welfare, the Ministry of Education, Science and Culture of Japan, Japan Human Science Foundation, Japan Rheumatism Foundation and Aichi D.R.G. Foundation.

References

[1] Mukaida, N., Mahe, Y. and Matsushima, K. (1990) J. Biol. Chem. 265, 21128–21133.
[2] Wesselborg, S., Bauer, M.K.A., Vogt, M., Schmitz, M.L. and Schulze-Osthoff, K. (1997) J. Biol. Chem. 272, 12422–12429.
[3] Beyaert, R., Cuenda, A., Berghe, W.V., Plaisance, S., Lee, J.C., Haegeman, G., Cohen, P. and Fiers, W. (1996) EMBO J. 15, 1914–1923.
[4] Livingstone, C., Patel, G. and Jones, N. (1995) EMBO J. 14, 1785–1797.
[5] Lee, J.C., Laydon, J.T., McDonnell, P.C., Gallagher, T.F., Kumar, S., Green, D., McNulty, D., Blumenthal, M.J., Heys, J.R., Landvatter, S.W., Stricker, J.E., McLaughlin, M.M., Siemens, I.R., Fisher, S.M., Livi, G.P., White, J.R., Adams, J.L. and Young, P.R. (1994) Nature 372, 739–746.
[6] Sakurada, S., Kato, T. and Okamoto, T. (1996) Int. Immunol. 8, 1483–1493.
[7] Yoshida, S., Kato, T., Sakurada, S., Kurono, C., Yang, J.P., Matsui, N., Soji, T. and Okamoto, T. (1999) Int. Immunol. 11, 151–158.
[8] Yoshida, S., Katoh, T., Tetsuka, T., Uno, K., Matsui, N. and Okamoto, T. (1999) J. Immunol. 163, 351–358.
[9] Arnett, F.C., Edworthy, S.M., Bloch, D.A., McShane, D.J., Fries, J.F., Cooper, N.S., Healey, L.A., Kaplan, S.R., Liang, M.H., Luthra, H.S., Medsger Jr., M.A., Michell, D.M., Neustadt, D.H., Pinals, R.S., Schaller, J.G., Sharp, J.T., Wilder, R.L. and Hunder, G.G. (1987) Arthritis Rheum. 31, 315–324.
[10] Raingeaud, J., Gupta, S., Rogers, J.S., Dickens, M., Han, J., Ulevitch, R.J. and Davis, R.J. (1995) J. Biol. Chem. 270, 7420–7426.
[11] Caivano, M. (1998) FEBS Lett. 429, 249–253.
[12] Pietersma, A., Tilly, B.C., Gaestel, M., de Jong, N., Lee, J.C., Koster, J.F. and Sluiter, W. (1997) Biochem. Biophys. Res. Commun. 230, 44–48.
[13] Hayashi, T., Sekine, T. and Okamoto, T. (1993) J. Biol. Chem. 268, 26790–26795.
[14] Brennan, F.M., Chantry, D., Jackson, A., Maini, R. and Feldmann, M. (1989) Lancet 29, 244–247.
[15] Elliott, M.J., Maini, R.N., Feldmann, M., Long-Fox, A., Charles, P., Katsikis, P., Brennan, F.M., Walker, J., Bijl, H., Ghrayeb, J. and Woody, J.N. (1993) Arthritis Rheum. 36, 1681–1690.
[16] Wendling, D., Racadot, E. and Wijdenes, J. (1993) J. Rheumanol. 20, 259–262.
[17] Bendele, A., McAb Sennello, G., Frazier, J., Chlipala, E. and McCabe, D. ee, T. (1999) Arthritis Rheum. 42, 498–506.
[18] Woronicz, J.D., Gao, X., Cao, Z., Rothe, M. and Goeddel, D.V. (1997) Science 278, 866–869.
[19] Okamoto, T., Sakurada, S., Yang, J.P. and Merin, J.P. (1997) Curr. Top. Cell. Regul. 35, 149–161.
[20] Cobb, M.H. and Goldsmith, E.J. (1995) J. Biol. Chem. 270, 14843–14846.
[21] Eliopoulos, A.G., Gallagker, N.J., Blake, S.M.S., Dawson, C.W. and Young, L.S. (1999) J. Biol. Chem. 274, 16085–16096.
[22] Krause, A., Holtmann, H., Eickemeier, S., Winzen, R., Szamel, M., Resch, K., Saklatvala, J. and Kracht, M. (1998) J. Biol. Chem. 273, 23681–23689.
[23] Baldassare, J.J., Bi, Y. and Bellone, C.J. (1999) J. Immunol. 162, 5367–5373.
[24] Vanden, B.W., Plaisance, S., Boone, E., De Bosscher, K., Schmitz, M.L., Fiers, W. and Haegeman, G. (1998) J. Biol. Chem. 273, 3285–3290.
[25] Zhang, Y.H. and Lin, J.X. (1990) J. Mol. Cell Biol. 10, 3818–3823.
[26] Miyazawa, K., Mori, A., Miyatu, H., Akahane, M., Ajisawa, Y. and Okudaira, H. (1998) Arthritis Rheum. 273, 24832–24838.
[27] Kopp, E. and Ghosh, S. (1994) Science 265, 956–959.
[28] Weber, C., Erl, W., Pietsch, A. and Weber, P.C. (1995) Circulation 91, 1914–1917.
[29] Yamamoto, Y., Yin, M.J., Lin, K.M. and Gaynor, R.B. (1998) J. Biol. Chem. 274, 27307–27314.
[30] Yang, J.P., Meirin, J.P., Nukano, T., Kato, T., Kitabe, Y. and Okamoto, T. (1995) FEBS Lett. 361, 89–96.

Exhibit 2

0022-3565/96/2793-1453$03.00/0
THE JOURNAL OF PHARMACOLOGY AND EXPERIMENTAL THERAPEUTICS
Vol. 279, No. 3
Printed in U.S.A.

JPET 279:1453–1461, 1996

Pharmacological Profile of SB 203580, a Selective Inhibitor of Cytokine Suppressive Binding Protein/p38 Kinase, in Animal Models of Arthritis, Bone Resorption, Endotoxin Shock and Immune Function

ALISON M. BADGER, JEREMY N. BRADBEER, BART VOTTA, JOHN C. LEE, JERRY L. ADAMS and DON E. GRISWOLD

Departments of Cellular Biochemistry (A.M.B., J.N.B., B.V., J.C.L.), Immunopharmacology (D.E.G.) and Medicinal Chemistry (J.L.A.), SmithKline Beecham Pharmaceuticals, King of Prussia, Pennsylvania

Accepted for publication August 9, 1996

ABSTRACT

SB 203580 [4-(4-fluorophenyl)-2-(4-methylsulfinylphenyl)-5-(4-pyridyl)imidazole], a selective cytokine suppressive binding protein/p38 kinase inhibitor, was evaluated in several models of cytokine inhibition and inflammatory disease. It was demonstrated clearly to be a potent inhibitor of inflammatory cytokine production *in vivo* in both mice and rats with IC_{50} values of 15 to 25 mg/kg. SB 203580 possessed therapeutic activity in collagen-induced arthritis in DBA/LACJ mice with a dose of 50 mg/kg resulting in significant inhibition of paw inflammation and serum amyloid protein levels. Antiarthritic activity was also observed in adjuvant-induced arthritis in the Lewis rat when SB 203580 was administered p.o. at 30 and 60 mg/kg. Evidence for disease-modifying activity in this model was indicated by an improvement in bone mineral density and by histological evaluation. Additional evidence for beneficial effects on bone resorption was provided in the fetal rat long bone assay in which SB 203580 inhibited ^{45}Ca release with an IC_{50} of 0.6 μM. In keeping with the inhibitory effects on lipopolysaccharide-induced tumor necrosis factor-α in mice, SB 203580 was found to reduce mortality in a murine model of endotoxin-induced shock. In immune function studies in mice treated with SB 203580 (60 mg/kg/day for 2 weeks), there was some suppression of an antibody response to ovalbumin, whereas cellular immune functions measured *ex vivo* were unaffected. This novel profile of activity strongly suggests that cytokine inhibitors could provide significant benefit in the therapy of chronic inflammatory disease.

Cytokines such as IL-1 and TNF-α play a predominant role during inflammatory responses and autoimmune disease (Dinarello, 1991). Evidence for their key participation in acute and chronic inflammation has been provided by the demonstration that protein antagonists such as IL-1ra and monoclonal antibodies to TNF-α, and its soluble receptor, can interfere with various acute and chronic inflammatory responses. Another approach to the control of proinflammatory cytokines is to inhibit their production, ideally through the use of p.o. active low molecular weight compounds. One class of compounds that is effective in this respect is the pyridinyl imidazoles which have been shown to inhibit cytokine production *in vitro*, and *in vivo* they can attenuate the inflammatory components of disease in the absence of generalized immunosuppression (Griswold *et al.*, 1988; Lee *et al.*, 1993; Reddy *et al.*, 1994).

SB 203580 [4-(4-fluorophenyl)-2-(4-methylsulfinylphenyl)-5-(4-pyridyl)imidazole] (fig. 1) is a member of a new series of pyridinyl imidazole compounds which inhibit IL-1 and TNF-α production from LPS-stimulated human monocytes and the human monocyte cell line THP-1 with IC_{50} values of 50 to 100 nM (Lee *et al.*, 1994a,b; Gallagher *et al.*, 1995). The term CSAID™ has been coined for these compounds and they have shown activity in a number of animal models of acute and chronic inflammation (Lee *et al.*, 1993). The molecular target of SB 203580 and related compounds has been identified as a pair of closely related mitogen-activated protein kinase homologs, alternatively termed CSBP (Lee *et al.*, 1994b), p38 (Han *et al.*, 1994) or RK (Rouse *et al.*, 1994). The binding of the CSAID™ compounds to the target CSBP in

Received for publication May 6, 1996.

ABBREVIATIONS: IL, interleukin; TNF, tumor necrosis factor; LPS lipopolysaccharide; CSBP, cytokine suppressive binding protein; CO, cyclooxygenase; RAP, rapamycin; RPMI, Roswell Park Memorial Institute; Con A, concanavalin A; OVA, ovalbumin; CFA, complete Freund's adjuvant; SAP, serum amyloid protein; AA, adjuvant arthritis; BMD, bone mineral density; BMC, bone mineral content; DXA, dual X-ray absorptiometry; PTH, parathyroid hormone; gal, galactosamine; LO, 5-lipoxygenase.

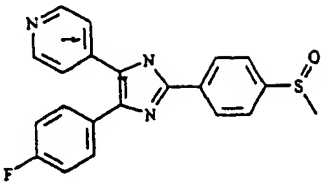

Fig. 1. Structure of SB 203580.

THP.1 cytosol correlates with their cytokine biosynthesis inhibition (Lee *et al.*, 1994b), indicating a role for CSBP in the production of cytokines in response to various stimuli (Lee and Young, 1996).

Compounds structurally related to SB 203580 have been tested previously in a number of animal models for their anti-inflammatory activity, including collagen-induced arthritis (Griswold *et al.*, 1988) and endotoxin shock (Badger *et al.*, 1989; Olivera *et al.*, 1992). These models are relatively insensitive to CO inhibitors, which adds credence to the cytokine suppressive nature of the CSAID™ molecules. In this manuscript, we show that cytokine inhibition with SB 203580 has beneficial effects in animal models of disease with only minor effects on immune function.

Materials and Methods

Animals. DBA/1 LACJ, BALB/c and C57BL/6 male mice were obtained from Jackson Laboratories (Bar Harbor, ME). Male Lewis rats were obtained from Charles River Laboratories (Raleigh, NC.) Within any given experiment, only animals of the same age were used. All experimental procedures were in accordance with National Institutes of Health guidelines and were reviewed by the SmithKline Beecham Animal Care and Use Committee (King of Prussia, PA).

Materials. SB 203580 [4-(4-fluorophenyl)-2-(4-methylsulfinylphenyl)-5-(4-pyridyl)imidazole] was synthesized at SmithKline Beecham Pharmaceuticals (fig. 1). For *in vivo* assays, SB 203580 was administered p.o. in 0.03 N HCl-0.5% tragacanth (Sigma Chemical Co., St. Louis, MO) at the doses indicated. RAP was prepared by fermentation at SmithKline Beecham Pharmaceuticals (Brockham Park, UK). RPMI 1640 was obtained from Flow Laboratories (Rockville, MD and contained 10% fetal bovine serum, 100 U/ml of penicillin, 100 μg/ml of streptomycin and 2 mM L-glutamine (GIBCO, Grand Island, NY). This medium will be known as RPMI-10. Con A was obtained from Pharmacia Fine Chemicals (Piscataway, NJ). Endotoxin (LPS) was either *Escherichia coli*, type W or *Salmonella typhosa* (Difco Laboratories, Detroit MI) and OVA was from Sigma.

LPS-induced TNF production in mice and rats. BALB/c male mice in groups of three to five were treated with vehicle or compound by p.o. gavage and 30 min later the animals were injected i.p. with 25 μg/mouse of endotoxin (*E. coli*, type W, Difco). Two hours later, the animals were euthanized by carbon dioxide asphyxiation and plasma was obtained from individual animals by collecting blood into heparinized tubes. The samples were clarified by centrifugation at 12,500 × *g* for 5 min at 4°C. The supernatants were decanted to new tubes (may be stored at −20°C) and were assayed for mouse TNF-α by ELISA (Olivera *et al.*, 1992). The range of sensitivity of the ELISA is 25 to 800 pg/ml of mouse TNF-α. For the induction of TNF-α in Lewis rats, the animals were treated with SB 203580 30 min before the injection of LPS (30 μg/kg i.p.). TNF-α levels were measured 90 min later by ELISA.

Collagen-induced arthritis. Type II collagen arthritis was induced in male DBA/1 LACJ mice (30–35 g, Jackson Laboratories) by the method of Wooley (1988). The mice were primed with an emulsion consisting of CFA (Difco Laboratories) combined with an equal volume of a freshly prepared solution of 2.0 mg of collagen type II (bovine nasal septum, Elastin Products Co., Inc., Owensville, MO) per ml of 0.01 N acetic acid. Extra *Mycobacterium butyricum* (Difco) was added to the CFA to make the concentration twice that present in the commercial preparation. The CFA/collagen emulsion was prepared by mixing through two connected 20-ml syringes. An intradermal injection of 0.1 ml of emulsion per mouse was administered at the base of the tail. Twenty-one days later, the mice were boosted by an i.p. injection of 0.1 ml of freshly prepared 1.0 mg of bovine collagen II/ml of 0.01 N acetic acid per mouse. Joint swelling presented within a few days and the mice were evaluated for incidence and severity of inflammation, assigned randomly to study groups, ear tagged and the individual mouse's dosing regimen was begun. Severity of joint swelling was determined subjectively for each limb by using a scale of 1 (one or more phlanges per limb) to 4 (maximum swelling per limb). A severity score of at least 2 on one limb (excluding phlanges) was required for an animal to be assigned to a study group. Before dosing, each mouse was bled by the tail vein for a serum sample (100–150 μl of blood). Disease severity was assessed on days 7 and 10 after which blood was collected (tail vein on day 7 and by exsanguination on day 10) for serum. The serum samples were assayed for mouse SAP by using a radio immunologically quantitated Western blot method (Griswold *et al.*, 1988).

Statistical analysis. Clinical severity and levels of SAP and TNF-α were analyzed by using the Student's *t* test, with P values less than .05 considered significant.

AA. AA was induced by a single injection of 0.75 mg of *M. butyricum* (Difco) suspended in paraffin oil into the base of the tail of male Lewis rats, 6 to 8 weeks old (160–180 g). Hindpaw volumes were measured by a water displacement method on day 16 and/or day 22. Test compounds were homogenized in acidified 0.5% tragacanth (Sigma) and were administered p.o. in a volume of 10 ml/kg. Control animals were administered vehicle (tragacanth) alone.

Percentage of inhibition of hindpaw lesions was calculated as follows:

$$\% \text{ Inhibition} = 1 - \frac{\text{AA (Treated)}}{\text{AA (Normal)}} \times 100$$

For statistical analysis, paw volumes of rats treated with SB 203580 were compared to the untreated controls by Student's *t* test.

BMD, as well as BMC and bone area were determined for the distal tibia by DXA by using the Hologic QDR-1000 equipped with high resolution scanning software as we have described previously (Bradbeer *et al.*, 1996).

Tibio-tarsal joints from representative animals from the following three groups of rats were examined histologically; normal rats, AA control rats and AA rats treated with SB 203580 at 60 mg/kg/day. Rats were sacrificed by CO_2 administration and the rear legs were fixed in formalin, decalcified in formic acid and the feet removed from the legs at the distal tibial diaphysis. After routine processing, the feet were embedded and coronal sections were cut in the plane midway through the tibiotarsal and tarsotarsal joints. Sections were stained with Safranin O and counterstained with fast green.

Bioassay for IL-6. Serum samples were obtained when the rats were euthanized. IL-6 levels were determined by using the previously described B9 bioassay (Aarden *et al.*, 1985). Briefly, B9 cells (5×10^3 cells/well in 96-well flat-bottomed plates) were cultured at 37°C with serial dilutions of rat serum in a final volume of 100 μl of RPMI-10. After 68 hr, 0.5 μCi of [^{3}H]thymidine was added and was incubated for 6 hr at 37°C. Cells were harvested and radioactivity incorporation was determined. IL-6 was quantified from a standard curve including known amounts of rat IL-6 (0.1–100 pg/ml). B9 proliferation was unaffected by any agents used in this study.

Fetal rat long bone resorption assay. This assay was performed essentially as described previously (Raisz, 1965; Stern and Raisz, 1979). Timed-pregnant Sprague Dawley rats (Taconic Farms, Germantown, NY) were injected s.c. with 200 μCi of $^{45}CaCl_2$ on day 18 of gestation, housed overnight, then anesthetized with Inovar-Vet (Pittman-Moore, Mundelein, IL) and sacrificed by cervical dislo-

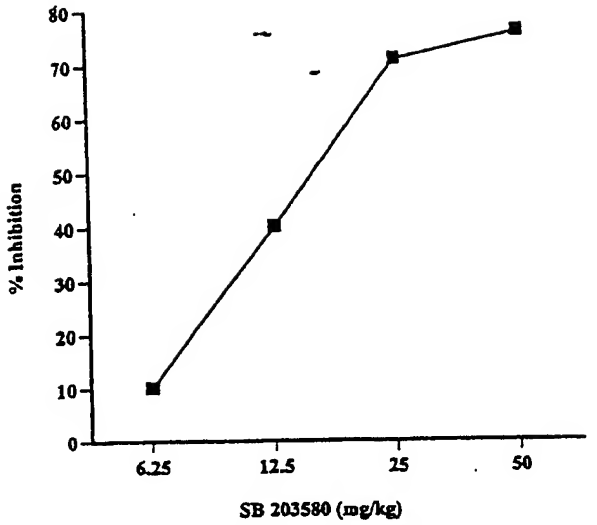

Fig. 2. Inhibition of plasma TNF levels in BALB/c mice. SB 203580 was administered 30 min before LPS challenge and TNF was measured by ELISA 2 hr later. Data are presented as percentage of inhibition by using three to five animals per group. Significant inhibition was observed at 50, 25 and 12.5 mg/kg ($P < .001$) with an IC_{50} of 15 mg/kg.

cation. Fetuses were removed aseptically and radii and ulnae were dissected free of surrounding soft tissue and cartilaginous ends. The bones were cultured 18 to 24 hr in BGJ_b medium (Sigma) containing 1 mg/ml of bovine serum albumin, then were transferred to fresh medium and cultured for an additional 48 hr in the absence or presence of 50 ng/ml of PTH (human, 1–34) and test compound. Calcium released into the medium and total residual calcium in the bones were measured by liquid scintillation spectrometry. Data are expressed as the percentage of calcium released from treated bones as compared to corresponding control bones. Statistical differences were assessed by using a one-way analysis of variance for nonpaired samples. Data are presented as mean ± S.E.

Endotoxin shock. Pathogen-free male C57BL/6 mice were obtained from Jackson Laboratories. Age-matched mice, 6 to 12 weeks old, were used. This model of shock was performed as described previously (Badger *et al.*, 1989; Olivera *et al.*, 1992). Briefly, 0.1 μg of LPS from *Salmonella typhosa* (Difco) mixed with D-(+)-gal (Sigma: 500 mg/kg) was injected i.v. in 0.25 ml of pyrogen-free saline (this mixture is referred to as LPS/D-gal). Compounds to be tested were administered p.o. 30 min before the i.v. injection of LPS/D-gal. Blood was collected *via* cardiac puncture 1 hr after LPS/D-gal and serum samples were stored at −20°C until evaluation for TNF-α by ELISA. Survival was monitored, in separate groups of animals, for 48 hr after LPS challenge, at which time no further deaths occurred in either treated or untreated control mice.

Immune function assays. Female BALB/c mice were immunized with 100 μg of OVA in 50 μl of CFA in both hind footpads (OVA was prepared at 4 mg/ml and diluted 1:1 in CFA). Mice were then treated for 5 days a week for 2 weeks with 60 mg/kg of SB 203580 or 50 mg/kg of RAP administered i.p. in a vehicle composed of 10% ethanol, 10% cremophor and 80% saline. At the termination of the experiment (day 12), spleen and lymph nodes were harvested and cell suspensions were prepared by standard procedures. For the response to OVA and Con A, lymph node cells (5×10^5) were established in 96-well round bottomed plates in the presence or absence of serially diluted Con A or OVA for 72 hr. For the mixed lymphocyte reaction, cells from treated BALB/c mice (1×10^6) were established in 96-well flat bottomed plates along with C57BL/6-irradiated (3000 R) stimulator cells (1×10^6). Cell cultures were incubated at 37°C/5% CO_2, with 0.5 μCi of [^{3}H]thymidine added for the last 18 hr of culture. Cell-associated radioactivity was measured after collection onto glass-fiber filters by scintillation counting. For OVA-specific antibody response, sera from immunized mice were tested for activity by ELISA which has been described in detail previously (Reddy *et al.*, 1994).

Results

Inhibition of TNF-α and collagen-induced arthritis in mice. Demonstration of the ability of SB 203580 [4-(4-fluorophenyl)-2-(4-methylsulfinylphenyl)-5-(4-pyridyl)imidazole] to inhibit inflammatory cytokine production *in vivo* was accomplished by using BALB/c mice challenged with LPS (25 μg i.p.). As seen in figure 2, SB 203580 given p.o. 30 min before LPS challenge inhibited the production of TNF-α (ED_{50}, 15 mg/kg p.o.).

Given the potent ability of SB 203580 to inhibit TNF-α production *in vivo*, it was of interest to evaluate the effect of the compound on a chronic inflammatory model. Collagen-induced arthritis was induced in DBA/1 LACJ mice by injection of bovine Type II collagen in CFA at the base of the tail, followed 21 days later by a booster injection of collagen solubilized in acetic acid (i.p.). Animals with significant disease were treated with SB 203580 (50 mg/kg p.o., b.i.d.). At the end of 7 days, the disease severity was judged on a scale of 0 to 4$^+$ and blood was obtained for analysis of serum amyloid P component. As seen in table 1, in two separate studies, SB 203580 significantly reduced disease severity (72%, $P < .01$ and 45%, $P < .05$, respectively) as well as acute phase reactant (SAP) levels (42%, $P < .05$ and 52%, $P < .001$, respectively).

Inhibition of TNF-α and AA in rats. TNF-α was also inhibited in SB 203580-treated Lewis rats. This was shown by treating normal rats with SB 203580 p.o. 30 min before a challenge with 30 mg/kg of LPS i.p. Plasma TNF-α levels measured 90 min later were inhibited by 53% at 25 mg/kg ($P < .01$) and by 38% at 12.5 mg/kg ($P < .01$) with no inhibition observed at 6.2 mg/kg (table 2).

In the rat model of AA, p.o. administration of SB 203580

TABLE 1

Effect of SB 203580 on type II collagen-induced Arthritis in DBA/1 mice

This table summarizes two studies in which the mice were dosed for 7 days at 50 mg/kg (p.o., b.i.d.), after the animals had presented with paw or joint edema/swelling. The data are the mean ± S.E. from a group of vehicle (0.03 N HCl/0.5% Tragacanth) and SB 203580-treated controls. In Experiment II, the mice were entered into the study as fully complemented groups. Data are significantly different from the control: * $P < .05$; ** $P < .01$; *** $P < .001$.

Treatment	*n*	Severity Index	%	*n*	SAP	%
Experiment I						
Control	9	5.86 ± 1.17		9	189.89 ± 28.29	
SB 203580	8	1.63 ± 0.79	72**	8	110.66 ± 17.75	42*
Experiment II						
Control	10	5.75 ± 0.83		8	181.30 ± 10.36	
SB 203580	10	3.15 ± 0.51	45*	8	86.61 ± 6.23	52***

TABLE 2

Inhibition of LPS-stimulated TNF-α levels in SB 203580 Lewis rats

Rats were dosed (p.o.) 30 min before treatment with LPS (30 μg/kg/i.p.). Plasma TNF was measured 90 min after LPS administration. Data are mean ± S.E. for six animals per group. * P < .05; ** P < .01.

Treatment	TNF-α	% Inhibition
	ng/ml	
Control (untreated)	42.15 ± 5.05	
SB 203580		
25 mg/kg	19.91 ± 2.77	53**
12.5 mg/kg	26.20 ± 4.56	38*
6.25 mg/kg	36.76 ± 3.56	13 N.S.

(10, 30 and 60 mg/kg p.o.) from day 0 to day 22 inhibited the development of immune-mediated hindpaw inflammation. On day 16, there was 86% inhibition at 60 mg/kg (P < .001) and 62% inhibition at 30 mg/kg (P < .01), with no effect observed at 10 mg/kg (fig. 3A). By day 22, the anti-inflammatory effect had lessened somewhat with 60% (P < .001) and 45% (P < .01) inhibition at 60 and 30 mg/kg, respectively (fig. 3B).

The anti-inflammatory and antiarthritic activities of SB 203580 were evaluated further by examining the BMC and BMD of the distal tibia region in treated AA rats. On day 22 when the rats were euthanized, hindlimbs were examined by DXA. When compared with the AA controls, there was a significant normalization of BMD (31%, P < .01) and BMC (26%, P < .01) in the rats treated with 60 mg/kg/day of the compound, indicating a protective effect on inflammation-mediated bone destruction and/or a direct effect on bone resorption proximal to the inflamed joint (fig. 4, A and B).

Histology of the tibio-tarsal joint from a normal rat and from rats challenged with adjuvant and then treated with vehicle (AA control) or SB 203580 is shown in figure 5. In the AA control joint, all of the original bone and marrow has been replaced by granulation tissue and newly formed woven bone. Remnants of articular cartilage are evident and the

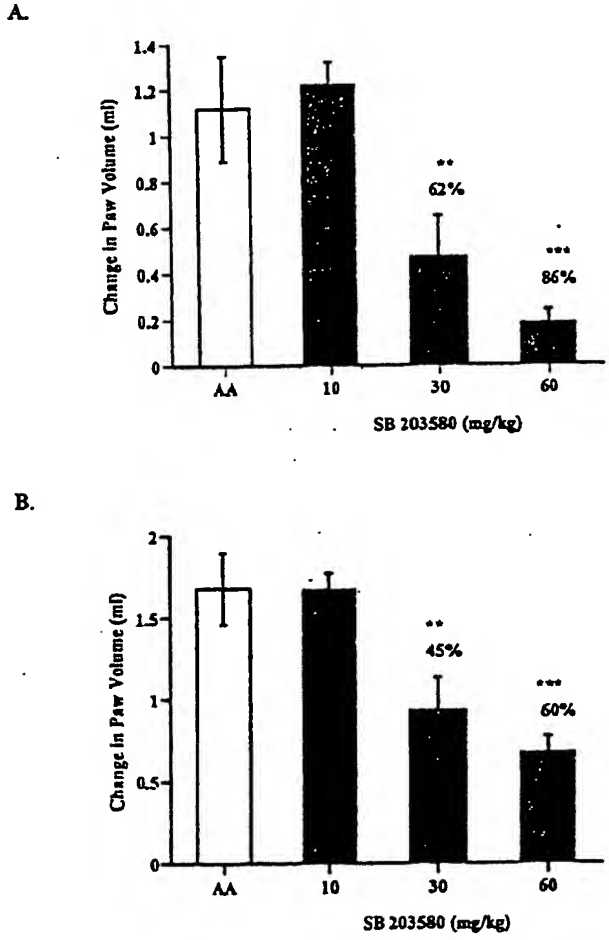

Fig. 3. Dose-dependent suppression of hindpaw inflammation in rats with AA by prophylactic administration of SB 203580 from days 0 to 22 (5 days a week). Paw inflammation was measured on day 16 (A) and on day 22 (B). Data are the mean and S.E.M. of 10 animals per group. **P < .01; ***P < .001, compared to the untreated AA controls.

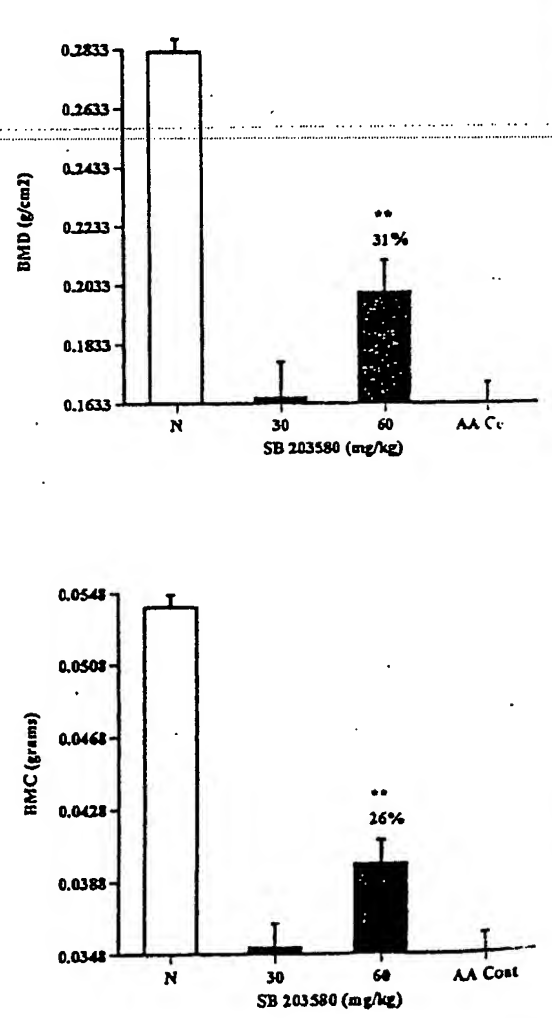

Fig. 4. Bone densitometry evaluation of the distal tibia in AA rats treated with SB 203580. Rats were treated with various doses 5 days a week from day 0 to day 22. Values are the percentage of normal (assigned a value of 100%), mean and S.E.M. of 10 animals per group. A, the BMD value was 0.2822 ± 0.0045 for normal rats and 0.01633 ± 0.0067 for AA rats, which is a 42% decrease in BMD in the diseased animals. B, the BMC value was 0.0540 ± 0.0007 for normal rats and 0.0348 ± 0.001 for AA rats which is a 36% decrease in BMC in the diseased animals. The effect of SB 203580 was statistically significant on both BMD and BMC. **P < .01.

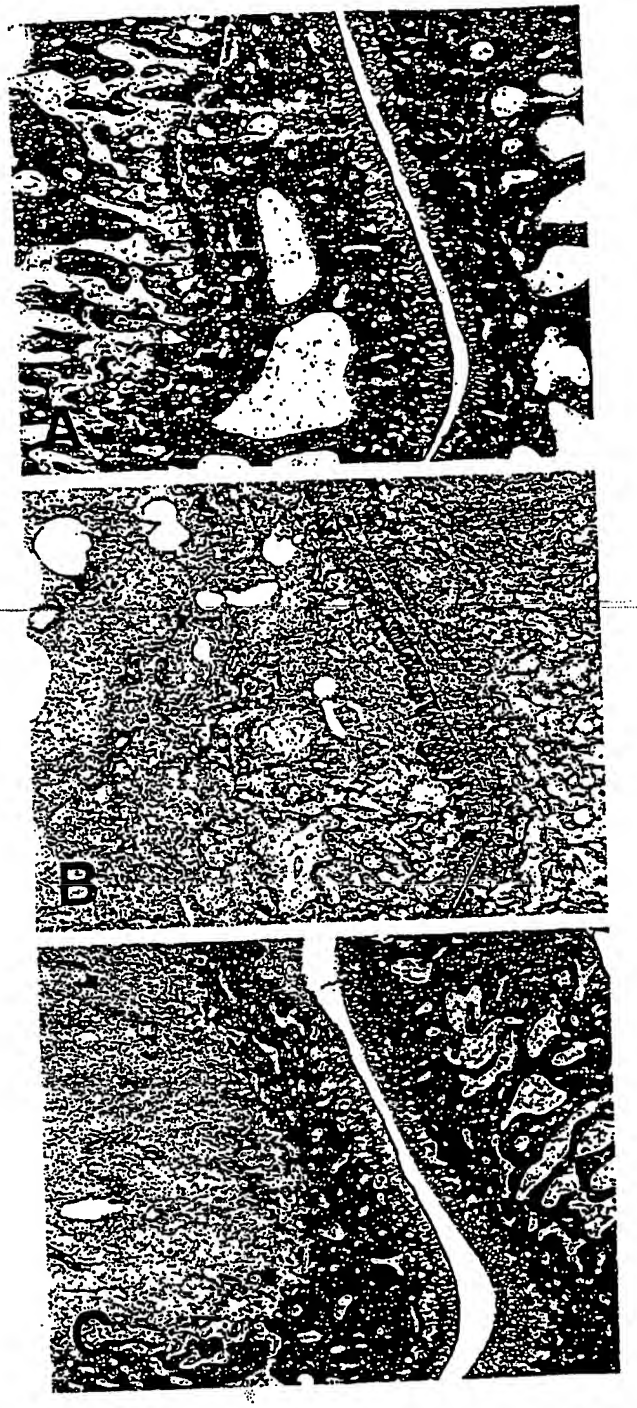

Fig. 5. A, photomicrograph of a normal tibio-tarsal joint. Cancellous bone of the metaphysis (left) is separated from the epiphysis (middle) by the growth plate (continuous pink line). The joint space between the tibia and tarsus (right) is clearly visible. B, photomicrograph of a tibio-tarsal joint typical of a rat suffering from AA. All of the original normal marrow and bone of the tibia and tarsus has been replaced by granulation tissue within which reactive woven bone has formed. The joint space (running vertically in approximately the same location as in the upper and lower panels) has been obliterated almost entirely by infiltrating granulation tissue and a large region of the articular cartilage on the tarsal side of the joint has been replaced by granulation tissue. C, photomicrograph of a tibio-tarsal joint from a rat which had been challenged with adjuvant and then treated with SB 203580 (60 mg/kg/day) for 22 days. Although a small amount of infiltration and cartilage erosion can be seen on the tibial side (top), the joint space and articular surface are otherwise normal. Whereas the cancellous bone of the tibial metaphysis has been lost and the marrow largely replaced by granulation tissue, woven bone has not yet formed. The bone and marrow of the tibial epiphysis and the tarsus are normal.

TABLE 3
Inhibition of serum IL-6 in AA rats treated with SB 203580

SB 203580 was administered orally 5 × a week from day 0 to 22. Serum IL-6 was measured on day 23. Data are mean ± S.E. for 10 animals per group. *** $P < .001$.

Treatment	IL-6	% Inhibition
	ng/ml	
Control AA rats	1.85 ± 0.10	
SB 203580		
60 mg/kg	1.11 ± 0.13	40***
30 mg/kg	1.43 ± 0.10	23***
10 mg/kg	1.75 ± 0.07	5 N.S.

former joint space has been infiltrated with granulation tissue. The joint from the rat treated with SB 203580 shows protection of the joint space, articular surfaces and subchondral bone. Although the tibial metaphyseal cancellous bone and marrow have been replaced by granulation tissue, these components of the tarsus are normal. This histological appearance is consistent with SB 203580 having retarded the progression of the adjuvant-induced arthritic lesion.

Serum IL-6 levels in AA rats treated with SB 203580 on days 0 to 22 were measured in a B9 hybridoma proliferation assay. Normal rats had serum IL-6 levels of < 50 pg/ml, whereas levels in rats with untreated AA were elevated as high as 1.85 ng/ml. In rats treated with SB 203580, there was a 40% reduction in IL-6 at the 60 mg/kg dose ($P < .001$) and 23% inhibition at 30 mg/kg ($P < .001$) (table 3).

Fetal rat long bone assay. As studies in the AA rat showed clearly that treatment with SB 203580 had disease-modifying activity and protective effects on both bone and cartilage, we examined the effect of the compound in a fetal rat long bone resorption assay. In this assay, osteoclast-mediated bone resorption is monitored by measuring the release of ^{45}Ca into the culture medium from preradiolabeled fetal long bones. SB 203580 inhibited resorption in a concentration-dependent manner; 3 μM (85%, $P < .001$), 1 μM (80%, $P < .001$) and 0.3 μM (38%, $P < .05$). The IC_{50} was 0.6 μM (fig. 6).

Endotoxin shock. The effect of SB 203580 was evaluated in a mouse model of endotoxin shock. In this model, C57BL/6 mice are sensitized with D-(+)-gal, which makes them highly susceptible to the lethal effects of endotoxin (LPS). One hour before an i.v. injection of LPS/D-gal, control mice have serum levels of TNF-α up to 4 ng/ml. This is reduced in a dose-dependent manner by prophylactic administration of SB 203580 given 30 min before the injection of LPS/D-gal. Doses of 100, 50 and 25 mg/kg were active and inhibited TNF-α levels by 87% ($P < .001$), 62% ($P < .001$) and 42% ($P < .001$), respectively (table 4). In a separate group of mice that were monitored for survival, 84% of mice treated with the 100 mg/kg dose of SB 203580 survived compared to only 17% of control mice.

Immune function. In order to determine whether chronic administration of a CSAID™ molecule such as SB 203580 had detrimental (suppressive) effects on the immune system, BALB/c mice were immunized with OVA in CFA and then treated for 2 weeks (5 days a week) with 60 mg/kg i.p. of the

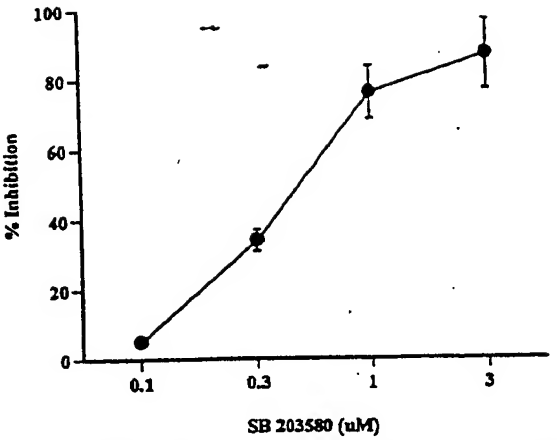

Fig. 6. SB 203580 inhibits PTH-stimulated fetal rat long bone resorption *in vitro* (IC_{50} = 0.6 μM). Fetal rat radii and ulnae (four bones per treatment per experiment) were cultured in the presence of 50 ng/ml of PTH and the indicated concentrations of SB 203580 for 48 hr as described under "Materials and Methods." Each data point represents mean and S.E.M. from three separate experiments. Bones cultured in the absence of PTH released approximately 14% of the incorporated ^{45}Ca. In the presence of PTH, control bones released approximately 45% of the incorporated ^{45}Ca.

compound or with RAP at 50 mg/kg. The serum antibody response of mice treated with RAP was suppressed totally by this treatment and there was a significant reduction in the anti-OVA serum antibody titer in mice treated with SB 203580 (fig. 7A). However, when lymph node cells from treated mice were examined for their response to the specific OVA antigen or to the mitogen Con A, no inhibition of proliferation was observed (fig. 7, B and C). Neither was there any inhibition of an allogeneic response in a mixed lymphocyte reaction between spleen cells from treated mice and C57BL/6 stimulator (3000 R) cells (fig. 7D). In all cases, the lymphocyte responses of RAP-treated mice were suppressed dramatically.

Discussion

The pyridinyl imidazoles are a novel class of compounds that have potent inhibitory effects on cytokine production both *in vitro* and *in vivo*, and also show anti-inflammatory activity in a variety of animal models (reviewed in Lee *et al.*, 1993). An early compound in this series, SK&F 86002, had cytokine suppressive activity (IC_{50}, 1 μM) (Lee *et al.*, 1993), but no significant antiproliferative activity (Reddy *et al.*, 1994). In addition to cytokine suppressive activity, SK&F 86002 and many structurally related analogs inhibited eicosanoid metabolism in LO and CO enzyme assays (Griswold *et al.*, 1987). In keeping with this profile of both cytokine and eicosanoid inhibition, SK&F 86002 and related compounds showed therapeutic activity in mouse collagen-induced arthritis (Griswold *et al.*, 1988) and carageenan-induced inflammation (Lee *et al.*, 1993), as well as analgesic activity in mouse abdominal constriction assays (Lee *et al.*, 1993). These activities, however, could not totally be attributed to LO/CO inhibition and the compounds clearly did not act as classical nonsteroidal anti-inflammatory drugs. Evidence for this was their activity in assays and models relatively insensitive to CO inhibition such as collagen-induced arthritis (Griswold *et al.*, 1988), the fetal rat long bone resorption assay (Votta and Bertolini, 1994) and mouse models of endotoxin shock (Badger *et al.*, 1989; Olivera *et al.*, 1992).

In studies designed to define the mechanism of cytokine suppression by the pyridinyl imidazoles, it was revealed that inhibition of TNF-α synthesis was primarily at the translational rather than the transcriptional level (Lee *et al.*, 1990; Young *et al.*, 1993), and that a block occurred before nascent peptide elongation (Young *et al.*, 1993; Prichett *et al.*, 1995; P. R. Young, unpublished data). Recent investigations using THP.1 cells, radiolabeled chemical probes for radioligand binding assays and photoaffinity labeling experiments have identified the molecular target of these compounds to be a pair of closely related mitogen-activated protein kinase homologs termed CSBPs (Lee *et al.*, 1994b). CSBP, alternatively termed p38 or RK, has subsequently been identified independently by several laboratories (Lee *et al.*, 1994b; Han *et al.*, 1994; Rouse *et al.*, 1994).

Inhibition of CSBP kinase activity by these compounds correlates with cytokine inhibition and THP.1 cytosol binding assays (Lee *et al.*, 1994b). SB 203580 [4-(4-fluorophenyl)-2-(4-methylsulfinylphenyl)-5-(4-pyridyl)imidazole], a newer member of the pyridinyl imidazoles, is the best studied compound and has an IC_{50} of 0.22 μM as a CSBP inhibitor (Cuenda *et al.*, 1995; Gallagher *et al.*, 1995; T. F. Gallagher *et al.*, in press, 1996). The compound is highly specific for CSBP kinase with no inhibitory activity observed on a variety of other kinases (Cuenda *et al.*, 1995). A physiological substrate of CSBP is MAPKAP kinase-2, and SB 203580 inhibits the activation of this kinase and its subsequent phosphorylation of hsp 27 in stress-stimulated cells (Cuenda *et al.*, 1995). In *in vitro* monocyte cultures, SB 203580 inhibits IL-1 and TNF-α from LPS-stimulated human monocytes (IC_{50}, 50–100 nM) as well as the production of leukotriene B_4 from calcium ionophore (A23187)-stimulated human monocytes (IC_{50}, 1.5 μM) (M. D. Chabot-Fletcher, unpublished observations). In HL-60 cells, SB 203580 had little effect on the LO pathway,

TABLE 4

SB 203580 inhibits serum TNFα and improves survival in a murine model of endotoxin shock

Male C57BL/6 mice were treated p.o. with SB 203580, 30 min before LPS/b-gal given i.v. Serum TNF was measured 1 hr later. Data are mean and S.E.M. of three to five animals per group. Survival was monitored in a separate group of mice (six per group). * $P < .05$ by Fisher's exact test. ND = not done.

Treatment/Dose	TNF-α	% Inhibition	% Survival
	pg/ml		
Control	3789 ± 142		17
SB 203580			
100 mg/kg	490 ± 172	87***	84*
50 mg/kg	1444 ± 130	62***	20 N.S.
25 mg/kg	2248 ± 130	42***	ND
12.5 mg/kg	3514 ± 214	7 N.S.	ND

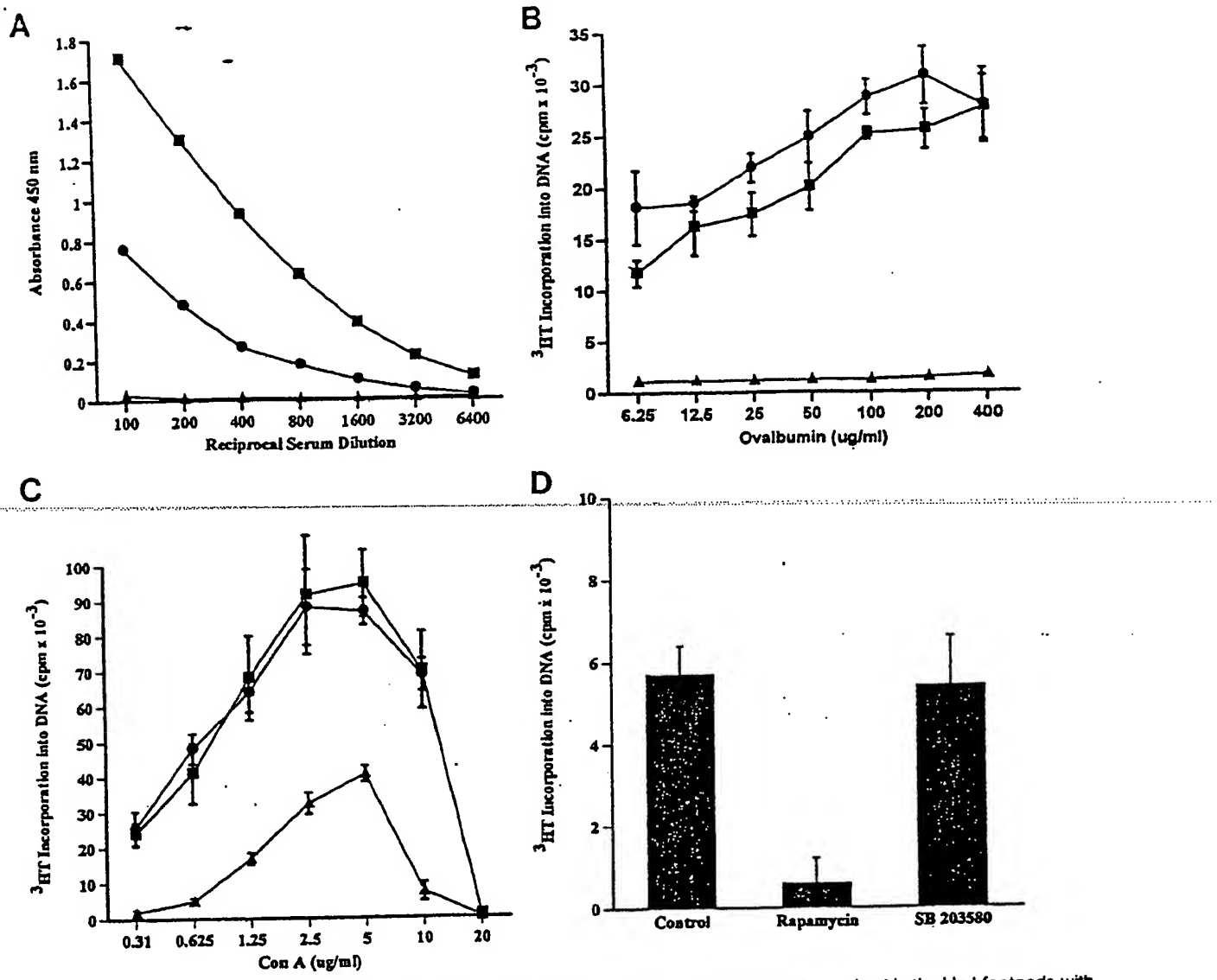

Fig. 7. Immune function in BALB/c mice treated with SB 203580 at 60 mg/kg i.p. for 2 weeks. Mice were immunized in the hind footpads with OVA in CFA as described under "Materials and Methods." A, serum antibody response to OVA measured in an ELISA assay. Data are from pooled serum samples. B, proliferative response of lymph node cells to varying doses of OVA. Data are mean and S.D. of six replicates. C, proliferative response of lymph node cells to varying doses of Con A. Data are mean and S.D. of six replicates. ■, control untreated; ●, SB 203580; ▲, RAP; and D, mixed lymphocyte reaction of treated BALB/c spleen cells against irradiated (3000 R) C57BL/6 stimulator cells. Data are mean and S.D. of six replicates.

but potently inhibited prostaglandin E_2 synthesis. SB 203580, however, had no direct inhibitory activity on pituitary growth hormone Synthase-1 and only modest inhibitory activity on LO (IC_{50}, 58 μM). The involvement of CSBP in the regulation of arachidonic acid availability, which is the rate limiting step for both LO and CO production, provides one mechanism which may explain these observations. In platelets, CSBP mediates the activation of cytosolic phospholipase A_2 by phosphorylation of cytosolic phospholipase A_2 in response to a thrombin agonist peptide (Kramer *et al.*, 1995). This activation was correlated with the subsequent release of arachidonic acid and formation of CO products. The observation that SB 203580 inhibits the synthesis of the inducible COX-2 enzyme provides an additional mechanism by which CSBP can regulate prostanoid synthesis (Lee *et al.*, 1994a).

In the studies reported in this paper, we have profiled SB 203580 in a number of pharmacological models both *in vitro* and *in vivo* and demonstrated its activity in a wide variety of TNF-α-mediated animal models. SB 203580 inhibited LPS-induced TNF-α *in vivo* in both mice and rats with IC_{50} values of 15 and 25 mg/kg, respectively. This inhibition of TNF-α was an indication that disease models such as mouse collagen-induced arthritis and rat adjuvant arthritis would be positively modulated by the compound. This was indeed the case and, in collagen-induced disease in DBA/1 LACJ mice, SB 203580 dosed for 7 days at 50 mg/kg p.o. (b.i.d.) reduced joint edema by 72 and 45% in two separate experiments. SAP, an acute inflammatory protein in mice, was also inhibited by 42 and 52%, respectively, in the two experiments. Evidence for the critical role of endogenous TNF-α in this disease model

has been provided by the observations that administration of anti-TNF-α antibodies can ameliorate the disease (Piguet *et al.*, 1992; Thorbecke *et al.*, 1992; Williams *et al.*, 1992) and that TNF-α transgenic mice spontaneously develop arthritis (Keffer *et al.*, 1991).

TNF-α clearly plays a proinflammatory role in another animal model of RA, the AA rat, in which elevated levels have been observed in the plasma and joints (DiMartino *et al.*, 1993; Smith-Oliver *et al.*, 1993). In this disease model, SB 203580 was very effective in reducing paw inflammation at doses of 30 and 60 mg/kg/day with optimum inhibition observed at 60 mg/kg/day (86% inhibition on day 16). Evidence for the protection of joint integrity at this dose was provided by the observation that there was a normalization of BMD (31%) and BMC (26%) as measured by DXA. This was also reflected in the histological evaluation of the affected joints, in which a clear beneficial effect was observed on both bone and cartilage. In keeping with the compound's disease-modifying activity, our studies also demonstrated that serum levels of IL-6 were reduced in treated rats. This cytokine has been shown to be increased in different biological fluids in patients with autoimmune disease, particularly RA (Houssiau *et al.*, 1988; Swaak *et al.*, 1988; Hirano *et al.*, 1988), and the level in various inflammatory compartments appears to be a sensitive marker of disease activity.

The protection of bone integrity in the AA rat led us to evaluate SB 203580 in a direct *in vitro* assay of bone resorption, the fetal rat long bone assay. Cytokines such as IL-1 and TNF-α have been shown to stimulate bone resorption *in vitro* and *in vivo* (Gowen and Mundy, 1986; Bertolini *et al.*, 1986; Tashijian *et al.*, 1987; Sabatini *et al.*, 1988), and it was reasonable to expect that a CSAID™ molecule would have a protective effect in this model system. SB 203580 dose-dependently (IC_{50}, 0.6 μM) inhibited PTH-stimulated bone resorption. Although the precise mechanism of action of the compound (and other pyridinyl imidazoles) on bone resorption has not been defined fully, it appears to be related to the compound's cytokine suppressive properties as selective CO, and dual CO/LO inhibitors were inactive in this organ culture system (Votta and Bertolini, 1994).

Another animal model in which TNF-α has been shown to play a predominant role is that of endotoxin-induced shock. We demonstrated previously that SK&F 86002, a dual inhibitor of arachidonic acid metabolism as well as a cytokine inhibitor, could reduce serum TNF-α levels and prolong survival in mouse shock models (Badger *et al.*, 1988). In addition, we were able to demonstrate that antibodies to mouse TNF-α could protect mice against endotoxin-induced shock in mice that were sensitized with *Proprionibacterium acnes* (Badger *et al.*, 1989). SB 203580, a more selective cytokine inhibitor with reduced inhibitory activity on LO and CO, reduced serum TNF-α in LPS/D-gal-sensitized mice and improved their survival at high doses.

It is clear that SB 203580 is a potent inhibitor of IL-1 and TNF-α *in vitro* and that it is pharmacologically active in a number of animal models *in vivo*. The question of whether such a potent cytokine inhibitor would be immunosuppressive as well as having anti-inflammatory activity has been addressed by examining its activity *in vivo* in mice immunized with OVA. Apart from partial inhibition of specific antibody levels against OVA, there was no suppression of OVA-specific T-cell proliferation, an allogeneic response or of mitogen (Con A)-induced proliferative responses. These results and those reported previously with the dual inhibitor of arachidonic acid metabolism, SK&F 86002 (Lee *et al.*, 1993; Reddy *et al.*, 1994), show clearly that these compounds do not have overt immunosuppressive activity.

Mechanistically, it is not clear at the present time to what extent the beneficial effects of SB 203580 are due to suppression of TNF-α production or suppression of cytokine signaling. Given that SB 203580 has been shown, at least *in vitro*, to be effective in inhibiting cytokine signaling leading to either cytokine production or other downstream effects, it is safe to assume that *in vivo*, the compound may induce its antiarthritic activity *via* both the inhibition of cytokine production and action. As an *in vitro* example, SB 203580 has been shown to block IL-6 production in L929 cells stimulated with TNF-α (Beyaert *et al.*, 1996).

The pharmacological profile that we have described here for SB 203580, a potent CSBP/p38 kinase inhibitor, would appear to be one that would be desirable for an antiarthritic therapeutic agent. Despite numerous attempts over the years to design drugs with therapeutic potential for RA, there is still a real need for more effective, less toxic treatments to control the progression of this disease. Most therapies, although supplying symptomatic relief, do not alter the progression of bone and cartilage destruction in the affected joints. In recent years, it has become clear that a multitude of cytokines contribute to the overall inflammatory and bone destructive sequelae that occur in RA, and that targeting one or more of these cytokines could modulate the disease (Arend and Dayer, 1955; Elliott and Maini, 1995). TNF-α has emerged as a cytokine of pivotal importance in the disease process and inhibition of the production and/or effects of this cytokine is a rational therapeutic strategy (Feldmann *et al.*, 1994; Brennan *et al.*, 1995). Indeed, ongoing studies are demonstrating the efficacy of treatment of RA with monoclonal antibodies to TNF-α in RA patients (Elliott *et al.*, 1993; Maini *et al.*, 1995). A small molecular weight orally active cytokine inhibitor with the pharmacological profile described in this manuscript could well provide significant beneficial effects in this disease.

Acknowledgments

The authors acknowledge the expert technical assistance of the following: Michael DiMartino, Len Hillegass, David Rieman, Barbara Swift, George Stroup, Sandra Hoffmann, Tonie Newman-Tarr and Hugh Zhao. We also thank Audrey Boyd for secretarial assistance.

References

Aarden, L. A., Lansdorp, P., and de Groot, E.: A growth factor for B-cell hybridomas produced by human monocytes. Lymphokines 10: 175–185, 1985.

Arend, W. P. and Dayer, J.-M.: Inhibition of the production and effects of interleukin-1 and tumor necrosis factor α in rheumatoid arthritis. Arthritis Rheum. 38: 151–160, 1995.

Badger, A. M., Olivera, D., Talmadge, J. E. and Hanna, N.: Protective effect of SK&F 86002, a novel dual inhibitor of arachidonic acid metabolism, in murine models of endotoxin shock: Inhibition of tumor necrosis factor as a possible mechanism of action. Circ. Shock 27: 51–61, 1989.

Bertolini, D. R., Nedwin, G. E., Bringman, T. S., Smith, D. D. and Mundy, G. R.: Stimulation of bone resorption and inhibition of bone formation *in vitro* by human necrosis factors. Nature (Lond.) 319: 515–518, 1986.

Beyaert, R., Cuenda, A., Berghe, W. V., Plaisance, S., Lee, J. C., Haegeman, G., Cohen, P. and Fiers, W.: The p38/RK mitogen-activated protein kinase pathway regulates interleukin-6 synthesis in response to tumor necrosis factor. EMBO J. 15: 1914–1923, 1996.

Bradbeer, J. N., Kapadia, R. S., Sarkar, S. K., Zhao, H., Stroup, G. B., Swift,

A., Riedan, D. J. and Badger, A. M.: Disease-modifying activity of SK&F 86615 in rat adjuvant-induced arthritis. Arthritis Rheum. 39: 504–514, 1996.

Brennan, F. M., Cope, A. P., Katsikis, P., Gibbons, D. L., Maini, R. N. and Feldmann, M.: Selective immunosuppression of tumour necrosis factor-alpha in rhuematoid arthritis. *In* Selective Immunosuppression: Basic Concepts and Clinical Applications, ed. by L. Adorini, pp. 48–60, S. Karger, Basel, 1995.

Cuenda, A., Rouse, J., Doza, Y. N., Meier, R., Cohen, P., Gallagher, T. F., Young, P. R. and Lee, J. C.: SB 203580 is a specific inhibitor of a MAP kinase homologue which is stimulated by cellular stresses and interleukin-1. FEBS Lett. 364: 229–233, 1995.

DiMartino, M., Slivjar, M., Esser, K., Wolff, C., Smith, E. and Gagnon, R.: Adjuvant arthritic (AA) rats exhibit enhanced endotoxin-induced plasma TNF (EIPT) levels. Agents Actions 39: C58–C60, 1993.

Dinarello, C. A.: Inflammatory cytokines: Interleukin-1 and tumor necrosis factor as effector molecules in autoimmune diseases. Curr. Opin. Immunol. 3: 941–948, 1991.

Elliott, M. J. and Maini, R. N.: Anticytokine Therapy in Rheumatoid Arthritis. *In* Bailliere's Clinical Rheumatology, Vol. 9 (issue 4), pp. 633–652, editors: P. M. Brooks and D. E. Furst, 1995.

Elliott, M. J., Maini, R. N., Feldmann, M., Long-Fox, A., Charles, P., Katsikis, P., Brennan, F. M., Walker, J., Bijl, H., Ghrayeb, J. and Woody, J. N.: Treatment of rheumatoid arthritis with chimeric monoclonal antibodies to tumor necrosis factor α. Arthritis Rheum. 36: 1681–1690, 1993.

Feldmann, M., Brennan, F. M., Elliott, M., Katsikis, P. and Maini, R. N.: TNFα as a therapeutic target in rheumatoid arthritis. Circ. Shock 43: 179–184, 1994.

Gallagher, T. F., Fier-Thompson, S. M., Garigipati, R. S., Sorenson, M. E., Smietana, J. M., Lee, D., Bender, P. E., Lee, J. C., Laydon, J. T., Griswold, D. E., Chabot-Fletcher, M. D., Breton, J. J. and Adams, J. L.: 2,4,5-Triarylimidazole inhibitors of IL-1 biosynthesis. Bioorg. Med. Chem. Lett. 5: 1171–1176, 1995.

Gallagher, T. F. *et al.*: Regulation of stress induced cytokine production by pyridinylimidazoles: Inhibition of CSBP kinase. In Press: Bioorganic and Medicinal Chemistry, 1996.

Gowen, M. and Mundy, G. R.: Action of recombinant interleukin-1, interleukin-2 and interferon gamma on bone resorption *in vitro*. J. Immunol. 136: 2478–2482, 1986.

Griswold, D. E., Marshall, P. J., Webb, E. F., Godfrey, R., DiMartino, M. J., Sarau, H. M., Newton, J., Jr., Gleason, J. G., Poste, G. and Hanna, N.: SK&F 86002: A structurally novel antiinflammatory agent that inhibits lipoxygenase- and cyclooxygenase-mediated metabolism of arachidonic acid. Biochem. Pharmacol. 36: 3463–3470, 1987.

Griswold, D. E., Hillegass, L. M., Meunier, P. C., DiMartino, M. J. and Hanna, N.: Effect of inhibitors of eicosanoid metabolism in murine collagen-induced arthritis. Arthritis Rheum. 31: 1406–1412, 1988.

Han, J., Lee, J. D., Bibb, S. L. and Ulevitch, R. J.: A MAP kinase targeted by endotoxin and in mammalian cells. Science (Wash. DC) 265: 808–811, 1994.

Hirano, T., Matsuda, T. and Turner, M.: Excessive production of IL-6/B cell stimulatory factor-2 in rheumatoid arthritis. Eur. J. Immunol. 18: 1797–1802, 1988.

Houssiau, F. A., Devogelaer, J.-P., van Damme, J., Nagant de Deuzchaisnes, D. and van Snick, J.: Interleukin-6 in synovial fluid and serum of patients with rheumatoid arthritis and other inflammatory arthritides. Arthritis Rheum. 31: 784–788, 1988.

Keffer, J., Probert, L., Cazlaris, H., Georgopoulos, S., Kaslaris, E., Kioussis, D. and Kollias, G.: Transgenic mice expressing human tumor necrosis factor: A predictive genetic model of arthritis. EMBO J. 10: 4025–4031, 1991.

Kramer, R. M., Roberts, E. F., Strifler, B. A. and Johnstone, E. M.: Thrombin induces activation of p38 MAP kinase in human platelets. J Biol. Chem. 270: 27395–27398, 1995.

Lee, J. C., Badger, A. M., Griswold, D. E., Dunnington, D., Truneh, A., Votta, B., White, J. R., Young, P. R. and Bender, P. E.: Bicyclic imidazoles as a novel class of cytokine biosynthesis inhibitors. Ann. N.Y. Acad. Sci. 696: 149–170, 1993.

Lee, J. C., Blumenthal, M. J., Laydon, J. T., Tan, K. B. and DeWitt, D. L.: Translational Regulation of Prostaglandin Endoperoxide Synthase-2 Expression in Human Monocytes, Presented at the 7th International Conference of the Inflammatory Research Association, Poconos, PA. 1994a.

Lee, J. C., Laydon, J. T., McDonnell, P. C., Gallagher, T. F., Kumar, S., Green, D., McNulty, D., Blumenthal, M. J., Heys, J. R., Landvatter, S. W., Strickler, J. E., McLaughlin, M. M., Siemens, I. R., Fisher, S. M., Livi, G. P., White, J. R., Adams, J. L. and Young, P. R.: A protein kinase involved in the regulation of inflammatory cytokine biosynthesis. Nature (Lond.) 372: 739–746, 1994b.

Lee, J. C., Votta, B., Dalton, B. J., Griswold, D. E., Bender, P. E. and Hanna, N.: Inhibition of human monocyte IL-1 production by SK&F 86002. Int. J. Immunother. 6: 1–12, 1990.

Lee, J. C. and Young, P. R.: Role of CSBP/p38/RK stress response kinase in LPS and cytokine signaling mechanisms. J. Leukocyte Biol. 59: 152–157, 1996.

Maini, R. N., Elliott, M. J., Brennan, F. M. and Feldmann, M.: Beneficial effects of tumour necrosis factor-alpha (TNF-α) blockade in rheumatoid arthritis (RA). Clin. Exp. Immunol. 101: 207–212, 1995.

Olivera, D. L., Esser, K. M., Lee, J. C., Greig, R. G. and Badger, A. M.: Beneficial effects of SK&F 105809, a novel cytokine-suppressive agent, in murine models of endotoxin shock. Circ. Shock 37: 301–306, 1992.

Piguet, P. F., Grau, G. E., Vesin, C., Loetscher, H., Gentz, R. and Lesslauer, W.: Evolution of collagen arthritis in mice is arrested by treatment with anti-tumour necrosis factor (TNF) antibody or a recombinant soluble TNF receptor. Immunology 77: 510–514, 1992.

Prichett, W., Hand, A., Sheilds, J. and Dunnington, D.: Mechanism of action of bicyclic imidazoles defines a translational regulatory pathway of tumor necrosis factor α. J. Inflamm. 45: 97–105, 1995.

Raisz, L. G.: Bone resorption in tissue culture. Factors influencing the response to parathyroid hormone. J. Clin. Invest. 44: 103–116, 1965.

Reddy, M. P., Webb, E. F., Cassatt, D., Maley, D., Lee, J. C., Griswold, D. E. and Truneh, A.: Pyridinyl imidazoles inhibit the inflammatory phase of delayed type hypersensitivity reactions without affecting T-dependent immune responses. Int. J. Immunopharmacol. 16: 795–804, 1994.

Rouse, J., Cohen, P., Trigon, S., Morange, M., Alonso-Llamazares, A., Zamanillo, D., Hunt, T. and Nebreda, A. R.: Identification of a novel protein kinase cascade stimulated by chemical stress and heat shock which activates MAP kinase-activated protein MAPKAP kinase-2 and induces phosphorylation of the small heat shock proteins. Cell 78: 1027–1037, 1994.

Sabatini, M., Boyce, B., Aufdermorte, T., Bonewald, L. and Mundy, G. R.: Infusion of interleukin-1α and β causes hypercalcemia in normal mice. Proc. Natl. Acad. Sci. U.S.A. 83: 5235–5239, 1988.

Smith-Oliver, T., Noel, L. S., Stempson, S. S., Yarnall, D. P. and Connolly, K. M.: Elevated levels of TNF in the joints of adjuvant arthritic rats. Cytokine 5: 298–304, 1993.

Stern P. H. and Raisz L. G.: Organ cultures of bone. *In* Skeletal Research: An Experimental Approach, pp. 21–59, editors: D. J. Simmons, and A. S. Kunin, Academic Press, New York, 1979.

Swaak, A. J. G., Rooyen, A., van Nieuwenhuis, E. and Aarden, L. A.: Interleukin-6 (IL-6) in synovial fluid and serum of patients with rheumatic diseases. Scand. J. Rheumatol. 17: 469–474, 1988.

Tashjian, A. H., Voekel, E. F., Lazzaro, M., Goad, D., Bosma, T. and Levine, L.: Tumor necrosis factor α (cachectin) stimulates bone resorption in mouse calvaria via a prostaglandin-mediated mechanism. Endocrinology 120: 2029–2036, 1987.

Thorbecke, G. J., Shah, R., Leu, C. H., Kuruvilla, A. P., Hardison, A. M. and Palladino, M. A.: Involvement of endogenous tumor necrosis factor α and transforming growth factor β during induction of collagen type II arthritis in mice. Proc. Natl. Acad. Sci. U.S.A. 89: 7375–7379, 1992.

Votta, B. J. and Bertolini, D. R.: Cytokine suppressive antiinflammatory compounds inhibit bone resorption *in vitro*. Bone 15: 533–538, 1994.

Williams, R. O., Feldmann, M. and Maini, R. N.: Anti-tumor necrosis factor ameliorates joint disease in murine collagen-induced arthritis. Proc. Natl. Acad. Sci. U.S.A. 89: 9784–9788, 1992.

Wooley, P. H.: Collagen-induced arthritis in the mouse. Methods Enzymol. 162: 361–373, 1988.

Young, P. R., McDonnell, P., Dunnington, D., Hand, A., Laydon, J. and Lee, J. C.: Bicyclic imidazoles inhibit IL-1 and TNF production at the protein level. Agents Actions 39: C67–C69, 1993.

Send reprint requests to: Dr. Alison M. Badger, Associate Director, Department of Cellular Biochemistry, SmithKline Beecham Pharmaceuticals, 709 Swedeland Rd., P.O. Box 1539, King of Prussia, PA 19406-0939.

Exhibit 3

ARTHRITIS & RHEUMATISM
Vol. 43, No. 1, January 2000, pp 175–183

DISEASE-MODIFYING ACTIVITY OF SB 242235, A SELECTIVE INHIBITOR OF p38 MITOGEN-ACTIVATED PROTEIN KINASE, IN RAT ADJUVANT-INDUCED ARTHRITIS

ALISON M. BADGER, DON E. GRISWOLD, RASESH KAPADIA, SIMON BLAKE, BARBARA A. SWIFT, SANDY J. HOFFMAN, GEORGE B. STROUP, EDWARD WEBB, DAVID J. RIEMAN, MAXINE GOWEN, JEFFREY C. BOEHM, JERRY L. ADAMS, and JOHN C. LEE

Objective. To evaluate the effects of SB 242235, a potent and selective inhibitor of p38 mitogen-activated protein (MAP) kinase, on joint integrity in rats with adjuvant-induced arthritis (AIA).

Methods. Male Lewis rats with AIA were orally treated either prophylactically (days 0–20) or therapeutically (days 10–20) with SB 242235. Efficacy was determined by measurements of paw inflammation, dual-energy x-ray absorptiometry for bone mineral density (BMD), magnetic resonance imaging (MRI), micro–computed tomography (CT), and histologic evaluation. Serum tumor necrosis factor α (TNFα) in normal (non-AIA) rats and serum interleukin-6 (IL-6) levels in rats with AIA were measured as markers of the antiinflammatory effects of the compound.

Results. SB 242235 inhibited lipopolysaccharide-stimulated serum levels of TNFα in normal rats, with a median effective dose of 3.99 mg/kg. When SB 242235 was administered to AIA rats prophylactically on days 0–20, it inhibited paw edema at 30 mg/kg and 10 mg/kg per day by 56% and 33%, respectively. Therapeutic administration on days 10–20 was also effective, and inhibition of paw edema was observed at 60, 30, and 10 mg/kg (73%, 51%, and 19%, respectively). Significant improvement in joint integrity was demonstrated by showing normalization of BMD and also by MRI and micro-CT analysis. Protection of bone, cartilage, and soft tissues was also shown histologically. Serum IL-6 levels were decreased in AIA rats treated with the 60 mg/kg dose of compound.

Conclusion. Symptoms of AIA in rats were significantly reduced by both prophylactic and therapeutic treatment with the p38 MAP kinase inhibitor, SB 242235. Results from measurements of paw inflammation, assessment of BMD, MRI, and micro-CT indicate that this compound exerts a protective effect on joint integrity, and thus appears to have disease-modifying properties.

SB 242235 is a new member of the pyridinyl imidazole class of compounds that has exhibited potent antiinflammatory activity (1–3). Early compounds in this class exerted this activity via inhibition of cyclooxygenase, 5-lipoxygenase, and proinflammatory cytokine biosynthesis (1). Inhibition of cytokine synthesis, however, has now been established as the primary pharmacologic action and is unrelated to the ability of the compounds to inhibit eicosanoids (4,5). Proinflammatory cytokines such as interleukin-1 (IL-1) and tumor necrosis factor α (TNFα) have been shown to play an important role in the pathogenesis of rheumatoid arthritis (RA), including inflammation (6–8), up-regulation of nitric oxide (9) and metalloproteinases (10), and bone resorption (11). The production of these cytokines from lipopolysaccharide (LPS)–stimulated human monocytes and from the human monocyte cell line THP-1 is inhibited by the pyridinyl imidazoles, with a 50% inhibition concentration (IC_{50}) of 50–100 n*M* (12,13).

Recent evidence that cytokines play a key role in acute and chronic inflammation has been provided by the demonstration that protein antagonists, such as IL-1 receptor antagonist and monoclonal antibodies to TNFα and its soluble receptor, can interfere with various acute and chronic inflammatory responses and are clinically

Alison M. Badger, PhD, Don E. Griswold, PhD, Rasesh Kapadia, PhD, Simon Blake, PhD, Barbara A. Swift, BS, Sandy J. Hoffman, BS, George B. Stroup, MS, Edward Webb, BS, David J. Rieman, BS, Maxine Gowen, PhD, Jeffrey C. Boehm, PhD, Jerry L. Adams, PhD, John C. Lee, PhD: SmithKline Beecham Pharmaceuticals, King of Prussia, Pennsylvania.

Address reprint requests to Alison M. Badger, PhD, SmithKline Beecham Pharmaceuticals, 709 Swedeland Road, King of Prussia, PA 19406.

Submitted for publication July 19, 1999; accepted in revised form September 21, 1999.

efficacious in RA (14,15). However, the need for orally active, small molecular weight compounds that would have the same effect as protein agents in inflammatory diseases is considerable.

SB 242235 and related compounds have been named cytokine-suppressive antiinflammatory drugs (CSAIDs), and the molecular target has been identified as the mitogen-activated protein (MAP) kinase homolog termed CSAID-binding protein 2 (CSBP2) (12), p38 (16), or RK (17,18). The binding of these compounds to the target CSBP/p38 protein in THP-1 cytosol and the inhibition of kinase activity for this recombinant protein has been correlated to their inhibition of cytokine biosynthesis (12,13), indicating a role for p38 in the regulation of cytokine production in response to various stimuli (19). Compounds structurally related to SB 242235 have been shown to attenuate the inflammatory components of disease in a number of animal models of acute and chronic inflammation in the absence of generalized immunosuppression (1,20,21) (examples include collagen-induced arthritis [2], adjuvant-induced arthritis [AIA] [20], and endotoxin shock [22,23]). In addition, inhibition of nitric oxide from IL-1–stimulated bovine cartilage and chondrocytes by the pyridinyl imidazole SB 203580 has recently been described (24).

SB 242235, when tested against a panel of representative protein kinases, shows a superior kinase selectivity profile in comparison with SB 203580. As reviewed by Lee et al (25), SB 203580 inhibits p38 isoform α with an IC_{50} of 48 nM (26) and p38β with an IC_{50} of 50 nM (27), as well as JNK2β1 (IC_{50} 280 nM) and c-raf (IC_{50} 360 nM) (28). However, SB 242235 is selective in that it does not inhibit ERK and JNK (up to 10 μM), which are structurally most related to p38 MAP kinase.

In this report, we have demonstrated significant antiinflammatory activity with SB 242235 in rats with AIA. This compound is a highly selective p38 inhibitor, which, unlike the earlier p38 inhibitor SB 203580 (29), has no direct effects on 5-lipoxygenase or cyclooxygenase-1 (Griswold D: unpublished observations). We have extended our previous findings in this animal model, in which we used SB 203580 (20), by examining the efficacy of SB 242235 when administered therapeutically as well as prophylactically to the AIA rat, a protocol reflecting the treatment of RA. In addition, we have utilized the advanced technology of magnetic resonance imaging (MRI) and micro–computed tomography (CT), as well as dual-energy x-ray absorptiometry (DEXA) and histology to clearly demonstrate the disease-modifying activity that a cytokine inhibitor of this compound class can have in an aggressive model of inflammatory disease. The effects observed in this rat model of arthritis indicated that treatment with small molecular weight, cytokine-suppressive agents may well have beneficial effects in RA.

MATERIALS AND METHODS

Animals. Inbred male Lewis rats were obtained from Charles River Breeding Laboratories (Raleigh, NC). Within any given experiment, only animals of the same age were used. All experimental procedures were in accordance with protocols approved by the SmithKline Beecham Institutional Animal Care and Use Committee, and met or exceeded the standards of the American Association for the Accreditation of Laboratory Animal Care, the United States Department of Health and Human Services, and all local and federal animal welfare laws.

Materials. SB 242235 was synthesized at SmithKline Beecham (Philadelphia, PA). For in vivo experiments, SB 242235 was administered orally in 0.03N HCl–0.5% tragacanth (Sigma, St. Louis, MO). Indomethacin was from Sigma.

LPS-induced TNFα production. Normal (non-AIA) rats were orally administered SB 242235 in acidified tragacanth at various times prior to challenge with LPS (3.0 mg/kg intraperitoneally). Ninety minutes later, the animals were killed by CO_2 inhalation, and blood samples were collected by cardiac puncture into heparinized tubes and stored on ice. The blood samples were centrifuged and the plasma collected and stored at −20°C until assayed for TNFα by specific enzyme-linked immunosorbent assay (ELISA) (23).

ELISA method. TNFα levels were measured using a sandwich ELISA, which utilized a hamster monoclonal anti-murine TNFα (Genzyme, Cambridge, MA) as the capture antibody and a polyclonal rabbit anti-murine TNFα (Genzyme) as the secondary antibody. For detection, a peroxidase-conjugated goat anti-rabbit antibody (Pierce, Rockford, IL) was added, followed by a substrate for peroxidase. TNFα levels in the plasma samples from each animal were calculated from a standard curve generated with recombinant murine TNFα (Genzyme).

Induction of arthritis. AIA was induced by a single injection of 0.75 mg of *Mycobacterium butyricum* (Difco, Detroit, MI) suspended in paraffin oil, into the base of the tail of male Lewis rats ages 6–8 weeks (weights 160–180 gm). Hindpaw volumes were measured by a water displacement method on day 16 and/or day 20 (30). Test compounds were homogenized in acidified 0.5% tragacanth (Sigma) and administered orally in a volume of 10 ml/kg. Control AIA animals were administered vehicle (tragacanth) alone. Two dosing protocols were used: prophylactic dosing (3, 10, and 30 mg/kg/day) initiated on the day of adjuvant injection, and therapeutic administration (10, 30, and 60 mg/kg/day) initiated on day 10. Indomethacin was included as a positive control (0.3 mg/kg prophylactically and 0.5 mg/kg therapeutically).

Change in paw volume is presented as the mean and SEM of 10–12 animals per group, and the percentage inhibition of hindpaw edema was calculated as follows:

$$\% \text{ inhibition} = 1 - \left[\frac{\text{AIA (treated)}}{\text{AIA (control)}}\right] \times 100,$$

where AIA (treated) and AIA (control) represent the mean paw volume (in ml) (minus the value in the normal non-AIA control) in rats treated with SB 242235 and rats treated with vehicle alone, respectively. For statistical analysis, paw volumes of rats treated with SB 242235 were compared with those of the untreated AIA controls by Student's *t*-test.

Bone mineral density (BMD) measurement. Animals were killed on day 21 and the hindlimbs removed and fixed in 70% ethanol. BMD of the distal tibia was determined by DEXA using the Hologic QDR-1000 equipped with high-resolution scanning software (Hologic, Waltham, MA). Quality control of the instrument was carried out each day prior to sample analysis by scanning both a human anthropomorphic spine phantom (low resolution) and the lumbar portion of a rat spine (high resolution), both of which were embedded in methylmethacrylate. All high-resolution scans were carried out with the sample placed on top of an acrylic block, 1.5 inches deep. The x-ray beam was collimated to a diameter of 1.27 mm, and line spacing and point resolution were 0.25 mm and 0.127 mm, respectively. Scans were made of the distal tibia region of excised bones stored in 70% ethanol in a square plastic container. The depth of the liquid was constant for all samples and sufficient to cover the limbs by ~0.5 inches.

BMD, as well as bone mineral content (BMC) and bone area, were determined for the distal tibia. The region of interest was defined as the area between a line drawn parallel to the proximal edge of the calcaneus and a second line drawn perpendicular to the long axis of the tibia midway between the first line and the point where the tibia meets the fibula. The point of connection between the fibula and tibia had to be approximated in some samples with low BMD. The width of the region of interest was kept constant between samples.

Magnetic resonance imaging. All MRI studies were carried out on a 9.4-Tesla AMX spectrometer with micro-imaging accessories (Bruker Instruments, Billerica, MA). Coronal sections (250 μm thick) of rat tibiotarsal joints were imaged with an in-plane resolution of 70 × 70 μm. A time to recovery of 1 second and an echo time of 7.5 ms were used, with a data matrix of 256 × 256. The morphologic changes in the joint architecture of the AIA control rats were compared with those in the normal, non-AIA controls and AIA rats treated with SB 242235. The joints were graded as the percentage of joints with no protection (i.e., severe disease, similar to AIA controls), moderate protection, or significant protection (i.e., similar to normal, non-AIA control animals).

Micro-CT imaging. All x-ray micro-CT images of the intact rat ankle joints were obtained on a micro-CT scanner (Scanco Medical, Auenring, Switzerland). A total of 380 slices covering a length of 12.9 mm (34 μm thick), with an in-plane resolution of 34 × 34 μm and an integration time of 80 ms/projection, yielding a total imaging time of 5 hours, were collected from each joint. The raw micro-CT images were gauss filtered (sigma = 1.2, base = 2) and binarized using a constant threshold for all the samples. Only the region around the tibiotarsal joint was rendered for 3-dimensional display.

Histology. Tibiotarsal joints from randomly selected animals from the following 3 groups of rats were examined histologically: normal, non-AIA rats, AIA control rats, or AIA rats treated orally with SB 242235 at 60 mg/kg/day. Rats were killed on day 21 by CO_2 administration, and then the hind legs were fixed in formalin and decalcified in Cal-Rite (Richard-Allen Scientific, Kalamazoo, MI) and the feet were removed from the legs at the distal tibial diaphysis. After routine processing, the feet were embedded and coronal sections were cut in the plane midway through the tibiotarsal and tarsotarsal joints. Sections were stained with Safranin O and counterstained with fast green.

Table 1. Determination of optimal pretreatment time for inhibition of LPS-induced TNFα production in rats by SB 242235*

Treatment	Pretreatment time, hours	TNFα, pg/ml	Inhibition, %
Vehicle	–	37,182 ± 2,791	–
SB 242235	4	11,236 ± 1,927	70†
	3	6,887 ± 1,997	81†
	2	4,318 ± 428	88†
	1	2,375 ± 449	94†

* A single dose of SB 242235 (15 mg/kg) or vehicle (0.5% tragacanth in 0.03N HCl) was given orally to normal rats at various times prior to challenge with lipopolysaccharide (LPS; 3 mg/kg intraperitoneally). Ninety minutes later, the animals were killed and plasma collected. Tumor necrosis factor (TNFα) levels were determined by specific enzyme-linked immunosorbent assay, and the results are expressed as the mean ± SEM of 6 rats per group.
† $P < 0.001$ versus treatment with vehicle alone.

Bioassay for IL-6. Serum samples were collected from the rats on day 21 following CO_2 administration. IL-6 levels were determined using the previously described B9 bioassay (31). Briefly, B9 cells (5×10^3 cells/well in 96-well, flat-bottom plates) were cultured with serial dilutions of rat serum in a final volume of 100 μl of RPMI 1640 (Flow Laboratories, Rockville, MD) containing 10% fetal bovine serum, 100 units/ml penicillin, 100 μg/ml streptomycin, and 2 m*M* L-glutamine (Grand Island Biological, Grand Island, NY). After 68 hours, 0.5 μCi of ^{3}H-thymidine was added to each well and the plates incubated for 6 hours at 37°C. Cells were harvested and the radioactivity incorporated was determined. IL-6 was quantitated from a standard curve including known amounts of rat IL-6 (0.1–100 pg/ml). B9 proliferation was unaffected by any agents used in this study.

RESULTS

Inhibition of TNFα in normal rats. To determine an optimal pretreatment time for inhibition of LPS-induced TNFα production in vivo, SB 242235 at a dose of 15 mg/kg was administered orally to normal rats at various times (4, 3, 2, and 1 hours) prior to LPS challenge (3 mg/kg, intraperitoneally). TNFα production was inhibited significantly ($P < 0.001$ versus treatment with vehicle alone) at all time points (70%, 81%, 88%, and 94% inhibition, respectively) (Table 1). A median effective dose (ED_{50}) was determined for SB 242235 in rats at a pretreatment time of 2 hours. SB 242235 at doses of 10, 5, and 2.5 mg/kg, administered orally in normal rats, significantly inhibited the LPS-induced production of TNFα (80% [$P < 0.001$], 68% [$P < 0.001$],

Table 2. Inhibition of LPS-induced TNFα production in normal rats by SB 242235*

Treatment	Oral dose, mg/kg	TNFα, pg/ml	Inhibition, %
Vehicle	–	70,661 ± 6,322	–
SB 242235	10	13,933 ± 3,027	80†
	5	22,316 ± 7,688	68†
	2.5	51,111 ± 7,318	28‡

* A single dose of compound or vehicle (0.5% tragacanth with 0.03N HCl) was given orally 2 hours prior to challenge with lipopolysaccharide (LPS; 3 mg/kg intraperitoneally). Ninety minutes later, the animals were killed and plasma collected. Tumor necrosis factor α (TNFα) levels were determined by specific enzyme-linked immunosorbent assay, and the results are expressed as the mean ± SEM of 6 rats per group. The median effective dose was calculated, by linear regression analysis, to be 3.99 mg/kg, orally, with 95% confidence limits of 2.19–5.82.
† $P < 0.001$ versus treatment with vehicle alone.
‡ $P < 0.05$ versus treatment with vehicle alone.

and 28% [$P < 0.05$] inhibition, respectively, versus treatment with vehicle alone) (Table 2).

Effect of prophylactic and therapeutic treatment with SB 242235 in AIA rats. *Paw inflammation.* The effect of SB 242235 was evaluated using the prophylactic dosing protocol, in which the compound was administered to male Lewis rats starting on the day of adjuvant injection. SB 242235 was administered in acidified tragacanth on a daily basis, and paw inflammation was measured on day 20. On day 21 the animals were killed and the hindlimbs were taken for measurement of BMD and for MRI. The data in Table 3 show that SB 242235 effectively inhibited paw edema in the AIA rat, with an

Table 3. Inhibition of paw edema in rats with adjuvant-induced arthritis (AIA) by SB 242235*

Treatment group	Oral dose, mg/kg	Paw volume, ml	Inhibition, %
Normal, non-AIA	–	1.56 ± 0.03	–
Vehicle-treated AIA control	–	3.30 ± 0.18	–
SB 242235-treated AIA	30	2.33 ± 0.12	56†
	10	2.72 ± 0.19	33‡
	3	2.95 ± 0.29	20§
Indomethacin-treated AIA	0.3	2.48 ± 0.14	47†

* AIA was induced by an injection of 0.75 mg of *Mycobacterium butyricum* in paraffin oil (Freund's complete adjuvant) into the base of the tail of male Lewis rats. AIA rats were treated prophylactically with SB 242235 on days 0–20, and hindpaw volumes (mean ± SEM of 10 rats per group) were measured by water displacement on day 20.
† $P < 0.001$ versus vehicle-treated AIA controls.
‡ $P < 0.01$ versus vehicle-treated AIA controls.
§ P not significant versus vehicle-treated AIA controls.

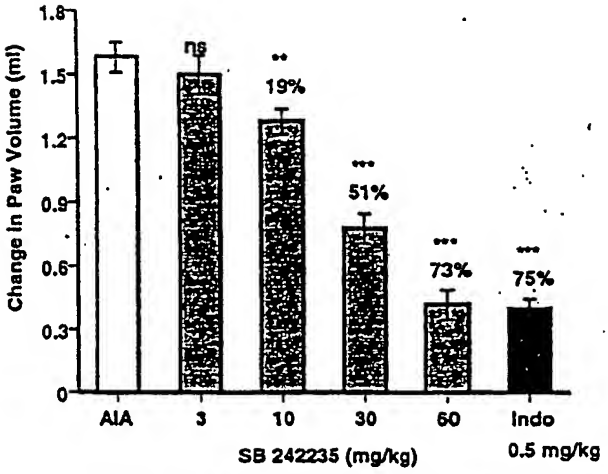

Figure 1. Therapeutic activity of SB 242235 on paw edema in adjuvant-induced arthritis (AIA) in Lewis rats. Rats were treated with SB 242235 in acidified tragacanth at 3, 10, 30, and 60 mg/kg orally or with vehicle alone (AIA controls) from day 10 to day 20, and paw edema was measured prior to killing of rats on day 21. Values are the mean ± SEM of 12 rats per group (with inhibition expressed as a percentage of AIA controls). ** = $P < 0.01$ and *** = $P < 0.001$ versus AIA controls. ns = not significant; Indo = indomethacin.

ED_{50} of ~30 mg/kg and a minimal effective dose of 10 mg/kg.

SB 242235 was also tested in the AIA rat using a therapeutic dosing protocol, which was used to more closely represent the treatment of RA in humans. In these experiments, rats were immunized with adjuvant on day 0 and treated with compound on days 10–20 (daily). Using this protocol, hindpaw inflammation was inhibited by 73% at 60 mg/kg ($P < 0.001$), by 51% at 30 mg/kg ($P < 0.001$), and 19% at 10 mg/kg ($P < 0.01$) compared with treatment with vehicle alone (Figure 1). There was no activity at 3 mg/kg.

Bone mineral density. BMD was determined by DEXA using the Hologic QDR-1000 equipped with high-resolution scanning software. Scans were made of the distal tibia obtained from the animals on day 21. BMD, as well as BMC and bone area, were determined. Bone integrity of normal control rats was assigned a value of 100%, and that of AIA control rats a value of 0%. Compared with the normal, non-AIA control rats, animals treated prophylactically with 30 mg/kg and 10 mg/kg of SB 242235 showed a significant normalization of BMD and BMC. There was 49% ($P < 0.001$) and 23% ($P < 0.05$) normalization of BMD at the 30 mg/kg and 10 mg/kg doses, respectively, and a 44% ($P < 0.001$) and

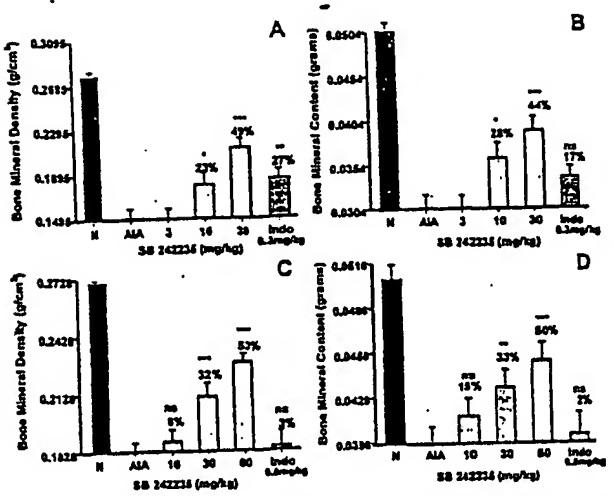

Figure 2. Bone densitometry evaluation of the distal tibia in AIA rats treated with SB 242235. Rats were treated with various doses of compound on days 0–20 (prophylactic) or days 10–20 (therapeutic). Values are the mean and SEM of 12 rats per group (with changes expressed as a percentage of normal controls [assigned a value of 100%]). A and B, Bone mineral density (BMD) and bone mineral content (BMC) of rats treated prophylactically. C and D, BMD and BMC of rats treated therapeutically. * = $P < 0.05$, ** = $P < 0.01$, and *** = $P < 0.001$ versus normal controls (N). See Figure 1 for other definitions.

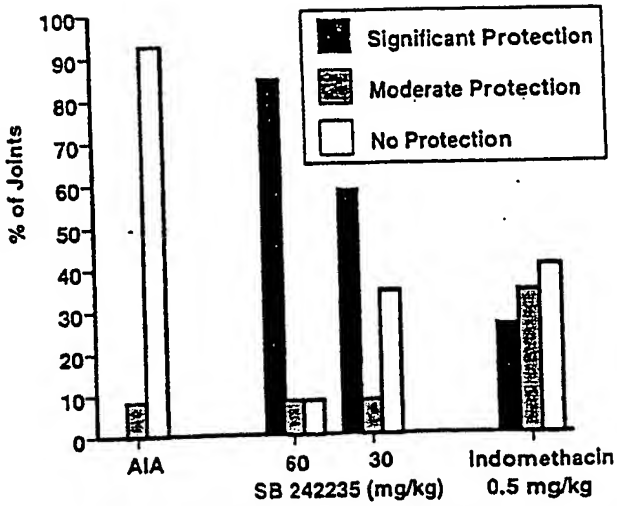

Figure 3. Magnetic resonance imaging of tibiotarsal joints of AIA rats treated therapeutically with SB 242235 (n = 10 at 30 mg/kg; n = 12 at 60 mg/kg). Data are the percentage of joints showing moderate, significant, or no protection by SB 242235 compared with AIA controls (n = 12) or normal controls (n = 6; data not shown). n = 10 AIA rats treated with indomethacin at 0.5 mg/kg. See Figure 1 for definitions.

28% ($P < 0.05$) normalization of BMC, respectively, at those doses (Figures 2A and B).

Following therapeutic treatment, in which animals were dosed starting on day 10 following adjuvant injection and then dosed daily until day 20, there was also a significant normalization of BMD and BMC. There was 53% ($P < 0.001$) and 32% ($P < 0.001$) normalization of BMD at the 60 mg/kg and 30 mg/kg doses, respectively, and a 50% ($P < 0.001$) and 33% ($P < 0.01$) normalization of BMC, respectively, at these doses (Figures 2C and D).

Magnetic resonance imaging. The morphologic changes in the joint architecture of AIA rats were assessed by MRI and compared with those in normal (non-AIA) control rats and in AIA rats treated therapeutically with SB 242235. Ex vivo MR images were obtained in the intact left and right tibiotarsal joints from normal, non-AIA rats (n = 6), AIA control rats (n = 12), and AIA rats treated with SB 242235 (30 mg/kg, n = 10; 60 mg/kg, n = 12) or with indomethacin (0.5 mg/kg, n = 10). The images were ranked as showing either significant protection (no change from control), moderate protection, or no protection observed (similar to AIA controls). SB 242235 demonstrated a dose-related efficacy, with 60% of the joints being protected at 30 mg/kg and 80% being protected at 60 mg/kg (Figure 3). In comparison, in the indomethacin-treated group, <30% of the joints were protected.

Figure 4 shows images of joints from 4 rats from the control, non-AIA group, from the AIA control group, and from the AIA rats treated with SB 242235. The joints from the normal rats (Figure 4A) exhibited intact joint architecture. The distal tibia, fibula, and talus were well defined and there was no edema. The joints from the AIA control group (Figure 4B) exhibited

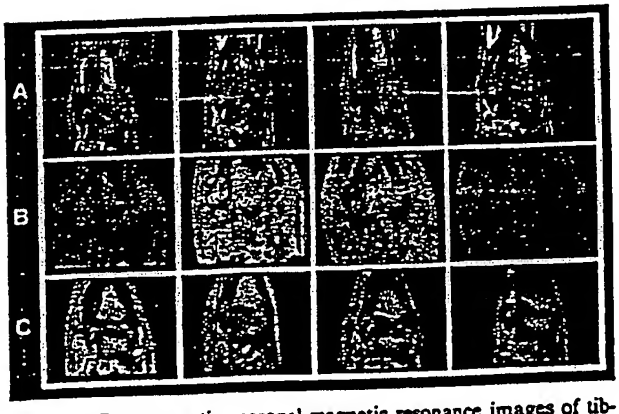

Figure 4. Representative coronal magnetic resonance images of tibiotarsal joints from A, normal, non-AIA rats; B, rats with AIA; and C, rats with AIA treated with SB 242235 at 60 mg/kg. See Figure 1 for definitions.

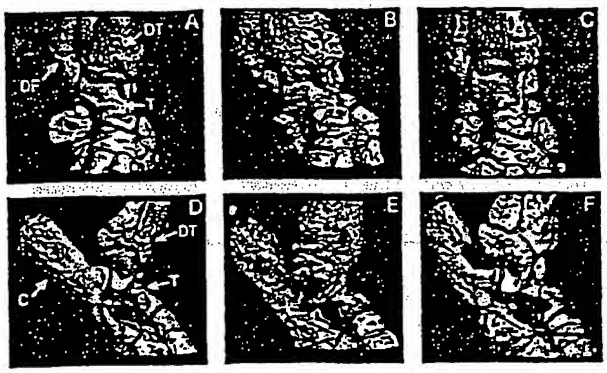

Figure 5. Micro–computed tomography views (coronal and sagittal) of rat tibiotarsal joints rendered in representative 3-dimensional images. A–C, Coronal views of a tibiotarsal joint from a normal, non-AIA rat, an AIA control rat, and an AIA rat treated therapeutically with SB 242235 (60 mg/kg), respectively. The distal tibia (DT), distal fibula (DF), and the talus (T) can be clearly visualized in the images. Significant bone-related damage can be seen in the image of the joint from the AIA control rat as compared with the joint from the normal rat, and significant protection is apparent with SB 242235. D–F, Sagittal views of the same joints as those shown in A–C. Sagittal images afford clear visualization of the calcaneus (C), where a significant amount of destruction has taken place. Again, significant protection is afforded by treatment with SB 242235. See Figure 1 for other definitions.

significant damage as well as swelling, and there was a marked loss in cortical as well as trabecular bone. The joints from the SB 242235–treated group (Figure 4C) exhibited significant inhibition of damage, and closely resembled the joints from the normal, non-AIA controls.

Micro-CT. The micro-CT images afforded a vivid, nondestructive visualization of the bone changes that occurred over the entire tibiotarsal joint. Coronal and sagittal views of the joints are shown in Figure 5. Images of a normal rat joint (Figures 5A and D) showed intact joint architecture as well as normal bone surfaces. The various bones that constitute the joint, namely, the distal tibia/fibula, talus, and the calcaneus, were clearly resolved. The joint from the AIA control rat (Figures 5B and E) showed marked erosion of several bone surfaces, especially at the junction of the distal tibia and fibula and also along the length of the calcaneus. Degenerative changes were also visible on the talus. The images of the joint from an AIA rat treated with SB 242235 (Figures 5C and F) showed the protective effects of the compound in inhibiting the degenerative changes. Isolated regions of bone erosion could be visualized, but the integrity of the joint architecture was clearly preserved.

Histology. For histologic evaluation, randomly selected limbs from the controls and treated groups of rats were sectioned through the tibiotarsal and tarsotarsal joints and examined for pathologic changes to the soft and connective tissues. Photomicrographs of a joint from a normal rat, a rat challenged with adjuvant and then treated with vehicle (AIA control), and from AIA

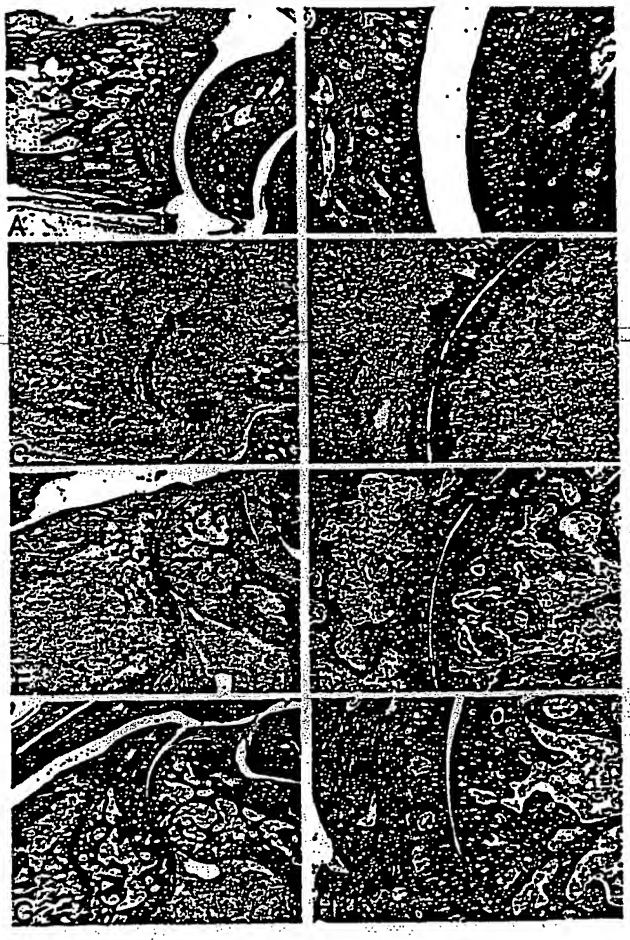

Figure 6. Photomicrographs of rat tibiotarsal joints. A and B, A normal tibiotarsal joint from a non-AIA rat. Articular cartilage is stained with Safranin O (pink), and other tissues are stained blue/green. The articulation of the distal tibia and the proximal tarsus runs vertically through the center of the image. Note the normal joint architecture. C and D, Coronal section of a tibiotarsal joint from a vehicle-treated control AIA rat. E and F, A tibiotarsal joint from an AIA rat administered 0.5 mg/kg/day indomethacin on days 10–20. Compared with the vehicle-treated AIA joint, treatment with indomethacin has limited the severity of the joint destruction. Numerous osteoclasts are evident on the subchondral bone surfaces. G and H, Coronal section of a tibiotarsal joint from an AIA rat administered 60 mg/kg/day SB 242235 therapeutically on days 10–20. Note that compared with the joint from the AIA control rat, joint integrity has been significantly maintained with SB 242235. See Figure 1 for definitions.

rats treated with either indomethacin or SB 242235 are shown in Figure 6. Joint architecture of a normal joint is shown in Figures 6A and B. In the AIA control joint (Figures 6C and D), all of the original bone and marrow had been replaced by granulation tissue and newly formed woven bone. Remnants of articular cartilage were evident and the former joint space had been infiltrated with granulation tissue. A representative joint from an AIA rat treated with indomethacin is shown in Figures 6E and F. When compared with the vehicle-treated joints, all joints examined from the indomethacin-treated group demonstrated some protection of joint integrity. Bone destruction and the replacement of marrow with granulation remained extensive throughout the tibia and tarsus. However, loss of proteoglycan from the articular cartilage was attenuated. A tibiotarsal joint from an AIA rat treated therapeutically with SB 242235 is shown in Figures 6G and H. In all of the joints examined from the rats administered SB 242235, there was a clear protective effect on the joint integrity. Treatment resulted in protection of the joint space, articular surfaces, proteoglycan loss, and subchondral bone architecture.

Serum IL-6. IL-6 has been shown to be increased markedly in different biologic fluids in patients with autoimmune disease, particularly those with RA (32–34), and the level in various inflammatory compartments appears to be a sensitive marker of disease activity. After therapeutic administration of SB 242235, there was a significant inhibition of this cytokine at the 60 mg/kg dose, but not at the lower doses (Figure 7).

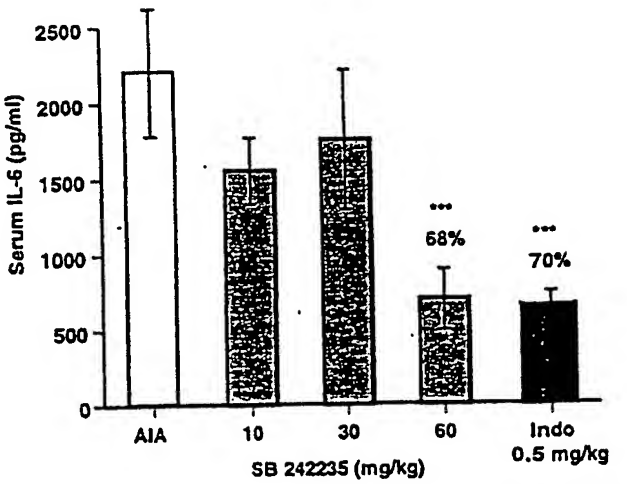

Figure 7. Inhibition of serum levels of interleukin-6 (IL-6) in AIA rats treated with SB 242235. Rats were administered SB 242235 orally from day 10 to day 20. Serum IL-6 levels were measured on day 21. Values are the mean ± SEM of 12 animals per group (with inhibition expressed as a percentage of AIA controls). *** = $P < 0.001$ versus AIA controls. See Figure 1 for other definitions.

DISCUSSION

The p38α MAP kinase, a member of the MAP kinase family of serine-threonine protein kinases, was first identified as a protein kinase activated in mouse macrophages in response to LPS (16). Subsequently, CSBP2, the human ortholog of p38, was identified as the molecular target of the pyridinyl imidazole class of antiinflammatory agents. The inhibition of p38 MAP kinase and subsequent inhibition of the synthesis of a number of important proinflammatory proteins has been identified as the primary mechanism contributing to the antiinflammatory activity of these compounds. Examples of inhibited cytokines are IL-1 and TNFα, IL-6, IL-8, and granulocyte–macrophage colony-stimulating factor, but not granulocyte colony-stimulating factor or IL-1 receptor antagonist (12,13,25,35).

The p38 pathway and the closely related JNK and ERK kinase signaling pathways are commonly associated with the early stages of host response to injury and infection, and their potential role in various pathologic conditions has made them targets for therapeutic intervention. The p38 MAP kinase signaling pathway is activated by a variety of stressful stimuli, including heat, ultraviolet light, LPS, inflammatory cytokines (IL-1 and TNF), and high osmolarity (16). When activated, p38 phosphorylates a number of down-stream substrates, which include kinases (MAPKAP K2 and K3, MST, MSK, PRAK) and transcription factors (CHOP, MEF2, CREB, and ATF2), and subsequently regulates the synthesis of several cytokines believed to be responsible for inflammation and tissue destruction in diseases such as RA. The pyridinyl imidazoles, by virtue of their inhibition of p38 kinase, have been shown to inhibit cytokine biosynthesis at both the transcriptional and translational level; however, at present, comprehensive mechanisms detailing all of the steps involved in cytokine regulation are unknown.

In general, the pyridinyl imidazole class inhibits the 2 splice forms of p38 (CSBP1 and CSBP2) as well as another homolog of p38 kinase, p38β2 (36), but not the closely related p38γ or p38δ, JNK, and ERK protein kinases. Although SB 203580 inhibits JNK2β1 and c-raf (28), a large number of other serine-threonine or tyrosine protein kinases are unaffected (36). Similar to SB 203580, SB 242235 inhibits CSBP/p38α MAP kinase

(IC_{50} 0.1 μM) and p38β2 MAP kinase (IC_{50} 1 μM), but not p38γ or p38δ MAP kinases. In contrast to SB 203580, SB 242235 does not inhibit JNK2β1 and ERK2 (Lee JC et al: unpublished observations). The mechanism of action of these p38 inhibitors is to compete with ATP by forming a 4-fluorophenyl binding pocket behind, and orthogonal to, the site normally occupied by the adenine ring of ATP (37).

Our previous studies with another member of this family of p38 inhibitors, SB 203580, showed it to be an effective antiinflammatory agent in the AIA rat when administered prophylactically (20), and also demonstrated that the antiinflammatory and disease-modifying activity was unlikely to be due to immunosuppression since little to no suppression was observed in mouse models of immune function (20,21). However, the evaluation of its activity when administered therapeutically, a more relevant model for RA, was not performed. In addition, although improvement in bone density by DEXA was observed, closer examination of joint integrity using imaging technologies such as MRI and micro-CT was also not performed.

In the studies described in the present report, we have shown that SB 242235 is a potent inhibitor of LPS-induced TNFα production in the plasma of normal rats. The optimal pretreatment time was 1–2 hours, although highly significant activity was seen 4 hours postdosing. SB 242235 demonstrated excellent inhibitory activity with regard to TNFα production after oral administration of a range of doses. The ED_{50} for inhibition of LPS-stimulated TNFα was 3.99 mg/kg given orally. The compound also inhibited LPS-induced TNFα production in the mouse with a potency similar to that in the rat (data not shown).

Antiinflammatory activity was observed in AIA in Lewis rats when SB 242235 was administered orally at 10, 30, and 60 mg/kg either prophylactically or therapeutically. There was a 73% inhibition of paw edema and a 53% normalization of BMD at the 60 mg/kg therapeutic dose, and 51% inhibition of paw edema with 32% normalization of BMD at the 30 mg/kg dose. This is significant activity for a small molecule cytokine inhibitor in such an aggressive arthritis model. Additional evidence for disease-modifying activity for the compound was provided by the obvious improvement observed in the MR images, in which 80% of the joints were significantly protected by treatment at the 60 mg/kg dose. In addition, micro-CT technology, which is uniquely suited for comprehensive 3-dimensional analysis of bone-related changes in the AIA rat, showed clear protection with SB 242235. This was particularly apparent in the distal tibia and the calcaneus. This is the first report describing the utility of this technology to evaluate joint integrity in the AIA rat. Histologic evaluation of representative joints showed that treatment resulted in protection of the joint space, the articular surfaces, and the subchondral bone structure, although synovial inflammation was still apparent. SB 242235 treatment at the 60 mg/kg dose also reduced circulating levels of IL-6. Previous studies in vitro have shown inhibition of IL-6 production from LPS-stimulated human monocytes, with an IC_{50} of 1.2 μM (Lee JC et al: unpublished observations).

The protection afforded by SB 242235 is considerable when compared with the nonsteroidal antiinflammatory drug (NSAID) indomethacin. Although indomethacin does have some bone-protective effects in the AIA rat, they are not significant. There was no improvement in BMD measurements compared with the arthritic controls following therapeutic treatment with indomethacin, and histologic evaluation indicated that, whereas protection of the cartilage was apparent, beneficial effects on bone were minimal. In addition, whereas NSAIDs have antiinflammatory effects in RA patients, they do not protect the bone from damage. Of particular relevance is the fact that indomethacin does not inhibit TNFα production in vitro or in vivo (Griswold D: unpublished observations), whereas this is a hallmark of CSAID activity. Inhibition of TNFα by these compounds makes them very attractive candidates for treatment of RA, particularly since inhibition of TNFα using monoclonal antibodies to the cytokine or its soluble receptor are clinically efficacious in RA (14,15).

The profile of activity described here for SB 242235 suggests strongly that orally active, small molecular weight cytokine inhibitors could provide significant benefit in the treatment of chronic inflammatory diseases such as RA.

REFERENCES

1. Lee JC, Badger AM, Griswold DE, Dunnington D, Truneh A, Votta B, et al. Bicyclic imidazoles as a novel class of cytokine biosynthesis inhibitors. Ann N Y Acad Sci 1993;696:149–70.
2. Griswold DE, Hillegass LM, Meunier PC, DiMartino MJ, Hanna N. Effect of inhibitors of eicosanoid metabolism in murine collagen-induced arthritis. Arthritis Rheum 1988;31:1406–12.
3. Marshall PJ, Griswold DW, Breton J, Webb EF, Hillegass LM, Sarau HM, et al. Pharmacology of the pyrroloimidazole, SK&F 105809. Biochem Pharmacol 1991;42:313–24.
4. Griswold DE, Hillegass LM, Breton JJ, Esser KM, Adams JL. In vivo differentiation of classical non-steroidal antiinflammatory drugs (NSAID) from cytokine suppressive antiinflammatory drugs (CSAID) and other pharmacological classes using mouse tumor

necrosis factor alpha (TNFα) production. Drugs Clin Res XIX 1993;6:243–8.
5. Boehm JC, Smietana JM, Sorenson ME, Garigipati RS, Gallagher TF, Sheldrake PL, et al. 1-substituted 4-aryl-5-pyridinylimidazoles: a new class of cytokine suppressive drugs with low 5-lipoxygenase and cyclooxygenase inhibitory potency. J Med Chem 1993;39: 3929–37.
6. Dinarello CA. Inflammatory cytokines: interleukin-1 and tumor necrosis factor as effector molecules in autoimmune diseases. Curr Opin Immunol 1991;3:941–8.
7. Arend WP, Dayer J-M. Cytokines and cytokine inhibitors or antagonists in rheumatoid arthritis. Arthritis Rheum 1990;33: 305–15.
8. Dayer JM, Demczuk S. Cytokines and other mediators in rheumatoid arthritis. Springer Semin Immunopathol 1984;7:387–413.
9. Cochran FC, Selph J, Sherman P. Insights into the role of nitric oxide in inflammatory arthritis. Med Res Rev 1966;16:547–63.
10. Werb Z, Alexander CM. Proteinases and matrix degradation. In: Kelley WN, Harris ED Jr, Ruddy S, Sledge CB, editors. Textbook of rheumatology. 4th ed. Philadelphia: WB Saunders; 1993. p. 248–68.
11. Roodman GD. Role of cytokines in the regulation of bone resorption. Calcif Tissue Int 1993;53:S94–8.
12. Lee JC, Laydon JT, McDonnell PC, Gallagher TF, Kumar S, Green D, et al. A protein kinase involved in the regulation of inflammatory cytokine biosynthesis. Nature 1994;372:739–46.
13. Gallagher TF, Fier-Thompson SM, Garigipati RS, Sorenson ME, Smietana JM, Lee D, et al. 2,4,5-triarylimidazole inhibitors of IL-1 biosynthesis. Bioorg Med Chem Lett 1995;5:1171–6.
14. Elliott MJ, Maini RN. New directions for biological therapy in rheumatoid arthritis. Int Arch Allergy Immunol 1994;104:112–5.
15. Moreland LW, Heck LW Jr, Koopman WJ. Biologic agents for treating rheumatoid arthritis: concepts and progress. Arthritis Rheum 1997;40:397–409.
16. Han J, Lee JD, Bibb SL, Ulevitch RJ. A MAP kinase targeted by endotoxin and in mammalian cells. Science 1994;265:808–11.
17. Rouse J, Cohen P, Trigon S, Morange M, Alonso-Llamazares A, Zamanillo D, et al. Identification of a novel protein kinase cascade stimulated by chemical stress and heat shock which activates MAP kinase-activated protein MAPKAP kinase-2 and induces phosphorylation of the small heat shock proteins. Cell 1994;78: 1027–37.
18. Freshney NW, Rawlinson L, Guesdon F, Jones E, Cowley S, Hsuan J, et al. Interleukin-1 activates a novel protein kinase cascade that results in the phosphorylation of Hsp27. Cell 1994; 78:1039–49.
19. Lee JC, Young PR. Role of CSBP/p38/RK stress response kinase in LPS and cytokine signaling mechanisms. J Leukoc Biol 1996; 59:152–7.
20. Badger AM, Bradbeer JN, Votta B, Lee JC, Adams JL, Griswold DE. Pharmacological profile of SB 203580, a selective inhibitor of cytokine suppressive binding protein/p38 kinase, in animal models of arthritis, bone resorption, endotoxin shock and immune function. J Pharmacol Exp Ther 1996;279:1453–61.
21. Reddy MP, Webb EF, Cassatt D, Maley D, Lee JC, Griswold DE, et al. Pyridinyl imidazoles inhibit the inflammatory phase of delayed type hypersensitivity reactions without affecting T-dependent immune responses. Int J Immunopharmacol 1994;16:795–804.
22. Badger AM, Olivera D, Talmadge JE, Hanna N. Protective effect of SK&F 86002, a novel dual inhibitor of arachidonic acid metabolism, in murine models of endotoxin shock: inhibition of tumor necrosis factor as a possible mechanism of action. Circ Shock 1989;27:51–61.
23. Olivera DL, Esser KM, Lee JC, Greig RG, Badger AM. Beneficial effects of SK&F 105809, a novel cytokine-suppressive agent, in murine models of endotoxin shock. Circ Shock 1992;37:301–6.
24. Badger AM, Cook MN, Lark MW, Newman-Tarr TM, Swift BA, Nelson AH, et al. SB 203580 inhibits p38 mitogen-activated protein kinase, nitric oxide production, and inducible nitric oxide synthase in bovine cartilage-derived chondrocytes. J Immunol 1998;161:467–73.
25. Lee JC, Kassis S, Kumar S, Badger A, Adams JL. p38 mitogen-activated protein kinase inhibitors—mechanisms and therapeutic potentials. Pharmacol Ther 1999;82:389–97.
26. Young PR, McLaughlin MM, Jumar S, Kassis S, Doyle ML, McNulty D, et al. Pyridinyl imidazole inhibitors of p38 mitogen-activated protein kinase bind in the ATP site. J Biol Chem 1997;272:12116–21.
27. Kumar S, McDonnell PC, Gum RJ, Hand AT, Lee JC, Young PR. Novel homologues of CSBP/p38 MAP kinase: activation, substrate specificity and sensitivity to inhibition by pyridinyl imidazoles. Biochem Biophys Res Commun 1997;235:533–8.
28. De Laszlo SE, Visco D, Agarwal L, Chang L, Chin J, Croft G, et al. Pyrroles and other heterocycles as inhibitors of p38 kinase. Bioorg Med Chem Lett 1998;8:2689–94.
29. Borsch-Haubold AG, Pasquet S, Watson SP. Direct inhibition of cyclooxygenase-1 and -2 by the kinase inhibitors SB 203580 and PD 98059. J Biol Chem 1998;273:28766–72.
30. Webb EF, Griswold DE. Microprocessor-assisted plethysmograph for the measurement of mouse paw volume. J Pharmacol Methods 1984;12:149–53.
31. Aarden LA, Lansdorp P, de Groot E. A growth factor for B-cell hybridomas produced by human monocytes. Lymphokines 1985; 10:175–85.
32. Houssiau FA, Devogelaer J-P, van Damme J, Nagant de Deuxchaisnes C, van Snick J. Interleukin-6 in synovial fluid and serum of patients with rheumatoid arthritis and other inflammatory arthritides. Arthritis Rheum 1988;31:784–8.
33. Swaak AJG, Rooyen A, van Nieuwenhuis E, Aarden LA. Interleukin-6 (IL-6) in synovial fluid and serum of patients with rheumatic diseases. Scand J Rheumatol 1988;17:469–74.
34. Hirano T, Matsuda T, Turner M. Excessive production of IL-6/B cell stimulatory factor-2 in rheumatoid arthritis. Eur J Immunol 1988;18:1797–802.
35. Lee JC, Votta B, Dalton BJ, Griswold DE, Bender PE, Hanna N. Inhibition of human monocyte IL-1 production by SK&F 86002. Int J Immunother 1990;VI:1–12.
36. Cuenda A, Rouse J, Doza YN, Meier R, Cohen P, Gallagher TF, et al. SB 203580 is a specific inhibitor of a MAP kinase homologue which is stimulated by cellular stresses and interleukin-1. FEBS Lett 1995;364:229–33.
37. Wang ZL, Canagarajah BJ, Boehm JC, Kassis S, Cobb MH, Young PR, et al. Structural basis of inhibitor selectivity in MAP kinases. Structure 1998;6:1117–28.

Exhibit 4

GASTROENTEROLOGY 2002;122:7–14

RAPID COMMUNICATIONS

Inhibition of Stress-Activated MAP Kinases Induces Clinical Improvement in Moderate to Severe Crohn's Disease

DAAN HOMMES,* BERNT VAN DEN BLINK,† TERRY PLASSE,§ JOEP BARTELSMAN,* CUIPING XU,† BRET MACPHERSON,§ GUIDO TYTGAT,* MAIKEL PEPPELENBOSCH,† and SANDER VAN DEVENTER*

*Department of Gastroenterology and Hepatology, †Laboratory of Experimental Internal Medicine, Academic Medical Center, University of Amsterdam, Amsterdam; the Netherlands, §Cytokine PharmaSciences, Inc., King of Prussia, Pennsylvania

Background & Aims: We investigated if inhibition of mitogen-activated protein kinases (MAPKs) was beneficial in Crohn's disease. *Methods:* Inhibition of JNK and p38 MAPK activation with CNI-1493, a guanylhydrazone, was tested in vitro. Twelve patients with severe Crohn's disease (mean baseline, CDAI 380) were randomly assigned to receive either 8 or 25 mg/m^2 CNI-1493 daily for 12 days. Clinical endpoints included safety, Crohn's Disease Activity Index (CDAI), Inflammatory Bowel Disease Questionnaire, and the Crohn's Disease Endoscopic Index of Severity. *Results:* Colonic biopsies displayed enhanced JNK and p38 MAPK activation. CNI-1493 inhibition of both JNK and p38 phosphorylation was observed in vitro. Treatment resulted in diminished JNK phosphorylation and tumor necrosis factor production as well as significant clinical benefit and rapid endoscopic ulcer healing. No serious adverse events were noted. A CDAI decrease of 120 at week 4 (P = 0.005) and 146.5 at week 8 (P = 0.005) was observed. A clinical response was seen in 67% of patients at 4 weeks and 58% at 8 weeks. Clinical remission was observed in 25% of patients at week 4 and 42% at week 8. Endoscopic improvement occurred in all but 1 patient. Response was seen in 3 of 6 infliximab failures, 2 of whom showed remission. Fistulae healing occurred in 4 of 5 patients, and steroids were tapered in 89% of patients. *Conclusions:* Inflammatory MAPKs are critically involved in the pathogenesis of Crohn's disease and their inhibition provides a novel therapeutic strategy.

Crohn's disease (CD) is a chronic inflammatory disorder of the gastrointestinal tract, which is thought to arise in genetically susceptible hosts caused by an inappropriate immunologic response against the microflora of the gut. The immune defect is unclear; however, recently a gene for CD was identified encoding NOD2, a protein involved in the recognition of microbes and signalling events leading to an immune response.[1,2] This finding directly links the mucosal immune response to enteric bacteria and the development of disease.

Tumor necrosis factor (TNF) plays a central role in the initiation and amplification of the inflammatory reaction observed in CD.[3] Monoclonal antibodies against TNF have been proven efficacious in both inducing clinical remission and endoscopic healing.[4,5] An alternative means of inhibiting TNF action is by inhibition of mitogen-activated protein kinases (MAPKs), signal-transducing enzymes that regulate important cellular processes like gene expression and cell proliferation.[6] Targeting the p38 MAPK signalling cascade led to reduction of lipopolysaccharide (LPS)-induced TNF production in rodents.[7] Hence, MAPK inhibition has been suggested as an anti-inflammatory strategy.[8] However, evidence that these proteins are required for the pathogenesis of inflammatory disease and that MAPK inhibition constitutes a therapeutic target is lacking.

An interesting candidate would be CNI-1493, a guanylhydrazone that inhibits the phosphorylation of both p38 MAP kinase and JNK.[8,9] CNI-1493 has been shown to inhibit macrophage activation and the production of several proinflammatory cytokines (TNF-α, IL-1, IL-6, MIP-1α, MIP-1β) and nitric oxide.[10,11] Furthermore, it was shown to be protective in a number of preclinical models, including endotoxic shock,[10,12] acute respiratory distress syndrome,[13,14] sepsis,[10] pancreatitis,[13,14] experimental allergic encephalomyelitis,[15] stroke,[16] rheumatoid arthritis, and dextran sulfate sodium colitis (data on file).

Abbreviations used in this paper: CDEIS, Crohn's Disease Endoscopic Index of Severity; CRP, C-reactive protein; HRP, horseradish peroxidase; IBDQ, Inflammatory Bowel Disease Questionnaire; LPS, lipopolysaccharide; MAPK, mitogen-activated protein kinase; PBMCs, peripheral blood mononuclear cell; TNF, tumor necrosis factor.

0016-5085/02/$35.00
doi:10.1053/gast.2002.30770

The goal of the current study was to investigate if MAP kinase activation was present in patients with CD, and to examine if inhibition of MAP kinase activation was a safe and effective novel therapeutic approach.

Materials and Methods

Effect of CNI-1493 on JNK and p38 MAPK Activation In Vitro

Peripheral blood mononuclear cells (PBMCs) obtained from healthy volunteers were stimulated with LPS for 15 minutes in the presence of increasing concentrations of CNI-1493 or diluent. Analysis of MAPK phosphorylation was performed using Western blotting and phosphospecific antibodies (Cell Signalling, Beverly, MA).

Patients

Twelve patients were enrolled in a doubled-blinded fashion to receive either 8 or 25 mg/m^2 of CNI-1493 intravenously once daily for 12 consecutive days. Patients were required to suffer from moderate to severe CD, i.e., a Crohn's Disease Activity Index (CDAI)[17] of $\geq$ 220 and $\leq$ 450; to have a CD history of at least 3 months duration, with colitis, ileitis, or ileocolitis confirmed by radiography, endoscopy, and histology. Furthermore, patients had to be on a stable dose of corticosteroids, aminosalicylates, or antibiotics at least 4 weeks before inclusion. Patients receiving methotrexate, 6-mercaptopurine, or azathioprine should have had stable dosages for at least 8 weeks before inclusion. Patients with extensive bowel resection (e.g., >100 cm of small bowel, proctocolectomy, or colectomy with ileorectal anastomosis) or fixed stenosis were excluded.

The primary endpoints were safety evaluations, as determined by occurrence of (1) adverse events and (2) stopping medication because of adverse events. The secondary endpoints were efficacy evaluations: (1) occurrence of a clinical response as defined by achieving a reduction of CDAI of $\geq$25% and $\geq$70 points as compared with baseline, occurring at least once after the start of treatment, and (2) occurrence of a clinical remission, defined as a reduction of CDAI to below 150, occurring at least once after the start of treatment. Safety and tolerability was evaluated by clinical assessment of adverse events and changes in standard hematologic and biochemical laboratory parameters. Other clinical assessments of efficacy included the Inflammatory Bowel Disease Questionnaire (IBDQ),[18] the Crohn's Disease Endoscopic Index of Severity (CDEIS),[19] and C-reactive protein (CRP) levels. Increasing IBDQ scores indicate improvement, values above 170 are considered normal. The CDEIS is a score, which is based on the presence of deep or superficial ulceration, the proportion of ulcerated surface, and the presence of ulcerated or nonulcerated stenosis in the terminal ileum and 4 different segments of the colon. At every visit, enterocutaneous or rectovaginal fistulas were examined to determine whether a fistula was present, open or closed. An enterocutaneous fistula was considered to be closed when it was no longer draining despite gentle compression. Rectovaginal fistulas were considered to be closed, based on either physical examination or absence of relevant symptoms (passage of rectal material or flatus from vagina). Written informed consent has been obtained from all patients, and the study has been approved by the Ethical Committee of the Academic Medical Center, Amsterdam.

Immunohistochemistry

Mucosal biopsy specimens of the intestine were obtained during videoendoscopy at the time of screening and at the end of week 4 for 6 patients. At both occasions biopsies were taken from most affected regions of inflammation, and subsequently formalin fixed and paraffin embedded. If patients were in remission at week 4, biopsies were taken form areas with apparent residual inflammatory changes. As a control, histological normal biopsies were obtained from non-CD patients. Paraffin sections (4 μm) were dewaxed and rehydrated in graded alcohols. Endogenous peroxidase activity was quenched with 1.5% H_2O_2 in phosphate-buffered saline (PBS) for 30 minutes at room temperature. Nonspecific staining was blocked with 10 mmol/L Tris, 5 mmol/L EDTA, 0.15 mol/L NaCl, 0.25% gelatin, 0.05% (vol/vol) Tween 20, pH 8.0, for 30 minutes at room temperature. After a washing with PBS the after primary Abs were applied: a mouse monoclonal anti-human antibody to phosphorylated JNK (Santa Cruz, CA; 1:400), a mouse monoclonal anti-human antibody to phosphorylated p38 MAPK (Cell Signalling, Beverly, MA; 1:25) or a mouse monoclonal immunoglobulin (Ig) M Ab against TNF-α, clone 4C6-H6 (Instruchemie, Hilversum, the Netherlands; 1:25). Sections were stored overnight at 4°C. The following day sections were washed in PBS and incubated with a secondary biotinylated goat anti-mouse Ig Ab (DAKO, Glostrup, Denmark; 1:200) for 1 hour at room temperature and washed with PBS. Detection was performed either with horseradish peroxidase (HRP) as an enzyme. Sections were incubated with HRP conjugated ABcomplex (DAKO) for 60 minutes and peroxidase activity was detected with diaminobenzidine (fast DAB, Sigma, St. Louis, MO). Sections were briefly counterstained with hematoxylin when appropriate, dehydrated in graded alcohols, and mounted. Controls consisted of omitting the primary and secondary Ab and use of an appropriate Ig control.

MAPKs Activation and TNF Immunohistochemistry

To assess the amount of TNF and the activity of JNK and p38 in situ in the human colon, screening and week 4 specimens available from 6 patients and controls were stained for TNF-α and phosphorylated JNK/p38. No counterstaining was applied to these sections to visualize positive cell more clearly. Three pictures of each section were taken at ×400 magnification, and positive cells were counted, blind to treatment and day of endoscopy, in each microscope field with the use of an image analysis program (EFM Software, Rotterdam, the Netherlands). Pictures appeared randomly on a computer

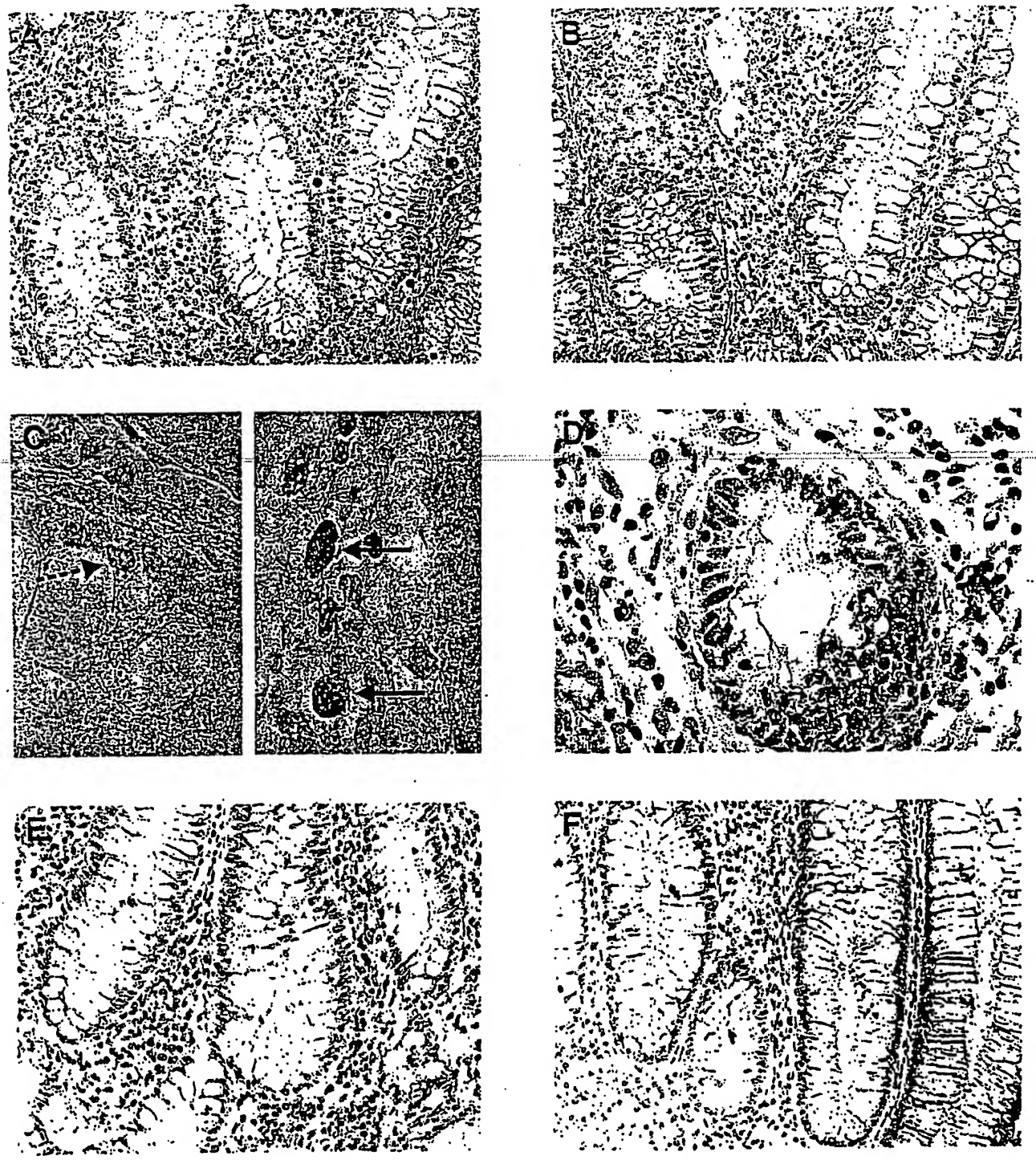

Figure 1. Involvement of MAPKs in CD. Patients received 12 days of intravenous infusions with CNI-1493 (8 or 25 mg/m^2). Paired biopsies were obtained at screening (day 1) and at week 4 for 6 patients. Sections were stained for phospho-JNK, phospho-p38 MAPK, and TNF-α. (*A*) Many inflammatory cells stained positive for phospho-JNK (original magnification, 200×). (*B*) After treatment with the MAPK inhibitor, a reduced number of cells stain positive for phospho-JNK (original magnification, 200×). (*C*) Inflammatory cell staining positive for phospho-JNK were IELs (*dotted arrow*, CD3+) or LP macrophages (*closed arrows*, CD68+) (1000×). (*D*) Activated p38 MAPK was observed in migrating neutrophils localized in crypt abscesses (1000×). The number of TNF staining cells in the lamina propria in biopsy specimens taken (*E*) before CNI-1493 treatment (400×) was significantly higher than in specimens taken (*F*) after treatment (400×).

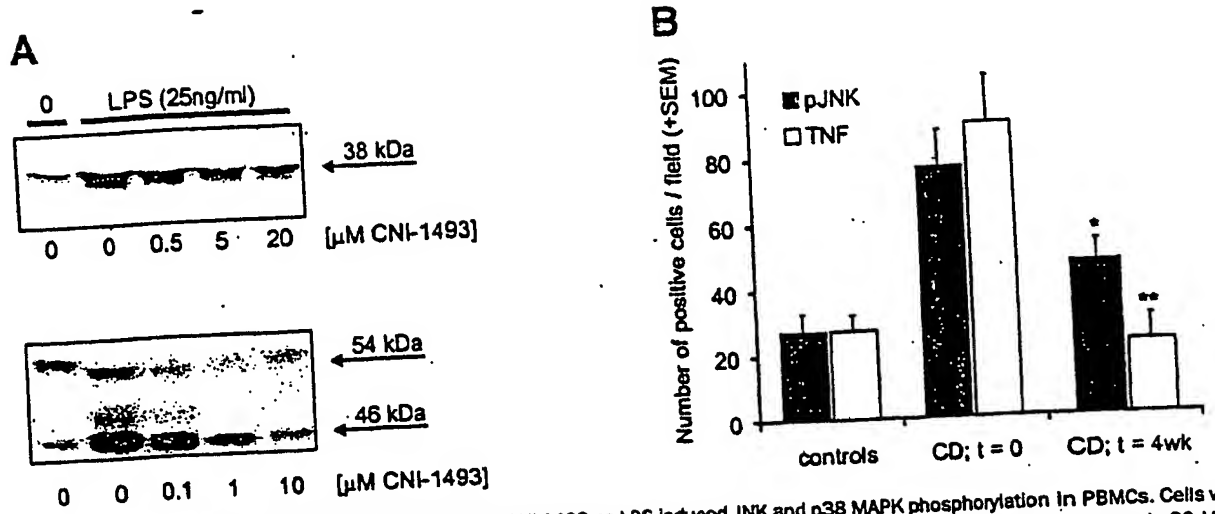

Figure 2. Effect of CNI-1493 in vitro and in CD. (*A*) Effect of CNI-1493 on LPS-induced JNK and p38 MAPK phosphorylation in PBMCs. Cells were stimulated with LPS (25 ng/mL) for 15 minutes or solvent control (0) in the presence of various concentrations CNI-1493. JNK and p38 MAPK activation was assessed with Western blotting using antibodies against phosphorylated JNK (against both 46- and 54-kilodalton isoforms, 1:1000) and p38 MAPK (38 kilodalton, 1:1000). (*B*) CNI-1493 inhibits the number of phospho-JNK and TNF-positive cells in CD. Patients received 12 days of intravenous infusions with CNI-1493 (8 or 25 mg/m^2). Paired biopsies were obtained at screening (day 1) and at week 4 for 6 patients. Sections were stained for phospho-JNK or TNF-α without applying hematoxylin counterstain. Three pictures of each section were taken at original magnification 400×, and positive cells were counted, blind to treatment and day of endoscopy, in each microscopic field with the use of an image analysis program. As a control, 8 histological normal biopsies were obtained from non-CD patients, and were counted in the same fashion. Differences between pretreatment and posttreatment reached statistical significance (JNK, $*P = 0.01$; TNF, $**P < 0.01$).

monitor and all intensely staining cells were marked positive by an observer, counted, and stored by the image analysis program for later data analysis.

Statistical Analysis

All measures of efficacy were evaluated by intention-to-treat analysis. Change from baseline within groups was analyzed by use of the Wilcoxon signed rank test. Change from baseline between groups at a specified time point was analyzed by use of the Wilcoxon rank-sum test. Comparisons between groups over the course of study were evaluated by use of repeated measures analysis of variance. Last observation carried forward analysis was implemented for missing data. The correlation between CDAI and CDEIS change from baseline was analyzed by use of the Pearson correlation coefficient. Baseline categorical variables were analyzed with Fisher exact test and continuous variables with the Wilcoxon rank-sum test.

Results

JNK and p38 MAPK Are Activated in Active CD

Although MAPKs have been implicated in regulation of inflammatory responses, actual involvement of MAPKs in chronic inflammatory disease has not yet been demonstrated. Recently, Waetzig et al.[20] reported increased activity of stress-activated MAPKs in CD. In colonic biopsies taken from patients with active CD, we show that activation of JNK and p38 MAPK is markedly present (Figure 1*A* and *D*). Activated p38 MAPK was observed in infiltrating neutrophils (Figure 1*D*) and in epithelial cells (not shown). Abundant active JNK was observed in inflammatory cells, especially intraepithelial lymphocytes (IELs, CD3$^+$) and lamina propria cells ([LPs] macrophages, CD68$^+$) stained positive (Figure 1*A* and *C*). Quantative comparison to histological normal biopsies showed that the number of phopspho-JNK positive cells was significantly increased (Figure 2*B*). As expected, the number of TNF-α positive cells in the colon mucosa of CD patients was also significantly increased compared with normal controls (Figure 2*B*).

CNI-1493 Is a Potent JNK and p38 MAPK Inhibitor In Vitro

CNI-1493 is reported to inhibit stress-activated MAP kinases in lymphocyte cell lines.[21] To confirm whether this compound exerts similar action in untransformed cells, we stimulated PBMCs with LPS in the presence of increasing concentrations of CNI-1493. CNI-1493 inhibited LPS-induced phosphorylation of both p38 MAPK and JNK in a dose-dependent fashion, although apparently with a higher efficacy for inhibiting JNK (Figure 2*A*). Thus, CNI-1493 effectively inhibits the stress-activated MAPKs in untransformed cells Therefore, we decided to use this inhibitor for elucidating their role in CD.

Safety and Efficacy of CNI-1493 in CD

We included 12 patients with severe CD (Table 1), 8 completed therapy. Two discontinued (after 6 and 9 doses of medication, both receiving 25 mg/m² daily) because of elevated alanine aminotransferase levels; one after 11 doses caused by a catheter-related infection (8 mg/m² daily), and one after 9 doses because of deterioration of CD (25 mg/m² daily). Treatment was generally well tolerated, side effects included phlebitis in 2 patients in each dosing group, and asymptomatic and transient elevation of liver enzymes in 1 patient in the low-dose and 5 patients in the high-dose group (Table 2).

For both dose groups combined, we observed a median change from baseline CDAI of −117.5 at 2 weeks (P = 0.003), −120 at 4 weeks (P = 0.005), −146.5 at 8 weeks (P = 0.005), and −148 at 16 weeks (P = 0.007). Figure 3*A* shows CDAI scores, data are censored at the last observation before any change in concomitant Crohn's therapy or addition of other medication, and the last observation is carried forward. Table 3 summarizes the response rates as well as the remission rates according to the predefined criteria. At 4 weeks from the start of treatment, 25% of patients were in remission, and 67% had responded. At 4 months after the start of treatment, without additional medications, half the patients were in remission and 58% were responders. The response rates in both treatment groups were similar, though the small sample size of each group precludes precise conclusions. Three of 6 patients who did not respond to prior infliximab therapy showed a response after CNI-1493 administration, of whom 2 entered remission. In parallel with the CDAI changes, we observed a median IBDQ increase from baseline of 21.5 at 2 weeks (P = 0.02), 36.5 at 4 weeks (P = 0.01), 43 at 8 weeks (P = 0.007), and 33.5 at 16 weeks (P = 0.002) in both groups combined (Figure 3*B*). CRP levels decreased significantly during the first weeks of treatment (Figure 3*C*). At week 4, 16 days after the end of therapy, endoscopic improvement was observed in all but 1 patient (Figure 3*C* and *D*), with a median change in CDEIS from baseline of −6.5 (P = 0.006).

Five patients suffered from active fistulizing CD, and closure of fistulae was observed in 4 patients during the study period (1 in the 8 mg/m² and 3 in the 25 mg/m² group). At baseline, 9 patients were receiving steroids, 5 used prednisolone (mean, 21 mg; range, 10–40 mg), and 4 used budesonide (all 9 mg). At week 8, steroids had been tapered in 8 patients (89%). In patients receiving prednisolone, the mean reduction was 12.5 mg at week 8; in the budesonide group, the mean reduction was 5 mg. CD-related arthralgia/arthritis was reported in 5 of 12 study patients at baseline, but resolved in all during the study period. We concluded that a 12-day infusion with CNI-1493 was safe and induces significant endoscopic healing and substantial clinical benefit in moderate to severe CD.

Table 1. Patient Characteristics

	8 mg/m²	25 mg/m²
Gender (M/F)	0/6	2/4
Age (yr)[a]	27.5 (19.8–35.6)	44.7 (18.7–54.4)
Duration of disease (yr)	5.7 (0.1–12.0)	13.8 (8.8–31.6)
CDAI[b]	382.5 (288–507)	377.5 (284–440)
IBDQ[c]	103 (50–149)	82.5 (79–132)
CDEIS[d]	14.4 (7.6–25)	12.2 (1.7–24.3)
Prior intestinal resection (N)	1	5
Fistulae	2/6	3/6
Concomitant medication[e]		
Mesalamine	1	3
Corticosteroids	4	5
Azathioprine	4	4
Prior infliximab (N)	3	3

[a]Values expressed as median (range); [b]CDAI; [c]IBDQ; [d]CDEIS; [e]Concomitant Crohn's disease therapy.

Table 2. Adverse Events

Body system/ adverse event	Daily dose, mg/m² 8	25	Body system/ adverse event	Daily dose, mg/m² 8	25
N=	6	6	Any AE possibly/ probably related	6	5
Body general	2	3	Digestive/hepatic	3	5
Abdominal pain	0	1	Alk phos increase	0	3
Asthenia	1	0	Bilirubinemia	1	0
Facial edema	0	1	Nausea	1	1
Flu syndrome	1	1	SGOT increase	1	5
Headache	1	1	SGPT increase	0	5
Cardiovascular	2	2	Stomatitis	0	1
Hematoma	1	0	Nervous	1	0
Phlebitis	2	2	Dizziness	1	0
Hematologic	4	2	Respiratory	1	1
Anemia	2	2	Rhinitis	0	1
Leukopenia	1	1	Skin	2	0
Thrombocytopenia	1	0	Herpes Zoster	1	0
			Maculopapular rash	1	0

CNI-1493 Inhibits JNK Phosphorylation In Vivo

To establish the effects of CNI-1493 treatment on MAPKs in vivo, paired biopsies (available from 6 patients), taken before (day 1) and after (week 4) treatment with CNI-1493 were stained for phospho-JNK and -p38 MAPK. The phospho-p38 MAPK staining was not consistent throughout all biopsies and thus, based on our immunohistochemistry, no assessment could be made of the effectiveness of CNI-1493 in inhibiting p38 MAPK

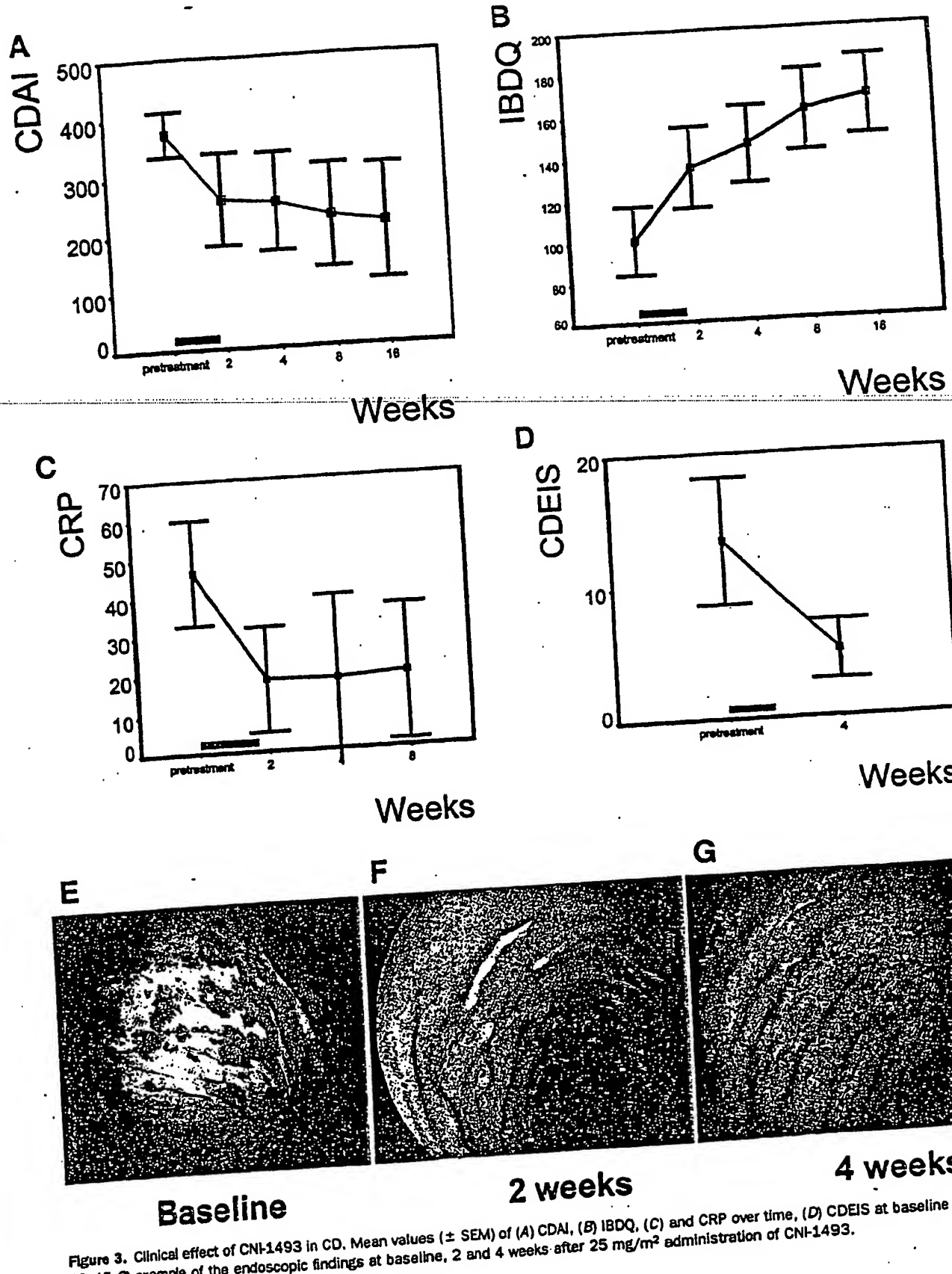

Figure 3. Clinical effect of CNI-1493 in CD. Mean values (± SEM) of (*A*) CDAI, (*B*) IBDQ, (*C*) and CRP over time, (*D*) CDEIS at baseline and da 29; (*E–G*) example of the endoscopic findings at baseline, 2 and 4 weeks after 25 mg/m² administration of CNI-1493.

Table 3. Number of Patients Showing a Response or Remission After Treatment With CNI-1493

Dose group (mg/m²)		Study day 8	15	29	57	112
		Number (%) in remission/responding				
8	Remission[a]	0	0	1 (17)	2 (33)	3 (50)
	Response[b]	2 (33)	5 (83)	5 (83)	4 (66)	4 (66)
25	Remission	0	3 (50)	2 (33)	3 (50)	3 (50)
	Response	3 (50)	3 (50)	3 (50)	3 (50)	3 (50)
Overall	Remission	0	3 (25)	3 (25)	5 (42)	6 (50)
	Response	5 (42)	8 (67)	8 (67)	7 (58)	7 (58)

[a]Occurrence of a clinical remission, defined as a reduction of CDAI to below 150, occurring at least once after the start of treatment.
[b]Occurrence of a clinical response as defined by achieving a reduction of CDAI of ≥25% and ≥70 points as compared with baseline, occurring at least once after the start of treatment.

in vivo. In contrast, treatment with CNI-1493 decreased the number of cells staining positive for active JNK (Figure 1*B*). Quantitatively confirmation came from experiments in which the number of phospho-JNK positive cells were counted in sections that were not counterstained with hematoxylin (in a blinded fashion). The MAPK inhibitor treatment strikingly reduced the number of phospho-JNK positive cells in these biopsies ($P = 0.01$, Figure 2*B*). We concluded that the clinical benefit of CNI-1493 coincides with reduction of active JNK.

Effects on Local TNF-α Production

The effectiveness of CNI-1493 treatment was further confirmed in patients and controls by staining for TNF-α, a proinflammatory cytokine that was reported to be under the regulatory control of JNK and p38 MAPK. Many TNF-α positive cells were found in the lamina propria (Figure 1*E*). After treatment with CNI-1493 the number of TNF-α positive cells in the colon mucosa significantly decreased, compared with the biopsies taken at time of screening (Figure 1*F*).

Discussion

We tested CNI-1493, a synthetic guanylhydrazone known to inhibit both JNK and p38 MAPK, in patients with moderate to severe CD. Although it is now generally recognized that inflammation involves the activation of stress-activated MAPKs, the actual importance of these kinases in human pathology is poorly understood. CNI-1493 has been shown to be protective in several experimental models involving inflammatory cytokine excess; however, clinical experience with CNI-1493 is limited. In a phase I study, CNI-1493 was studied in melanoma and renal cancer patients receiving high-dose IL-2.[22] CNI-1493 was well tolerated and inhibited the IL-2-induced increase in TNF-α in a dose-dependent fashion. A pilot study of CNI-1493 in patients with moderate to severe psoriasis showed a marked response in several patients to a brief course of therapy, which lasted for up to several months without further therapy (data on file).

In this pilot study, we show that CNI-1493 has significant therapeutic impact on severe CD, resulting in endoscopic healing, as well as remarkable and sometimes long-lasting clinical benefit. Concomitantly, the strong JNK phosphorylation observed in patients before the onset of treatment was reduced, implying that CNI-1493 treatment caused JNK inhibition in vivo. These results support the notion that inflammatory MAPKs are critically involved in the pathogenesis of CD.

Immunohistochemical staining of colon biopsies for p38 MAPK did not yield consistent results, nor was a decrease in phosphorylated p38 MAPK staining detected after CNI-1493 treatment. In agreement, directly determining p38 MAPK activity, using immunoprecipated p38 MAPK from colon biopsies in in vitro kinase assays (not shown), did not reveal an influence of CNI-1493 treatment on p38 MAPK enzymatic activity. Together with our data showing that CNI-1493 more potently inhibits JNK phosphorylation in LPS-stimulated PBMCs in vitro and in mucosal inflammatory cells in vivo, our studies suggest that JNK is the more relevant target for CNI-1493 treatment. These findings would correspond well with recent results obtained in our laboratory obtained with TNBS-induced colitis in mice, which revealed that although the p38 MAPK inhibitor SB20358 effectively inhibited p38 MAPK enzymatic activity in these mice, no attenuation of disease progression was observed.[23] Hence, we favor the hypothesis that JNK inhibition underlies the clinical benefit of CNI-1493 in CD, but until more JNK-specific inhibitors are tested other possibilities must be kept in mind.

To our knowledge, this is the first article that reports immunocompetent cells within the inflamed human intestinal lamina propria expressing phosphorylated JNK and p38 MAPK. Whatever the exact nature of these underlying inflammatory MAPKs, the present study indicates that activity of these kinases is essential for CD-pathogenesis. In this open-label pilot study we observe that inhibition of these kinases may have significant clinical benefit, resulting even in endoscopic healing. As inhibition of such kinases may be achieved with small, orally available, and relatively cheap compounds we propose that such a therapy may constitute a promising novel avenue for the treatment of CD.

References

1. Hugot JP, Chamaillard M, Zouali H, Lesage S, Cezard JP, Belaiche J, Almer S, Tysk C, O'Morain CA, Gassull M, Binder V, Finkel Y, Cortot A, Modigliani R, Laurent-Puig P, Gower-Rousseau C, Macry J, Colombel JF, Sahbatou M, Thomas G. Association of NOD2 leucine-rich repeat variants with susceptibility to Crohn's disease. Nature 2001;411:599–603.
2. Ogura Y, Bonen DK, Inohara N, Nicolae DL, Chen FF, Ramos R, Britton H, Moran T, Karaliuskas R, Duerr RH, Achkar JP, Brant SR, Bayless TM, Kirschner BS, Hanauer SB, Nunez G, Cho JH. A frameshift mutation in NOD2 associated with susceptibility to Crohn's disease. Nature 2001;411:603–606.
3. van Deventer SJ. Review article: targeting TNF alpha as a key cytokine in the inflammatory processes of Crohn's disease–the mechanisms of action of infliximab. Aliment Pharmacol Ther 1999;13(Suppl 4):3–8.
4. van Dullemen HM, van Deventer SJ, Hommes DW, Byl HA, Jansen J, Tytgat GN, Woody J. Treatment of Crohn's disease with anti-tumor necrosis factor chimeric monoclonal antibody (cAz). Gastroenterology 1995;109:129–135.
5. Targan SR, Hanauer SB, van Deventer SJ, Mayer L, Present DH, Braakman T, DeWoody KL, Schaible TF, Rutgeerts PJ. A short-term study of chimeric monoclonal antibody cA2 to tumor necrosis factor alpha for Crohn's disease. Crohn's Disease cA2 Study Group. N Engl J Med 1997;337:1029–1035.
6. Kyriakis JM, Avruch J. Mammalian mitogen-activated protein kinase signal transduction pathways activated by stress and inflammation. Physiol Rev 2001;81:807–869.
7. Badger AM, Bradbeer JN, Votta B, Lee JC, Adams JL, Griswold DE. Pharmacological profile of SB 203580, a selective inhibitor of cytokine suppressive binding protein/p38 kinase, in animal models of arthritis, bone resorption, endotoxin shock and immune function. J Pharmacol Exp Ther 1996;279:1453–1461.
8. Cohen PS, Schmidtmayerova H, Dennis J, Dubrovsky L, Sherry B, Wang H, Bukrinsky M, Tracey KJ. The critical role of p38 MAP kinase in T cell HIV-1 replication. Mol Med 1997;3:339–346.
9. Cohen PS, Nakshatri H, Dennis J, Caragine T, Bianchi M, Cerami A, Tracey KJ. CNI-1493 inhibits monocyte/macrophage tumor necrosis factor by suppression of translation efficiency. Proc Natl Acad Sci U S A 1996;93:3967–3971.
10. Bianchi M, Ulrich P, Bloom O, Meistrell M III, Zimmerman GA, Schmidtmayerova H, Bukrinsky M, Donnelley T, Bucala R, Sherry B. An inhibitor of macrophage arginine transport and nitric oxide production (CNI-1493) prevents acute inflammation and endotoxin lethality. Mol Med 1995;1:254–266.
11. Bianchi M, Bloom O, Raabe T, Cohen PS, Chesney J, Sherry B, Schmidtmayerova H, Calandra T, Zhang X, Bukrinsky M, Ulrich P, Cerami A, Tracey KJ. Suppression of proinflammatory cytokines in monocytes by a tetravalent guanylhydrazone. J Exp Med 1996;183:927–936.
12. Molina PE, Qian L, Schuhlein D, Naukam R, Wang H, Tracey KJ, Abumrad NN. CNI-1493 attenuates hemodynamic and pro-inflammatory responses to LPS. Shock 1998;10:329–334.
13. Denham W, Yang J, Wang H, Botchkina G, Tracey KJ, Norman J. Inhibition of p38 mitogen activate kinase attenuates the severity of pancreatitis-induced adult respiratory distress syndrome. Crit Care Med 2000;28:2567–2572.
14. Yang J, Denham W, Tracey KJ, Wang H, Kramer AA, Salhab KF, Norman J. The physiologic consequences of macrophage pacification during severe acute pancreatitis. Shock 1998;10:169–175.
15. Martiney JA, Rajan AJ, Charles PC, Cerami A, Ulrich PC, MacPhail S, Tracey KJ, Brosnan CF. Prevention and treatment of experimental autoimmune encephalomyelitis by CNI-1493, a macrophage-deactivating agent. J Immunol 1998;160:5588–5595.
16. Meistrell ME, III, Botchkina GI, Wang H, Di Santo E, Cockroft KM, Bloom O, Vishnubhakat JM, Ghezzi P, Tracey KJ. Tumor necrosis factor is a brain damaging cytokine in cerebral ischemia. Shock 1997;8:341–348.
17. Best WR, Becktel JM, Singleton JW, Kern F, Jr. Development of a Crohn's disease activity index. National Cooperative Crohn's Disease Study. Gastroenterology 1976;70:439–444.
18. Guyatt G, Mitchell A, Irvine EJ, Singer J, Williams N, Goodacre R, Tompkins C. A new measure of health status for clinical trials in inflammatory bowel disease. Gastroenterology 1989;96:804–810.
19. Mary JY, Modigliani R. Development and validation of an endoscopic index of the severity for Crohn's disease: a prospective multicentre study. Groupe d'Etudes Therapeutiques des Affections Inflammatoires du Tube Digestif (GETAID). Gut 1989;30:983–989.
20. Waetzig GH, Seegert D, Nikolaus S, Rosenstiel P, Sfikas N, Schreiber S, Albrechts C. Differential activity and expression of mitogen-activated protein kinases in inflammatory bowel disease (abstr). Gastroenterology 2001;121:A522.
21. Hunt AE, Lali FV, Lord JD, Nelson BH, Miyazaki T, Tracey KJ, Foxwell BM. Role of interleukin (IL)-2 receptor beta-chain subdomains and Shc in p38 mitogen-activated protein (MAP) kinase and p54 MAP kinase (stress-activated protein kinase/c-Jun N-terminal kinase) activation. IL-2- driven proliferation is independent of p38 and p54 MAP kinase activation. J Biol Chem 1999;274:7591–7597.
22. Atkins MB, Redman B, Mier J, Gollob J, Weber J, Sosman J, MacPherson BL, Plasse T. A phase I study of CNI-1493, an inhibitor of cytokine release, in combination with high-dose interleukin-2 in patients with renal cancer and melanoma. Clin Cancer Res 2001;7:486–492.
23. Ten Hove T, van den Blink B, Pronk I, Drillenburg P, Peppelenborch MP, van Deventer SJ. Inhibition of p38 MAPK with SB 203580 in experimental colitis. Gut 2002;50 (in press).

Received July 16, 2001. Accepted November 2, 2001.

Address requests for reprints to: Daan W. Hommes, M. D., Department of Gastroenterology and Hepatology, Academic Medical Center, C2-116, Meibergdreef 9, 1105 AZ Amsterdam, the Netherlands. e-mail: d.w.hommes@amc.uva.nl; fax: (31) 20 566 9285.

Exhibit 5

Am J Physiol Heart Circ Physiol
280: H1970–H1981, 2001.

Role of p38 mitogen-activated protein kinase in cardiac myocyte secretion of the inflammatory cytokine TNF-α

CHERRY BALLARD-CROFT, D. JEAN WHITE, DAVID L. MAASS,
DIXIE PETERS HYBKI, AND JURETA W. HORTON
Department of Surgery, University of Texas Southwestern Medical Center, Dallas, Texas 75390-9160

Received 25 September 2000; accepted in final form 14 December 2000

Ballard-Croft, Cherry, D. Jean White, David L. Maass, Dixie Peters Hybki, and Jureta W. Horton. Role of p38 mitogen-activated protein kinase in cardiac myocyte secretion of the inflammatory cytokine TNF-α. *Am J Physiol Heart Circ Physiol* 280: H1970–H1981, 2001.—This study examined the hypothesis that burn trauma promotes cardiac myocyte secretion of inflammatory cytokines such as tumor necrosis factor (TNF)-α and produces cardiac contractile dysfunction via the p38 mitogen-activated protein kinase (MAPK) pathway. Sprague-Dawley rats were divided into four groups: *1*) sham burn rats given anesthesia alone, *2*) sham burn rats given the p38 MAPK inhibitor SB203580 (6 mg/kg po, 15 min; 6- and 22-h postburn), *3*) rats given third-degree burns over 40% total body surface area and treated with vehicle (1 ml of saline) plus lactated Ringer solution for resuscitation (4 ml·kg^{-1}·percent burn^{-1}), and *4*) burn rats given injury and fluid resuscitation plus SB203580. Rats from each group were killed at several times postburn to examine p38 MAPK activity (by Western blot analysis or in vitro kinase assay); myocardial function and myocyte secretion of TNF-α were examined at 24-h postburn. These studies showed significant activation of p38 MAPK at 1-, 2-, and 4-h postburn compared with time-matched shams. Burn trauma impaired cardiac mechanical performance and promoted myocyte secretion of TNF-α. SB203580 inhibited p38 MAPK activity, reduced myocyte secretion of TNF-α, and prevented burn-mediated cardiac deficits. These data suggest p38 MAPK activation is one aspect of the signaling cascade that culminates in postburn secretion of TNF-α and contributes to postburn cardiac dysfunction.

rat model of burn trauma; Langendorff perfusion; cardiac contraction-relaxation; tumor necrosis factor-α

IN SEVERAL INJURY AND DISEASE STATES inflammatory cytokines such as tumor necrosis factor (TNF)-α play a significant role in the inflammatory sequelae that culminates in multiple organ failure. Recent studies (7–10, 25, 33, 39, 44, 48, 58) have shown that cardiac myocytes themselves secrete inflammatory cytokines in response to trauma or sepsis, producing myocardial cytokine levels that exceed those measured in the systemic circulation. In addition, cardiac secretion of the inflammatory cytokine TNF-α has been shown to correlate with cardiac contraction and relaxation deficits (7, 25) and has been proposed to mediate cardiac deficits in burn trauma (32, 34), ischemia-reperfusion (44), and hemorrhagic shock (45). Anticytokine strategies such as monoclonal antibodies to TNF-α have had limited success in models of ischemia-reperfusion, trauma, or sepsis (1, 2, 19–21). Recent approaches to limiting cytokine-mediated organ injury and dysfunction have included defining the signal transduction pathways that regulate cytokine synthesis, with the goal of developing therapeutic approaches to interrupt specific aspects of this pathway (10). This approach could limit cardiodepression mediated by cardiac cytokine secretion without producing generalized immunosuppression or increasing susceptibility to subsequent infection.

One aspect of the signal transduction pathway that regulates cytokine synthesis in other cell populations is the p38 mitogen-activated protein kinase (MAPK). Activation of the p38 MAPK signaling cascade is one of the mechanisms by which cells respond to environmental stress (47). In fact, p38 was first identified as a protein undergoing rapid tyrosine phosphorylation after exposure to lipopolysaccharide (LPS), a bacterial surface component released on host infection (28). Later, Lee and colleagues (41) described a protein that was the binding site for pyridinyl imidazole compounds that had been shown to inhibit LPS-stimulated inflammatory cytokine production (41). This cytokine-suppressive binding protein was subsequently cloned and was identified as p38 MAPK (42).

While p38 MAPK plays a role in regulating inflammatory cytokine production as well as many other cellular responses to stress, the biological consequences of MAPK activation in the heart are diverse and not clearly understood. Recently, p38 MAPK has been implicated in cardiac hypertrophy, ischemia-reperfusion, and cardiomyocyte apoptosis (52, 55). Furthermore, Weinbrenner and colleagues (56) showed that upregulation of p38 MAPK activity correlates with ischemic preconditioning, most likely through the phosphorylation of heat shock protein 27 (40, 52). Some downstream targets of p38 MAPK activation may include several transcription factors including activating

Address for reprint requests and other correspondence: J. W. Horton, Dept. of Surgery, Univ. of Texas Southwestern Medical Center, 5323 Harry Hines Blvd., Dallas, TX 75390-9160 (E-mail: jureta.horton@UTSOUTHWESTERN.edu).

The costs of publication of this article were defrayed in part by the payment of page charges. The article must therefore be hereby marked "*advertisement*" in accordance with 18 U.S.C. Section 1734 solely to indicate this fact.

transcription factor-2 (ATF2), nuclear factor (NF)-κB, and p53 (43, 47, 51).

Because p38 MAPK activation appears to be involved in other cardiac abnormalities, it is possible that this MAPK may also mediate the contractile deficits observed in burn trauma. Therefore, the purpose of this present study was to determine whether burn trauma activates p38 MAPK in the heart; in addition, the effects of inhibiting cardiac MAPK activity on cardiomyocyte secretion of the inflammatory cytokine TNF-α and on cardiac mechanical function were studied.

MATERIALS AND METHODS

Experimental Animals

Adult Sprague-Dawley rats (Harlan Laboratories; Houston, TX) weighing 325–360 g were used throughout the study. Animals were allowed 5–6 days to acclimate to their surroundings. Commercial rat chow and tap water were available at will throughout the experimental protocol. All work described herein was approved by the University of Texas Southwestern Medical Center Institutional Animal Care and Research Advisory Committee and was performed according to the guidelines outlined in the "Guide for the Care and Use of Laboratory Animals" published by the American Physiological Society.

Catheter Placement and Burn Procedure

Rats were briefly anesthetized with methoxyflurane 18 h before the burn experiment. Body hair was closely clipped, the neck region was treated with a surgical scrub (Betadine), and a polyethylene (PE) catheter (PE-50 tubing) was inserted into the left carotid artery with the tip advanced to the level of the aortic arch. In addition, a PE catheter (PE-50) was placed in the right external jugular vein for administration of fluids. The catheters were filled with heparinized saline and exteriorized at the nape of the neck, and the skin was closed. After the animals had recovered from the anesthesia for catheter placement, they were housed in individual cages, and body temperature was maintained throughout the experimental period with a heating pad and a heating lamp.

Hemodynamic, metabolic, and hematological measurements were collected 18 h after catheter placement (preburn data); the animals were then deeply anesthetized with methoxyflurane and secured in a constructed template device as previously described (3, 25, 36). The surface area of the skin exposed through the template device was immersed in 100°C water for 12 s on each side; with the use of this technique, full-thickness dermal burns comprising 40% of the total body surface area were obtained. This burn technique produces complete destruction of the underlying neural tissue and a transient (<45 s) increase in internal body temperature of 1–3°C. Sham burn rats were subjected to an identical preparation except that they were immersed in room temperature water. After immersion, the rats were immediately dried, and each animal was placed in an individual cage; the external jugular catheter was then connected to a swivel device (model 923, Holter pump, Critikon; Tampa, FL) for fluid administration during the 24-h postburn period (4 $ml \cdot kg^{-1} \cdot$percent $burn^{-1}$ lactated Ringer solution, with one-half of the calculated volume given during the first 8-h postburn and the remaining volume given during the next 16-h postburn). In the control group, the external jugular vein was cannulated but no fluid resuscitation was administered. Twenty-four hours after burn injury (or sham burn), hemodynamic parameters including systemic blood pressure [using a model P23 ID, Gould-Statham pressure transducer (Gould; Oxnard, CA) connected to a model 7D Polygraph recorder (Grass Instruments; Quincy, MA)] and heart rate (using a model 7P4F tachycardiograph, Grass Instruments) were measured. A small sample of arterial blood (0.25 ml) was withdrawn from the arterial catheter for measuring packed cell volume, hematocrit, arterial pH, and blood gases. Body temperature was measured with a rectal temperature probe (model 44TA, YS1-Tele Thermometer, Yellow Springs Instruments; Yellow Springs, OH), and respiratory rate was monitored by counting respiratory movement.

Experimental Groups

All rats had catheters placed before inclusion in an experimental group. Eighteen hours after catheter placement, rats were randomly divided into two major experimental groups as follows: cutaneous burn injury over 40% of the total body surface area ($n = 68$) or sham burn injury ($n = 66$). These two experimental groups were then subdivided such that one-half of the sham burns ($n = 33$) and one-half of the burns ($n = 34$) were given the selective inhibitor of p38 MAPK SB203580 [4-(4-fluorophenyl)-2-(4-methyl-sulfinylphenyl)-5-(4-pyridinyl)imidazole, SmithKline Beecham Pharmaceuticals; Brocham Park, UK]. SB203580 was dissolved in 0.03 N HCl-0.5% tragacanth (Sigma; St. Louis, MO) and was administered by oral gavage at 6 mg/kg at 15 min and 6 and 22 h after either burn or sham burn (4, 6). The remaining sham ($n = 33$) and burn rats ($n = 34$) were given vehicle (0.03 N HCl-0.5% tragacanth) to serve as appropriate control groups. Initial studies were designed to measure the time course of p38 MAPK activation after burn trauma. For these studies, three hearts were collected from each of the four experimental groups at several time points after injury (30 min and 1, 2, 4, 6, 12, and 24 h). The hearts were cleared of fat and epicardial vessels, freeze-clamped in liquid nitrogen, and stored at −80°C until used for immunoprecipitation of p38 MAPK for in vitro kinase assay or Western blot analysis. Thirty-two rats were used to assess ventricular function 24 h after burn trauma (Langendorff perfusion); rats ($n = 8$ rats/group) from each of the four experimental groups (sham plus vehicle, sham plus inhibitor, burn plus vehicle, and burn plus inhibitor) were studied. Four to five rats from each of the four experimental groups were used to prepare cardiomyocytes 24 h after burn injury to assess TNF-α secretion by this cell population. The time frame selected to assess ventricular function and TNF-α secretion was based on previous studies (unpublished data) from our laboratory examining the time course of cardiac contractile defects, NF-κB activation, and myocyte secretion of inflammatory cytokines.

Isolated Perfused Hearts (Langendorff Model)

For studies of cardiac contraction and relaxation, awake animals were anticoagulated with heparin sodium (1000 units, Elkins-Sinn; Cherry Hill, NJ) 24-h postburn (or sham burn) and decapitated with a guillotine. The hearts were rapidly removed and placed in ice-cold (4°C) Krebs-Henseleit bicarbonate-buffered solution [containing (in mM) 118 NaCl, 4.7 KCl, 21 $NaHCO_3$, 2.5 $CaCl_2$, 1.2 $MgSO_4$, 1.2 KH_2PO_4, and 11 glucose]. All solutions were prepared on the day of experimental performance and bubbled with 95% O_2-5% CO_2 (pH 7.4; Po_2, 550 mmHg; Pco_2, 38 mmHg). A 17-gauge cannula placed in the ascending aorta was connected to a buffer-filled reservoir for perfusion of the coronary circulation at a constant flow rate of 5 ml/min. Hearts were suspended in a temperature-controlled chamber maintained at 38 ± 0.5°C,

and a constant flow pump (model 911, Holter pump, Critikom) was used to maintain perfusion of the coronary arteries by retrograde perfusion of the aortic stump cannula. Coronary perfusion pressure was measured and effluent was collected to confirm coronary flow rate. Contractile function was assessed by measuring intraventricular pressure with a saline-filled latex balloon placed in the left ventricular chamber. Left ventricular pressure (LVP) was measured with a Statham pressure transducer (model P23 ID, Gould) attached to the balloon cannula; the rate of LVP rise ($+dP/dt_{max}$) and fall ($-dP/dt_{max}$) was obtained using an electronic differentiator (model 7P20C, Grass Instruments) and recorded (model 7DWL8P, Grass Recording Instruments).

A Frank-Starling relationship for each heart was determined by plotting left ventricular developed pressure (peak systolic pressure minus left ventricular end-diastolic pressure) and $\pm dP/dt_{max}$ responses to increases in preload (left ventricular end-diastolic volume). Because the heart rate varied after burn injury, hearts were paced through an electrode attached to the right atrium (3–4 Hz, 2–10 W for 4-ms duration; Grass stimulator, Grass Instruments). Hearts were paced at twice the minimum capture voltage; thus in vitro heart rates were similar in all experimental groups, and differences in cardiac performance could not be attributed to burn-related differences in heart rate. In addition, ventricular performance was assessed in all hearts as coronary flow rate was increased from 3 to 12 ml/min or as perfusate calcium concentration was increased from 1 to 8 mM.

Cardiomyocyte Isolation

To isolate cardiac myocytes, animals from each experimental group were heparinized 24-h postburn and decapitated, and the hearts were removed through a medial sternotomy with the use of sterile techniques. The isolated heart was immediately placed in ice-cold calcium-free Tyrode solution [containing (in mM) 136 NaCl, 5 KCl, 0.57 $MgCl_2$, 0.33 NaH_2PO_4, 10 HEPES, and 10 glucose]. The aorta was cannulated within 60 s, and the excised heart was perfused with calcium-free Tyrode solution using a Langendorff perfusion apparatus. Perfusion was maintained for 5 min and then switched to a collagenase solution, which contained 80 ml of calcium-free Tyrode, 40 mg of collagenase A (0.05%, Boehringer Mannheim; Indianapolis, IN), and 4 mg of protease (Polysaccharide XIV, Sigma) with continuous oxygenation (95% O_2-5% CO_2). After this enzymatic digestion over a 10-min period was completed, the heart was removed from the cannula, and the ventricular tissue was separated from the base of the heart. This tissue was plated in a petri dish containing Tyrode solution with 100 μM calcium and gently minced to increase cell dispersion over 6 min. The myocyte suspension was then filtered, and the cells were allowed to settle. This rinsing and settling step was repeated three times with 10 min between each step and with gentle swirling between each step to allow myocyte separation. The calcium concentration of the rinsing solution was gradually increased during these steps from 100 to 200 μM and finally to 1.8 mM. The cell viability was measured (Trypan blue dye exclusion), and cell suspensions with >85% viability were used for subsequent studies. Myocytes with a rodlike shape, clearly defined edges, and sharp striations were prepared with a final cell count of 5×10^4 cells·ml^{-1}·well^{-1} (38).

Cytokine Secretion by Cardiomyocytes

Myocytes were pipetted into microtiter plates at 5×10^4 cells·ml^{-1}·well^{-1} (12-well cell culture cluster, Corning; Corning, NY) and subsequently stimulated with either 0, 10, 25, or 50 μg/well of LPS (from *Escherichia coli*; lot 65H 4053, Difco Laboratories; Detroit, MI) for 18 h (CO_2 incubator at 37°C). Supernatants were collected to measure myocyte-secreted TNF-α (TNF-α, rat ELISA, Endogen; Woburn, MA). We previously examined the contribution of contaminating cells (nonmyocytes) in our cardiomyocyte preparations using flow cytometry, cell staining (hematoxylin and eosin), and light microscopy. We confirmed that <2% of the total cell number in a myocyte preparation was noncardiomyocytes (33). Because our cardiomyocyte preparations were 98% pure, we concluded that the majority of the TNF-α measured in the cardiomyocyte supernatant was indeed cardiomyocyte derived.

In Vitro p38 MAPK Assay

The in vitro kinase assay was performed on rat heart tissue extracts in which p38 MAPK had been immunoprecipitated. Briefly, 100 μg of extract was incubated with 2 μg p38 antibody (courtesy of Dr. M. Cobb, Dept. of Pharmacology, Univ. of Texas Southwestern Medical Center, Dallas, TX; Santa Cruz Biotechnology; Santa Cruz, CA), lysis buffer [containing phosphate-buffered saline (pH 7.4), 1% Nonidet P-40, 0.5% sodium deoxycholate, 0.1% SDS, 0.1 mg/ml phenylmethylsulfonyl fluoride, 45 μg/μl aprotinin, 1 mM sodium orthovanadate, and 0.5 mM β-glycerophosphate], and protein A sepharose beads for 2 h at 4°C with gentle agitation. After sedimentation, the protein A sepharose beads were washed twice with lysis buffer, twice with buffer B [containing 0.25 M Tris (pH 7.6) and 0.1 M NaCl], and once with kinase buffer [containing 20 mM HEPES (pH 8.0) and 20 mM $MgCl_2$]. The resulting p38 MAPK immunoprecipitates were resuspended in 30 μl of kinase assay reaction buffer, which contained kinase buffer (as indicated above) plus 50 μM ATP, 15 μCi [γ-^{32}P]ATP, and 20 μg glutathione-*S*-transferase (GST)-ATF2 (Upstate Biotechnology; Lake Placid, NY). The kinase reaction was initiated by incubating the samples at 30°C for 30 min. Termination of the kinase reaction was accomplished by sedimentation of the beads and addition of the supernatant to Laemmli buffer. After the samples were boiled for 5 min, SDS-PAGE (12%) was used to separate the kinase reaction product, and autoradiography was then performed on the dried gel. A beta scintillation counter was used to quantify incorporation of radiolabel into the reaction product.

Western Blot Analysis

Protein samples (30 μg) were separated on a 12% SDS-polyacrylamide gel and transferred to a polyvinylidene difluoride membrane (Millipore; Bedford, MA). The membrane was blocked by a 1-h incubation in a Tris-buffered saline solution [containing 20 mM Tris (pH 7.6), 135 mM NaCl, and 0.1% Tween] containing 3% bovine serum albumin and 1% nonfat dry milk. The phospho-p38 antibody or phospho-c-Jun NH_2-terminal kinase (JNK) antibody (Santa Cruz Biotechnology) was then added to the membranes at a dilution of 1:400 and incubated for 1 h at room temperature. After the primary antibody incubation, the membrane was washed three times with Tris-buffered saline solution with 0.1% Tween. The secondary antibody was then added to the membrane (1:2,500, Promega; Madison, WI) and incubated for 1 h at room temperature. The membrane was again washed three times with Tris-buffered saline with 0.1% Tween. The bound antibodies were visualized by enhanced chemiluminescence (Amersham; Piscataway, NJ).

Table 1. *Hemodynamic and metabolic responses to burn trauma or to burn trauma with MAPK inhibitor*

	Vehicle-Treated Sham	Sham + p38 MAPK Inhibitor	Vehicle-Treated Burn	Burn + p38 MAPK Inhibitor
MAP, mmHg	126 ± 4	145 ± 3*	94 ± 4*	116 ± 6*†
HR, beats/min	480 ± 22	516 ± 12	433 ± 21*	513 ± 17†
Body temperature, °C	38.9 ± 0.3	38.9 ± 0.2	38.8 ± 0.2	38.7 ± 0.2
pH	7.45 ± 0.02	7.54 ± 0.02	7.48 ± 0.01	7.51 ± 0.02
Hct, %	37.4 ± 2.3	38.8 ± 0.6	28.3 ± 1.6*	31.6 ± 1.6*
PCV, %	39.5 ± 3.7	43.0 ± 1.4	35.5 ± 0.6*	35.0 ± 1.5*
P_{CO_2}, mmHg	29 ± 2	29 ± 2	26 ± 2*	25 ± 2*
P_{O_2}, mmHg	113 ± 5	117 ± 6	120 ± 5	110 ± 4

All values are means ± SE. MAP, mean arterial pressure; HR, heart rate; Hct, hematocrit; PCV, packed cell volume; MAPK, mitogen-activated protein kinase. *Significant difference among groups, $P < 0.05$. †Significant difference between burn groups, $P < 0.05$.

In Vitro Effects of MAPK Inhibitor

To examine the cell-specific effects of MAPK inhibition on cardiomyocyte secretion of TNF-α, myocytes were harvested from additional rats 24 h after either burn trauma ($n = 5$) or sham burn ($n = 5$). Myocytes (5×10^4 cells/well) were incubated (37°C) for 60 min in Tyrode solution containing 1.8 mM calcium. SB203580 (0.2 or 20 μM) was then added, and the myocytes were incubated for an additional 60 min. The supernatant was removed and replaced with fresh Tyrode solution containing 1.8 mM calcium. After viability measurements, cells were challenged with LPS (0, 10, 25, or 50 μg/well). After 18 h, supernatants were collected to measure myocyte secretion of TNF-α. In this manner, the cell-specific effects of the MAPK inhibitor on cytokine secretion by cardiac myocytes was assessed in vitro.

Statistical Analysis

All values are expressed as means ± SE. Analysis of variance (ANOVA) was used to assess an overall difference among the groups for each of the variables. Levene's test for equality of variance was used to suggest the multiple comparison procedure to be used if the ANOVA was significant. If equality of variance among the four groups was suggested, multiple comparison procedures were performed (Bonferroni). If inequality of variance was suggested, Tamhane's multiple comparisons were performed. P values <0.05 were considered statistically significant (analysis was performed using SPSS for Windows, version 7.5.1).

RESULTS

Effects of Burn Trauma

Survival and hemodynamic responses to burn injury. All animals survived the respective experimental protocols. Despite aggressive fluid resuscitation during the 24-h postburn period, mean arterial blood pressure (MABP) was significantly lower in rats with burns compared with that measured in the sham burn rats (Table 1). Packed cell volume and hematocrit fell significantly in all burn rats, and this hemodilution was attributed to the aggressive fluid resuscitation after burn trauma (Table 1).

Cardiac function after burn trauma. Cardiac contraction and relaxation deficits occurred in burns despite aggressive fluid resuscitation. As shown in Table 2, LVP, $\pm dP/dt_{max}$, left ventricular developed pressure at 40 mmHg, the time to peak tension, time to 90% relaxation of the ventricle, and the time to $-dP/dt_{max}$ were significantly lower in burn rats than values measured in sham burn rats. In addition, burn-mediated cardiac contractile deficits were evident from the left ventricular function curves. As seen in Fig. 1, Frank-Starling relationships calculated for burn rats were shifted downward and rightward compared with those calculated for vehicle-treated shams. In addition, burn

Table 2. *p38 MAPK inhibitor alters cardiodynamic responses to burn trauma*

	Vehicle-Treated Sham	Sham + p38 MAPK Inhibitor	Vehicle-Treated Burn	Burn + p38 MAPK Inhibitor
LVP, mmHg	88 ± 3	91 ± 3	65 ± 5*	80 ± 2†
$+dP/dt_{max}$, mmHg/s	2,192 ± 32	2,050 ± 71	1,321 ± 117*	2,067 ± 111†
$-dP/dt_{max}$, mmHg/s	1,776 ± 68	1,725 ± 25	999 ± 91*	1,625 ± 52†
$LVDP_{40}$, mmHg/s	1,987 ± 23	1,900 ± 71	1,249 ± 110*	1,845 ± 124†
TPP, ms	78.9 ± 1.1	84.0 ± 4.1	88.0 ± 3.9*	88.8 ± 3.0*
RT_{90}, ms	74.6 ± 2.0	82.5 ± 6.0	82.9 ± 2.0*	83.3 ± 2.7*
Time to $+dP/dt_{max}$, ms	45.9 ± 1.8	52.5 ± 2.0	49.1 ± 1.2	57.0 ± 2.4*†
Time to $-dP/dt_{max}$, ms	45.0 ± 1.6	46.2 ± 1.4	40.3 ± 0.5*	50.0 ± 0.2†
CPP, mmHg	49.2 ± 3.4	50.5 ± 3.3	52.9 ± 6.6	46.8 ± 6.6
CVR, mmHg/s	9.87 ± 0.67	10.1 ± 0.7	10.6 ± 1.32	9.35 ± 0.32
HR, beats/min	256 ± 18	266 ± 7	252 ± 13	258 ± 4

All values are means ± SE. LVP, left ventricular pressure; $+dP/dt_{max}$ and $-dP/dt_{max}$, rate of LVP rise and fall, respectively; $LVDP_{40}$, left ventricular developed pressure at 40 mmHg; TPP, time to peak pressure; RT_{90}, time to 90% relaxation; CPP, coronary perfusion pressure; CVR, coronary vascular resistance. *Significant difference among groups, $P < 0.05$ (ANOVA and Bonferroni). †Significant difference between burn groups, $P < 0.05$ (unpaired Student t-test).

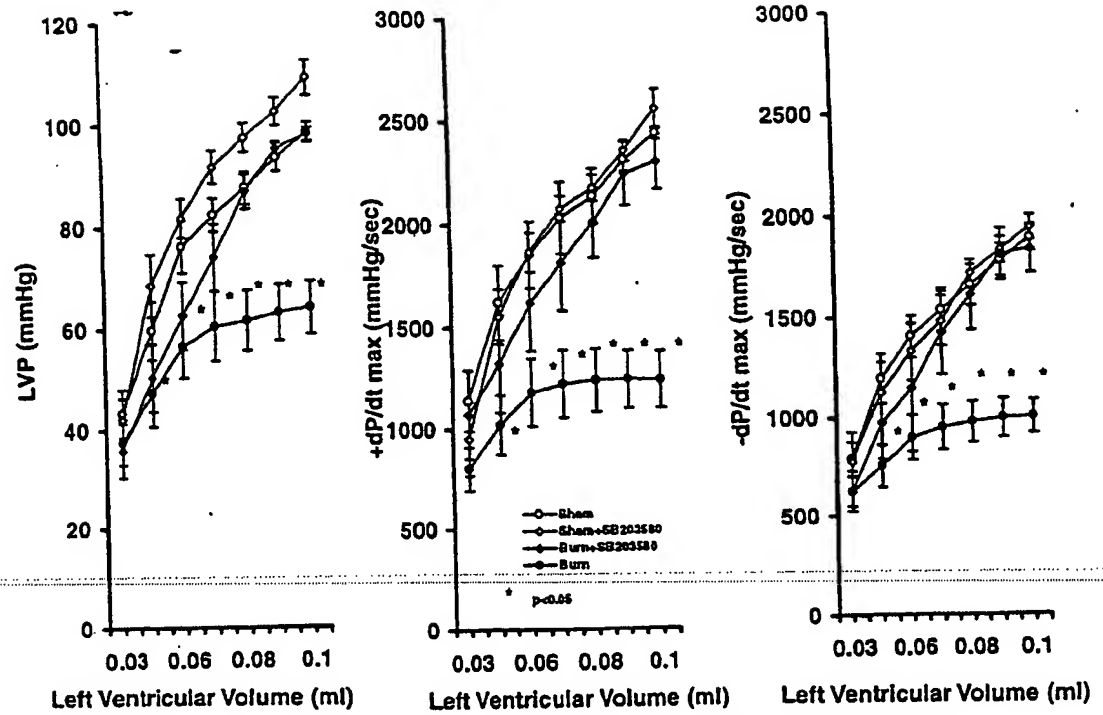

Fig. 1. Left ventricular developed pressure (LVP) calculated from peak systolic pressure minus end-diastolic pressure and the rate of LVP rise ($+dP/dt_{max}$) and fall ($-dP/dt_{max}$) responses to increases in preload (ventricular volume) (n = 8 animals/group). All values are means ± SE. Statistical analysis included ANOVA and a multiple comparison procedure (Bonferroni). *Significant difference among groups, $P < 0.05$.

trauma decreased ventricular responses to increases in coronary flow rate (Fig. 2) and to increases in perfusate calcium levels (Fig. 3).

p38 MAPK activity after burn trauma. To determine whether burn upregulated cardiac MAPK activity, hearts were collected at several time points after burn injury. As measured by Western blot, upregulation of p38 MAPK activity was observed as early as 1-h postburn (Fig. 4, *A* and *B*); this burn-mediated increase in p38 MAPK activity was confirmed by a specific p38 MAPK assay (Fig. 4*C*). Sixty minutes after burn trauma, p38 activity had increased from 1.28 ± 0.15 measured in the sham burn rats to 1.77 ± 0.055 relative units measured in the burn rats. Peak p38 MAPK activation occurred 2-h postburn, persisted through 4-h postburn, and returned to baseline values 6-h postburn (Fig. 4*C*).

Effects of MAPK Inhibition on Hemodynamic and Cardiodynamic Function

To determine whether upregulation of p38 MAPK plays a role in cardiac dysfunction after burn trauma, the specific p38 MAPK inhibitor SB203580 was administered with aggressive fluid resuscitation from burn trauma. A group of sham burn rats were treated with SB203580 to provide suitable controls. p38 MAPK inhibition in sham burn rats did not alter MABP, body temperature, or any measure of acid-base balance compared with those values measured in vehicle-treated sham rats (Table 1). While heart rate tended to increase after SB203580 administration in shams, this increase did not achieve statistical significance. Administration of the MAPK inhibitor in sham animals did not alter LVP, $\pm dP/dt_{max}$, time to peak tension, time to 90% relaxation, time to $\pm dP/dt_{max}$, coronary perfusion pressure, or coronary vascular resistance. Similarly, administration of the inhibitor in shams did not alter ventricular responsiveness to increases in left ventricular volume, increases in coronary flow rate, or increases in perfusate calcium concentration (Figs. 1–3).

MAPK inhibition in burn rats tended to improve MABP, but MABP remained significantly lower than values measured in the SB203580-treated sham rats. Inhibiting MAPK (by SB203580) in burn rats significantly improved LVP and $\pm dP/dt_{max}$, whereas burn-mediated changes in time to peak pressure, time to 90% relaxation of the ventricle, and time to $+dP/dt_{max}$ persisted. In addition, administration of SB203580 in burns significantly improved LVP and $\pm dP/dt_{max}$ responses to increases in ventricular volume (Fig. 1) and improved ventricular responsiveness to increases in either coronary flow rate (Fig. 2) or to increases in perfusate calcium (Fig. 3).

Effects of MAPK Inhibition on Cardiac MAPK/JNK Activity after Burn Trauma

To ensure that SB203580 blocked the MAPK pathway in the heart, p38 MAPK activity was determined

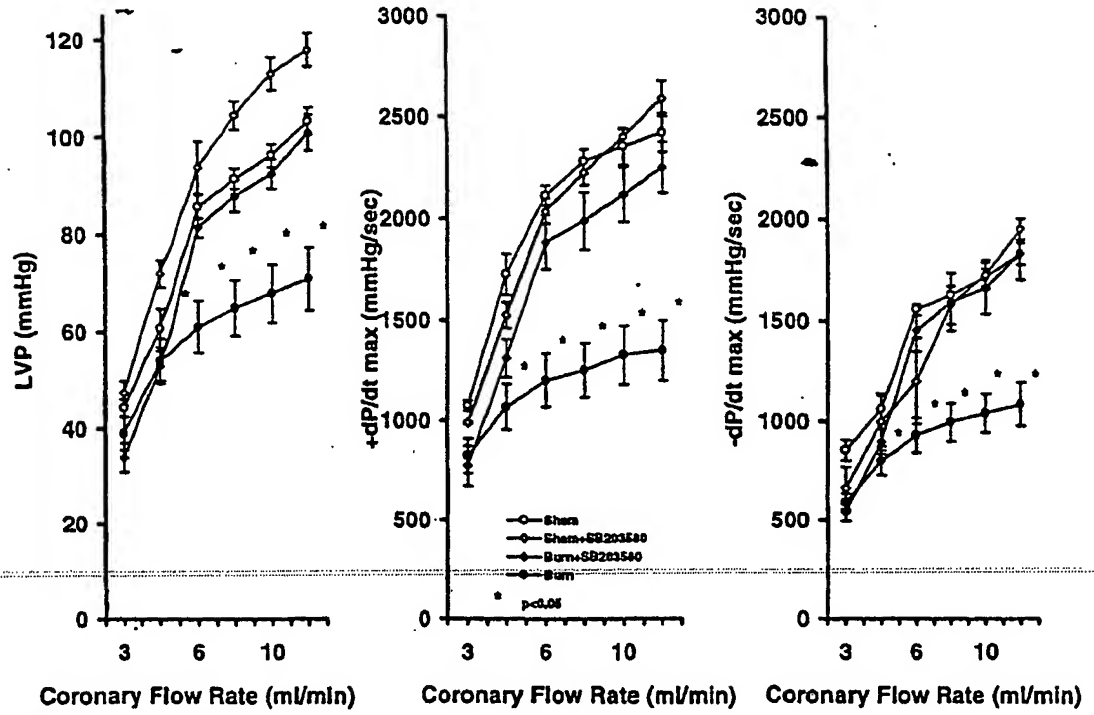

Fig. 2. Effects of increases in coronary flow rate on LVP and $\pm dP/dt_{max}$ in all experimental groups. All values are means ± SE. Statistical analysis included ANOVA and a multiple comparison procedure (Bonferroni). *Significant difference among groups, $P < 0.05$.

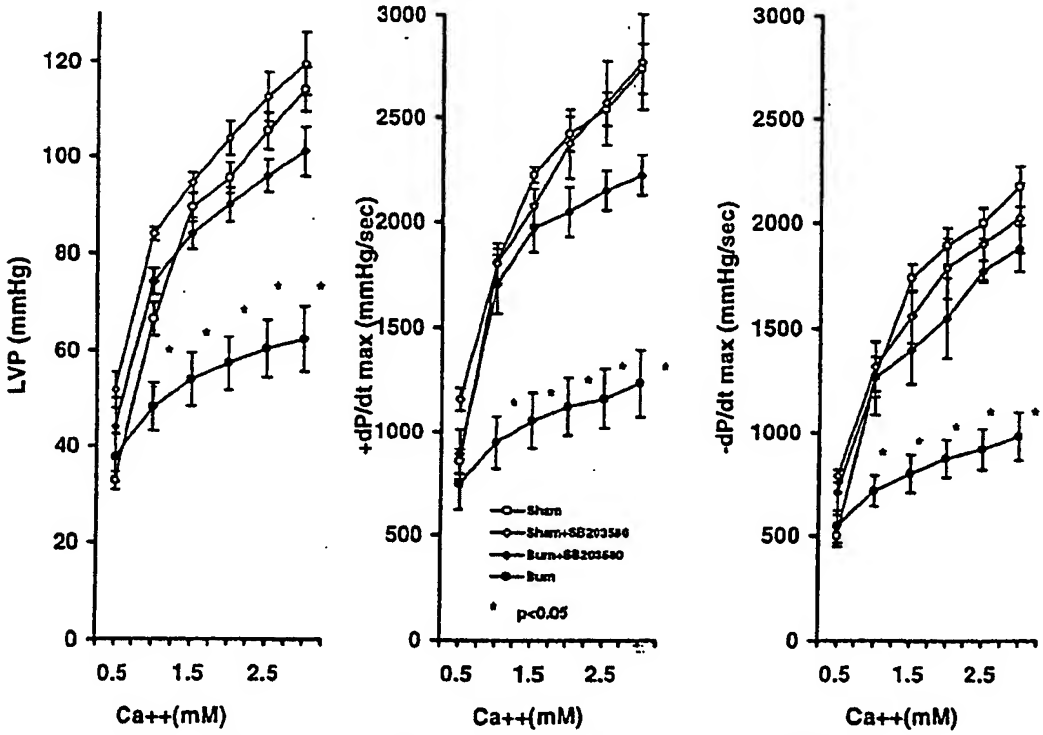

Fig. 3. The effects of increases in perfusate calcium levels on left ventricular contraction and relaxation in all experimental groups. All values are means ± SE. Statistical analysis included ANOVA and a multiple comparison procedure (Bonferroni). *Significant difference among groups, $P < 0.05$.

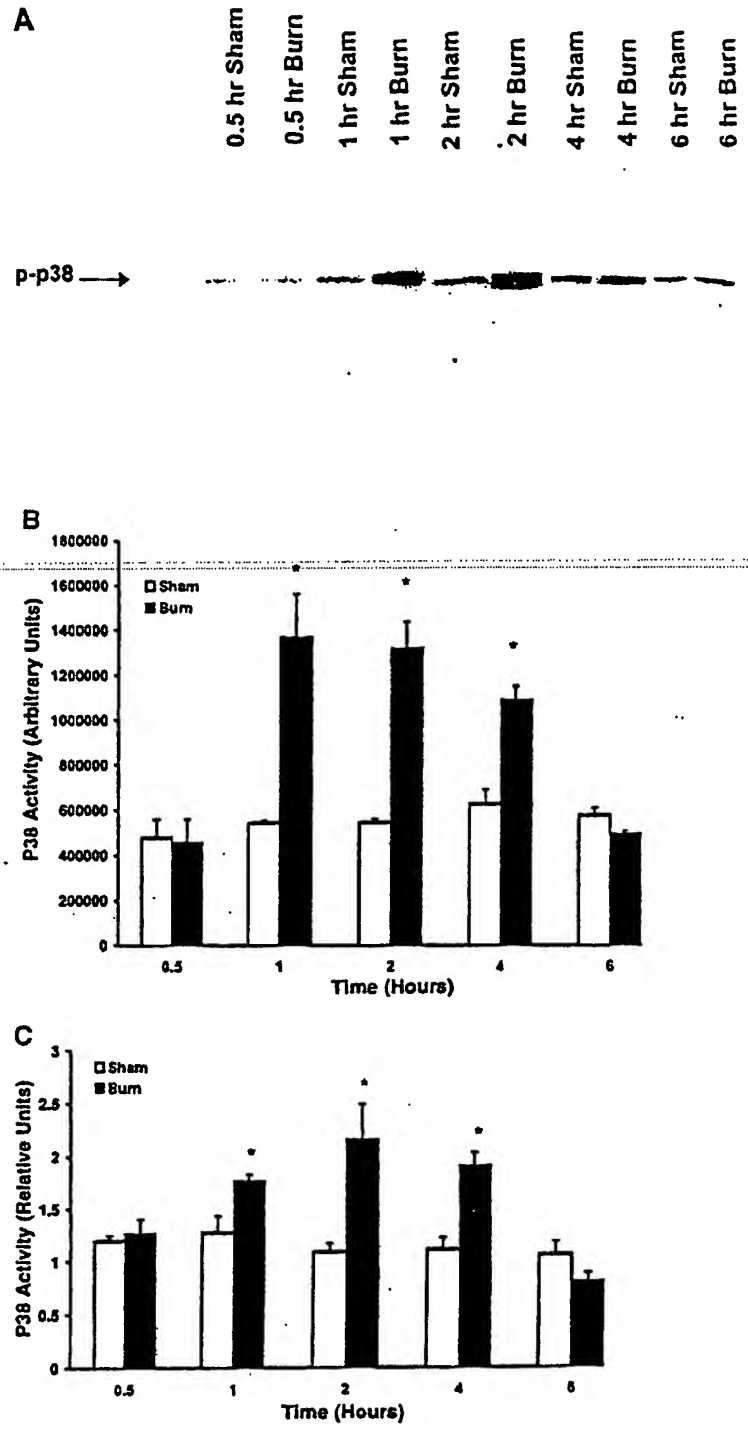

Fig. 4. Burn trauma activates p38 mitogen-activated protein kinase (MAPK) in the heart. *A*: Western blot analysis using an antibody that recognizes only the active, phosphorylated form of p38 MAPK (p-p38) indicated that upregulation of p38 MAPK activity occurred at 1-, 2-, and 4-h postburn. *B*: densitometric analysis of pooled anti-active p38 MAPK Western blots. *Significant increase in p38 MAPK activity (as indicated by p38 activity) in burn versus time-matched sham rats at 1-, 2-, and 4-h postburn, $P < 0.05$. *C*: in vitro p38 MAPK assay confirmed that burn trauma promoted activation of p38 MAPK (indicated as p38 activity) at 1-, 2-, and 4-h postburn. *Significant difference between burn and sham rats, $P < 0.05$.

in cardiac tissue harvested from the SB203580-treated experimental groups (SB203580-treated shams and SB203580-treated burn rats). This inhibitor abolished p38 MAPK activation at all times after burn injury; there were minimal effects of SB203580 in time-matched sham burn animals (Fig. 5, *A* and *B*). These data determined by Western blot were confirmed by an in vitro p38 MAPK specific assay (Fig. 5*C*). In addition, there was no effect of SB203580 on burn-mediated activation of JNK (Fig. 5*A*). Whereas burn trauma increased JNK activity in cardiac tissue, SB203580 had no significant effect on the burn-mediated increase in JNK activity.

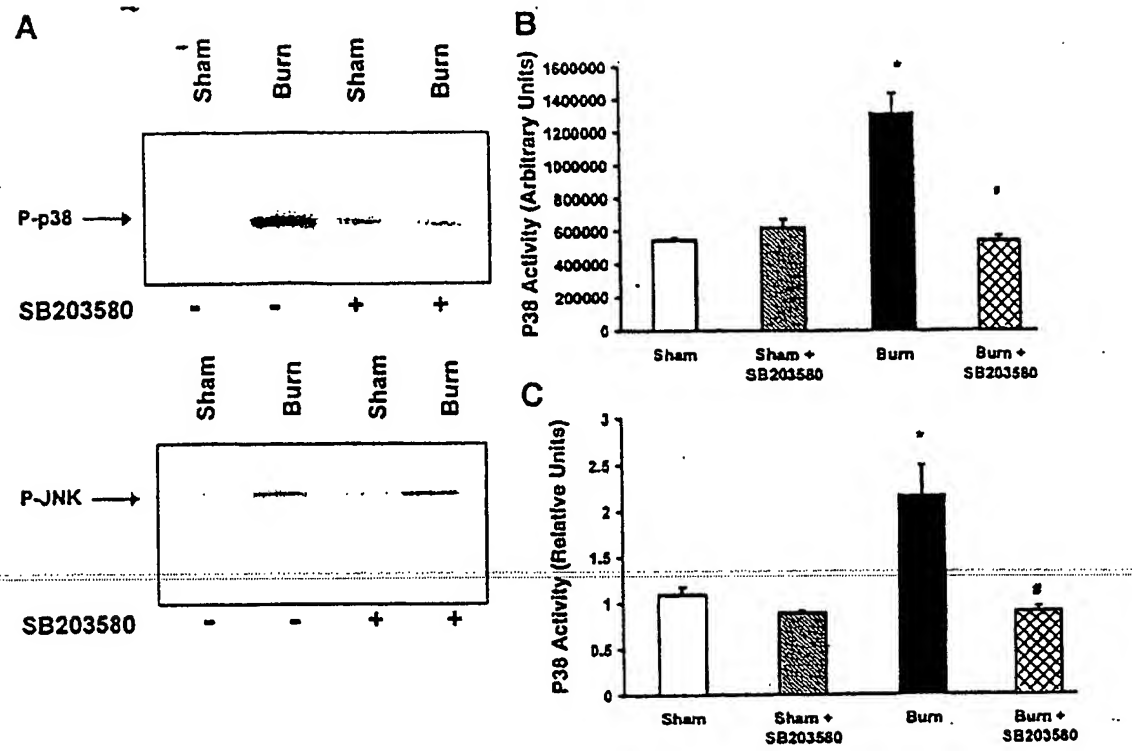

Fig. 5. Effects of SB203580 on burn-mediated activation of p38 MAPK and c-Jun NH_2-terminal kinase (JNK) in the heart. *A, top*: Western blot analysis with anti-active p38 MAPK antibody indicated that the burn-mediated increase in p38 MAPK activity (p-p38) at 2-h postburn was blocked by in vivo administration of SB203580. *Bottom*: Western blot analysis with anti-active JNK antibody demonstrated activation of JNK (p-JNK) 1-h postburn that was not inhibited by in vivo treatment with SB203580. + and −, Presence and absence, respectively, of SB203580. *B*: densitometric analysis of pooled anti-active p38 MAPK Western blots. *Significant elevation in p38 MAPK activity (indicated as p38 activity) in burn vs. sham rats, $P < 0.05$. #Significant difference in p38 MAPK activity in the SB203580-treated burn versus burn rats, $P < 0.05$. *C*: p38 MAPK assay confirmed that SB203580 prevented p38 MAPK activity (indicated as p38 activity) in burn rats. *Significant difference between burn and sham rats, $P < 0.05$. #Significant difference between vehicle-treated burn and SB203580-treated burn rats, $P < 0.05$.

Effects of MAPK Inhibition on Cardiac Myocyte Secretion of TNF-α

Primary cardiac myocytes were isolated from all four experimental groups (vehicle-treated sham, SB203580-treated sham, vehicle treated burn, and SB203580-treated burn rats). As shown in Fig. 6, burn trauma increased cardiac myocyte secretion of TNF-α ($P < 0.05$). Administration of the MAPK inhibitor during the postburn period significantly reduced this burn-mediated TNF-α response. Furthermore, MAPK inhibition during burn trauma produced cardiomyocyte TNF-α levels that were comparable to those measured in SB203580-treated sham burn rats.

As shown in Fig. 7, cardiomyocytes from vehicle-treated experimental groups responded to in vitro LPS challenge with a dose-dependent increase in TNF-α secretion ($P < 0.05$). However, cardiomyocytes harvested from vehicle-treated burn rats secreted significantly more TNF-α at each LPS concentration compared with the TNF-α responses measured in myocytes prepared from vehicle-treated sham rats ($P < 0.05$). Myocytes prepared from rats given SB203580 after burn trauma had reduced TNF-α responses to LPS challenge with significantly less TNF-α secreted at each LPS dose compared with those values measured in vehicle-treated burn rats ($P < 0.05$).

Fig. 6. Burn trauma produced a significant rise in cardiac myocyte secretion of tumor necrosis factor (TNF)-α at $P < 0.05$. All values are means ± SE. *Significant difference among groups, $P < 0.05$. †In vivo administration of the MAPK inhibitor SB203580 significantly reduced burn-mediated cytokine secretion by cardiac myocytes.

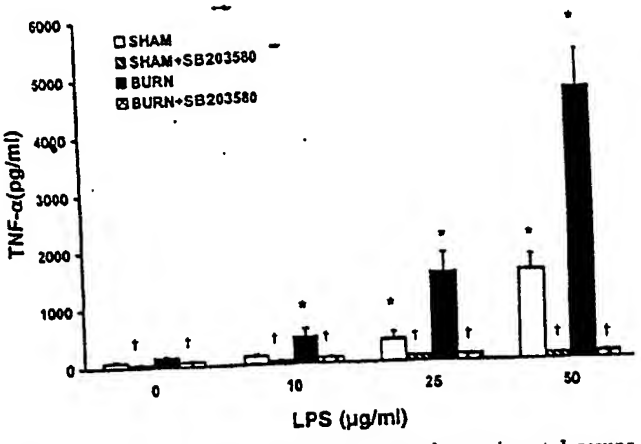

Fig. 7. Cardiac myocytes from vehicle-treated experimental groups responded to an in vitro lipopolysaccharide (LPS) challenge with a significant and dose-dependent increase in TNF-α secretion. All values are means ± SE. *Significant increase in cytokine secretion with LPS challenge compared with values measured in the respective experimental groups in the absence (0) of LPS. †Within each in vitro experimental challenge (i.e., at each LPS dose), in vivo administration of SB203580 reduced cardiomyocyte secretion of inflammatory cytokine by myocytes from both sham and burn rats (ANOVA and repeated measures).

In Vitro Effects of MAPK Inhibition on Cardiomyocyte Cytokine Secretion

Because the in vivo administration of the p38 MAPK inhibitor may affect cytokine production in both the reticuloendothelial system as well as by cardiac myocytes, the cell-specific effects of SB203580 on cardiac myocyte secretion of TNF-α were examined. This was accomplished by the in vitro addition of SB203580 to myocytes prepared from either sham burn or burn rats. The viability and morphological characteristics of myocytes harvested after exposure to either Tyrode solution alone or Tyrode solution containing SB203580 were nearly identical. As shown in Fig. 8, exposure of myocytes to SB203580 before LPS challenge significantly decreased myocyte secretion of TNF-α regardless of a previous burn injury. These data indicate the effects of p38 MAPK inhibition on TNF-α secretion were specific to the cardiac myocytes.

DISCUSSION

The data from this present study showed that burn trauma upregulated cardiac p38 MAPK activity, promoted secretion of the inflammatory cytokine TNF-α by cardiomyocytes, and impaired cardiac mechanical function. The in vivo administration of the selective p38 MAPK inhibitor SB203580 decreased burn-induced MAPK activity in the myocardium, abolished burn-mediated secretion of TNF-α by cardiac myocytes, and prevented postburn cardiac contractile dysfunction. In addition, in vitro treatment of cardiac myocytes with SB203580 inhibited the cytokine response elicited by LPS challenge.

We and others (34, 37, 48) confirmed that inflammatory cytokines such as TNF-α impair several aspects of cardiac contraction and relaxation. Further evidence that TNF-α produces cardiac contractile dysfunction has been provided by studies showing that 75-TNF receptor linked to the Fc portion of IgG-1 (an anti-TNF strategy) ablated systolic and diastolic cardiac dysfunction after experimental burn trauma or sepsis (24, 25) and in isolated hearts challenged with TNF-α (34). Because TNF-α mediates, at least in part, the cardiac mechanical defects that have been shown to occur after burn trauma, it was reasonable to expect that inhibiting one aspect of the signal transduction pathway that regulates TNF-α transcription and translation would provide a measure of postburn cardioprotection. Indeed, our finding that SB203580 inhibited cardiomyocyte secretion of TNF-α and prevented burn-mediated cardiac dysfunction is consistent with studies by Cain and colleagues (9), who reported that SB203580 diminished ischemia-induced TNF-α secretion and improved postischemic function in isolated atria trabeculae.

Because burn trauma elicits a systemic inflammatory cascade by stimulating cytokine synthesis in both cells of the reticuloendothelial system as well as in cardiac myocytes, the in vivo administration of SB203580 would likely interrupt several aspects of postburn inflammation. The question of whether this inhibitor would specifically target cardiac myocyte secretion of TNF-α was addressed by the in vitro studies where myocytes were pretreated with SB203580 before LPS challenge. The p38 MAPK inhibitor directly suppressed cytokine secretion elicited by LPS challenge of cardiac myocytes, suggesting that SB203580 can target cardiac myocytes.

Although little is known about the signaling pathway by which a cutaneous burn injury transmits an

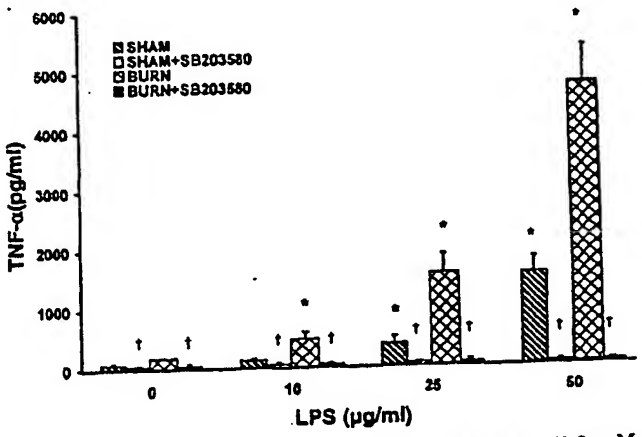

Fig. 8. These data describe the in vitro treatment (0.2 μM SB203580) of cardiac myocytes harvested after either sham or burn injury (24-h postburn). The addition of SB203580 to cardiac myocytes prepared from either sham or burn rats blunted the TNF secretory response to in vitro LPS challenge. All values are means ± SE. *Significant increase in cytokine secretion with LPS challenge compared with values measured in the respective experimental groups in the absence of LPS. †Within each in vitro experimental challenge (i.e., at each LPS dose), SB203580 reduced cardiomyocyte secretion of inflammatory cytokine by myocytes from both sham and burn rats (ANOVA and repeated measures).

extracellular stimulus to the nucleus to trigger an inflammatory response by cardiac myocytes, the data from this present study suggest that this pathway likely includes MAPK. Several previous studies (17, 18, 29, 30, 46, 54) proposed a significant role for LPS in this signaling cascade. It is well recognized that burn trauma promotes loss of gut mucosal barrier integrity and translocation of bacteria. While we failed to show a significant rise in serum LPS levels after burn trauma (unpublished data), the idea that LPS initiates a signal transduction pathway that culminates in cardiomyocyte TNF-α secretion has not been ruled out. In addition to LPS, it is clearly recognized that cutaneous burn promotes the formation of several reactive oxygen species (ROS) (31, 36), and several studies have suggested that ROS alter several aspects of inflammatory cytokine signaling. The in vivo administration of SB203580 in our study may have altered many of the upstream events, providing an indirect means of interrupting MAPK activation. There are no data, to our knowledge, regarding the effects of SB203580 on gut barrier function, LPS-LPS binding protein binding, or free radical generation. In this regard, Clerk and colleagues (12–14, 50) showed that ROS activate p38 MAPK pathway in cultured cardiac myocytes. Alternatively, emigration of activated leukocytes from the coronary microcirculation (35) or coronary endothelium-derived TNF-α (11) may serve as the initiating stimulus for postburn TNF-α secretion by cardiac myocytes. Because several putative burn-derived extracellular signals have been shown to activate p38 MAPK in other experimental models, our current finding that burn trauma upregulated the p38 MAPK pathway was not surprising.

Whereas the signal transduction cascade that regulates TNF-α synthesis and secretion by cardiac myocytes has not been defined in burn trauma, synthesis of inflammatory cytokines such as TNF-α by macrophages has been studied in considerable detail. In the macrophage population, LPS complexes with LPS binding protein and binds to CD14 (27, 57). Geppert et al. (23) have shown that the LPS-generated signal is then transmitted to regulate TNF-α transcription via the ras/raf-1/mitogen-activated protein or extracellular signal-regulated kinase (ERK) kinase (MEK)/ERK1,2 pathway (23). Similarly, Swantek et al. (53) showed that JNK activities are upregulated by macrophage exposure to LPS. In the present study, cardiomyocytes isolated from burn rats secreted significantly more TNF-α in response to LPS challenge than myocytes prepared from sham burn rats, and this effect was blocked by p38 MAPK inhibition with SB203580.

The MAPK inhibitor SB203580 is a pyridinyl imidiazole compound with potent inhibitory effects on cytokine production by LPS-stimulated human monocytes and thp-1 cells (a human monocytic cell line) (22, 42). In addition, the pyridinyl imidiazoles exhibit anti-inflammatory effects in several animal models (41) and have been shown to exert beneficial effects in experimental arthritis and in experimental endotoxin shock (4–6, 46). Although the specificity of SB203580 for p38 MAPK has been established by an absence of inhibitory effects of this compound on various other kinases (15), recently SB203580 was shown to inhibit JNK in rat neonatal ventricular myocytes. In these myocytes, the IC_{50} for p38 MAPK and JNK was 0.07 and 3–10 μM, respectively (14). Because 0.2 μM SB203580 was employed in this study, it was likely that this compound was specific for p38 MAPK at the dosage used. However, we chose to examine the effects of SB203580 on JNK activity in our model of burn trauma. Whereas burn injury produced significant JNK activation 1- and 2-h postburn, this activity was not inhibited by in vivo administration of SB203580, confirming the selectivity of this inhibitor for p38 MAPK.

While this present study confirms that burn trauma activates p38 MAPK in the myocardium, the downstream substrates for this kinase group within the heart remain undefined. One potential target in the p38 MAPK pathway is the redox-sensitive transcription factor NF-κB. Nuclear translocation of NF-κB has been shown to occur in the heart after burn trauma (32), and previous studies (43, 44) have confirmed that p38 MAPK activity promotes NF-κB activation in several tissues. Because NF-κB is one of the transcription factors involved in TNF-α gene transcription, it is likely that burn trauma and p38 MAPK upregulation promote the release of inflammatory cytokines via a NF-κB-dependent mechanism. In addition, AP1, a transcription factor that is also activated by p38 MAPK, may play a role in the transcriptional regulation of postburn inflammatory cytokine production. It must also be considered that the upregulation of the p38 MAPK pathway after burn trauma may induce inflammatory enzymes such as inducible nitric oxide synthase and cyclooxygenase-2 as well as the increased expression of adhesion proteins such as vascular cellular adhesion molecule-1 (5, 16, 26, 49).

While much of the previous work examining the activation and regulation of p38 MAPK pathway used noncardiac myocyte cells, this pathway is likely of primary importance in the myocardium under stressful conditions such as ischemia and reperfusion, trauma with blood loss, and burn trauma. The data from this present study clearly indicate that this kinase pathway is activated by burn trauma, and activation of this pathway occurs early in the postburn period (1 h) and occurs before other signaling events within the myocardium, such as nuclear translocation of NF-κB and cardiomyocyte secretion of TNF-α (32). Clear definition of the p38 MAPK pathway, including delineating upstream activators of this pathway as well as downstream targets, will likely provide potential sites for therapeutic intervention after major traumatic injury.

REFERENCES

1. Abraham E, Glauser MP, Butler T, Barbino J, Gelmont D, Laterre PF, Kudsk K, Ha HAB, Otto C, Tobin E, Zwingelstein C, Lesslauer W, and Leighton A. p55 Tumor necrosis factor receptor fusion protein in the treatment of patients with severe sepsis and septic shock. A randomized controlled multicenter trial. Ro 45-2081 Study Group. *JAMA* 277: 1531–1538, 1997.

2. Abraham E, Wunderink R, Silverman H, Perl TM, Nasraway S, Levy H, Bone R, Wenzel RP, Balk R, Allred R, Pennington JE, and Wherry JC. Efficacy and safety of monoclonal antibody to human tumor necrosis factor alpha in patients with sepsis syndrome. *JAMA* 273: 934–941, 1995.
3. Adams HR, Baxter CR, and Izenberg SD. Decreased contractility and compliance of the left ventricle as complications of thermal trauma. *Am Heart J* 108: 1477–1487, 1984.
4. Badger AM, Bradbeer JN, Votta B, Lee JC, Adams JL, and Griswold DE. Pharmacological profile of SB203580, a selective inhibitor of cytokine suppressive binding protein/p38 kinase, in animal models of arthritis, bone resorption, endotoxin shock and immune function. *J Pharmacol Exp Ther* 279: 1452–1461, 1996.
5. Badger AM, Cook MN, Lark MW, Newman-Tarr TM, Swift BA, Nelson AH, Barone FC, and Kumar S. SB 203580 inhibits p38 mitogen-activated protein kinase, nitric oxide production, and inducible nitric oxide synthase in bovine cartilage-derived chondrocytes. *J Immunol* 161: 467–473, 1998.
6. Badger AM, Olivera D, Talmadge JE, and Hanna N. Protective effect of SK&F 86002, a novel dual inhibitor of arachidonic acid metabolism, in murine models of endotoxin shock: Inhibition of tumor necrosis factor as a possible mechanism of action. *Circ Shock* 27: 51–61, 1989.
7. Bryant D, Becker L, Richardson J, Shelton J, Franco F, Peshock R, Thompson M, and Giroir B. Cardiac failure in transgenic mice with myocardial expression of tumor necrosis factor-alpha. *Circulation* 97: 1375–1381, 1998.
8. Cain BS, Harken AH, and Meldrum DR. Therapeutic strategies to reduce TNF-α mediated cardiac contractile depression following ischemia and reperfusion. *J Mol Cell Cardiol* 31: 931–947, 1999.
9. Cain BS, Meldrum DR, Dinarello CA, Meng X, Joo KS, Banergee A, and Harken AH. Tumor necrosis factor-α and interleukin-1β synergistically depress human myocardial function. *Crit Care Med* 27: 1309–1318, 1999.
10. Cain BS, Meldrum DR, Meng X, Dinarello CA, Shames BO, Banerjee A, and Harken AH. p38 MAPK inhibition decreases TNF-α production and enhances postischemic human myocardial function. *J Surg Res* 83: 7–12, 1999.
11. Chan EL, Haudek SB, and Murphy JT. NF-κB regulation of TNF-α mRNA expression in endotoxin stressed human coronary endothelial cells. *National ACS Committee On Trauma Resident Paper Competition, Reno, Nevada.* March 9, 2000.
12. Clerk A, Michael A, and Sugden PH. Stimulation of multiple mitogen-activated protein kinase sub-families by oxidative stress and phosphorylation of the small heat shock protein, HSP25/27, in neonatal ventricular myocytes. *Biochem J* 333: 581–589, 1998.
13. Clerk A and Sugden PH. Mitogen-activated protein kinases are activated by oxidative stress and cytokines in neonatal rat ventricular myocytes (Abstract). *Biochem Soc Trans* 25: 566S, 1997.
14. Clerk A and Sugden PH. The p38 MAPK inhibitor, SB203580, inhibits cardiac stress-activated protein kinases/C-jun N-terminal kinases (SAPKs/JNKs). *FEBS Lett* 426: 93–96, 1998.
15. Cuenda A, Royse J, Doza YN, Meier R, Cohen P, Gallagher TF, Young PR, and Lee JC. SB203580 is a specific inhibitor of a MAP kinase homologue which is stimulated by cellular stresses and interleukin-1. *FEBS Lett* 364: 229–233, 1995.
16. Davis RJ. Transcriptional regulation by MAP kinases. *Mol Reprod Dev* 42: 459–467, 1995.
17. Deitch EA and Bridges RM. Effect of stress and trauma on bacterial translocation from the gut. *J Surg Res* 42: 536–542, 1987.
18. Deitch EA, Winterton J, and Berg R. Thermal injury promotes bacterial translocation from the gastrointestinal tract in mice with impaired T-cell-mediated immunity. *Arch Surg* 121: 97–101, 1986.
19. Dinarello CA, Gelfand JA, and Wolff SM. Anticytokine strategies in the treatment of the systemic inflammatory response syndrome. *JAMA* 269: 1829–1835, 1993.
20. Evans TJ, Moyes D, Carpenter A, Martin R, Loetscher H, Lesslauer W, and Cohen J. Protective effect of 55- but not 75-kDa soluble tumor necrosis factor receptor-immunoglobin G fusion proteins in an animal model of gram-negative sepsis. *J Exp Med* 180: 2173–2179, 1994.
21. Fisher SCJ, Opal SM, Dhainaut JF, Stephens S, Zimmerman JL, Nightingale P, Harris SJ, Schein RMH, Panacep EA, Vincent JL, Foulke GE, Warren EL, Garrard C, Park G, Bodmer MW, Cohen J, Linden CV, Cross AS, and Sadoff JC. Influence of an anti-tumor necrosis factor monoclonal antibody on cytokine levels in patients with sepsis. *Crit Care Med* 21: 318–327, 1993.
22. Gallager TF, Fier-Thompson SM, Garigipati RS, Sorenson ME, Smietana JM, Lee D, Bender PE, Lee JC, Laydon JT, Griswold DE, Chabot-Fletcher MD, Breton JJ, and Adams JL. 2,4,5-Triarylimidiazole inhibitors of IL-1 biosynthesis. *Bioorg Med Chem* 5: 1171–1176, 1995.
23. Geppert TD, Whitehurst CE, Thompson P, and Beutler KBK. Lipopolysaccharide signals activation of tumor necrosis factor biosynthesis through the Ras/Raf-1/MEK/MAPK pathway. *Mol Med* 1: 93–103, 1994.
24. Giroir B, Arteaga G, White J, and Horton J. Prevention of endotoxin-induced myocardial dysfunction with TNF blockade or IL-1 blockade (Abstract). *Crit Care Med* 24, *Suppl*: A144, 1996.
25. Giroir BP, Horton JW, White DJ, McIntyre KL, and Lin CQ. Inhibition of tumor necrosis factor prevents myocardial dysfunction during burn shock. *Am J Physiol Heart Circ Physiol* 267: H118–H124, 1994.
26. Guan Z, Buckman SY, Pentland AP, Templeton DJ, and Morrison AR. Induction of cyclooxygenase-2 by the activated MEKK1→SEK1/MKK4→p38 mitogen-activated protein kinase pathway. *J Biol Chem* 273: 12901–12908, 1998.
27. Hailman E, Lichenstein HS, Wurfel MM, Miller DS, Johnson Da Kelley M, Busse LA, Zakowski MM, and Wright SD. Lipopolysaccharide (LPS)-binding protein accelerates the binding of LPS to CD14. *J Exp Med* 179: 269–277, 1994.
28. Han J, Lee JD, Tobias PS, and Ulevitch RJ. Endotoxin induces rapid tyrosine phosphorylation in 70Z/3 cells expressing CD14. *J Biol Chem* 268: 25009–25014, 1993.
29. Herndon DN and Zeigler ST. Bacterial translocation after thermal injury. *Crit Care Med* 21: 50–54, 1993.
30. Horton JW. Bacterial translocation after burn injury: the contribution of ischemia and permeability changes. *Shock* 4: 286–290, 1994.
31. Horton JW. Oxygen free radicals contribute to postburn cardiac cell membrane dysfunction. *J Surg Res* 61: 97–102, 1996.
32. Horton J, Maass D, Haudek S, and Giroir B. The role of NF-κB in cardiac TNF-α secretion after trauma (Abstract). *Proc Am Assoc Surg Trauma*, 1999.
33. Horton JW, Maass D, White J, and Sanders B. Nitric oxide modulation of TNF-α induced cardiac contractile dysfunction is concentration dependent. *Am J Physiol Heart Circ Physiol* 278: H1955–H1965, 2000.
34. Horton JW, Maass D, White J, and Sanders B. Hypertonic saline dextran suppresses burn-related cytokine secretion by cardiomyocytes. *Am J Physiol Heart Circ Physiol* 280: 1591–1601, 2001.
35. Horton JW, Mileski WJ, White DJ, and Lipsky P. Monoclonal antibody to intercellular adhesion molecule-1 reduces cardiac contractile dysfunction after burn injury in rabbits. *J Surg Res* 64: 49–56, 1996.
36. Horton JW and White DJ. Role of xanthine oxidase and leukocytes in postburn cardiac dysfunction. *J Am Coll Surg* 181: 129–137, 1995.
37. Kappadia S, Lee J, Torre-Amione G, Birdsall HH, Ma TS, and Mann DL. Tumor necrosis factor-α gene and protein expression in adult feline myocardium after endotoxin administration. *J Clin Invest* 96: 1042–1052, 1995.
38. Keller RS, Parker JL, Adams HR, and Rubin LJ. Contractile dysfunction and inositol phosphates in ventricular myocytes isolated from endotoxemic guinea pigs (Abstract). *Circ Shock* 37: 29, 1992.
39. Kumar A, Thota V, Dee L, Olson J, Uretz E, and Parillo JE. Tumor necrosis factor-alpha and interleukin 1-beta are responsible for the in vitro myocardial cell depression induced by human septic shock serum. *J Exp Med* 183: 949–958, 1996.

40. Lavoie JN, Lambert H, Hickey E, Weber LA, and Landry J. Modulation of cellular thermoresistance and actin filament stability accompanies phosphorylation-induced changes in the oligomeric structure of heat shock protein 27. *Mol Cell Biol* 15: 505–516, 1995.
41. Lee JC, Badger AM, Griswold DE, Dunnington D, Truneh A, Votta B, White JR, Young PR, and Bender PE. Bicyclic imidiazoles as a novel class of cytokine biosynthesis inhibitors. *Ann NY Acad Sci* 696: 149–170, 1993.
42. Lee JC, Laydon JT, McDonnel PC, Gallagher TF, Kumar S, Green D, McNulty D, Blumenthal MJ, Heys JR, Landvatter SW, Strickler JE, McLaughlin MM, Siemens IR, Fisher SM, Livi GP, White JR, Adams JL, and Young PR. A protein kinase involved in the regulation of inflammatory cytokine biosynthesis. *Nature* 372: 739–745, 1994.
43. Maulik N, Sato M, Price BD, and Das DK. An essential role of NF-κB in tyrosine kinase signaling of p38 MAP kinase regulation of myocardial adaptation to ischemia. *FEBS Lett* 429: 365–369, 1998.
44. Meldrum DR. Tumor necrosis factor in the heart. *Am J Physiol Regulatory Integrative Comp Physiol* 274: R577–R595, 1998.
45. Meldrum DR, Shenkar R, Sheridan BC, Cain BS, Abraham E, and Harken AH. Hemorrhage activates myocardial NF-κB and increases tumor necrosis factor in the heart. *J Mol Cell Cardiol* 29: 2849–2854, 1997.
46. Olivera DL, Esser KM, Lee JC, Greig RG, and Badger AM. Beneficial effects of SK&F 105809, a novel cytokine-suppressive agent, in murine models of endotoxin shock. *Circ Shock* 37: 301–306, 1992.
47. Ono K and Han J. The p38 signal transduction pathway: Activation and function. *Cell Signal* 12: 1–13, 2000.
48. Oral H, Dorn GW, and Mann DL. Sphingosine mediates the immediate negative inotropic effects of tumor necrosis factor-α in the adult mammalian cardiac myocyte. *J Biol Chem* 272: 4836–4842, 1997.
49. Pietersma A, Tilly BC, Gaestel M, de Jong N, Lee JC, Koster JF, and Sluiter W. p38 Mitogen activated protein kinase regulates endothelial VCAM-1 expression at the post-transcriptional level. *Biochem Biophys Res Commun* 230: 44–48, 1997.
50. Seko Y, Takahashi N, Tobe K, Kadowaki T, and Yazaki Y. Hypoxia and hypoxia/reoxygenation activate p65^{PAK}, p38 mitogen-activated protein kinase (MAPK), and stress-activated protein kinase (SAPK) in cultured rat cardiac myocytes. *Biochem Biophys Res Commun* 239: 840–844, 1997.
51. She QB, Chen N, and Dong Z. ERKs and p38 kinase phosphorylate p53 protein at serine 14 in response to UV radiation. *J Biol Chem* 275: 20444–20449, 2000.
52. Sugden PH and Clerk A. "Stress-responsive" mitogen-activated protein kinases (c-Jun N-terminal kinases and p38 mitogen-activated protein kinases) in the myocardium. *Circ Res* 83: 345–352, 1998.
53. Swantek JL, Cobb MH, and Geppert TD. Jun N-terminal kinase/stress-activated protein kinase (JNK/SAPK) is required for lipopolysaccharide stimulation of tumor necrosis factor alpha (TNF-α) translation: glycacorticoids inhibit TNF-α translation by blocking JNK/SAPK. *Mol Cell Biol* 17: 6274–6282, 1997.
54. Tokyay R, Zeigler ST, Traver DL, Stothert JC Jr, Loick HM, Heggers JP, and Herndon DN. Postburn gastrointestinal vasoconstriction increases bacterial and endotoxin translocation. *J Appl Physiol* 74: 1521–1527, 1993.
55. Wang Y, Huang S, Sah VP, Ross J, Brown JH, Han J, and Chien KR. Cardiac muscle cell hypertrophy and apoptosis induced by distinct members of the p38 mitogen-activated protein kinase family. *J Biol Chem* 273: 2161–2168, 1998.
56. Weinbrenner C, Liu GS, Cohen MV, and Downey JM. Phosphorylation of tyrosine 182 of p38 mitogen-activated protein kinase correlates with the protection of preconditioning in the rabbit heart. *J Mol Cell Cardiol* 29: 2383–2391, 1997.
57. Wright SD, Ramos RA, Tobias PS, Ulevitch RJ, and Mathison JC. CD14, a receptor for complexes of lipopolysaccharide (LPS) and LPS binding protein. *Science* 249: 1431–1433, 1990.
58. Yokoyama T, Vaca L, Rossen RD, Durante W, Hazarika P, and Mann DL. Cellular basis for the negative inotropic effects of tumor necrosis factor-α in the adult mammalian cardiac myocyte. *J Clin Invest* 92: 2303–2312, 1993.

Exhibit 6

INHIBITION OF P38 MITOGEN-ACTIVATED PROTEIN KINASE SUPPRESSES INTERLEUKIN-1β-EXPRESSION AND PREVENTS PROGRESSION OF CARDIAC HYPERTROPHY AND CONGESTIVE HEART FAILURE IN RATS.

Akira Shimamoto, Tomoyuki Oda, Hiroshi Kodama, Masahiro Shimada, Shinji Kanemitsu, Kazuya Fujinaga, Motoshi Takao, Kòji Onoda, Takatsugu Shimono, Kuniyoshi Tanaka, Hideto Shimpo, Isao Yada, MIE Univ Sch of Medicine, Tsu Japan

Background: Proinflammatory cytokines have been reported to participate in cardiac hypertrophy and congestive heart failure (CHF) induced by mechanical overload. Intercellular signaling leading to proinflammatory cytokine production involves p38 mitogen-activated protein kinase (MAPK). We evaluated the effects of a p38 MAPK inhibitor in Dahl salt-sensitive rats (DS) with hypertension-induced left ventricular (LV) hypertrophy at risk of progression to CHF. Methods: DS rats were divided into four groups: a 7W in which a p38 MAPK inhibitor (FR167653; 2 mg/kg/day) was administered from age 7 weeks when we initiated a high-salt diet in all groups; an 11W in which FR167653 was administered beginning at 11 weeks, when concentric LV hypertrophy appeared; a 15W in which FR167653 was administered beginning at 15 weeks, when CHF developed; and an untreated group (UN). Dahl salt-resistant rats (DR), a control group, were not given FR167653. Results: At 19 weeks of age, interleukin-1β(IL-1β) mRNA expression was significantly less in all treated groups than in UN ($p<.01$), indeed nearly the same as in DR. Expression of monocyte chemoattractant protein-1 (MCP-1) mRNA and the number of macrophages in LV did not decrease in any treated group. Echocardiographical findings indicated the presence of LV concentric hypertrophy in 11W and LV wall dilation in 15W, but no such changes in 7W, and preserved LV wall motion in all treated groups. Hypertrophy of myocytes and increased interstitial fibrosis were observed in LV sections from 11W, 15W, and UN but not in 7W or DR. All UN had died of pulmonary congestion due to LV dysfunction by 22 weeks. The survival rate at 22 weeks was 90% in 7W, 50% in 11W, and 30% in 15W groups. Kaplan-Meier survival analysis demonstrated a significant improvement in 7W ($p=.0015$) and 11W ($p=.0320$) compared with UN. Conclusion: The p38 MAPK inhibitor suppressed IL-1βproduction by macrophages infiltrating the LV in response to MCP-1. The inhibitor prevented progression of cardiac hypertrophy and CHF.

Exhibit 7

Role of p38 Mitogen-Activated Protein Kinase in a Murine Model of Pulmonary Inflammation[1]

Jerry A. Nick,[2*†] Scott K. Young,[*] Kevin K. Brown,[*†] Natalie J. Avdi,[*] Patrick G. Arndt,[*†] Benjamin T. Suratt,[*†] Michael S. Janes,[‡] Peter M. Henson,[‡] and G. Scott Worthen[*†§]

Early inflammatory events include cytokine release, activation, and rapid accumulation of neutrophils, with subsequent recruitment of mononuclear cells. The p38 mitogen-activated protein kinase (MAPK) intracellular signaling pathway plays a central role in regulating a wide range of inflammatory responses in many different cells. A murine model of mild LPS-induced lung inflammation was developed to investigate the role of the p38 MAPK pathway in the initiation of pulmonary inflammation. A novel p38 MAPK inhibitor, M39, was used to determine the functional consequences of p38 MAPK activation. In vitro exposure to M39 inhibited p38 MAPK activity in LPS-stimulated murine and human neutrophils and macrophages, blocked TNF-α and macrophage inflammatory protein-2 (MIP-2) release, and eliminated migration of murine neutrophils toward the chemokines MIP-2 and KC. In contrast, alveolar macrophages required a 1000-fold greater concentration of M39 to block release of TNF-α and MIP-2. Systemic inhibition of p38 MAPK resulted in significant decreases in the release of TNF-α and neutrophil accumulation in the airspaces following intratracheal administration of LPS. Recovery of MIP-2 and KC from the airspaces was not affected by inhibition of p38 MAPK, and accumulation of mononuclear cells was not significantly reduced. When KC was instilled as a proinflammatory stimulus, neutrophil accumulation was significantly decreased by p38 MAPK inhibition independent of TNF-α or LPS. Together, these results demonstrate a much greater dependence on the p38 MAPK cascade in the neutrophil when compared with other leukocytes, and suggest a means of selectively studying and potentially modulating early inflammation in the lung. *The Journal of Immunology*, 2000, 164: 2151–2159.

The rapid accumulation of neutrophils to the lung in response to a proinflammatory stimulus is one of the first recognizable events in the pathogenesis of many pulmonary diseases. The process by which neutrophils cross the pulmonary vasculature, migrate through the lung interstitium, and ultimately accumulate in the airways requires complex interactions between circulating leukocytes and the cells of the lung (1). Although many aspects of neutrophil accumulation are poorly understood, a number of discrete events have been identified. In health, a significant proportion of the circulating neutrophils are passing through the lung capillary bed at any point in time, contributing to the marginating pool (2). In the setting of lung injury, effective migration and accumulation of neutrophils into the airspaces requires coordinated responses including up-regulation of adhesion molecules, cytoskeletal rearrangement, increases in cell size and stiffness, and chemotaxis (2–4). To a large extent, cytokines and other soluble proinflammatory stimuli orchestrate the responses of the leukocytes. Synthesis of cytokines by the neutrophil itself may serve to amplify and perpetuate the recruitment of leukocytes to the airspaces in certain disease states (5). Monocyte and macrophage accumulation in the lung typically occurs following an initial recruitment of neutrophils. In some animal models of acute inflammation, accumulation of monocytes in the lung was found to be neutrophil dependent (6).

Of particular interest is the ability of LPS to induce lung inflammation, as local or systemic endotoxin release is an important feature of many diseases, including focal pneumonias, cystic fibrosis, and the acute respiratory distress syndrome. LPS is not an effective chemoattractant for neutrophils, but can trigger an inflammatory cascade via the synthesis of cytokines and other proinflammatory mediators by resident alveolar macrophages (AM),[3] local mast cells, fibroblasts, epithelia, and endothelial cells. The release of TNF-α and neutrophil-directed chemokines such as IL-8 are essential to early LPS-mediated neutrophil recruitment.

The combined effects of TNF-α and IL-8 on neutrophil recruitment are complex and incompletely understood. Known roles of TNF-α include activation of endothelial cells to express adherence proteins, induction of an array of secondary inflammatory mediators, and "priming" of neutrophils for enhanced phagocytic and bactericidal activity (7). Through studies with specific Abs and genetically modified mice, the requirement for TNF-α in the pathogenesis of LPS-induced shock and tissue injury has been confirmed. However, these techniques do not allow for selective reduction of the release of TNF-α by a cell type, nor modulation of the ability of neutrophils to respond to TNF-α. As a single agent, TNF-α also does not induce chemotaxis of neutrophils. However, the ELR(+)CXC chemokine IL-8 is one of the most specific neutrophil chemoattractants yet described (8–10). IL-8 has not been

Departments of *Medicine and ‡Pediatrics, and §Program in Molecular Signal Transduction, National Jewish Medical and Research Center, Denver, CO 80206; and †Division of Pulmonary Science and Critical Care Medicine, University of Colorado School of Medicine, Denver, CO 80262

Received for publication June 11, 1999. Accepted for publication December 9, 1999.

The costs of publication of this article were defrayed in part by the payment of page charges. This article must therefore be hereby marked *advertisement* in accordance with 18 U.S.C. Section 1734 solely to indicate this fact.

[1] This work was supported by Grants K08 HL03657, HL-40784, HL-34303, HL-09640, and GM-30324 from the National Institutes of Health.

[2] Address correspondence and reprint requests to Dr. Jerry A. Nick, National Jewish Medical and Research Center, D403, 1400 Jackson Street, Denver, CO 80206. E-mail address: nickj@njc.org

[3] Abbreviations used in this paper: AM, alveolar macrophages; ATF-2, activated transcription factor-2; BAL, bronchial alveolar lavage; ERK, extracellular signal-regulated kinases; JNK, c-Jun NH_2-terminal kinase; MAPK, mitogen-activated protein kinase; MIP-2, macrophage inflammatory protein-2; MPO, myeloperoxidase.

0022-1767/00/$02.00

identified in mice. but macrophage inflammatory protein-2 (MIP-2) and KC share the same ELR(+)CXC structure and act as functional homologue of human IL-8 (11, 12).

Selective responses of cells to external stimuli may be understood through differential activation of intracellular signaling mechanisms. The mitogen-activated protein kinase (MAPK) superfamily are highly conserved signaling kinases that regulate cell growth, differentiation, and stress responses (13). At least three distinct families of MAPKs exist in mammalian cells: the p42/44 extracellular signal-regulated kinase (ERK) MAPKs, c-Jun NH_2-terminal kinases (JNKs), and p38 MAPK (14–16). Both the coordinated release of cytokines by host defense cells and the functional response of neutrophils to cytokines and other proinflammatory agents are to varying degrees regulated by p38 MAPK. In the neutrophil, p38α MAPK is activated in response to many stimuli, including LPS and TNF-α (17, 18). Once activated, p38α MAPK is capable of modulating functional responses through phosphorylation of transcription factors and activation of other kinases. In LPS-stimulated neutrophils, p38α MAPK regulates distinctly different functions, including adhesion, activation of NF-κB, and the synthesis of TNF-α and IL-8 (19–21). In neutrophils stimulated with the chemoattractant FMLP, activation of p38α MAPK regulates both superoxide anion release and chemotaxis (19, 20). In the LPS-stimulated monocyte/macrophage, inhibition of p38α MAPK blocks TNF-α and IL-8 release (16, 22). In cells other than leukocytes, p38 MAPK also regulates stress-responses, including release of IL-8 by bronchial epithelial cells in response to TNF-α or other inflammatory stimuli (23). LPS stimulation also causes activation of p38 MAPK in endothelial cells, resulting in up-regulation of the ICAM-1 adhesion molecule (24).

Given this central role of p38 MAPK as a regulator of multiple inflammatory responses in many diverse cell types, we questioned the effect of in vivo p38 MAPK inhibition on neutrophil accumulation in the lung. For these studies, we employed a murine model of mild pulmonary inflammation in response to a single administration of LPS in the airspace. Inhibition of p38α MAPK was accomplished with the novel compound M39, which is the most highly selective and potent inhibitor of p38 MAPK described to date (25). We studied the effects of selective inhibition of p38 MAPK on several events critical in the pathogenesis of the early inflammatory response of the murine lung. Herein we report that in vitro inhibition of p38 MAPK resulted in a significant decrease in murine neutrophil function, but a limited effect on other inflammatory responses. In vivo, this resulted in the loss of initial neutrophil recruitment to the airspaces, while later accumulation of mononuclear cells remained largely intact. Together, these data indicate the potential for relatively selective in vivo inhibition of neutrophilic responses.

Materials and Methods

Materials

Endotoxin-free reagents and plastics were used in all experiments. Aprotinin, leupeptin, Tris-HCl, Triton X-100, igepal, PMSF, EDTA, EGTA, Nonidet P-40, and protein A-Sepharose were purchased from Sigma (St. Louis, MO), and [γ-^{32}P]ATP was purchased from Amersham (Arlington Heights, IL). M39 [(*S*)-5-[2-(1-phenylethylamino)pyrimidin-4-yl]-1-methyl-4-(3-trifluoromethylphenyl)-2-(4-piperidinyl) imidazole] was provided by Merck (Rahway, NJ) and stored in DMSO at −20°C. LPS was purified from *Escherichia coli* 0111:B4 (List Biological Laboratories, Campbell, CA). Recombinant KC and MIP-2 were purchased from R&D Systems (Minneapolis, MN). Activated transcription factor (ATF)-2_{1-110} was prepared as previously described (17, 19).

Animals

Female C57BL/6 mice (Harlan Sprague Dawley, Indianapolis, IN), 6–12 wk of age and weighing 16–20 g, were used in all experiments. They were given commercial pellet food and water ad libitum. All experiments were performed in accordance with the Animal Welfare Act and the U.S. Public Health Service Policy on Humane Care and Use of Laboratory Animals after review of the protocol by the Animal Care and Use Committee of the National Jewish Medical and Research Center. Anesthesia was provided by a single i.p. injection of 333 mg/kg avertin. Avertin was prepared by mixing 10 g tribromoethyl alcohol (Aldrich, Milwaukee, WI) with 10 ml tertiary amyl alcohol (Aldrich) and diluting this stock to a 2.5% solution in sterile saline.

Murine bronchial alveolar lavage (BAL)

BAL was performed immediately following sacrifice of the animals by pentobarbital overdose or cervical dislocation. The procedure was performed with the lungs in situ but with the chest cavity opened by midline incision. The trachea was intubated orally or directly through a small cutdown of the skin overlying the trachea with a 20-g angiocath (Baxter Quik-Cath, Baxter Health Care, Deerfield, IL). Two to four 0.8-ml aliquots of saline with 20 U/ml heparin were instilled and sequentially removed by gentle hand suction with a 1-ml syringe. The volume of BAL recovered was quantified and cells recovered were counted in a hemocytometer. Cell types were determined by Wright staining of a spun sample. All slides were counted twice by different observers blinded to the status of the animal. Samples for cytokine analysis were immediately frozen in a dry ice/ethanol bath and stored at −70°C.

Isolation of cells

Human neutrophils were isolated by the plasma Percoll method (26) and suspended in Krebs-Ringer phosphate buffer with 0.2% dextrose at pH 7.2 or in RPMI 1640 culture medium (BioWhittaker, Walkersville, MD). Mature murine bone marrow neutrophils were isolated from mouse femurs and tibias. Animals were sacrificed by cervical dislocation, and the bones were dissected. Both ends of each bone were removed, and a 25-gauge needle on a 5-ml syringe containing HBSS (without calcium, magnesium, bicarbonate, or phenol red) was employed to express marrow from the bones. Marrow cords were collected in a 50-ml polypropylene conical tube (Becton Dickinson, Bedford, MA) and subsequently resuspended by gentle aspiration of the suspension through a 19-gauge needle. The marrow cells were pelleted by centrifugation at 112 × *g* for 6 min, washed once with HBSS, and resuspended in HBSS to a final volume of 2 ml in preparation for density gradient centrifugation. A stock solution of Percoll (100% fine grade; Pharmacia Fine Chemicals, Piscataway, NJ) was prepared in 10× HBSS in a ratio of 9:1 (v/v) Percoll:10× HBSS. A 3 × 2-ml Percoll discontinuous density gradient (72, 64, and 52% with 1× HBSS) was prepared in a 15-ml polypropylene conical tube (Becton Dickinson). The marrow suspension was layered on top of the Percoll gradient and centrifuged at 1060 × *g* for 30 min. Morphologically mature appearing neutrophils at a concentration of >95% formed a band at the interface of the 64 and 72% Percoll layers. This band was carefully aspirated and mixed with 12 ml of 1× HBSS in a 15-ml conical tube, centrifuged at 112 × *g* for 6 min, washed twice with 1× HBSS, and resuspended in 1× HBSS to a volume of 2 ml and counted by hemocytometer. Typical yields were ~1–2 × 10^7 mature bone marrow neutrophils per mouse. In separate studies, the marrow neutrophils were shown to have equivalent functional responses and recirculation patterns when compared with peripheral murine neutrophils (B.T.S., unpublished observations). Murine peripheral blood neutrophils were isolated by modification of methods previously reported (27) for the purification of rabbit peripheral neutrophils. Mice were volume expanded and exsanguinated into a 3.8% citrate solution followed by centrifugation at 300 × *g* for 20 min. The cell pellet was resuspended in 6% dextran and 0.9% NaCl solution (in a ratio of 1:5.25, dextran:saline) to a final volume of 150% the original blood volume and sedimented at unity gravity for 30 min. The leukocyte-rich supernatant was aspirated, washed once in HBSS, layered over a Percoll gradient (78, 66, and 54%) and centrifuged at 1060 × *g* for 30 min. Cytospun samples of the dense band revealed >90% neutrophils. Following lysis with hypotonic saline, typical yields were ~2–4 × 10^5 peripheral blood neutrophils per mouse. Trypan blue dye exclusion showed the cells to be >97% viable following purification. Murine AM were isolated by two sequential BALs. Typical yields were ~2 × 10^5 cells per mouse and were 97–99% AM as assessed by Wright staining of spun samples.

Neutrophil functional assays

All experiments were done in the presence of 1% human or murine heat-inactivated platelet-poor plasma. Cytokine release assays were performed with murine neutrophils isolated from peripheral blood or murine AM resuspended in RPMI 1640 containing 2% murine heat-inactivated platelet-poor plasma at a concentration of 5 × 10^6 cells/ml. One milliliter of cells

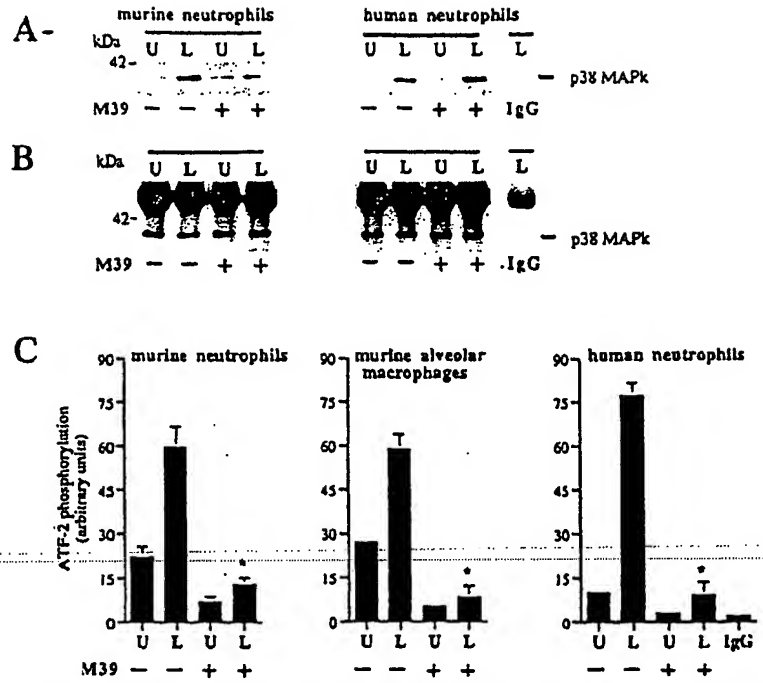

FIGURE 1. M39 inhibits LPS-induced activation of p38α MAPK in the murine neutrophil. *A*, Tyrosine phosphorylation of p38α MAPK. Murine and human neutrophils (4×10^6 per condition) were exposed to M39 (1 μM) for 60 min at 37°C or left untreated, then stimulated with LPS (100 ng/ml) for 20 min at 37°C (L) or left unstimulated (U). The cells were lysed, and p38α MAPK was immunoprecipitated and separated by SDS-PAGE. Western blots were probed with an anti-phosphotyrosine Ab capable of reacting with phosphorylated tyrosine residues of p38α MAPK. A nonimmune IgG control is shown in *lane 5* for human neutrophils to confirm the specificity of our p38α MAPK antiserum. *B*, Equivalent immunoprecipitation of p38α MAPK. Blots from *A* were reprobed with an anti-p38 MAPK Ab to demonstrate an equal amount of p38 MAPK immunoprecipitated for each condition studied. *C*, Activation of p38α MAPK. p38α MAPK was immunoprecipitated from the lysates depicted in *A* and *B* and combined with $ATF\text{-}2_{1-110}$ in the presence of [^{32}P]ATP. The peptide was subjected to SDS-PAGE, and the amount of [^{32}P] phosphorylation of $ATF\text{-}2_{1-110}$ was assessed by phosphor screen autoradiography. Under identical conditions, p38α MAPK immunoprecipitated from murine AM was also analyzed for inhibition by M39. Immunoprecipitation with the nonimmune IgG control shown in *lane 5* of *A* and *B* for human neutrophils confirmed a lack of nonspecific phosphorylation of $ATF\text{-}2_{1-110}$. Plots depict means ± SEM from three consecutive experiments expressed in arbitrary units. *, $p < 0.01$ by Student's *t* test, compared with the LPS-stimulated sample in the absence of M39 for each cell type.

suspension was added per well of a 12-well flat-bottom tissue culture-treated polystyrene plate (Costar, Corning, NY). Cells were allowed to settle without agitation for 60 min at 37°C (in the presence or absence of the p38 MAPK inhibitor), followed by addition of stimuli for the designated periods. At the end of the stimulation, the supernatant was removed for quantification of KC, MIP-2, or TNF-α by immunoassay (R&D Systems). In vitro inhibition of p38 MAPK was performed by incubation of neutrophils or macrophages with M39 over a range of concentrations for 60 min at 37°C. Collagen gel migration assays were performed as previously described (27) with minor modifications. Throughout all migration assays, Krebs-Ringer-phosphate dextrose with 0.25% human serum albumin was used as the buffer. Between 2 and 5×10^6 neutrophils were loaded per gel for each condition studied. Gels were inverted onto mounting media containing 0.1% *p*-phenylenediamine and 70% glycerol with 1 drop of defined diameter fluorescent beads (DNA-Check; Coulter, Hialeati, FL) to establish the scale. All gels were examined with a ×40 dry objective and numerical aperture 0.55. Diagrams of cells in each gel section were made at 5-μm intervals, and the number of cells at each depth were recorded. A minimum of three gel sections were examined for each condition, and averages were calculated for each depth. Values for cell distribution at each depth were expressed as a percent of total cells observed in the entire vertical section.

P38 MAPK immunoprecipitation assays

Kinase activity of p38α MAPK was assayed from immunoprecipitated samples by the ability to phosphorylate $ATF\text{-}2_{1-110}$ as previously described (19).

Intratracheal instillation of proinflammatory stimuli

Following anesthesia with avertin, a 300-ng aliquot of LPS or 1 μg KC dissolved in 50 μl saline containing 0.1% human serum albumin was injected into the mouse airways by passing a 22-gauge bent feeding needle with a 1.25-mm ball diameter (Popper & Sons, New Hyde Park, NY) through the oropharynx into the trachea.

In vivo inhibition of p38 MAPK

Anesthetized mice were administered M39 by gastric intubation of a 22-gauge straight feeding needle with a 2.25-mm ball diameter (Popper & Sons). Fasting mice were placed in a semiupright position, and M39 suspended in 100 μl hydroxypropylmethylcellulose (Abbott Laboratories, Abbott Park, IL) was instilled at a dose of 3 mg/kg. The M39 was administered 2 h before and 12 h following intratracheal instillation of KC or LPS, except for time points earlier than 12 h, in which a single dose of M39 was administered.

Histological examination and quantification of neutrophil accumulation of murine lung tissue

Animals were treated with saline or LPS in the presence or absence of M39. At 24 h, the animals were sacrificed by pentobarbital overdose and a midline incision was performed. A 20-g catheter (Baxter Health Care) was inserted into the trachea and secured by tying with 2–0 silk followed by careful dissection to remove the lungs from the thoracic cavity. After full inflation with air to 25 cm water pressure, the trachea was tied and the lungs submerged in 1.5% glutaraldehyde solution in sodium cacodylate buffer for 24 h. Sections (4 μm) taken across the entire lung were embedded in paraffin. Sagittal sections were stained with hematoxylin-eosin and examined by light microscopy. Between two and four animals were studied for each condition, and representative sections of lungs were chosen by two

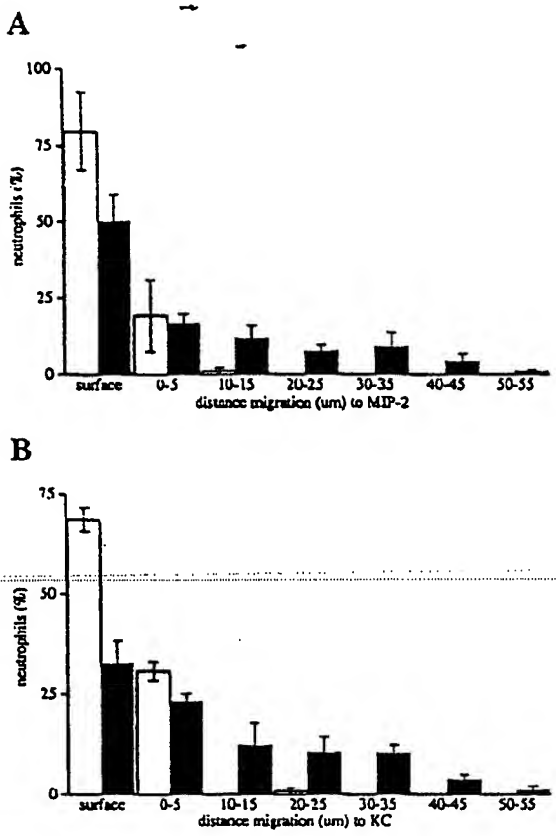

FIGURE 2. Inhibition of p38 MAPK blocks neutrophil migration toward MIP-2 and KC. *A*, Neutrophils (3×10^6) were treated with 1 μM M39 (□) or left untreated (■) for 60 min at 37°C and then subjected to an in vitro collagen gel migration assay (see *Materials and Methods*) toward MIP-2 (10^{-7} M) for 75 min at 37°C. Each plot depicts distance of migration in 10-μm intervals, expressed in mean percent of total cells counted ± SEM from three consecutive experiments, with three independent readings at each depth. Cells that failed to penetrate the gel were quantified in the interval labeled "surface." The failure of neutrophils to migrate beyond the gel surface following inhibition of p38 MAPK was significant ($p < 0.0001$) by χ^2 analysis when compared with untreated cells. *B*, Under identical conditions, neutrophils were treated with M39 (□) or left untreated (■) and then subjected to an in vitro collagen gel migration assay toward KC (10^{-7} M). The observed loss of migration following inhibition of p38 MAPK was significant ($p < 0.0001$) by χ^2 analysis.

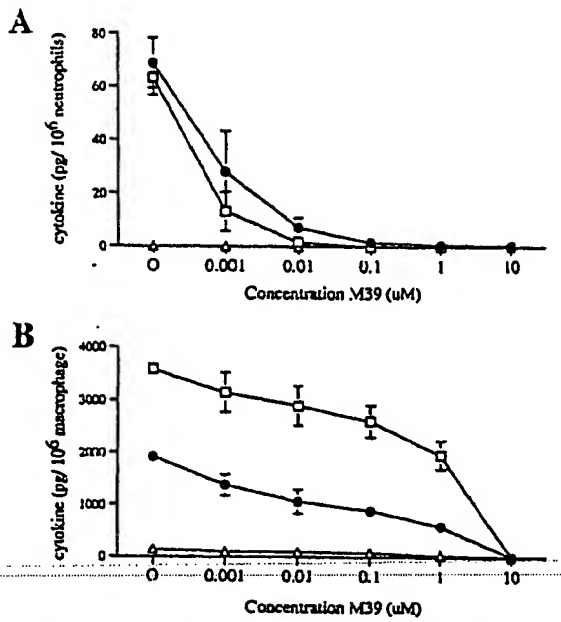

FIGURE 3. Effect of p38 MAPK inhibition on cytokine release of LPS-stimulated murine neutrophils and AM. *A*, Murine neutrophils were treated with M39 (0.001–10 μM at 37°C) or left untreated and allowed to adhere to plastic. The cells were then stimulated with LPS (100 ng/ml) for 4 h at 37°C, and the quantity of TNF-α (●), MIP-2 (□), or KC (△) released was quantified. Each plot depicts mean cytokine release (pg per 10^6 cells) ± SEM for each concentration of M39 from three consecutive experiments. The M39 concentration-dependent inhibition of cytokine release is significant for TNF-α and MIP-2 ($p < 0.001$) by one-way ANOVA, but not for KC. *B*, Under identical conditions, murine AM were treated with M39 or left untreated and allowed to adhere to plastic. The cells were then stimulated with LPS (100 ng/ml) for 4 h at 37°C and the quantity of TNF-α (●), MIP-2 (□), or KC (△) released was quantified. Each plot depict mean cytokine release (pg per 10^6 cells) ± SEM for each concentration of M39 from three consecutive experiments. The M39 concentration-dependent inhibition of cytokine release is significant for TNF-α and MIP-2 ($p < 0.001$) by one-way ANOVA, but not for KC.

independent observers blinded to the treatment status of the animals. Photomicrographs were taken at ×400 magnification. Quantification of neutrophil accumulation in the whole lung excluding the airspaces was performed by myeloperoxidase (MPO) assay as previously described (28) with minor modifications. Following BAL, isolated whole lungs were frozen in liquid nitrogen, weighed, and then homogenized. Following centrifugation at 20,000 × *g* for 30 min, the insoluble pellet was resuspended in 50 mM potassium phosphate buffer, pH 6.0, with 0.5% hexadecyltrimethylammonium bromide. Samples were sonicated, incubated at 60°C for 2 h, and assayed for activity in a hydrogen peroxide/*o*-dianisidine buffer at 460 nm. Results are expressed as units of MPO activity per gram of lung tissue.

Statistical analysis

Data were analyzed using JMP statistical software (SAS Institute, Cary, NC). Student's unpaired *t* test (two-tailed) was use to determine significance of p38 MAPK inhibition (Fig. 1) and neutrophil accumulation and MPO content (Fig. 8) for a single time point. Differences in chemotaxis (Fig. 2) were analyzed by a χ^2 test. One-way ANOVA was used to analyze the effect of LPS-induced cytokine release and leukocyte accumulation over time (Figs. 3 and 4). Differences in in vivo cell accumulation and cytokine release over time in the presence and absence of p38 MAPK inhibition (Figs. 5, 6, and 9) were analyzed by two-way ANOVA. When a significant interaction between inhibition and time existed, the effect of inhibition was analyzed separately for each time point. For all tests, $p < 0.01$ was considered significant unless otherwise indicated.

Results

Inhibition of p38α MAPK activation in murine neutrophils

Previous reports have demonstrated phosphorylation and activation of p38α MAPK in human neutrophils following stimulation with LPS (17, 18). To determine whether activation of p38α MAPK occurs in murine neutrophils in response to LPS, and assess the ability of M39 to inhibit p38α MAPK activity, murine bone marrow neutrophils were stimulated with LPS in the presence and absence of M39. Activity and phosphorylation of p38α MAPK were assessed simultaneously by immunoprecipitation of the kinase from neutrophil lysates stimulated with LPS or left unstimulated. The p38α MAPK was resolved by SDS-PAGE, and the Western blot was stained with an Ab capable of detecting tyrosine phosphorylation of p38α MAPK (Fig. 1*A*). For comparison, an equal number of human neutrophils were stimulated and analyzed

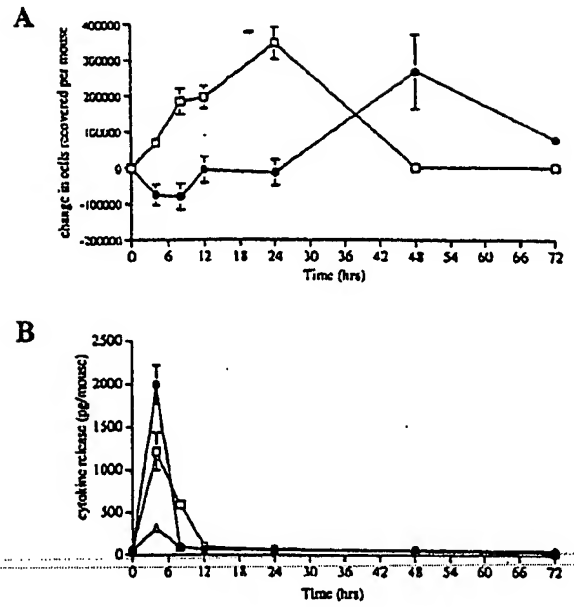

FIGURE 4. Features of pulmonary inflammation induced by intratracheal administration of LPS. *A*, Influx of leukocytes in the murine airspaces in response to intratracheal LPS. Mice were administered LPS (300 ng) at time 0, and the difference in numbers of neutrophils (□) and mononuclear cells (●) recovered by BAL compared with baseline levels was plotted over a series of time points. Each data point represents the mean change in number of cells ± SEM from three to five animals. The effect of LPS on leukocyte accumulation over time is significant by one-way ANOVA for both neutrophils ($p < 0.001$) and monocytes ($p = 0.003$). *B*, Cytokines in the murine airspaces in response to LPS. BAL samples recovered following administration of LPS (300 ng) were analyzed for TNF-α (●), MIP-2 (□), and KC (△). Quantities of cytokine recovered per mouse were plotted against time (see *Materials and Methods*). Each data point represents the mean amount ± SEM of cytokine recovered from the BAL of three to five animals. The effect of LPS on cytokine release over time is significant by one-way ANOVA ($p < 0.001$).

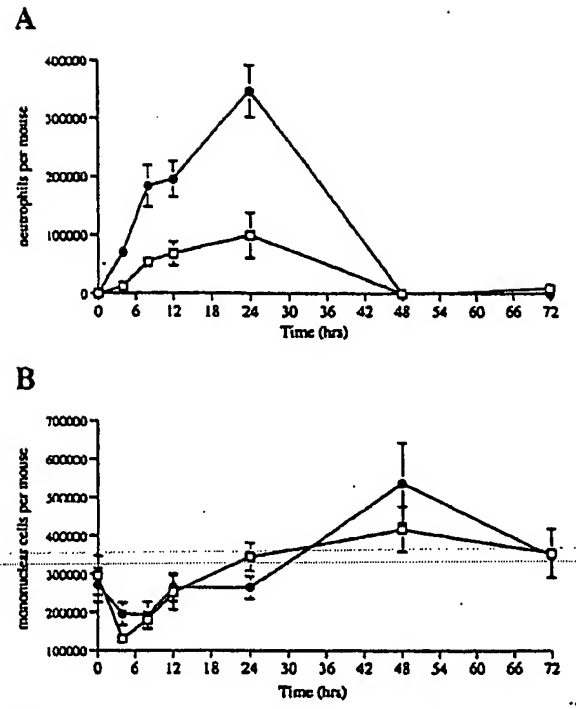

FIGURE 5. Effect of in vivo inhibition of p38 MAPK on leukocyte accumulation in the airspaces. *A*, Neutrophil accumulation in the murine airspaces following intratracheal LPS. Mice pretreated with M39 (□) were administered LPS (300 ng) at time 0, and cell analysis of BAL was compared with untreated mice (●) over a series of times (see *Materials and Methods*). Each point represents mean number of neutrophils ± SEM from three to five animals. The effect of M39 on LPS-induced neutrophil accumulation over time is significant ($p = 0.0005$) by two-way ANOVA. *B*, Mononuclear cells accumulation in the murine airspaces following LPS. Mononuclear cells from BAL samples depicted in Fig. 4*A* were analyzed in mice administered M39 (□) and compared with untreated mice (●) over a series of times. Each point represents mean number of cells ± SEM from three to five animals. The effect of M39 on LPS-induced mononuclear cell accumulation over time is not significant ($p = 0.39$) by two-way ANOVA.

in the identical manner (Fig. 1*A*). The blot was then reprobed with a second Ab against p38α MAPK, confirming that equivalent amounts of kinase were immunoprecipitated for each condition (data not shown). Activity of p38α MAPK was determined by combining immunoprecipitated p38α MAPK with $ATF\text{-}2_{(-)10}$, a known substrate (29), in the presence of [^{32}P]ATP (Fig. 1*B*). LPS stimulation resulted in robust tyrosine phosphorylation of p38α MAPK in both murine and human neutrophils. However, p38α MAPK isolated from LPS-stimulated cells treated with M39 had significantly reduced kinase activity. Inhibition of p38 MAPK by M39 may result in varying degrees of decreased tyrosine phosphorylation between different cell types and species (our unpublished observations). These results demonstrate phosphorylation and activation of p38α MAPK in the murine neutrophil and the ability of M39 to inhibit LPS-induced activation of p38α MAPK.

Inhibition of p38 MAPK blocks chemokine-induced chemotaxis of murine neutrophils

Chemotaxis is a complex response involving coordination of adhesion and actin assembly. We have reported previously that inhibition of p38 MAPK results in loss of chemotaxis response by human neutrophils to FMLP (19). We tested the effect of p38 MAPK inhibition on migration of murine neutrophils toward the chemoattractants MIP-2 and KC. Neutrophil chemotaxis through a three-dimensional collagen matrix was quantified by counting the number of cells within a series of 5-μm intervals after 75 min of exposure to the chemokines. In the presence of M39, neutrophil chemotaxis to MIP-2 (Fig. 2*A*) and KC (Fig. 2*B*) was blocked.

Effect of p38 MAPK inhibition on cytokine release of LPS-stimulated murine neutrophils and AM

An important role of AM is cytokines release in response to LPS, thus triggering and coordinating early inflammation. Neutrophils also have the capability to synthesize and release a limited number of cytokines (30) and under certain conditions may be important in perpetuating the inflammatory response. Activation of p38 MAPK has been associated with cytokine production by both monocytes/macrophages and neutrophils. We tested the effect of p38 MAPK inhibition with M39 on LPS-induced release of TNF-α, MIP-2, and KC from adherent neutrophils and AM (see *Materials and Methods*). An IC_{50} of M39 inhibition of TNF-α and MIP-2 release by LPS-stimulated neutrophils was achieved with a concentration of M39 <0.1 nM (Fig. 3*A*). In contrast, the IC_{50} of M39 for LPS-activated AM to achieve inhibition of TNF-α and MIP-2 release

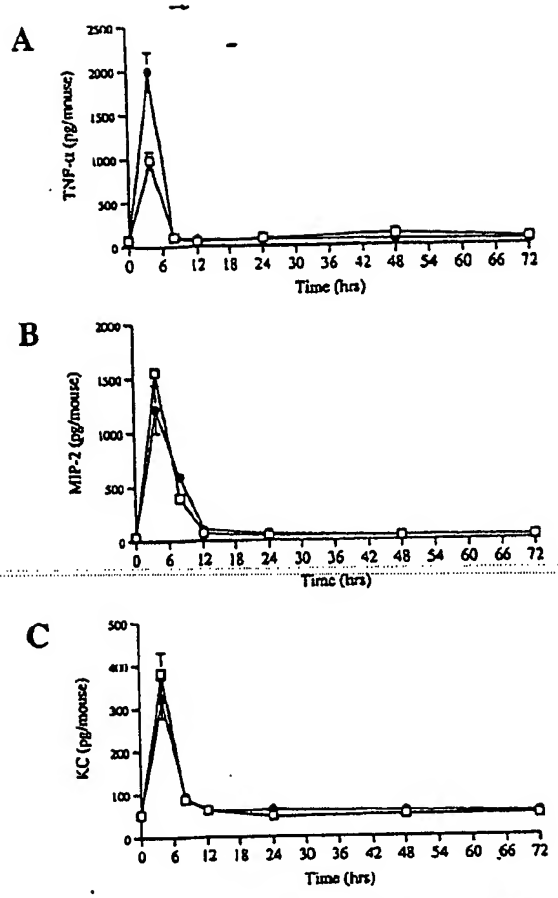

FIGURE 6. Effect of in vivo inhibition of p38 MAPK on cytokine release in the airspaces. *A*, TNF-α in the murine airspaces in response to LPS. Untreated mice (●) were administered LPS (300 ng) at time 0, and the quantity of TNF-α in the BAL were compared with mice pretreated with M39 (□) over a series of times (see *Materials and Methods*). Each point represents the mean amount (pg/mouse) ± SEM of TNF-α recovered from the BAL from three to five animals. *, $p < 0.01$, compared with M39 treated mice at the same time point. The effect of M39 on LPS-induced TNF-α release over time is significant ($p < 0.0001$) by two-way ANOVA. *B*, MIP-2 in the murine airspaces in response to LPS. BAL samples from Fig. 5*A* were reanalyzed for MIP-2 in untreated mice (●) compared with mice administered M39 (□) over a series of times. Each point represents the mean amount (pg/mouse) ± SEM of MIP-2 recovered from the BAL from three to five animals. The effect of M39 on LPS-induced MIP-2 release over time is not significant ($p = 0.49$) by two-way ANOVA. *C*, KC in the murine airspaces in response to LPS. BAL samples from Fig. 5*A* were reanalyzed for KC in untreated mice (●) compared with mice administered M39 (□) over a series of times. Each point represents the mean amount (pg/mouse) ± SEM of KC recovered from the BAL from three to five animals. The effect of M39 on LPS-induced KC release over time is not significant ($p = 0.73$) by two-way ANOVA.

was >1000-fold higher (Fig. 3*B*). Neither LPS-stimulated neutrophils nor AM were found to release significant quantities of KC under the conditions studied (Fig. 3, *A* and *B*). Viability of neutrophils and macrophages treated with 10 μM M39 ranged from 97 to 99%, equal to the viability of the untreated cells (data not shown). These results support the conclusion that in vitro inhibition of p38 MAPK may result in a relatively greater loss of functional response by the neutrophil than by the AM.

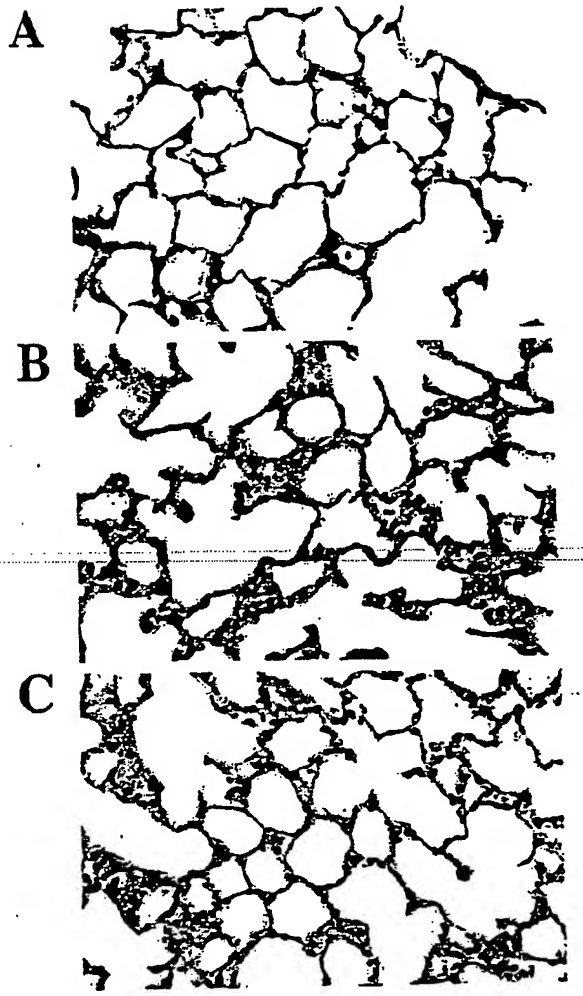

FIGURE 7. Systemic inhibition of p38 MAPK results in diminished pulmonary inflammation. *A*, Pulmonary histology of a saline-treated mouse. At 24 h following intratracheal instillation of saline, the murine lungs were fixed and stained with hematoxylin and eosin (see *Materials and Methods*). Plate represents a representative field from one of two mice at ×400 magnification. *B*, Histologic changes associated with intratracheal administration of LPS. Murine lung 24 h following intratracheal administration of LPS (300 ng/mouse). Plate depicts a representative field from one of four mice. *C*, Effect of in vivo p38 MAPK inhibition on LPS-induced histological changes. Mice were administered M39 by gastric intubation (see *Materials and Methods*) and then exposed to LPS in an identical manner as Fig. 4*B*. Plate depicts a representative field from one of four mice.

Characterization of murine pulmonary inflammation in response to intratracheal LPS

To study the role of p38 MAPK activation in the lungs, a model of mild pulmonary inflammation was developed. Following intratracheal administration of LPS, leukocytes and selected cytokines were quantified from BAL samples over a series of time points. A dose of LPS was selected that would elicit an exuberant neutrophil influx, followed by a secondary accumulation of mononuclear cells (primarily macrophages and monocytes), with near complete resolution by 72 h (Fig. 4*A*). The maximal neutrophil accumulation in the airspaces occurred at 24 h following LPS installation (Fig. 4*A*).

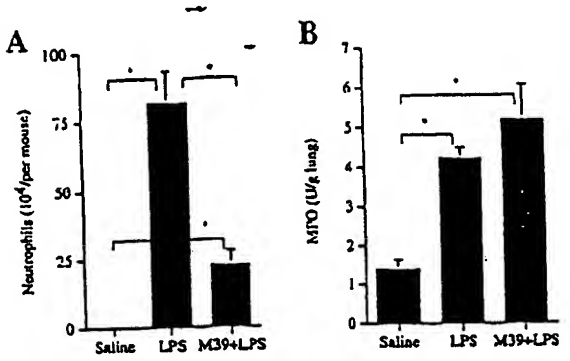

FIGURE 8. Systemic inhibition of p38 MAPK results in decreased accumulation of neutrophils in the airspaces independent of the whole lung. *A*, Neutrophil accumulation in airspaces. Neutrophils recovered by BAL at 24 h following intratracheal instillation of saline or LPS (300 ng/mouse) with and without administration of M39 by gastric intubation (identical with the conditions depicted in Fig. 7). Each bar represents mean number of neutrophils ± SEM from three animals. *, $p < 0.01$ by Student's *t* test comparing indicated condition. *B*, MPO content in lungs following BAL. To determine relative quantities of neutrophils present in the lungs excluding the neutrophils accumulated in the airspaces, the isolated lungs from the animals depicted in *A* were assayed for MPO following BAL. Each bar represents mean ± SEM of MPO activity per gram of lung tissue from three animals. *, $p < 0.01$ by Student's *t* test comparing indicated condition.

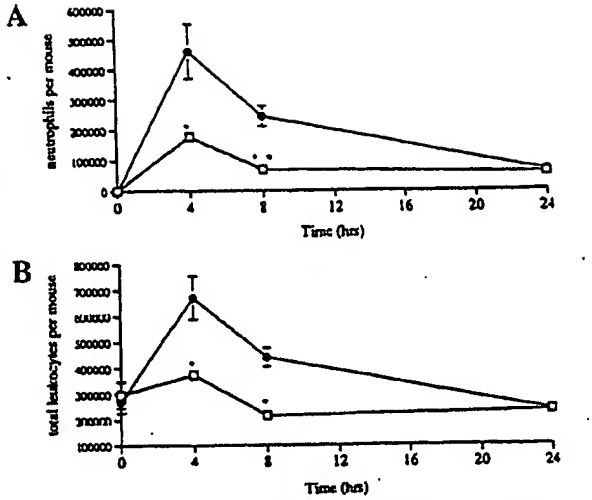

FIGURE 9. Effect of in vivo inhibition of p38 MAPK on KC-induced leukocyto accumulation and cytokine release. *A*, Neutrophil accumulation in the murine airspaces in response to intratracheal KC. Mice pretreated with M39 (□) were administered KC (1 μg) at time 0, and cell analysis of BAL was compared with untreated mice (●) over a series of times (see *Materials and Methods*). Each point represents mean number of neutrophils ± SEM from three to seven animals. Analysis of data by two-way ANOVA indicated a significant interaction between M39-induced inhibition and time, therefore the effect at each time point was analyzed separately. Significant inhibition (*, $p < 0.01$) was found at 4 h, with inhibition approaching significance at 8 h (**, $p = 0.028$). No significant changes were present at 24 h ($p = 0.95$). *B*, Leukocyte accumulation in the murine airspaces in response to KC. The total white blood cell count in BAL samples depicted in Fig. 8*A* was counted in mice administered M39 (□) compared with untreated mice (●) over a series of times. Each point represents mean number of cells ± SEM from three to seven animals. Analysis of data by two-way ANOVA indicated a significant interaction between M39-induced inhibition and time, therefore the effect at each time point was analyzed separately. Significant inhibition (*, $p < 0.01$) was found at 4 and 8 h. No significant changes were present at 24 h ($p = 0.99$).

In association with administration of LPS, production of TNF-α, MIP-2, and KC peaked within 4 h, returning to baseline by 12 h (Fig. 4*B*). Cytokine recovery was negligible by 24 h, the point at which neutrophil influx was greatest, suggesting that cytokine release by neutrophils is minimal in this model.

Inhibition of p38 MAPK in vivo results in decreased leukocyte accumulation in the airspaces

To quantify changes in inflammation observed in the setting of in vivo p38 MAPK inhibition, we conducted BAL studies over 72 h following administration of LPS. Numbers of neutrophils and mononuclear cells recovered by BAL in mice following intratracheal LPS were counted. Administration of M39 resulted in significant reduction of neutrophil accumulation from 4 to 24 h (Fig. 5*A*). By 48 h, neutrophils were no longer present in the airways, but were replaced by monocytes/macrophages. When total mononuclear cells were evaluated, the effect of systemic p38 MAPK inhibition was not statistically significant (Fig. 5*B*). Together, these plots support the conclusion that in vivo inhibition of p38 MAPK result primarily in reduction of the early neutrophil accumulation, with little effect on the later recruitment of monocytes/macrophages.

Inhibition of p38 MAPK in vivo results in decreased TNF-α release in the airspaces

BAL studies of mice 0–72 h following administration of LPS were analyzed for TNF-α, MIP-2, and KC. Only TNF-α was found to be significantly reduced by in vivo inhibition of p38 MAPK with M39 (Fig. 6*A*), with no detectable change in the release of MIP-2 (Fig. 5*B*) or KC (Fig. 5*C*). This data suggests that systemic inhibition of p38 MAPK can have divergent effects on cytokine release, and that release of the KC and MIP-2 chemokines by resident pulmonary immune cells in the mouse is relatively less dependent on p38 MAPK signaling than TNF-α under the conditions studied.

Inhibition of p38 MAPK in vivo results in diminished histological evidence of pulmonary inflammation

The effect of in vivo p38 MAPK inhibition on the histological changes of mild LPS-induced pulmonary inflammation were evaluated. Animals were administered LPS intratracheally in the presence and absence of M39and compared with saline-treated controls. After 24 h, LPS-treated mice (Fig. 7*B*) demonstrated a significant interstitial and intraalveolar accumulation of leukocytes and edema when compared with saline treated animals (Fig. 7*A*). In the presence of 38 MAPK inhibition, inflammatory changes were evident, but to a lesser extent (Fig. 7*C*).

Inhibition of p38 MAPK selectively blocks the accumulation of neutrophils into the airspaces

Decreased neutrophil accumulation in the airspaces in response to LPS following inhibition of p38 MAPK could possibly be due to decreased retention of neutrophils in the pulmonary vasculature or lung interstitium, or by loss of the ability of the cells to migrate into the alveoli. The MPO assay was used to quantify the neutrophil burden in the pulmonary vasculature and interstitium. Animals were administered LPS intratracheally in the presence and absence of M39 and compared with saline-treated controls at 24 h, identical with the conditions depicted in Fig. 7, *A–C*. Neutrophil accumulation in the airspaces was determined by BAL (Fig. 8*A*), and

following BAL the isolated lungs were subjected to the MPO assay (Fig. 8*B*). Although significant reduction in neutrophil accumulation is observed in the setting of in vivo p38 MAPK inhibition (Fig. 8*A*), the amount of neutrophils present in the isolated lungs with or without p38 MAPK inhibition are equivalent (Fig. 8*B*). These results support the conclusion that systemic inhibition of p38 MAPK results in a loss of migration of neutrophils into the airways, consistent with the effects of in vitro p38 MAPK inhibition on neutrophil chemotaxis (Fig. 2).

Decreased neutrophil accumulation by inhibition of p38 MAPK in vivo occurs due to reduced neutrophil chemotaxic response

Observed decreases in pulmonary inflammation following systemic inhibition of p38 MAPK might occur due to diminished response of neutrophils to LPS, as a result of decreased TNF-α release (Fig. 6*A*) or as a selective inhibition of neutrophil chemotaxis (Fig. 2*B*). To evaluate the effect of systemic p38 MAPK inhibition on neutrophil chemotaxis independent of LPS and TNF-α, a model using KC-induced pulmonary inflammation was studied. KC is a potent and selective chemoattractant for murine neutrophils that triggers little of the inflammatory cascade. KC was administered intratracheally in mice in the presence and absence of M39, and BAL studies were performed from 0 to 48 h. Under the conditions studied, KC induced a rapid and self-limited migration of neutrophils that was significantly decreased by in vivo p38 MAPK inhibition (Fig. 9*A*). Unlike LPS, a substantial later accumulation of mononuclear cells did not occur in response to KC (Fig. 9*B*). BAL analysis demonstrated no measurable release of MIP-2 and TNF-α and levels of KC within the airspaces decreased rapidly following administration (data not shown). These results suggest that decreases in LPS-induced neutrophil accumulation following systemic inhibition of p38 MAPK can occur due to reduced neutrophil response, independent of TNF-α production.

Discussion

The murine model of lung inflammation described above uses a single, low-dose intratracheal administration of LPS to induce an acute inflammatory response characterized by rapid but self-limiting release of cytokines, followed by the transient influx of neutrophils and a secondary accumulation of mononuclear cells. This model was designed to study the critical early stages of lung inflammation in which neutrophil recruitment is a central feature. By limiting the extent of the initial insult, many of the features that contribute to the perpetuation of severe inflammation were avoided, including sustained release of cytokines, ongoing recruitment of leukocytes, significant damage of the parenchyma, and ultimately a significant mortality rate.

Through in vitro studies of various cell lines and primary cells, p38 MAPK has been linked to a variety of inflammatory responses. With the recent development of potent and specific inhibitors, the role of p38 MAPK in both in vitro systems and complex in vivo models of inflammation can be studied. Murine neutrophils were found to have nearly identical activation of p38α MAPK in response to stimulation by LPS with what has previously been reported in human neutrophils. Treatment of murine neutrophils with the novel p38 MAPK inhibitor M39 resulted in significant inhibition of p38α MAPK activity. Important functional effects of p38 MAPK inhibition in the murine neutrophil were the loss of chemotaxis toward MIP-2 and KC and the loss of TNF-α and MIP-2 release in response to LPS. Unexpectedly, parallel studies of murine AM demonstrated a 1000-fold greater concentration of M39 is required to block release of TNF-α, MIP-2, or KC. The greater sensitivity of neutrophils to inhibition of the p38 MAPK cascade was also observed in vivo. In response to intratracheal administration of LPS, the influx of neutrophils, but not mononuclear cells, was significantly decreased in the setting of systemic p38 MAPK inhibition. Quantification of the neutrophil accumulation in the whole lung demonstrated that under the conditions studied only the airspaces have a reduction of the influx of neutrophils, supporting the in vitro analysis of the dependence of neutrophil chemotaxis on p38 MAPK activation. Recovery of TNF-α in the airspaces was reduced through p38 MAPK inhibition, but quantities of MIP-2 and KC were not affected. When KC was used as a primary neutrophil chemoattractant, secondary release of TNF-α and MIP-2 was not evoked, but neutrophil influx was significantly blocked by systemic p38 MAPK inhibition.

Although the MAPK cascades are highly conserved, it is now understood that specific utilization of the MAPK cascades differs between neutrophils, macrophages, and other cells. In monocytes or macrophage cell lines, LPS has been reported to activate p42/44 (ERK) MAPK and JNK as well as the p38 MAPK cascade (31–33). Release of TNF-α by monocytes or macrophage cell lines can be blocked through selective inhibition of either the JNK (32), p38 MAPK (16), or the p42/44 (ERK) MAPK cascade (34). Disruption of a component of the p38 MAPK cascade in *MKK3*$^{-/-}$ mice failed to reduce TNF-α release by peritoneal macrophages in response to LPS (35). In T cells, inhibition of p38 MAPK has less of an effect on TNF-α release than does inhibition of the p42/44 (ERK) cascade (36). In contrast, LPS stimulation of neutrophils does not result in activation of the p42/44 (ERK) MAPKs or the JNKs (17, 18, 37). As a short-lived, terminally differentiated primary cell, the neutrophil possesses a more limited synthetic capability and, in response to LPS, uses fewer of the available intracellular signal transduction mechanisms. Thus, the selective loss of neutrophil function in the setting of systemic p38 MAPK inhibition suggests that neutrophils are relatively more dependent on signal transduction via the p38 MAPK cascade than AM.

Although considerable recent interest has been focused on the activation and function of p38 MAPK, there are few reports of in vivo inhibition of this signaling pathway. The pyridinyl imadazole compounds, including SB203580 and SK&F86002, are the most widely studied p38 MAPK inhibitors and have been shown to possess antiinflammatory properties in animal models. These early p38 MAPK inhibitors were shown to reduce neutrophil influx in response to monosodium urate- or carrageenan-induced peritonitis (38) and collagen-induced arthritis (39, 40). In response to i.p. injection of LPS, administration of these compounds resulted in decreased recovery of TNF-α by peritoneal washout (41) and decreased serum TNF-α and mortality in a murine model of endotoxin shock (40, 42, 43). The antiinflammatory effects of these p38 MAPK inhibitors occurred in the absence of generalized immunosupression (40, 41, 44, 45). The effects of systemic p38 MAPK inhibition on pulmonary inflammation has not been described. To date, nearly all studies of the functional role of p38 MAPK have used the compound SB203580, which has an $IC_{50} = 39 \pm 11$ nM for p38 MAPK as well as considerable inhibitory effects toward c-Raf ($IC_{50} = 330 \pm 155$ nM) and JNK2α1 ($IC_{50} = 290 \pm 110$ nM). In comparison, M39 has an $IC_{50} = 0.11 \pm 0.046$ nM for p38 MAPK and is significantly less active toward c-Raf ($IC_{50} = >1000$ nM) or JNK2α1 ($IC_{50} = 675$ nM) (25). As a more potent and selective p38 MAPK inhibitor, M39 is better suited for in vivo studies than previously available compounds.

In the murine model of mild LPS-induced pulmonary inflammation, the predominant effect of in vivo p38 MAPK inhibition was to reduce recruitment of neutrophils. Based on in vitro chemotaxis assays to MIP-2 and KC, it would appear that this effect

can occur as a result of decreased neutrophil response. BAL measurement of chemokine levels support this conclusion, as neither KC nor MIP-2 release was decreased in animals treated with M39. In addition, in vivo inhibition of p38 MAPK blocked neutrophil accumulation in response to intratracheal administration of KC, independent of LPS or TNF-α. Although decreased TNF-α release following LPS stimulation was detected in animals treated with M39, this effect appears to be of secondary importance under the conditions studied. The apparently greater dependence of neutrophils on p38 MAPK signaling when compared with resident cells of the lung suggests the potential for selective analysis and modulation of neutrophil influx in pulmonary inflammation.

References

1. Worthen, G. S., and J. A. Nick. 1998. Leukocyte accumulation in the lung. In *Pulmonary Diseases and Disorders*. Vol. 1. A. P. Fishman, ed. McGraw-Hill, New York, p. 325.
2. Lien, D. C., W. W. Wagner, R. L. Capen, C. L. Haslett, W. L. Hanson, S. E. Hofmeister, P. M. Henson, and G. S. Worthen. 1987. Physiologic neutrophil sequestration in the canine pulmonary circulation: evidence for localization in capillaries. *J. Appl. Physiol. 62:1236.*
3. Worthen, G. S., B. Schwab, E. L. Elson, and G. P. Downey. 1989. Mechanics of stimulated neutrophils: cell stiffening induces retention in capillaries. *Science 245:183.*
4. Downey, G. P., D. E. Doherty, B. Schwab, III, E. L. Elson, P. M. Henson, and G. S. Worthen. 1990. Retention of leukocytes in capillaries: role of cell size and deformability. *J. Appl. Physiol. 69:1767.*
5. Xing, Z., H. Kirpalani, D. Torry, M. Jordana, and J. Gauldie. 1993. Polymorphonuclear leukocytes as a significant source of TNF-α in endotoxin-challenged lung tissue. *Am. J. Pathol. 143:1009.*
6. Doherty, D. E., G. P. Downey, B. I. Schwab, E. Elson, and G. S. Worthen. 1994. Lipopolysaccharide-induced monocyte retention in the lung: role of monocyte stiffness, actin assembly, and CD18-dependent adherence. *J. Immunol. 153:241.*
7. Fantone, J. C. 1997. Cytokines and neutrophils: neutrophil-derived cytokines and the inflammatory response. In *Cytokines in Health and Disease*. D. G. Remick and J. S. Friedland, eds. Marcel Dekker, New York, p. 373.
8. Rollins, B. 1997. Chemokines. *Blood 90:909.*
9. Harada, A., N. Sekido, T. Akahoshi, T. Wada, N. Mukaida, and K. Matsushima. 1994. Essential involvement of IL-8 in acute inflammation. *J. Leukocyte Biol. 56:559.*
10. VanZee, K., L. DeForge, E. Fischer, M. Marano, J. Kenney, D. Remick, S. Lowry, and L. Moldawer. 1991. IL-8 in septic shock, endotoxemia, and after IL-1 administration. *J. Immunol. 146:3478.*
11. Wolpe, S., B. Sherry, D. Juers, G. Davatelis, R. Yurt, and A. Cerami. 1989. Identification and characterization of macrophage inflammatory protein 2. *Proc. Natl. Acad. Sci. USA 86:612.*
12. Bozic, C., J. L. F. Kolakowski, N. P. Gerard, C. Garcia-Rodrig, C. v. Uexkull-Guldenband, M. J. Conklyn, R. Breslow, H. J. Showell, and C. Gerard. 1995. Expression and biologic characterization of the murine chemokine KC. *J. Immunol. 154:6048.*
13. Cobb, M. H., and E. J. Goldsmith. 1995. How MAP kinases are regulated. *J. Biol. Chem. 270:14843.*
14. Han, J., J.-D. Lee, L. Bibbs, and R. J. Ulevitch. 1994. A MAP kinase targeted by endotoxin and hyperosmolarity in mammalian cells. *Science 265:808.*
15. Rouse, J., P. Cohen, S. Trigon, M. Morange, A. Alonso-Llamazares, D. Zamanillo, T. Hunt and A. R. Nebreda. 1994. A novel kinase cascade triggered by chemical stress and heat shock which stimulates MAP kinase-activatedprotein kinase-2 and phosphorylation of the small heat shock proteins. *Cell 78:1027.*
16. Lee, J. C., J. T. Laydon, P. C. McDonnell, T. F. Gallagher, S. Kumar, D. Green, D. McNulty, M. J. Blumenthal, J. R. Heys, S. W. Landvatter, et al. 1994. A protein kinase involved in the regulation of inflammatory cytokine biosynthesis. *Nature 372:739.*
17. Nick, J. A., N. J. Avdi, P. Gerwins, G. L. Johnson, and G. S. Worthen. 1996. Activation of a p38 mitogen-activated protein kinase in human neutrophils by lipopolysaccharide. *J. Immunol. 156:4867.*
18. Nahas, N., T. F. P. Molski, G. A. Fernandez, and R. I. Sha'afi. 1996. Tyrosine phosphorylation and activation of a new mitogen-activated protein (MAP)-kinase cascade in human neutrophil stimulated with various agonists. *Biochem. J. 318: 247.*
19. Nick, J. A., N. J. Avdi, S. K. Young, C. Knall, G. L. Johnson, and G. S. Worthen. 1997. Common and distinct intracellular signalling pathways in human neutrophil utilized by platelet activating factor and FMLP. *J. Clin. Invest. 99:975.*
20. Zu, Y.-L., J. Qi, A. Gilchrist, G. A. Fernandez, D. Vazquez-Abad, D. L. Kreutzer, C.-K. Huang, and R. I. Sha'afi. 1998. p38 Mitogen-activated protein kinase activation is required for human neutrophil function triggered by TNF-α or FMLP stimulation. *J. Immunol. 160:1982.*
21. Demers, P. A., D. Zhou, E. Polizzi, R. Thieringer, W. A. Hanlon, S. Vaidya, and V. Bunsal. 1998. Role of stress-activated mitogen-activated protein kinase (p38) in β_2-integrin-dependent neutrophil adhesion and the adhesion-dependent oxidative burst. *J. Immunol. 161:1921.*
22. Manthey, C. L., S.-W. Wang, S. D. Kinney, and Z. Yao. 1998. SB202190, a selective inhibitor of p38 mitogen-activated protein kinase, is a powerful regulator of LPS-induced mRNA-s in monocytes. *J. Leukocyte Biol. 64:409.*
23. Matsumoto, K., S. Hashimoto, Y. Gon, T. Nakayama, and T. Horie. 1998. Proinflammatory cytokine-induced and chemical mediator-induced IL-8 expression in human bronchial epithelial cells through p38 mitogen-activated protein kinase-dependent pathway. *J. Allergy Clin. Immunol. 101:823.*
24. Schumann, R. R., D. Pfeil, N. Lamping, C. Kirschning, G. Scherzinger, P. Schlag, L. Karawajew, and F. Herrmann. 1996. LPS induces the rapid tyrosine phosphorylation of the MAP kinases ERK-1 and p38 in cultured human vascular endothelial cells requiring the presence of soluable CD14. *Blood 87:2805.*
25. Liverton, N. J., J. W. Butcher, C. F. Claiborne, D. A. Claremon, B. E. Libby, K. T. Nguyen, S. M. Pitzenberger, H. G. Selnick, G. R. Smith, A. Tebben, et al. 1999. The design and synthesis of potent, selective and orally bioavailable tetrasubstituted imidazole inhibitors of p38 MAP kinase. *J. Med. Chem. 42:2180.*
26. Haslett, C., L. A. Guthrie, M. Kopaniak, R. B. Johnston, Jr., and P. M. Henson. 1985. Modulation of multiple neutrophil functions by trace amounts of bacterial LPS and by preparative methods. *Am. J. Pathol. 119:101.*
27. Haslett, C., G. S. Worthen, P. C. Giclas, D. C. Morrison, J. E. Henson, and P. M. Henson. 1987. The pulmonary vascular sequestration of neutrophils in endotoxemia is initiated by an effect of endotoxin on the neutrophil in the rabbit. *Am. Rev. Respir. Dis. 136:9.*
28. Rosengren, S., P. M. Henson, and G. S. Worthen. 1994. Migration-associated volume changes in neutrophils facilitate the migratory process. *Am. J. Physiol. Cell. Physiol. 267:C1623.*
29. Goldblum, S. E., K.-M. Wu, and M. Jay. 1985. Lung myeloperoxidase as a measure of pulmonary leukostasis in rabbits. *J. Appl. Physiol. 59:1978.*
30. Raingeaud, J., S. Gupta, J. S. Rogers, M. Dickens, J. Han, R. J. Ulevitch, and R. J. Davis. 1995. Pro-inflammatory cytokines and environmental stress cause p38 mitogen-activated protein kinase activation by dual phosphorylation on tyrosine and threonine. *J. Biol. Chem. 270:7420.*
31. Cassatella, M. 1995. The production of cytokines by polymorphonuclear neutrophils. *Immunol. Today 16:21.*
32. Weinstein, S. L., J. S. Sanghera, K. Lemke, A. L. DeFranco, and S. L. Pelech. 1992. Bacterial lipopolysaccharide induces tyrosine phosphorylation and activation of mitogen-activated protein kinases in macrophages. *J. Biol. Chem. 267: 14955.*
33. Swantek, J. L., M. H. Cobb, and T. D. Geppert. 1997. Jun N-terminal kinase/stress-activated protein kinase (JNK/SAPK) is required for lipopolysaccharide stimulation of tumor necrosis factor α (TNF-α) translation: glucocorticoids inhibit TNF-α translation by blocking JNK/SAPK. *Mol. Cell. Biol. 17:6274.*
34. Hambleton, J., S. L. Weinstein, L. Lem, and A. L. DeFranco. 1996. Activation of c-Jun N-terminal kinase in bacterial LPS-stimulated macrophages. *Proc. Natl. Acad. Sci. USA 93:2774.*
35. Scherle, P. A., E. A. Jones, M. F. Favata, A. J. Daulerio, M. B. Covington, S. A. Numberg, R. L. Magolda, and J. M. Trzaskos. 1998. Inhibition of MAP kinase kinase prevents cytokine and prostaglandin E_2 production in LPS-stimulated monocytes. *J. Immunol. 161:5681.*
36. Lu, H.-T., D. D. Young, M. Wysk, E. Gatti, I. Mellman, R. J. Davis, and R. A. Flavell. 1999. Defective IL-12 production in mitogen-activated protein (MAP) kinase kinase 3 (Mkk3)-deficient mice. *EMBO J. 1845.*
37. Schafer, P. H., L. Wang, S. A. Wadsworth, J. E. Davis, and J. J. Siekierka. 1999. T cell activation signals up-regulate p38 mitogen-activated protein kinase activity and induce TNF-α production in a manner distinct from LPS activation of monocytes. *J. Immunol. 162:659.*
38. Fonda, B. L., T. F. P. Molski, M. S. Ashour, and R. I. Sha'afi. 1995. Effect of lipopolysaccharide on mitogen-activated protein kinases and cytosolic phospholipase A2. *Biochem. J. 308:815.*
39. Griswold, D. E., S. Hoffstein, P. J. Marshall, E. F. Webb, L. Hillegass, P. E. Bender, and N. Hanna. 1989. Inhibition of inflammatory cell infiltration by bicyclic imidazoles, SK&F 86002 and SK&F 104493. *Inflammation 13:727.*
40. Griswold, D. E., L. M. Hillegass, P. C. Meunier, M. J. DiMartino, and N. Hanna. 1988. Effect of inhibitors of eicosanoid metabolism in murine collagen-induced arthritis. *Arthritis Rheum. 31:1406.*
41. Badger, A. M., J. N. Bradbeer, B. Votta, J. C. Lee, J. L. Adams, and D. E. Griswold. 1996. Pharmacologic profile of SB 203580, a selective inhibitor of cytokine suppressive binding protein/p38 kinase, in animal models of arthritis, bone resorption, endotoxin shock and immune function. *J. Pharmacol. Exp. Ther. 279:1453.*
42. Lee, J. C., A. M. Badger, D. E. Griswold, D. Dunnington, A. Truneh, B. Votta, J. R. White, P. R. Young, and P. E. Bender. 1993. Bicyclic imidazoles as a novel class of cytokine biosynthesis inhibitors. *Ann. NY Acad. Sci. 696:149.*
43. Badger, A. M., D. L. Olivera, J. E. Talmadge, and N. Hanna. 1989. Protective effects of SK&F 86002, a novel dual inhibitor of arachidonic acid metabolism, in murine models of endotoxic shock: inhibition of TNF as a possible mechanism of action. *Circ. Shock 27:51.*
44. Olivera, D. L., K. K. Esser, J. C. Lee, R. G. Greig, and A. M. Badger. 1992. Beneficial effects of SK&F 105809, a novel cytokine-suppressive agent, in murine models of endotoxin shock. *Circ. Shock 37:301.*
45. Reddy, M. P., E. F. Webb, D. Cassani, D. Maley, J. C. Lee, D. E. Griswold, and A. Truneh. 1994. Pyridinyl imidazoles inhibit the inflammatory phase of delayed type hypersensitivity reactions without affecting T-dependent immune responses. *Int. J. Immunopharmacol. 16:795.*

Exhibit 8

ELSEVIER

Brain Research 892 (2001) 70–77

BRAIN RESEARCH

www.elsevier.com/locate/bres

Research report

SB 239063, a novel p38 inhibitor, attenuates early neuronal injury following ischemia

Jeffrey J. Legos[a,d,*], Joseph A. Erhardt[a], Raymond F. White[a], Stephen C. Lenhard[b], Sudeep Chandra[b], Andrew A. Parsons[a,c], Ronald F. Tuma[d], Frank C. Barone[a]

[a]Department of Cardiovascular Pharmacology, SmithKline Beecham Pharmaceuticals, King of Prussia, PA, USA
[b]Department of Physical and Structural Chemistry, SmithKline Beecham Pharmaceuticals, King of Prussia, PA, USA
[c]Department of Neuroscience Research, SmithKline Beecham Pharmaceuticals, Harlow, UK
[d]Department of Physiology, Temple University School of Medicine, Philadelphia, PA, USA

Accepted 8 November 2000

Abstract

The aim of the present study was to evaluate p38 MAPK activation following focal stroke and determine whether SB 239063, a novel second generation p38 inhibitor, would directly attenuate early neuronal injury. Following permanent middle cerebral artery occlusion (MCAO), brains were dissected into ischemic and non-ischemic cortices and Western blots were employed to measure p38 MAPK activation. Neurologic deficit and MR imaging were utilized at various time points following MCAO to monitor the development and resolution of brain injury. Following MCAO, there was an early (15 min) activation of p38 MAPK (2.3-fold) which remained elevated up to 1 h (1.8-fold) post injury compared to non-ischemic and sham operated tissue. Oral SB 239063 (5, 15, 30, 60 mg/kg) administered to each animal 1 h pre- and 6 h post MCAO provided significant ($P<0.05$) dose-related neuroprotection reducing infarct size by 42, 48, 29 and 14%, respectively. The most effective dose (15 mg/kg) was further evaluated in detail and SB 239063 significantly ($P<0.05$) reduced neurologic deficit and infarct size by at least 30% from 24 h through at least 1 week. Early (i.e. observed within 2 h) reductions in diffusion weighted imaging (DWI) intensity following treatment with SB 239063 correlated ($r=0.74$, $P<0.01$) to neuroprotection seen up to 7 days post stroke. Since increased protein levels for various pro-inflammatory cytokines cannot be detected prior to 2 h in this stroke model, the early improvements due to p38 inhibition, observed using DWI, demonstrate that p38 inhibition can be neuroprotective through direct effects on ischemic brain cells, in addition to effects on inflammation.

Theme: Disorders of the nervous system

Topic: Ischemia

Keywords: Stroke; p38 MAPK; Neuronal Injury; Neuroprotection; Focal ischemia

1. Introduction

The mitogen activated protein kinase (MAPK) family is composed of three main groups of kinases. Included among these kinases are the p42/44 extracellular-signal regulating kinase (ERK), c-Jun N-terminal kinase (JNK), and the p38 kinases [28,37]. The MAPK can be further divided into two major subfamilies; those regulated by growth factors promoting survival (ERK) and the stress activated protein kinases (SAPKs) which regulate apoptosis and inflammatory cell death [27,29,31,42].

Activation of the p38 MAPK pathway (phosphorylated p38 MAPK) has been implicated in playing a role in the regulation of pro-inflammatory cytokines and apoptosis [27,30,31,42]. In particular, in vitro studies demonstrated that monocytes require activation of p38 MAPK for LPS induced cytokine release. Inhibition of the p38 MAPK pathway using SB 203580 (specific for p38α and p38β) resulted in an inhibition of cytokine release from stimulated monocytes [26]. Several studies have demonstrated that p38 MAPK may regulate the transcription of cytokine mRNA [2] and/or possibly the translation of cytokines by

*Corresponding author. Department of Cardiovascular Pharmacology, SmithKline Beecham Pharmaceuticals, PO Box 1539, 709 Swedeland Road, King of Prussia, PA 19406, USA. Tel.: +1-610-270-6547; fax: +1-610-270-4114.
E-mail address: jeffrey_2_legos@sbphrd.com (J.J. Legos).

0006-8993/01/$ – see front matter
PII: S0006-8993(00)03228-5

inhibiting the critical step of phosphorylation of an AU-rich (AUUUA) repeat in the 3′ end of mRNA [25]. SB 203580 also was effective at reducing TNFα, IL-1β production [25,29,30,39,43] as well as the expression of several other inflammatory cytokines, including IL-6 [10,24] and IL-8 [17,19,20,24,29,35], thus significantly impacting on the inflammatory process and ultimate degree of tissue injury. Inhibition of p38 with SB 239063 suppressed LPS-induced increased plasma TNF levels and reduced adjuvant arthritis paw inflammation in the Lewis rat [4] and was 3-fold more potent than the first generation inhibitor SB 203580. Although the exact mechanism is not fully understood, both in vitro and in vivo studies have demonstrated that inhibition of p38 MAPK correlates with decreased levels of pro-inflammatory cytokine release [1,25,29,30].

In a recent study, we also demonstrated that protein concentrations for IL-6 and IL-1ra did not significantly increase until 12 h following distal electrocoagulation of the middle cerebral artery [32]. In addition, the increased levels of IL-1β were biphasic increasing at 4 h, approaching baseline, and then significantly increasing again at 12 h. The timing of increased protein levels agrees with the infiltration of inflammatory cells as assessed by myeloperoxidase activity in this particular model. Since cytokine production and neutrophil infiltration can be delayed up to 12 h or may fall below the lower limit of quantification at these time points, p38 MAPK inhibitors may be beneficial via additional/alternative mechanisms.

The rapid phosphorylation of p38 following severe stroke [22] suggests that the activation of this signaling cascade may be, to some degree, independent of the brain inflammatory response. The effects of SB 239063, a novel, second-generation p38 inhibitor, have been evaluated in an in vitro model of oxygen-glucose deprivation induced neuronal cell death [4]. SB 239063 significantly reduced hippocampal CA1 cell death (up to 40%) produced by this in vitro ischemia in cultured organotypic brain slices. These in vitro data suggest that p38 inhibition may directly protect neurons, independent of blood flow effects, in addition to effects at blocking inflammatory cytokine/mediator production. Therefore, the aim of the present study was to examine the temporal profile of p38 MAPK phosphorylation following moderate focal stroke and to determine whether SB 239063 provides very early direct neuronal protection in vivo.

2. Methods

2.1. Middle cerebral artery occlusion

Male spontaneously hypertensive rats (SHR; Taconic Farms, Germantown, NY) weighing 300–350 g, were used in this study. Body temperature was maintained at 37°C during all surgical procedures and during recovery from anesthesia (i.e. until normal locomotor activity returned). Animals were anesthetized with pentobarbital (65 mg/kg, i.p.) and underwent permanent middle cerebral artery occlusion (MCAO) as described previously [5–7]. Briefly, the middle cerebral artery was exposed through a 2–3-mm^2 craniotomy made just rostral to the zygomatic-squamosal skull suture and occlusion of the middle cerebral artery was achieved at the level of the inferior cerebral vein.

2.2. Western analyses for p38 MAPK

For Western blotting experiments, the brain was removed and rapidly dissected into ischemic (I) and non-ischemic control cortices (C) and snap frozen at −80°C. Both cortices were homogenized in 1 ml of standard lysis buffer for every 100 mg of tissue wet weight. Based on protein assay, equivalent amounts of protein (e.g. 30 μg/well) were be loaded onto a 10% Bis Tris Gel from Novex. The gel was run at a constant 130 V for 90 min. The gel was transferred at 100 V for 1 h at room temperature or overnight at 4°C at 23 V to a nitrocellulose membrane (Protran, Schleicher and Schuell BA85, 0.45-μm pore). After the transfer step, the membrane was soaked in blocking solution (ZyMed) for 1 h at room temperature. The membrane was then washed quickly twice and then three times with 1× Tween/DPBS for 10 min each on an orbital shaker. The primary antibody (New England Biolabs kit #9210) was diluted 1:1000 in blocking solution and allowed to incubate overnight at 4°C on slow shake. The membrane was then washed three times as described above. The 2°C HRP-linked antibody (New England Biolabs) was diluted 1:2000 (anti-rabbit HRP) in blocking solution for 1 h at room temperature on a slow shaker. Following incubation with the secondary antibody, the membrane was washed twice quickly followed by two 10-min washes as above. The membrane was then soaked in ECL reagent (Amersham RPN 2106 1:1 ration of reagent 1 and reagent 2) for 1 min (ECL was not mixed more than 15 min prior to use). The membrane was placed in a hypercassette (Amersham RPN 11648) with hyperfilm (Amersham RPN 1674H) and exposed for between 30 s and 1 min to develop the film. Western blots were scanned and densitometries were calculated using NIH 1.62 Image Quant software. Data are represented as a relative fold increase in the amount of p38 MAPK in the ischemic and non-ischemic cortices relative to sham operated tissue on the same side of the brain. This ratio allows for direct comparisons between blots as well as for different exposure times.

2.3. Dose range for oral SB 239063

The dose volume for oral studies using SB 239063 was 10 ml/kg. The vehicle was prepared using a 0.5% tragacanth (Sigma, St. Louis, MO) solution and hydrochlo-

ric acid (pH 3.0–3.5). SB 239063 powder was added to the solution and the pH was maintained at 3.0–3.5 for optimal effectiveness. In order to determine the most effective dose, the animals received a dose of 5, 15, 30, and 60 mg/kg 1 h prior to middle cerebral artery occlusion and a subsequent dose of SB 239063 at 6 h post MCAO.

2.4. Histologic evaluation of infarct size

Rats were euthanized by an overdose of sodium pentobarbital (200 mg/kg, i.p.). The brains were immediately removed and 2-mm coronal sections were cut from the entire forebrain area (i.e. from the olfactory bulbs to the cortical-cerebellar junction), using a brain slicer (Zivic-Miller Laboratories). The coronal sections were immediately stained in a solution of 1% triphenyltetrazolium chloride as described [8]. Sections were transferred to 10% formalin (in 0.1% sodium phosphate buffer) for at least 24 h and then photographed and analyzed as described previously [6,7]. Briefly, brain injury was quantified using an Optimas image analysis system (DataCell) and the degree of brain damage was corrected for the contribution made by brain edema/swelling as described previously [33,38]. Hemispheric swelling and infarct volume (mm^3) were calculated from infarct areas measured from the sequential forebrain sections. Infarct size was expressed as the percent infarcted tissue in reference to the contralateral hemisphere. Slice by slice analysis was also performed to evaluate the extent of agreement between histology and MRI determinations of brain injury.

2.5. Diffusion weighted imaging

The magnet was programmed to acquire both diffusion weighted and T2 weighted images. For magnetic resonance imaging, the animals were intubated for respiratory gating and were subsequently maintained on a mixture of 1.5–3% isoflurane and 0.8 l/min of medical grade air. The core body temperatures of the animals were monitored with a rectal probe and maintained at 37±1°C. Diffusion weighted imaging (DWI) was performed using a full birdcage resonator on a 4.7 T/40 cm Bruker ABX spectrometer equipped with a gradient coil insert as described previously [12]. Briefly, DWI data were collected as follows: SE: TR/TE=1500/45 ms; 128×128; FOV=3×3 cm; slice thickness=2 mm; G=10 G/cm; Δ=25 ms; 4 NEX; δ=10 ms; b-factor=1550 s/mm^2. The animals were placed in the magnet within the 1st hour and a half post surgery and data were acquired at a 2-h time point. Following imaging, the animals were allowed to recover from anesthesia under supervision. All MR images were transferred to an SGI UNIX workstation and were analyzed with the software package ANALYZE™ (CN Software, UK) in exactly the same manner as histologic sections were analyzed. Infarct assessment and hemispheric volume was obtained by manual tracing. The percent of hemispheric infarct was calculated over all slices (Σ the area of lesion per slice/Σ the contralateral area per slice) for each animal using three data sets acquired at 2 h. T2 weighted MR images were acquired at 24 h and 7 days post injury and hemispheric infarct was calculated as described above.

2.6. Assessment of neurologic deficit

Each rat then was evaluated for neurological deficits using two graded scoring systems as previously described [6,7,9]. The neurologic condition of the rat was assessed at 24 h and 7 days after the ischemic insult. The animals were assigned a numerical score ranging from 0 (no observable evidence of neurologic deficit) to 3 (most severely injured) as described by Bederson et al. [9]. In addition to the Bederson test, rats underwent various sensorimotor and proprioception behavioral tests further evaluating forelimb and hindlimb function. Collectively, the Bederson score, hindlimb, and forelimb individual scores were added together. A normal healthy rat would have a global neurologic score of 0. A rat with maximal neurologic deficit would have a global neurologic score of 7.

2.7. Statistics

Absolute measurements (e.g. infarct volume, densitometry) for each individual parameter were analyzed by parametric and non-parametric analyses of variance (ANOVA). Post hoc comparisons among groups were evaluated using Fisher's protected least significant differences (LSD) and Dunnett's test where appropriate. Neurobehavioral scores were evaluated using Kruskal–Wallis median test. Differences among groups were assessed using Mann–Whitney U-test.

3. Results

3.1. Evidence of p38 phosphorylation

To determine whether the activity of p38 MAPK was altered following permanent middle cerebral artery occlusion, ischemic (n=4) and control cortices (n=4) were subjected to Western analysis using p38 and phospho p38 MAPK antibodies. There were no significant changes in non-phosphorylated p38 MAPK levels between sham-operated and MCAO animals from 15 min to 5 days post stroke (figure not shown). Fig. 1 demonstrates a very rapid activation of p38 MAPK. Levels of phosphorylated p38 MAPK were significantly ($P<0.05$) upregulated at both 15 min (2.3-fold) and 1 h (1.8-fold) post injury compared to non-ischemic and sham-operated tissue. The levels returned to baseline by 4 h and there were no significant changes up to 5 days post injury or in sham operated tissue at 15 min, 1, 4, or 24 h.

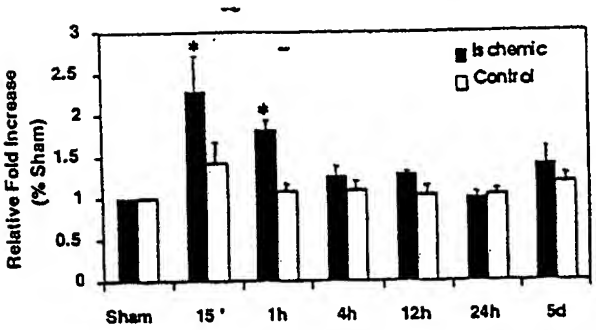

Fig. 1. Changes in phosphorylated p38 MAPK following MCAO in the rat. Ischemic tissue ($n=4$) and control tissue ($n=4$) are represented as mean±S.E. The mean for each group is normalized to sham tissue run on the same gel. Comparisons were considered significant if * $P<0.05$.

3.2. Dose related neuroprotection

In order to further evaluate whether selective p38 inhibition, using a well-characterized p38 inhibitor, is neuroprotective following MCAO, simple behavioral tests to assess neurologic function and triphenyltetrazolium chloride staining for histologic measures were utilized to evaluate several doses of SB 239063 ($n=6$–10 per group). Control animals received an equal volume of acidified tragacanth (vehicle). SB 239063 provided significant neuroprotection in stroke (Fig. 2). The vehicle treated group exhibited an infarct volume of 148±8 mm^3 and a consistent neurologic grade score of 2.6±0.1. Animals, which received the lowest dose (5 mg/kg) of SB 239063, had significantly ($P<0.05$) less neurologic deficits as evidenced by a mean neurologic score of 1.9±0.5 compared to the vehicle treated group. This neurologic protection correlated to a 42% ($P<0.01$) reduction in total infarct volume (86±12 mm^3). The most dramatic neuroprotection, with improvements in behavior, and reductions in infarct size, were observed in the group of animals treated with 15 mg/kg of SB 239063. Animals within this group had a significantly ($P<0.01$) lower mean neurologic score (1.5±0.3) as compared to the vehicle treated group. The behavioral improvements correlated to a 48% reduction in infarct volume (77±11 mm^3) which was significant ($P<0.01$) over vehicle treated animals. A higher dose of SB 239063 (30 mg/kg) was also neuroprotective. At this dose, behavioral deficits were significantly ($P<0.05$) reduced and infarct volume was reduced ($P<0.05$) by ~29%. At a dose of 60 mg/kg, SB 239063 did not reduce functional deficits (2.3±0.4) or confer any significant histologic protection (14%). Fig. 3 demonstrates that the optimal dose of SB 239063 (15 mg/kg) provided significant neuroprotection throughout the forebrain. These relationships for total infarct volume were also evident for percent hemispheric infarct as well as infarct measurements that were corrected for swelling.

3.3. Development and resolution of infarct size

To better evaluate the neuroprotective effects following p38 inhibition with the most effective oral dose of SB 239063 (15 mg/kg), global neurologic deficit (GND), diffusion weighted imaging (DWI), and T2 weighted MRI were evaluated following MCAO to monitor both the development and resolution of the infarct. DWI was used to measure the early effects of cytotoxic edema to reflect the areas ultimately at risk of irreversible injury. This has been shown previously to reflect ultimate degree of injury/protection in this model [12]. We have previously demon-

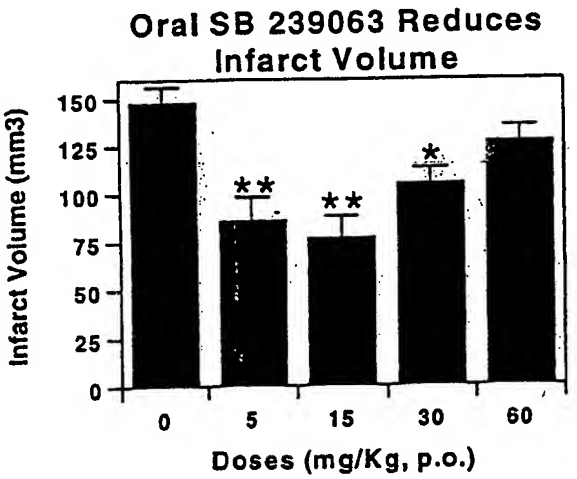

Fig. 2. Dose-related effects of oral SB 239063 on infarct volume following MCAO. Oral administration of SB 239063 at 5, 15, and 30 mg/kg significantly reduced total infarct volume at 24 h following MCAO ($n=6$–10/group). All data are represented as mean±S.E. Differences were considered significant at * $P<0.05$ and ** $P<0.01$ compared with vehicle treated group.

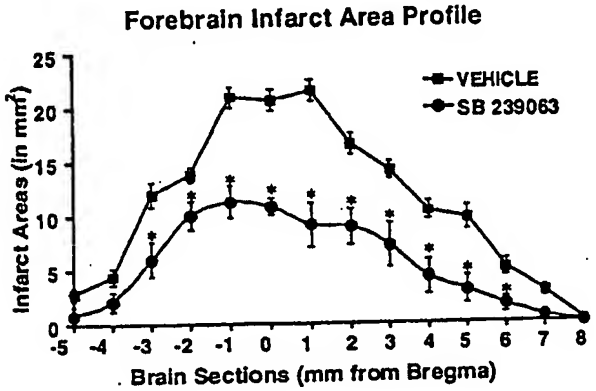

Fig. 3. Effects of SB 239063 (15 mg/kg) on infarct volume over sequential forebrain slices. Brain sections correspond to various distances from the skull landmark bregma for vehicle treated and SB 239063 (15 mg/kg) groups. This figure demonstrates the significant neuroprotection exhibited throughout the forebrain as a result of oral administration of SB 239063 (15 mg/kg). All data are represented as mean±S.E. Differences were considered significant at * $P<0.05$ compared with vehicle treated group.

strated a very high correlation ($r>0.90$, $P<0.01$) between TTC histology and T2 weighted MRI at 24 h post MCAO. In this particular study, using a separate group of animals treated with either vehicle ($n=5$) or 15 mg/kg SB 239063 ($n=5$), this relationship was reconfirmed and again highly correlative ($r=0.94$, $P<0.01$). At 2 h post injury, there was a significant ($P<0.05$) reduction in the area at risk (e.g. cell depolarization, diffusibility of water) for the SB 239063 (109.7±9.7 mm^3) treated group compared to the vehicle group (160.8±9.3 mm^3). At 24 h post injury, there was ~30% reduction in infarct size between the SB 239063 (146.8±7.8 mm^3) and the vehicle treated group (206.4±11.3 mm^3). There was a good correlation ($r=0.74$, $P<0.01$) between the protection observed using early DWI ($n=9$/group) and 24 h T2 MR imaging ($n=9$/group). At 1 day post MCAO, SB 239063 (15 mg/kg) therefore, provided dramatic neuroprotection which was associated with a significant ($P<0.01$) reduction in neurologic deficit from 4.4±0.4 in the vehicle treated group to 1.6±0.3 in animals receiving SB 239063 (15 mg/kg). At 7 days post MCAO, animals receiving SB 239063 (15 mg/kg) maintained a 30% reduction in infarct size which was significant ($P<0.05$) compared to the vehicle treated group. The neuroprotection that was observed with T2 weighted MRI over time is represented in Fig. 4. The neuroprotection as assessed by infarct size was not attributable to any significant differences in amount of swelling within the injured brain between the treatment groups. By day 7, the ischemic hemisphere had become significantly smaller due to macrophage. Identical results were obtained when the infarct volumes were corrected for swelling. At 7 days post injury, SB 239063 (15 mg/kg) also significantly ($P<0.01$) improved neurologic outcome assessed by a GND of 1.2±0.2 compared to 3.8±0.5 for the vehicle treated group.

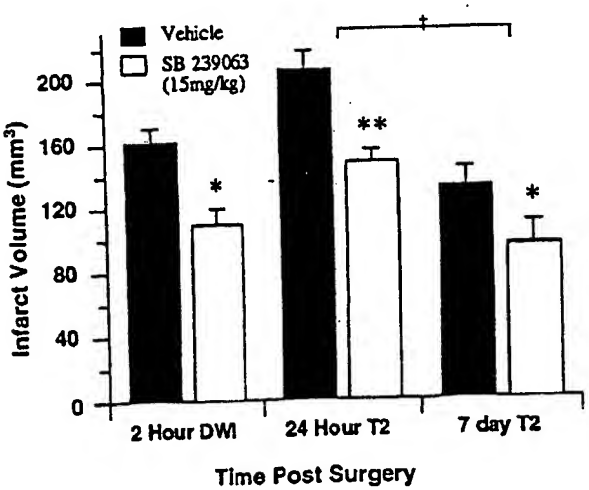

Fig. 4. Effects of SB 239063 (15 mg/kg) on infarct volume over a 7-day period. All data are represented as mean±S.E. Differences were considered significant at * $P<0.05$ compared to vehicle, ** $P<0.01$ compared to vehicle, and † $P<0.05$ compared to day 1.

4. Discussion

4.1. p38 Mitogen activated protein kinases

This was the first study designed to examine the temporal relationship of p38 activation following moderate focal stroke, where this type of ischemia produces a discrete cortical infarct. In the normal brain, p38 (non-phosphorylated) is present in a wide variety of cell types including neurons, astrocytes, endothelial cells and leukocytes. Following permanent middle cerebral artery occlusion, we did not expect or observe any changes in non-phosphorylated p38 MAPK at any of the time points (15 min to 5 days) evaluated. The levels of non-phosphorylated p38 MAPK were nearly identical between both the ischemic and contralateral control hemispheres for injured and sham-operated animals. These results are consistent with an earlier study where Walton et al. reported no change in p38 MAPK levels following bilateral common carotid occlusion [41].

4.2. p38 MAPK and delayed cell death

In the same study, however, following 7 min of global ischemia, gradual changes in activated/phosphorylated p38 MAPK activation were observed over 47 days with the peak appearing at 4 days [41]. This type of stimulus usually leads to apoptotic cell death over the course of 1 week. Bhat et al. have studied this response in more detail using Nissl-stained sections and demonstrated that the loss of CA1 pyramidal neurons was maximal between 3 and 4 days after ischemia. Taken together, these results along with several others suggest that p38 activation may play a role in apoptotic cell death [11,21,27,36,42]. Several studies have evaluated the effects of p38 inhibition following apoptosis [18,21,23,27,34,36,42]. In cultured cerebellar granule neurons, SB 203580 prevented the activation of caspase 3 activity as well as glutamate-induced apoptosis [18,23]. In PC12 pheochromocytoma cells, withdrawal of nerve growth factor induces apoptotic cell death, which is preceded by p38 MAPK activation [27]. Within PC12 cells, apoptosis (programmed cell death) may be regulated by a balance of survival promoting extracellular signal regulating kinases (ERK) and stress-activated protein kinases (SAPK) [42]. SB 203580 abolished this apoptotic cell death and enhanced neuronal survival within this cell culture system [21,42]. However, there are only limited studies evaluating the effects of p38 activation and inhibition following stimuli that result primarily in necrotic cell death [4].

4.3. Activation of the p38 pathway following focal stroke

In the present study, p38 MAPK activity was evaluated following moderate focal stroke where cell death primarily occurs in cortical tissue via necrosis. Following MCAO, there was an early and robust activation of p38 MAPK at 15 min post injury which was maintained at 1 h but then returned to baseline levels by ~4 h post MCAO. These data are consistent with previous data demonstrating that p38 MAPK activation is an early response to the cellular stress (i.e. ischemia, ATP depletion, ionic changes) elicited by severe focal ischemia [4]. The early increases in p38 activation are also in agreement with immunohistochemical changes in p38 MAPK phosphorylation observed in other models of focal stroke. In particular, p38 activity increased early as observed at 1, 3 and 6 h following thread MCAO [4], and was prolonged, remaining elevated for at least 24 h, following transient MCAO [22]. Therefore, the changes in p38 MAPK activation may be differentially regulated in response to either the duration and/or intensity of the stimuli. The rapid activation of p38 post-ischemia may be directly neurodestructive to the neurons rather than inducing a delayed cell death via apoptosis. In this SHR model of moderate focal stroke, the damage is maximal within the first 24 h and primarily restricted to the cortex. In addition, there is little evidence for apoptotic cell death in this model.

Rapid activation of p38 MAPK has also been observed following myocardial/ischemia reperfusion injury [34]. The maximal level of p38 MAPK activation in isolated Langerdorff perfused hearts was at 10 min following reperfusion which is consistent with the results obtained in this study. Pre-treatment with SB 203580, a specific p38 inhibitor, significantly improved post-ischemic cardiac function but treatment initiated after 10 min had no effect. Having established significant activation/phosphorylation of p38 MAPK in the brain up to and including 1 h following moderate focal stroke, the current study was designed to determine whether inhibition of p38 MAPK activation would provide early direct neuroprotection following ischemia.

4.4. Early neuronal protection using SB 239063

SB 239063 is a second generation pyridinyl imidazole compound with potent activity and improved selectivity [4]. Specific p38 MAPK inhibitors have been widely studied in both in vivo and in vitro models. The early rapid activation of p38 in this model suggests that treatment may be most beneficial if initiated prior to or at the time of peak activation. In the present study, SB 239063 (administered 1 h pre- and 6 h post MCAO) provided significant neuroprotection following focal stroke. We have also previously demonstrated that intravenous treatment, with SB 239063, was neuroprotective when initiated within the first 15 min following MCAO [4]. In a separate study intravenous treatment with SB 239063 prevented activated p38 from phosphorylating its downstream targets at plasma levels that provided significant neuroprotection from brain injury [3]. Although we have demonstrated that SB 239063 blocks p38 activity at 1 h and is neuroprotective when administered prior to or at the time of peak activation, we have not fully evaluated the therapeutic window for this class of drug. The most effective dose of SB 239063 (15 mg/kg) was then evaluated using MR imaging to monitor both the development and resolution of the infarct from 2 h to 7 days post MCAO. There was a striking difference in diffusion weighted imaging (DWI) at 2 h post MCAO. The DWI contrast is based on lack of mobility of water in the extra-cellular environment. During the initial phases of ischemic injury, areas where the extracellular space is dramatically reduced (restricted for free water mobility due to cell swelling) are highlighted by this technique [40]. Therefore, it is implied that DWI measures the early effects of cytotoxic edema. Thus, the size of the infarct very early following stroke in essence reflects the areas ultimately at risk of irreversible injury but not necessarily irrevocably injured at that early time point. In fact, a good agreement with post-mortem histology demonstrates that areas at risk, as predicted by DWI early following MCAO in this model, do finally get damaged permanently as measured by TTC staining at 24 h [12]. At 24 h post injury, the animals treated with SB 239063 exhibited a 30% reduction in infarct volume compared to vehicle treated animals. Therefore, the data demonstrate that the protection observed at 2 h is identical to the neuroprotection seen at 24 h. By 7 days post injury, both infarct size and hemispheric size had decreased due to the phagocytic activity of macrophages which creates a cavitation within the necrotic tissue and was probably responsible for the decrease in hemispheric volume [13] but the 30% protection in the drug treated group was maintained. Overall, the data demonstrate that treatment with SB 239063 (15 mg/kg) provides dramatic neuroprotection up to and including 7 days post MCAO. Since the protection observed at 7 days was identical to that assessed by DWI at 2 h, it appears that no additional cell death (e.g. via apoptosis) had occurred over 1 week. The data also suggest that the reduction in DWI hyperintensity observed at 2 h following treatment with SB 239063 may be attributed to a direct protective effect on brain cells. This in vivo study is in agreement with previous findings where SB 239063 (20 μM) significantly reduced hippocampal CA1 cell death (up to 40%) produced by OGD in cultured organotypic brain slices [4]. These in vitro data suggest that p38 inhibition may directly protect neurons, independent of blood flow effects, in addition to effects at blocking inflammatory cytokine/mediator production. We have previously demonstrated that SB 239063 has no cardiovascular or cerebrovascular effects in spontaneously hypertensive rats (SHR) [4]. SHR were chosen because they exhibit a more

consistent degree of brain damage following permanent or transient focal ischemia than do normotensive rats using dorsal electrocoagulation of the MCA [6] because of their limited collateral circulation [14–16]. These early improvements in neuronal injury following p38 inhibition do reflect final outcome up to and including 1 week post injury.

Studies are ongoing to determine the effective therapeutic window for SB 239063 following focal stroke. In addition multiple in vitro cell systems are being utilized to better understand how SB 239063 may be interfering with the early pathophysiological events. These detailed in vitro studies are necessary to fully understand the role of p38 following ischemia and the mechanism(s) by which it can be beneficial.

Acknowledgements

This work was supported in part by a grant from the American Heart Association (Award # 9910080U). The authors would also like to thank Thomas R. Schaeffer for his technical assistance in carrying out the experiments involving the use of the MRI.

References

[1] A.M. Badger, J.N. Bradbeer, B. Votta, J.C. Lee, J.L. Adams, D.E. Griswold, Pharmacological profile of SB 203580, a selective inhibitor of cytokine suppressive binding protein/p38 kinase, in animal models of arthritis, bone resorption, endotoxin shock and immune function, J. Pharmacol. Exp. Ther. 279 (1996) 1453–1461.

[2] A.M. Badger, M.N. Cook, M.W. Lark, T.M. Newman-Tarr, B.A. Swift, A.H. Nelson, F.C. Barone, S. Kumar, SB 203580 inhibits p38 mitogen-activated protein kinase, nitric oxide production, and inducible nitric oxide synthase in bovine cartilage-derived chondrocytes, J. Immunol. 161 (1998) 467–473, (published erratum appears in J. Immunol. 162 (5) (1999) 3105).

[3] F. Barone, E.A. Irving, A.M. Ray, J.C. Lee, S. Kassis, S. Kumar, A.M. Badger, J.J. Legos, J.A. Erhardt, A.H. Nelson, E.H. Ohlstein, A.J. Hunter, D.C. Harrison, K. Philpott, B.R. Smith, J.L. Adams, A.A. Parsons, Inhibition of p38 mitogen activated protein kinase provides neuroprotection in cerebral focal ischemia, Med. Res. Rev. in press.

[4] F. Barone, E.A. Irving, A.M. Ray, J.C. Lee, S. Kassis, S. Kumar, A.M. Badger, R.F. White, J.J. Legos, J.A. Erhardt, A.H. Nelson, E.H. Ohlstein, A.J. Hunter, K. Ward, B.R. Smith, J.L. Adams, A.A. Parsons, SB 239063, A second generation p38 mitogen-activated protein kinase inhibitor, reduces brain injury and neurological deficits in cerebral focal ischemia, J. Pharm. Exp. Ther. 296 (2) (2001) 1–10.

[5] F.C. Barone, L.M. Hillegass, M.N. Tzimas, D.B. Schmidt, J.J. Foley, R.F. White, W.J. Price, G.Z. Feuerstein, R.K. Clark, D.E. Griswold, H.M. Sarau, Time-related changes in myeloperoxidase activity and leukotriene B-4 receptor binding reflect leukocyte influx in cerebral focal stroke, Mol. Chem. Neuropathol. 24 (1995) 13–30.

[6] F.C. Barone, W.J. Price, R.F. White, R.N. Willette, G.Z. Feuerstein, Genetic hypertension and increased susceptibility to cerebral ischemia, Neurosci. Biobehav. Rev. 16 (1992) 219–233.

[7] F.C. Barone, R.F. White, P.A. Spera, J. Ellison, R.W. Currie, X. Wang, G.Z. Feuerstein, Ischemic preconditioning and brain tolerance: temporal histological and functional outcomes, protein synthesis requirement, and interleukin-1 receptor antagonist and early gene expression, Stroke 29 (1998) 1937–1950, (discussion 1950-1).

[8] J.B. Bederson, L.H. Pitts, S.M. Germano, M.C. Nishimura, R.L. Davis, H.M. Bartkowski, Evaluation of 2,3,5-triphenyltetrazolium chloride as a stain for detection and quantification of experimental cerebral infarction in rats, Stroke 17 (1986) 1304–1308.

[9] J.B. Bederson, L.H. Pitts, M. Tsuji, M.C. Nishimura, R.L. Davis, H. Bartkowski, Rat middle cerebral artery occlusion: evaluation of the model and development of a neurologic examination, Stroke 17 (1986) 472–476.

[10] R. Beyaert, A. Cuenda, W. Vanden Berghe, S. Plaisance, J.C. Lee, G. Haegeman, P. Cohen, W. Fiers, The p38/RK mitogen-activated protein kinase pathway regulates interleukin-6 synthesis response to tumor necrosis factor, EMBO J. 15 (1996) 1914–1923.

[11] B.S. Cain, D.R. Meldrum, X. Meng, C.A. Dinarello, B.D. Shames, A. Banerjee, A.H. Harken, p38 MAPK inhibition decreases TNF-alpha production and enhances postischemic human myocardial function, J. Surg. Res. 83 (1999) 7–12.

[12] S. Chandra, R.F. White, D. Everding, G.Z. Feuerstein, R.W. Coatney, S.K. Sarkar, F.C. Barone, Use of diffusion-weighted MRI and neurological deficit scores to demonstrate beneficial effects of isradipine in a rat model of focal ischemia, Pharmacology 58 (1999) 292–299.

[13] R.K. Clark, E.V. Lee, C.J. Fish, R.F. White, W.J. Price, Z.L. Jonak, G.Z. Feuerstein, F.C. Barone, Development of tissue damage, inflammation and resolution following stroke: an immunohistochemical and quantitative planimetric study, Brain Res. Bull. 31 (1993) 565–572.

[14] P. Coyle, Different susceptibilities to cerebral infarction in spontaneously hypertensive (SHR) and normotensive Sprague–Dawley rats, Stroke 17 (1986) 520–525.

[15] P. Coyle, D.D. Heistad, Blood flow through cerebral collateral vessels in hypertensive and normotensive rats, Hypertension 8 (1986) II67–II71.

[16] P. Coyle, D.D. Heistad, Development of collaterals in the cerebral circulation, Blood Vessels 28 (1991) 183–189.

[17] Y. Gon, S. Hashimoto, K. Matsumoto, T. Nakayama, I. Takeshita, T. Horie, Cooling and rewarming-induced IL-8 expression in human bronchial epithelial cells through p38 MAP kinase-dependent pathway, Biochem. Biophys. Res. Commun. 249 (1998) 156–160.

[18] J. Harada, M. Sugimoto, An inhibitor of p38 and JNK MAP kinases prevents activation of caspase and apoptosis of cultured cerebellar granule neurons, Jpn. J. Pharmacol. 79 (1999) 369–378.

[19] S. Hashimoto, K. Matsumoto, Y. Gon, S. Maruoka, I. Takeshita, S. Hayashi, T. Koura, K. Kujime, T. Horie, p38 Mitogen-activated protein kinase regulates IL-8 expression in human pulmonary vascular endothelial cells, Eur. Respir. J. 13 (1999) 1357–1364.

[20] S. Hashimoto, K. Matsumoto, Y. Gon, T. Nakayama, I. Takeshita, T. Horie, Hyperosmolarity-induced interleukin-8 expression in human bronchial epithelial cells through p38 mitogen-activated protein kinase, Am. J. Respir. Crit. Care Med. 159 (1999) 634–640.

[21] S. Horstmann, P.J. Kahle, G.D. Borasio, Inhibitors of p38 mitogen-activated protein kinase promote neuronal survival in vitro, J. Neurosci. Res. 52 (1998) 483–490.

[22] E.A. Irving, F.C. Barone, A.D. Reith, S.J. Hadingham, A.A. Parsons, Differential activation of MAPK/ERK and p38/SAPK in neurones and glia following focal cerebral ischaemia in the rat, Mol. Brain Res. 77 (2000) 65–75.

[23] H. Kawasaki, T. Morooka, S. Shimohama, J. Kimura, T. Hirano, Y. Gotoh, E. Nishida, Activation and involvement of p38 mitogen-activated protein kinase in glutamate-induced apoptosis in rat cerebellar granule cells, J. Biol. Chem. 272 (1997) 18518–18521.

[24] A. Krause, H. Holtmann, S. Eickemeier, R. Winzen, M. Szamel, K. Resch, J. Saklatvala, M. Kracht, Stress-activated protein kinase/Jun N-terminal kinase is required for interleukin (IL)-1-induced IL-6 and

IL-8 gene expression in the human epidermal carcinoma cell line KB, J. Biol. Chem. 273 (1998) 23681–23689.
[25] S. Kumar, M.S. Jiang, J.L. Adams, J.C. Lee, Pyridinylimidazole compound SB 203580 inhibits the activity but not the activation of p38 mitogen-activated protein kinase, Biochem. Biophys. Res. Commun. 263 (1999) 825–831.
[26] S. Kumar, P.C. McDonnell, R.J. Gum, A.T. Hand, J.C. Lee, P.R. Young, Novel homologues of CSBP/p38 MAP kinase: activation, substrate specificity and sensitivity to inhibition by pyridinyl imidazoles, Biochem. Biophys. Res. Commun. 235 (1997) 533–538.
[27] J.L. Kummer, P.K. Rao, K.A. Heidenreich, Apoptosis induced by withdrawal of trophic factors is mediated by p38 mitogen-activated protein kinase, J. Biol. Chem. 272 (1997) 20490–20494.
[28] J.M. Kyriakis, J. Avruch, Sounding the alarm: protein kinase cascades activated by stress and inflammation, J. Biol. Chem. 271 (1996) 24313–24316.
[29] J.C. Lee, A.M. Badger, D.E. Griswold, D. Dunnington, A. Truneh, B. Votta, J.R. White, P.R. Young, P.E. Bender, Bicyclic imidazoles as a novel class of cytokine biosynthesis inhibitors, Ann. NY Acad. Sci. 696 (1993) 149–170.
[30] J.C. Lee, J.T. Laydon, P.C. McDonnell, T.F. Gallagher, S. Kumar, D. Green, D. McNulty, M.J. Blumenthal, J.R. Heys, S.W. Landvatter et al., A protein kinase involved in the regulation of inflammatory cytokine biosynthesis, Nature 372 (1994) 739–746.
[31] J.C. Lee, P.R. Young, Role of CSB/p38/RK stress response kinase in LPS and cytokine signaling mechanisms, J. Leukocyte Biol. 59 (1996) 152–157.
[32] J.J. Legos, R.G. Whitmore, J.A. Erhardt, A.A. Parsons, R.F. Tuma, F.C. Barone, Quantitative changes in interleukin proteins following focal stroke in the rat, Neurosci. Lett. 282 (2000) 189–192.
[33] T.N. Lin, Y.Y. He, G. Wu, M. Khan, C.Y. Hsu, Effect of brain edema on infarct volume in a focal cerebral ischemia model in rats, Stroke 24 (1993) 117–121.
[34] X.L. Ma, S. Kumar, F. Gao, C.S. Louden, B.L. Lopez, T.A. Christopher, C. Wang, J.C. Lee, G.Z. Feuerstein, T.L. Yue, Inhibition of p38 mitogen-activated protein kinase decreases cardiomyocyte apoptosis and improves cardiac function after myocardial ischemia and reperfusion, Circulation 99 (1999) 1685–1691.
[35] K. Matsumoto, S. Hashimoto, Y. Gon, T. Nakayama, T. Horie, Proinflammatory cytokine-induced and chemical mediator-induced IL-8 expression in human bronchial epithelial cells through p38 mitogen-activated protein kinase-dependent pathway, J. Allergy Clin. Immunol. 101 (1998) 825–831.
[36] D.S. Nagarkatti, R.I. Sha'afi, Role of p38 MAP kinase in myocardial stress, J. Mol. Cell. Cardiol. 30 (1998) 1651–1664.
[37] M.J. Robinson, M.H. Cobb, Mitogen-activated protein kinase pathways, Curr. Opin. Cell Biol. 9 (1997) 180–186.
[38] R.A. Swanson, M.T. Morton, G. Tsao-Wu, R.A. Savalos, C. Davidson, F.R. Sharp, A semiautomated method for measuring brain infarct volume, J. Cereb. Blood Flow Metab. 10 (1990) 290–293, (see comments).
[39] H. Tomimoto, I. Akiguchi, H. Wakita, A. Kinoshita, A. Ikemoto, S. Nakamura, J. Kimura, Glial expression of cytokines in the brains of cerebrovascular disease patients, Acta Neuropathol. 92 (1996) 281–287.
[40] H.B. Verheul, R. Balazs, J.W. Berkelbach van der Sprenkel, C.A. Tulleken, K. Nicolay, K.S. Tamminga, M. van Lookeren Campagne, Comparison of diffusion-weighted MRI with changes in cell volume in a rat model of brain injury, NMR Biomed. 7 (1994) 96–100, (published erratum appears in NMR Biomed 7(8) (1994) 374).
[41] K.M. Walton, R. DiRocco, B.A. Bartlett, E. Koury, V.R. Marcy, B. Jarvis, E.M. Schaefer, R.V. Bhat, Activation of p38MAPK in microglia after ischemia, J. Neurochem. 70 (1998) 1764–1767.
[42] Z. Xia, M. Dickens, J. Raingeaud, R.J. Davis, M.E. Greenberg, Opposing effects of ERK and JNK-p38 MAP kinases on apoptosis, Science 270 (1995) 1326–1331.
[43] P.R. Young, M.M. McLaughlin, S. Kumar, S. Kassis, M.L. Doyle, D. McNulty, T.F. Gallagher, S. Fisher, P.C. McDonnell, S.A. Carr, M.J. Huddleston, G. Seibel, T.G. Porter, G.P. Livi, J.L. Adams, J.C. Lee, Pyridinyl imidazole inhibitors of p38 mitogen-activated protein kinase bind in the ATP site, J. Biol. Chem. 272 (1997) 12116–12121.

Exhibit 9

Journal of Cardiovascular Pharmacology™
35:474–483 © 2000 Lippincott Williams & Wilkins, Inc., Philadelphia

Inhibition of the Cardiac p38-MAPK Pathway by SB203580 Delays Ischemic Cell Death

*†Miroslav Barancik, *Patrik Htun, *Claudia Strohm, *Sven Kilian, and *Wolfgang Schaper

*Department of Experimental Cardiology, Max-Planck-Institute for Physiological and Clinical Research, Bad Nauheim, Germany; and †Institute for Heart Research, Slovak Academy of Sciences, Bratislava, Slovak Republic

Summary: We report that SB203580 (SB), a specific inhibitor of p38-MAPK, protects pig myocardium against ischemic injury in an in vivo model. SB was applied by local infusion into the subsequently ischemic myocardium for 60 min before a 60-min period of coronary occlusion followed by 60-min reperfusion (index ischemia). Infarct size was reduced from a control value of 69.3 ± 2.7% to 36.8 ± 3.7%. When SB was infused systemically for 10 min before index ischemia, infarct size was reduced to 36.1 ± 5.6%. We measured the content of phosphorylated p38-MAPK after systemic infusion of SB and Krebs–Henseleit buffer (KHB; negative control) and during the subsequent ischemic period using an antibody that reacts specifically with dual-phosphorylated p38-MAPK (Thr180/Tyr182). Ischemia with and without SB significantly increased phospho-p38-MAPK, with a maximum reached at 20 min but was less at 30 and 45 min under the influence of the inhibitor. The systemic infusion of SB for 10 min before index ischemia did not significantly change the p38-MAPK activities (compared with vehicle, studied by in-gel phosphorylation) ≤20 min of ischemia, but activities were reduced at 30 and 45 min. Measurements of p38-MAPK activities in situations in which SB was present during in-gel phosphorylation showed significant inhibition of p38-MAPK activities. The systemic infusion of SB significantly inhibited the ischemia-induced phosphorylation of nuclear activating transcription factor 2 (ATF-2). Using a specific ATF-2 antibody, we did not observe significant changes in ATF-2 abundance when nuclear fractions from untreated, KHB-, and SB-treated tissues were compared. We investigated also the effect of local and systemic infusion of SB on the cardioprotection induced by ischemic preconditioning (IP). The infusions (local or systemic) of SB before and during the IP protocol did not influence the infarct size reduction mediated by IP. The observed protection of the myocardium against ischemic damage by SB points to the negative role of the p38-MAPK pathway during ischemia. **Key Words:** SB203580—Protein kinases—p38-MAPK—Ischemia/reperfusion—Pig.

Stressful stimuli applied as brief pulse trains condition most tissues so that they become more tolerant against longer lasting stresses, significantly delaying the onset of irreversible damage (1). The molecular mechanism of this increase in stress tolerance, especially that toward ischemia, is not entirely clear, but mitogen activated protein kinases (MAPKs), which are involved in the signal-transduction pathways, may play a role. In previous reports we have shown that brief ischemic pulses lead to changes in the expression of the cardiac protooncogenes that may participate in the adaptive response (2,3). Since the protooncogene-based transcription factors are activated by membrane and cytoplasmic signaling cascades, we studied the involvement of three MAPK pathways (extracellular signal-regulated kinases, ERKs; stress-activated/c-Jun N-terminal kinases, SAPK/JNKs; and p38-MAPK) and found that they react to brief ischemia and reperfusion in a very specific way: the ERKs moderately increased activity during brief ischemia but markedly during reperfusion, the SAPK/JNKs become active only during reperfusion, and the p38-MAPK was activated only during ischemia and deactivated during the following reperfusion and subsequent period of ischemia (4). MAPK pathways can also be influenced by pharmacologic agents that specifically influence the activity of members of the MAPKs, particularly those of the stress-activated protein kinases (SAPK/JNKs, p38-MAPK) (5,6). A common feature of all MAPKs is their

Received July 28, 1999; revision accepted November 15, 1999.
Address correspondence and reprint requests to Dr. W. Schaper at Max-Planck-Institute, Department of Experimental Cardiology, Benekestrasse 2, D-61231 Bad Nauheim, Germany. E-mail: w.schaper@kerckhoff.mpg.de
Drs. Barancik and Htun contributed equally to this article.

ability to phosphorylate the transactivation domains of numerous transcription factors and thus modulate transcriptional activity. However, it cannot be excluded that MAPK activation also has effectors outside the nucleus. The fact that repeated brief occlusion, which can amplify the conditioning effect of the first occlusion, induced an attenuation of p38-MAPK activity suggested that p38-MAPK activation may cause premature ischemic cell death. We hypothesized that SB203580 (SB), an inhibitor of p38-MAPK, may be able to protect the heart against the consequences of prolonged ischemia. This hypothesis was tested in an in vivo model by two different application methods of SB: intramyocardial and intravenous infusion.

MATERIALS AND METHODS

The experimental protocol described in this study was approved by the Bioethical Committee of the District of Darmstadt, Germany. Furthermore, all animals in this study were handled in accordance with the guiding principles in care and use of animals as approved by the American Physiology Society, and the investigation conformed with the Guide for Care and Use of Laboratory Animals published by the U.S. National Institutes of Health.

Chemicals

Azaperone, metomidate, and piritramide were purchased from Janssen Pharmaceutica (Meckenheim, Germany). SB, protein kinase inhibitor (PKI), α-chloralose, triphenyl tetrazolium chloride (TTC), and other biochemicals were from Sigma (Deisenhofen, Germany). The fluorescent zinc-cadmium sulfide microspheres (diameter, 2–15 μm) were purchased from Duke Scientific Corp (AC Leusden, Netherlands). The polyclonal antibody against p38-MAPK was from Santa Cruz Biotechnology (Heidelberg, Germany). Phospho-p38-MAPK, phospho-SAPK/JNK, ATF-2, and phospho-ATF-2 antibodies were from New England Biolabs (Schwalbach/Taunus, Germany). Nitrocellulose membranes, rainbow molecular mass markers, the horseradish peroxidase–linked goat anti-rabbit immunoglobulin, the enhanced chemiluminescence (ECL) reagents, autoradiography films, and [γ-^{32}P]-ATP were from Amersham (Pharmacia Biotech, Europe GmbH, Freiburg, Germany). Recombinant MAPKAPK-2 (residues 46–400 encompassing the catalytic domain) was expressed in *Escherichia coli* as glutathione-*S*-transferase fusion protein (clone provided by C. J. Marshall, a kind gift from P. H. Sugden) and was purified by glutathione-Sepharose (Pharmacia) chromatography.

Animal preparation

Male castrated German landrace-type domestic pigs (32.6 ± 2.3 kg) were premedicated with azaperone (2 mg/kg of body weight, i.m.) and 2 mg/kg BW piritramide, s.c., 30 min before the initiation of anesthesia with 10 mg/kg BW metomidate. After tracheal intubation, a bolus of α-chloralose (25 mg/kg) was given intravenously. Anesthesia was maintained by a continuous intravenous infusion of α-chloralose (25 mg/kg/h). The animals were ventilated artificially with a pressure-controlled respirator (Stephan Respirator ABV, F. Stephan GmbH, Gackenbach, Germany) with room air enriched with 2 L/min of oxygen. Arterial blood gases were analyzed frequently to guide adjustment of the respirator settings. Additional doses of piritramide (10 mg) were given i.v. every 60 min. Both internal jugular veins were cannulated with polyethylene tubes for administration of saline, piritramide, and α-chloralose. Arterial sheath catheters (7F) were inserted into both carotid arteries. To measure arterial blood pressure, the left sheath was advanced into the aortic arch and connected with a Statham transducer (P23XL; Statham, San Juan, Puerto Rico). After a midsternal thoracotomy, the heart was suspended in a pericardial cradle. Arterial pressure, heart rate, and the ECG were continuously monitored and recorded on the hard disk of a MacLab computer. A loose reversible ligature was placed halfway around the left anterior descending artery (LAD), and was subsequently tightened to occlude the vessels. In pigs subjected to intramyocardial microinfusion, eight 26-gauge needles connected by tubing with a peristaltic pump (Miniplus; Gilson, Villiers-le-Bel, France) were placed in pairs along the LAD into the myocardium perpendicular to the epicardial surface. After preparation, a stabilization period of 30 min was allowed and the experimental protocols were started. The p38-MAPK inhibitor, SB, was dissolved in DMSO and finally diluted in Krebs–Henseleit buffer (KHB; final concentration of DMSO was 0.1%). For this reason, the infusion of KHB with DMSO served as a negative control (KHB).

Experimental groups

This study consisted of eight experimental groups (Fig. 1). Group I was subjected to 60 min of occlusion and 60 min of reperfusion (control group 1). In group II, SB (40 n*M*) or KHB (with 0.1% DMSO) was administered by local infusion for 60 min before the index ischemia of 60 min and the following reperfusion period of 60 min. In group III, SB (5 mg/animal) or KHB was applied by systemic infusion for 10 min before the index ischemia (60 min occlusion and 60 min reperfusion periods). In group IV, the animals were subjected to 40 min of occlusion followed by 60 min of reperfusion (control group 2). In group V, the animals were subjected to the preconditioning protocol (two cycles of 10-min ischemia and 10-min reperfusion) followed by a period of 40-min index ischemia and 60 min of reperfusion. In group VI, SB (40 n*M*) or KHB was administered by local microinfusion for 15 min before the brief occlusions/reperfusions and during reperfusion periods of the preconditioning protocol. This was followed by 40 min of ischemia and 60 min of reperfusion. In group VII, SB (5 mg/animal) or KHB was applied by intravenous infusion for 15 min before the brief occlusions/reperfusions and during reperfusion periods of the preconditioning protocol. This was followed by 40 min of index ischemia and 60 min of reperfusion. In group VIII, SB (5 mg/animal) or KHB was applied by intravenous infusion for 10 min before the index ischemia of 60 min, and left ventricular biopsies for in vitro assays were obtained at the end of SB and KHB infusion and at 5, 10, 20, 30, 45, and 60 min of the following index ischemia. Drill biopsies were taken from control tissue, KHB-, and SB-treated tissue (Fig. 1). Biopsies weighed ~80 mg and were ~4 mm long (i.e., they reached from epi- to midmyocardium).

Determination of infarct size

At 45 min into the last reperfusion period, 1 g of fluorescein dissolved in 10 ml Ringer's solution was injected into the right ventricle. This stained the entire myocardium and detected nonreperfused tissue. Hearts with traces of nonreperfused myocardium were excluded from analysis. At the end of the experi-

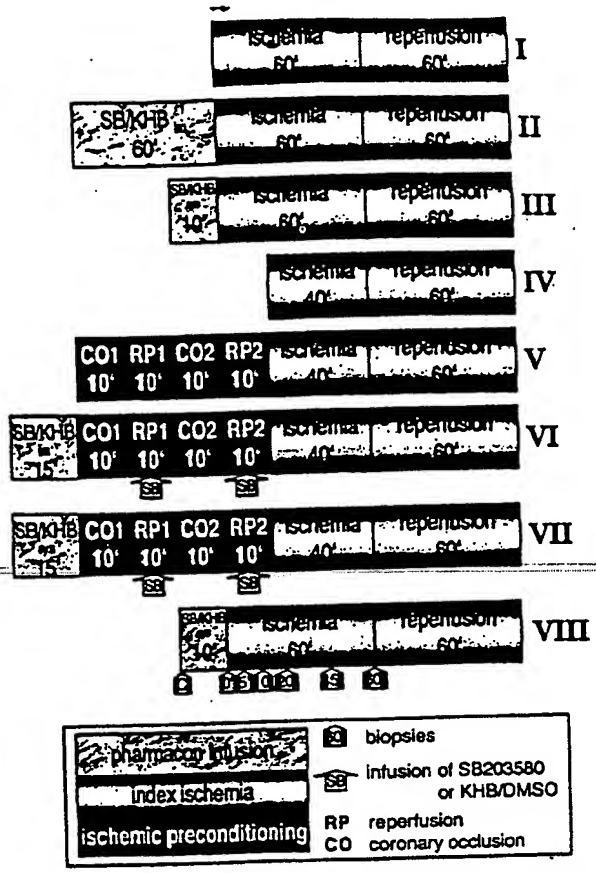

FIG. 1. This study consisted of eight experimental groups. Group I was subjected to 60 min of occlusion and 60 min of reperfusion (control group 1). In group II, SB203580 (40 n*M*) or KHB (with 0.1% DMSO, negative control) were administered by local intramyocardial infusion (i.m.; infusion rate, 20 μl/min) for 60 min before the index ischemia of 60 min and the following reperfusion period of 60 min. In group III, SB203580 (5 mg/animal) or KHB was applied by systemic infusion (sys) for 10 min before the index ischemia of 60 min and the following reperfusion period of 60 min. In group IV, the animals were subjected to 40 min of occlusion followed by 60 min of reperfusion (control group 2). In group V, the animals were subjected to a preconditioning protocol of two cycles of 10-min ischemia and 10-min reperfusion followed by the index ischemia of 40-min occlusion and a reperfusion period of 60 min. In group VI, SB203580 (40 n*M*) or KHB was administered by local microinfusion for 15 min before preconditioning and during the reperfusion phase of the preconditioning protocol. This was followed by index ischemia of 40-min occlusion and a reperfusion period of 60 min. In group VII, SB203580 (5 mg/animal) or KHB was applied by systemic infusion for 15 min before preconditioning and during the reperfusion phases. This was followed by the index ischemia of 40-min occlusion and the reperfusion period of 60 min. In group VIII, SB203580 (5 mg/animal) or KHB was systematically infused for 10 min before index ischemia of 60 min, and left ventricular biopsies for in vitro assays were obtained at the end of SB and KHB infusion and at various intervals of index ischemia.

mental protocol, the LAD and the aorta were occluded, clamped, and 500 mg of zinc cadmium fluorescent microspheres in 10 ml of Ringer's solution were injected into the ascending aorta. Shortly thereafter, the animals were injected with an intravenous bolus of 20% potassium chloride to arrest the heart. After excision, both atria and the right ventricle were removed. The left ventricle was cut into slices along the microinfusion needle pairs perpendicular to the LAD. Heart slices were weighed and incubated at 37°C in 1% triphenyltetrazolium chloride (TTC) in PBS, pH 7.0, for 20 min. Myocardium at risk of infarction was identified as the nonfluorescent (by microspheres) area by UV light (366 nm). The infarcted area was demarcated by the absence of the characteristic red TTC stain. The slices were photographed by double exposure with UV and artificial daylight, and the pictures were used for further planimetric evaluation. Planimetry of the infarct areas was performed on the basal aspect of the apex, the apical and basal sides of the following four consecutive myocardial slices, and on the apical aspect of the basal section of the left ventricle. We expressed infarct size (IS) as the infarct area (IA) relative to the risk area (RA). Infarct sizes were then averaged per group and depicted graphically (Figs. 3 and 5).

Preparation of soluble and nuclear fractions

The biopsies for the kinase assays were suspended in ice-cold buffer containing in m*M*: 20 Tris-HCl, 250 sucrose, 1.0 EDTA, 1.0 EGTA, 1.0 dithiothreitol (DTT), 0.1 sodium orthovanadate, 10 NaF, and 0.5 PMSF, pH 7.4, (buffer A), and were homogenized with a Teflon-glass homogenizer. The homogenates were centrifuged at 14,000 *g* for 30 min at 4°C. The supernatants represented the soluble (cytosolic) fractions. The pellets were resuspended in buffer B containing in m*M*: 20 Tris-HCl, 1,000 sucrose, 1.0 EDTA, 1.0 EGTA, 1.0 DTT, 0.1 sodium orthovanadate, 10 NaF, 10 KCl, and 0.1 PMSF (pH 7.4), and were centrifuged for 30 min at 10,000 *g* (4°C). The resulting pellets were resuspended in buffer C containing 10% glycerol, 20 m*M* Tris-HCl, 400 m*M* KCl, 1.0 m*M* EGTA, 1.0 m*M* DTT, 0.1 m*M* sodium orthovanadate, 10 m*M* NaF, 0.5 m*M* PMSF, and 0.1% Triton X-100, and sonicated and used for the detection of transcription factor ATF-2. For the preparation of electrophoretic probes, Laemmli sample buffer was added and the proteins were denatured by heating. The denatured probes were applied to sodium dodecyl sulfate–polyacrylamide gel electrophoresis (SDS-PAGE), and used for MAPK assays by in-gel kinase assays and for Western blot analysis.

Measurement of p38-MAPK activities by in-gel phosphorylation

Equivalent amounts of proteins were separated on 10% SDS-polyacrylamide gels containing 0.5 mg/ml of GST-MAPKAPK-2_{46-400}. After electrophoresis, the gels were washed for 1 h with 20% (vol/vol) 2-propanol in 50 m*M* Tris-HCl (pH 8.0), followed by 1 h with 5 m*M* 2-mercaptoethanol in 50 m*M* Tris-HCl, pH 8.0. The in-gel proteins were denatured by incubation for 2 h with 50 m*M* Tris-HCl, pH 8.0, containing 6 *M* guanidine-HCl. Renaturation was achieved by incubation with 50 m*M* Tris-HCl, pH 8.0, containing 0.1% (vol/vol) Nonidet P-40 and 5 m*M* 2-mercaptoethanol for 16 h. After preincubation of gels in 40 m*M* HEPES (pH 8.0) containing 2 m*M* DTT and 10 m*M* magnesium chloride, the in-gel phosphorylation of substrates was performed in 40 m*M* HEPES (pH 8.0), 0.5 m*M* EGTA, 10 m*M* magnesium chloride, 1.0 μ*M* protein kinase A inhibitory peptide, and 25 μ*M* [γ-^{32}P]-ATP (5 μCi/ml) at 25°C for 4 h. In some experiments, the sample preparation, incubation of gels, and phosphorylation were performed in the presence of 50 n*M* SB. After extensive washing in 5% (wt/vol) trichloroacetic acid containing 2% (wt/vol) sodium pyrophosphate, the gels were dried, and quantitative analysis was

performed using a Phosphorimager SF (Molecular Dynamics, Krefeld, Germany).

Immunoblot analysis

Soluble or nuclear fractions of heart were subjected to SDS-PAGE in 10% polyacrylamide gels, and proteins were transferred onto nitrocellulose membranes. Anti-p38-MAPK, anti-phospho-p38-MAPK, anti-phospho-SAPK/JNK, anti-ATF-2, and anti-phospho-ATF-2 antibodies were used for primary immunodetection. The secondary antibody directed against all antibodies was peroxidase-labeled anti-rabbit immunoglobulin. Bound antibodies were detected by the ECL Western blot detection method.

Statistics

For the IS quantification, we used the unpaired Student's *t* test; $p < 0.05$ was accepted as significant. For in-gel phosphorylation and Western blot assays, the SB-treated tissue biopsy material was compared with control (untreated) and KHB-treated tissue (negative control). The differences were evaluated with a Student's *t* test. The accepted level of significance was $p < 0.05$.

RESULTS

Hemodynamic data

The infusion of SB, systemic and local, had no effect on blood pressure and heart rate. Coronary occlusion produced a decrease in blood pressure that usually returned to normal values before reperfusion.

The effect of SB203580 infusion on infarct size

The effects of local and systemic infusions of the p38-MAPK inhibitor SB on IS in pig myocardium are shown in Figs. 2 and 3. The local intramyocardial infusion of SB203580 (40 n*M*) for 60 min before index ischemia (group II) significantly reduced infarct size from 69.3 ± 2.7% (control, group I) to 36.8 ± 3.7% ($p < 0.002$; Fig. 3). When SB was infused intravenously (5 mg/animal) for 10 min before the onset of 60-min coronary occlusion (group III), we also observed a significant reduction of IS as compared with control (group I; 36.1 ± 5.6% for SB, 69.3 ± 2.7% for control). The remaining infarcts were not solid but rather spotty. Important also is the fact that both local and systemic infusions of KHB/DMSO (0.1%

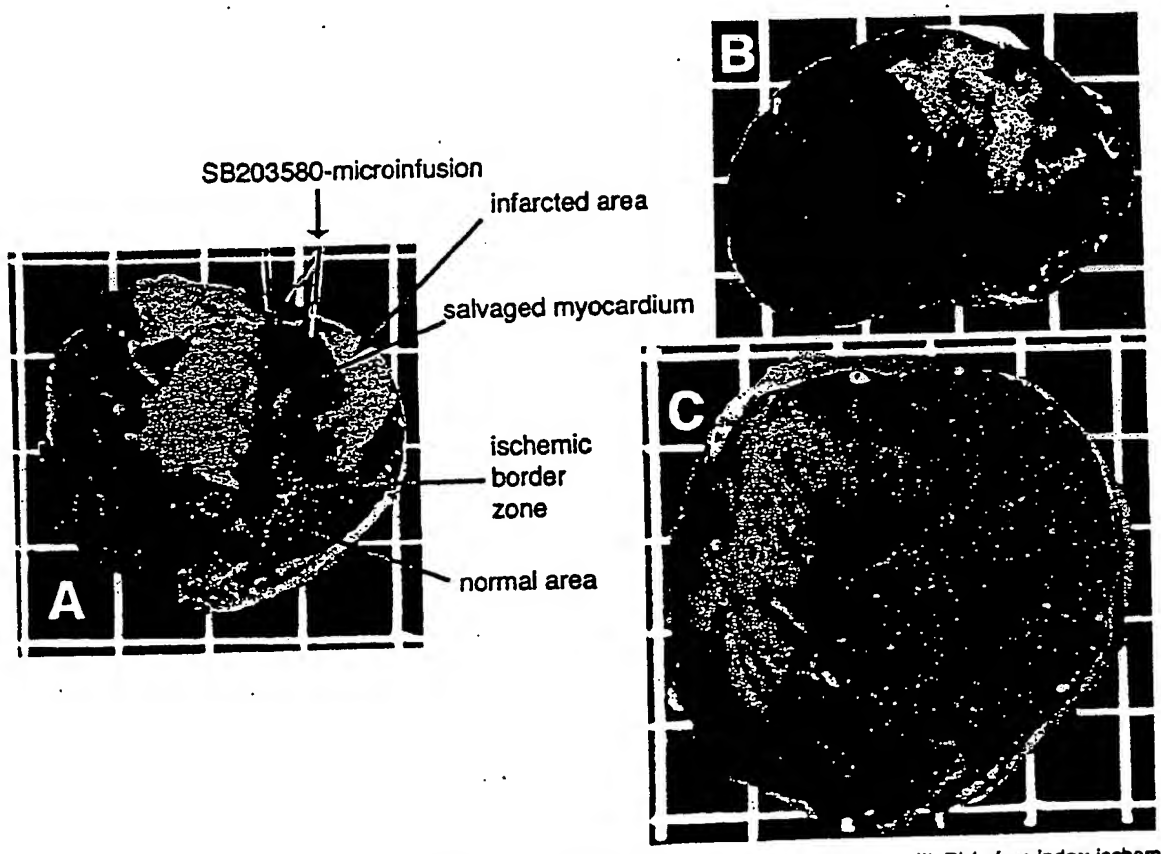

FIG. 2. Intramyocardial infusion of SB203580 (group II; A) and systemic infusion of SB203580 (group III; B) before index ischemia of 60-min occlusion followed by reperfusion of 60 min. The needles for intramyocardial microinfusion were placed into the subsequently ischemic part of the left ventricle. The fluorescent microspheres demarcate the nonfluorescent area of risk. After TTC staining, the myocardial protection was defined as stained tissue surrounding the microinfusion needles in transmurally infarcted myocardium. A: Microinfusion of SB203580 (40 n*M*, needle on the right). B: Systemic infusion of SB203580 (5 mg/animal). C: Index ischemia for 60-min occlusion followed by reperfusion of 60 min (control group 1).

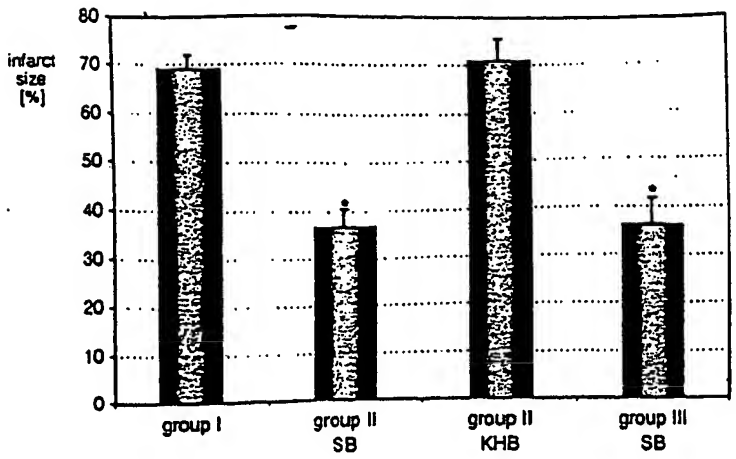

FIG. 3. Effect of local intramyocardial (group II) and systemic infusion (group III) of SB203580 before index ischemia on infarct size in pig myocardium. Group II: Effect of KHB/DMSO infusion on infarct size. Values are expressed as percentage of the area at risk of infarction (group I, control group 1). Each bar represents the mean ± SEM. *$p < 0.002$ (vs. group I).

DMSO in KHB, negative control) before index ischemia did not influence the IS as compared with control (Fig. 3).

The effect of SB203580 on ischemic preconditioning

The effect of local and systemic infusion of SB on cardioprotection by ischemic preconditioning is shown in Figs. 4 and 5. When SB was applied locally before and during the ischemic preconditioning protocol (group VI), the IS represented 3.8 ± 0.5%. This IS was significantly lower than that in control 2 (group IV; IS, 54.0 ± 2.5%) and was not different from group V (IS, 2.5 ± 0.7%; Fig. 5). Systemic application of SB203580 before and during the preconditioning protocol (group VII) did not influence the IS limitation mediated by ischemic preconditioning (3.2 ± 0.5% for SB systemic; Fig. 5). Also in this case, IS was significantly lower than in the control group 2 (group IV). These results show that the infusion (local or systemic) of SB before and during ischemic preconditioning did not influence the IS limitation mediated by ischemic preconditioning. The infusion of KHB/DMSO before and during the preconditioning protocol did not influence the effect of ischemic preconditioning (Fig. 5).

Effect of SB203580 on p38-MAPK activities

The p38-MAPK activity and the phosphorylation state of this enzyme were investigated during index ischemia that followed the systemic infusion of SB or of the solvent. The ventricular drill biopsies were taken from the ischemic and nonischemic regions at time points described in the experimental protocol VIII (Fig. 1). Using an antibody that reacts specifically with dual-phosphorylated p38-MAPK (Thr180/Tyr182), we investigated the content of phosphorylated p38-MAPK after systemic infusion. In both SB and KHB infusion, we found a significant increase of phospho-p38-MAPK during ischemia (Fig. 6A and B), with a maximum reached at 20 min of ischemia and without significant differences between KHB- and SB-treated tissue. Only at 30 and 45 min of ischemia did SB significantly reduce the content of phospho-p38-MAPK. With an antibody that reacts specifically with the phosphorylated form of SAPK/JNKs, we did not detect significant changes in phosphorylation of these kinases during ischemia after SB or KHB treatment (Fig. 6C). Western blot assay with a specific p38-MAPK antibody showed that there were no significant changes in p38-MAPK abundance when cytosolic fractions from untreated, KHB-, and SB-treated tissue were compared (Fig. 7A and B). Some decrease in content of p38-MAPK after SB infusion was observed after 45 min of ischemia, but this difference was not statistically significant. By means of in-gel phosphorylation of a specific p38-MAPK substrate (GST-MAPKAPK-2_{46-400}), we investigated the effect of SB on p38-MAPK activity. We found that systemic infusion of SB for 10 min before index ischemia did not significantly change the p38-MAPK activities when compared with KHB (DMSO) infusion ≤20 min of ischemia (Fig. 8A and B). Only at 30 and 45 min of ischemia did SB significantly reduce the activity of p38-MAPK. The influence of SB on p38-MAPK activities during ischemia correlates with the observed time course of p38-MAPK phosphorylation (Fig. 6B). SB is an inhibitor that directly and reversibly influences the p38-MAPK. However, SB does not change the phosphorylation state of p38-MAPK itself (a factor important for activation of this enzyme), and after washout of the inhibitor by homogenization and buffer washes, the p38-MAPK is reactivated. For this reason, we investigated the p38-MAPK activities also when SB was present during the whole experimental procedure (especially by in-gel phosphorylation). In this case, we observed significant reduction of p38-MAPK activities (reduced phosphorylation of MAPKAPK-2) in the presence of SB (Fig. 8A and C).

Effect of SB203580 on the phosphorylation of ATF-2

To determine the in vivo effect of SB on p38-MAPK activities, we determined also the in vivo phosphorylation of activating transcription factor-2 (ATF-2). This transcription factor serves as an endogenous substrate for p38-MAPK, and we investigated its phosphorylation af-

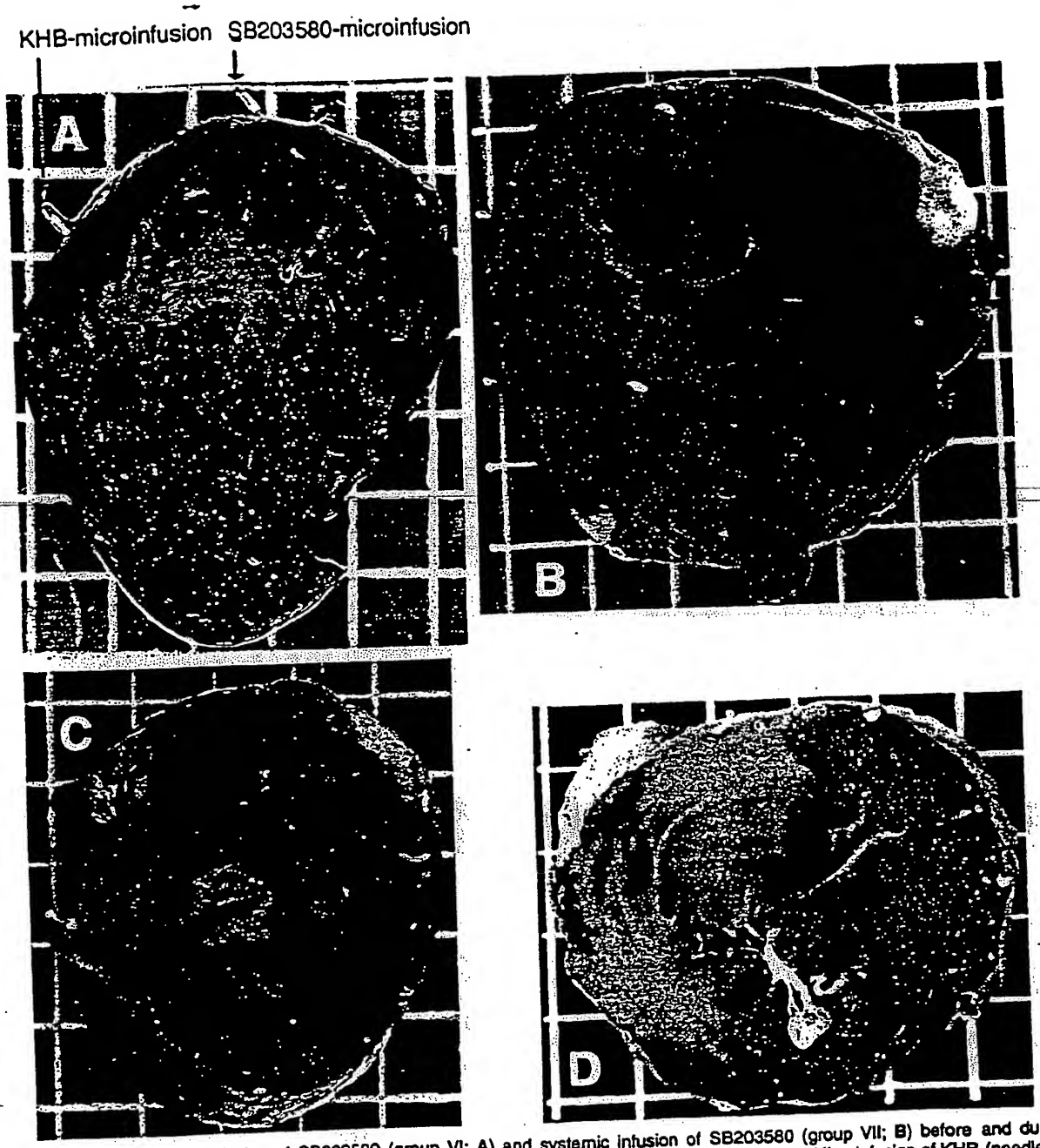

FIG. 4. Intramyocardial infusion of SB203580 (group VI; A) and systemic infusion of SB203580 (group VII; B) before and during ischemic preconditioning followed by index ischemia of 60-min occlusion and reperfusion of 60 min. A: Microinfusion of KHB (needle on the left) and SB203580 (40 n*M*, needle on the right). B: Systemic infusion of SB203580 (5 mg/animal). C: Preconditioning protocol (two cycles of 10-min ischemia and 10-min reperfusion; group V) followed by index ischemia of 40-min occlusion and reperfusion (60 min). D: Index ischemia for 40-min occlusion followed by reperfusion (60 min, group IV, control group 2).

ter systemic infusion of SB (or KHB as negative control) and during the following ischemia (group VIII; Fig. 1). We found that the presence of SB significantly inhibited the ischemia-induced phosphorylation of ATF-2 (Fig. 9). The content of phospho-ATF-2 was decreased after infusion of SB (compared with KHB control). In negative controls (KHB infusion), we observed during ischemia increased phosphorylation of ATF-2 (maximum at 20 min of ischemia), but the presence of SB prevented the ischemia-induced p38-MAPK–mediated phosphorylation of ATF-2. Western blot assays with a specific ATF-2 antibody showed that there were no significant changes in ATF-2 abundance when nuclear fractions from untreated, KHB-, and SB-treated tissue were com-

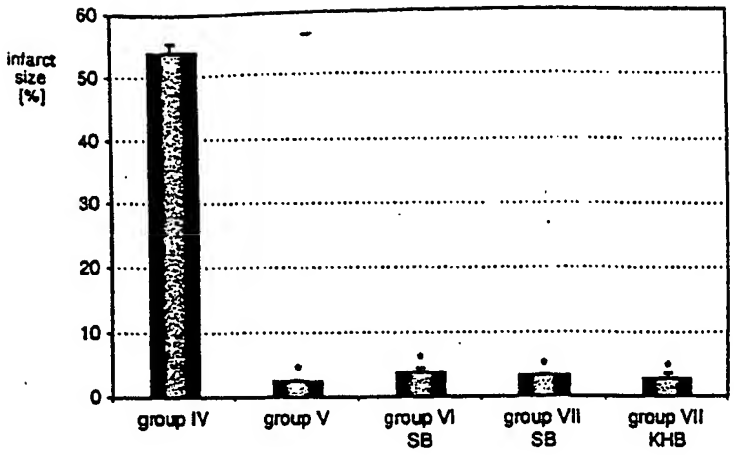

FIG. 5. Effect of local (group VI) and systemic (group VII) infusion of SB203580 on the cardioprotection induced by ischemic preconditioning. Group IV: Effect of KHB/DMSO infusion on infarct size after ischemic preconditioning. Values are expressed as percentage of the area at risk of infarction. Group IV is control group 2; group V underwent the ischemic preconditioning protocol. Each bar represents the mean ± SEM. *p < 0.001 (vs. group IV).

pared. This observation proves that the changes of phospho-ATF-2 reflect the different degree of phosphorylation of this transcription factor.

DISCUSSION

The most important findings are our observations that (a) the inhibition of p38-MAPKinase pathway with the specific inhibitor SB before and during ischemia protects the myocardium against ischemic cell death, and (b) the systemic or local application of SB before and during the ischemic preconditioning (IP) protocol did not influence the IP-mediated cardioprotection. We have previously reported that ischemia increased p38-MAPK activity, that reperfusion downregulated, and that repeated brief ischemia further downregulated its activity (4). We showed also the protective effect of p38-MAPK inhibition during ischemia (7). These results suggested an inverse correlation between p38-MAPK activation and survival (i.e., low p38-MAPK activity correlated well with an improved chance of survival and vice versa). Because uninterrupted ischemia is the fastest way to cell death,

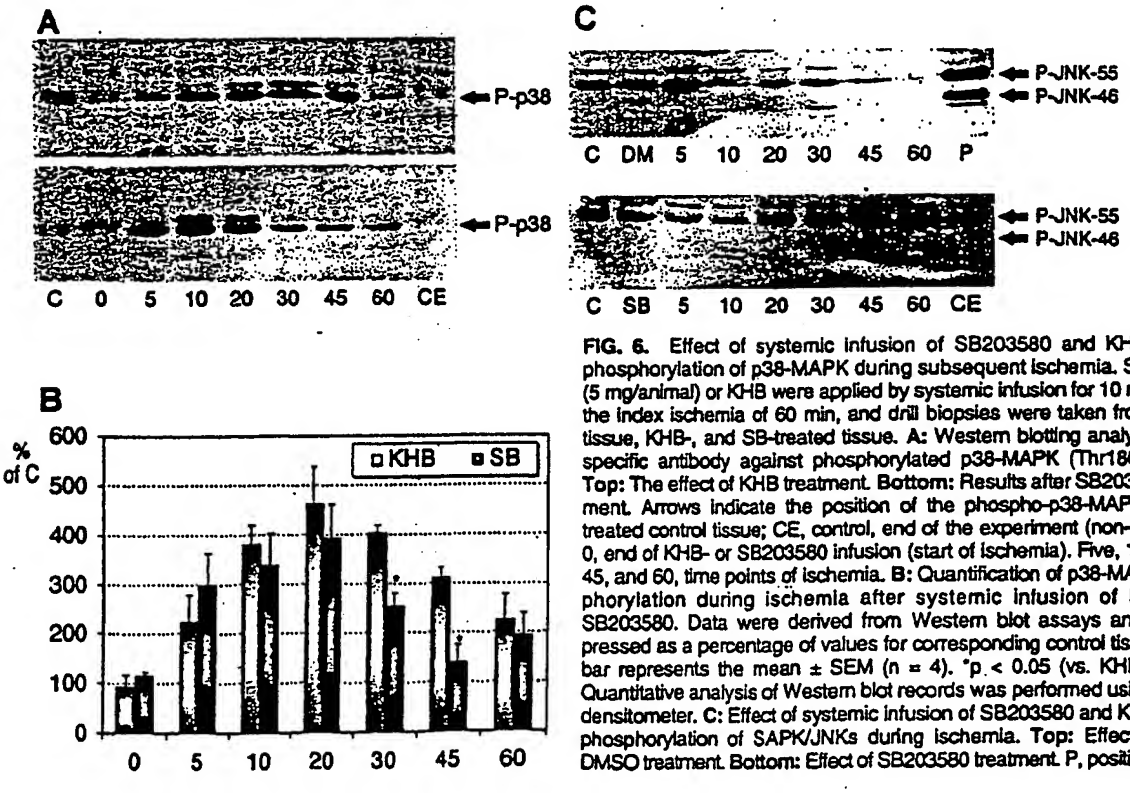

FIG. 6. Effect of systemic infusion of SB203580 and KHB on the phosphorylation of p38-MAPK during subsequent ischemia. SB203580 (5 mg/animal) or KHB were applied by systemic infusion for 10 min before the index ischemia of 60 min, and drill biopsies were taken from control tissue, KHB-, and SB-treated tissue. A: Western blotting analysis with a specific antibody against phosphorylated p38-MAPK (Thr180/Tyr182). Top: The effect of KHB treatment. Bottom: Results after SB203580 treatment. Arrows indicate the position of the phospho-p38-MAPK. C, untreated control tissue; CE, control, end of the experiment (non-risk area); 0, end of KHB- or SB203580 infusion (start of ischemia). Five, 10, 20, 30, 45, and 60, time points of ischemia. B: Quantification of p38-MAPK phosphorylation during ischemia after systemic infusion of KHB and SB203580. Data were derived from Western blot assays and are expressed as a percentage of values for corresponding control tissue. Each bar represents the mean ± SEM (n = 4). *p < 0.05 (vs. KHB/DMSO). Quantitative analysis of Western blot records was performed using a laser densitometer. C: Effect of systemic infusion of SB203580 and KHB on the phosphorylation of SAPK/JNKs during ischemia. Top: Effect of KHB/DMSO treatment. Bottom: Effect of SB203580 treatment. P, positive control.

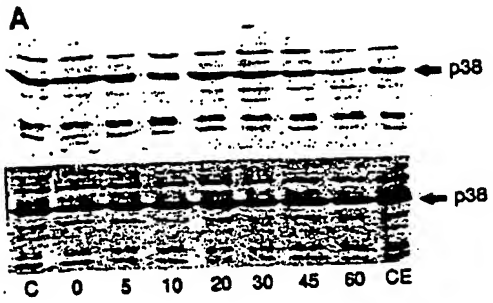

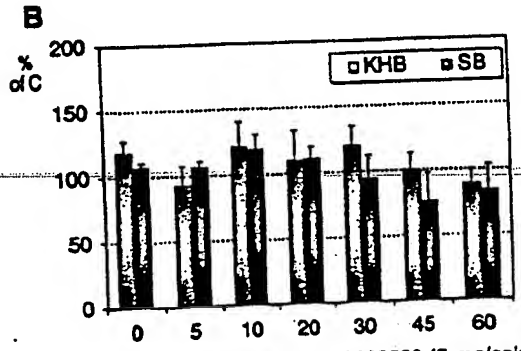

FIG. 7. Effect of systemic infusion of SB203580 (5 mg/animal) and KHB on the content of p38-MAPK during ischemia. A: Western blot analysis with a specific antibody against p38-MAPK. Top: Results after KHB treatment. Bottom: After SB203580. Arrows indicate the position of the p38-MAPK. C, untreated control tissue; CE, control, end of experiment (non-risk area); 0, end of KHB or SB203580 infusion (start of ischemia); 5, 10, 20, 30, 45, and 60, time points of ischemia. B: Quantification of p38-MAPK content during ischemia after systemic infusion of KHB and SB203580. Each bar represents the mean ± SEM (n = 4).

we hypothesized that p38-MAPK stimulation is the cause for accelerated or premature cell death. This hypothesis was tested by systemic and by local infusion of a p38-MAPK inhibitor, the pyridinyl imidazole compound SB. The infusion of SB markedly increased the tolerance to ischemia, especially when infused locally into the myocardium, a useful method for the study of tool drugs that are either too costly or too toxic for systemic use (8,9). SB also significantly reduced IS after systemic i.v. injection. When care was taken that the SB also was present during the phosphorylation step by in-gel phosphorylation, it exhibited a powerful inhibitory effect on p38-MAPK. ATF-2 is a transcription factor that serves in vivo as a substrate for the p38-MAPK cascade. We observed increased phosphorylation of this transcription factor during ischemia, but the phosphorylation was significantly reduced as a consequence of p38-MAPK inhibition by SB. It was reported that SB at high concentrations inhibits 52- and 54-kDa SAPK/JNK but not the 46-kDa JNK-1 (10). Ten micromolar SB completely inhibited the 54-kDa SAPK/JNK and partially inhibited the activity of 52-kDa SAPK/JNK. The IC_{50} for inhibition of p38-MAPK–mediated stimulation of MAPKAPK-2 observed in the cited study was ~70 n*M* and 3–10 μ*M* for total SAPK/JNK activity. The concentration of SB used in our study was 40 n*M*. The concentrations that would inhibit also SAPK/JNKs were therefore not reached. Moreover, we and others found that the activities of SAPK/JNKs are unaffected by ischemia, and activation occurs only during reperfusion (4,11,12). In this study we did not observe stimulation (increased phosphorylation) of SAPK/JNKs activities during ischemia. For this reason, the SAPK/JNKs are unlikely contributors in the increased phosphorylation of ATF-2 during ischemia. Our findings strongly suggest that p38-

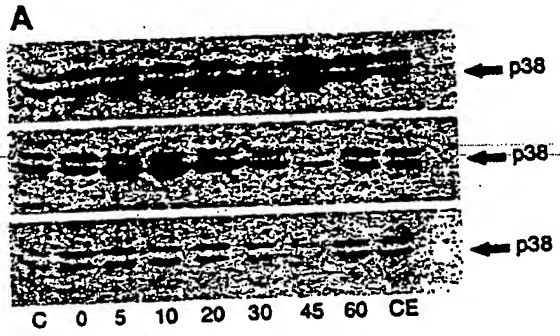

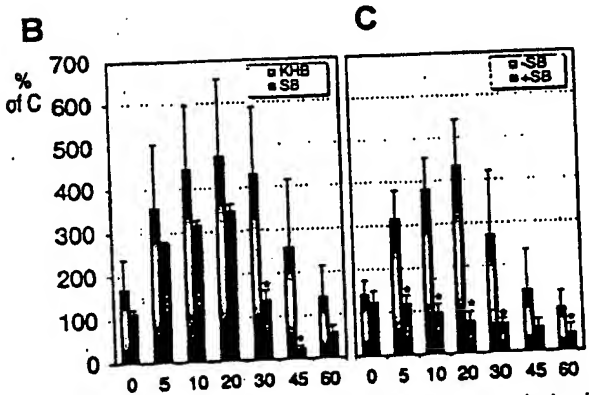

FIG. 8. Effect of systemic infusion of SB203580 (5 mg/animal) and KHB on the activity of p38-MAPK during ischemia. A: The in-gel phosphorylation of MAPKAPK-2 was performed as described under Materials and Methods. Top: Gel after KHB infusion. Middle: Gel after SB203580 infusion. Bottom: In-gel phosphorylation of MAPKAPK-2 in the presence of SB203580. The arrows indicate the positions of p38-MAPK. C, control tissue; CE, control, end of experiment (non-risk area); 0, end of KHB or SB203580 infusion (start of ischemia); 5, 10, 20, 30, 45, and 60, time points of ischemia. B: Quantification of p38-MAPK activation during ischemia after systemic infusion of KHB and SB203580. Data were derived from in-gel kinase assays and are expressed as a percentage of value for corresponding control-untreated tissue. Each bar represents the mean ± SEM (n = 4). *p < 0.05 (vs. KHB/DMSO). C: Quantification of p38-MAPK activities from gels when SB203580 was absent (–) or present (+) during in-gel phosphorylation. Each bar represents the mean ± SEM. *p < 0.05 (vs. SB). Quantitative gel analysis was performed using Phosphorimager SF (Molecular Dynamics).

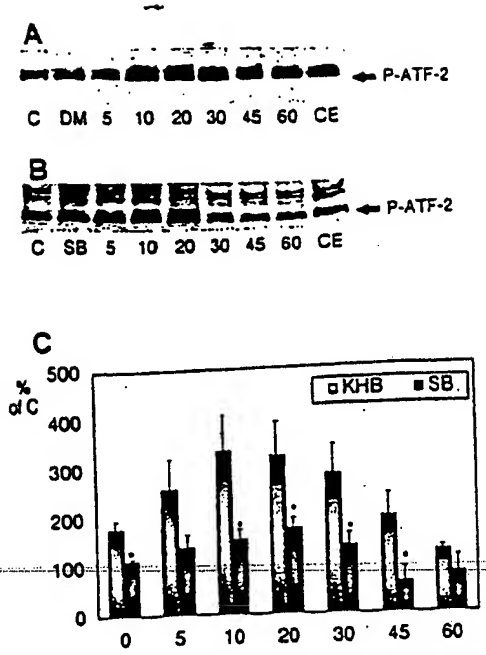

FIG. 9. Western blotting analysis with a specific antibody against phospho-ATF-2. A: After KHB treatment. B: After SB203580 treatment. Arrows indicate the position of the phospho-ATF-2. C, untreated control tissue; CE, control, end of experiment (non-risk area); DM, end of KHB infusion; SB, end of SB203580 infusion (start of ischemia); 5, 10, 20, 30, 45, and 60, time points of ischemia. C: Quantification of content of phosphorylated ATF-2 during ischemia after systemic infusion of KHB and SB203580. Data were derived from Western blot assays and are expressed as a percentage of values for corresponding control tissue. Each bar represents the mean ± SEM (n = 4). *p < 0.05 (vs. KHB/DMSO). Quantitative analysis of Western blot records was performed using a laser densitometer.

MAPK is part of a pathway accelerating cell death. These findings are in contrast to those of others who found, in the rabbit, that p38-MAPK is the pathway favoring survival. In the study of Weinbrenner et al. (13), it was shown that ischemia caused no increased phosphorylation of the tyrosine residue of p38-MAPK in the rabbit heart, and the increased phosphorylation occurred only when the heart was preconditioned. However, our previous findings with regard to p38-MAPK activation (increased phosphorylation) during ischemia (4) in pig myocardium are in agreement with Bogoyevitch et al. (11), who found in isolated rat heart that the p38-MAPK activity was strongly activated by ischemia alone. In contrast to our findings, this activation was further increased during reperfusion. These somewhat divergent results strongly suggest the existence of species differences. Our results are in support of those by Ma et al. (14), who showed that administering SB before ischemia and during reperfusion completely inhibited p38-MAPK activation and exerted a beneficial effect on the recovery of myocardial function and reduced the incidence of apoptosis. The study of Mackay and Mochly-Rosen (15) demonstrated a protective effect of SB against extended ischemia in cultured neonatal rat cardiomyocytes. These cited studies, which all supported the view of a negative survival value of p38-MAPK in ischemia, are in contrast to the earlier results by Weinbrenner et al. (13), who observed that SB completely abolished the protection from ischemic preconditioning in isolated cardiomyocytes and suggested a positive role of p38-MAPK in preconditioning. Nagarkatti and Sha'afi (16) also found that the protective effect of preconditioning stimuli was abolished in the presence of SB but not in the presence of MEK inhibitor PD98059 in the rat myoblast cell line H9C2. In contrast to the results of these studies, we found that both systemic and local applications of SB before and during brief coronary occlusions did not influence the protection by ischemic preconditioning. Moreover, in contrast to the results of Nagarkatti and Sha'afi (16), we recently found that the MEK inhibitor PD98059 abolished the protective effect of preconditioning (17). Paradoxically the study of Nagarkatti and Sha'afi reported a protective effect of SB203580 when present during the lethal ischemic stress. We found previously that ischemia in our experimental model stimulated the p38-MAPK activity, but attenuation occurred during repeated ischemia (4). It is of interest that Nagarkatti and Sha'afi (16) support our finding that ischemic stress activates p38-MAPK and that preconditioning decreased activation of p38-MAPK in response to repeated ischemia. Our results with the p38-MAPK inhibitor and SAPK/JNK activators (7,18,19) support those of a recent report by Wang et al. (20), who studied the role played by MKK7 and found that p38-MAPKs promote cell death in cultured cardiac myocytes and that the JNKs were important for hypertrophy but also favored survival. It was shown that in isolated perfused rat hearts, ischemic stress was associated with nuclear translocation and activation of nuclear factor κB (NFκB), which was significantly blocked by genistein and SB (21). It was also reported that the activation of p38-MAPK and of NFκB leads to tumor necrosis factor (TNF) production (22), which contributes to postischemic myocardial dysfunction. In isolated perfused rat hearts, it was found that p38-MAPK inhibition or treatment with TNF-binding protein decreased myocardial TNF production, cardiomyocyte death, and myocardial dysfunction (23). These observations also suggest the negative survival value of p38-MAPK during ischemia and show that inhibition of p38-MAPK increases the ischemic tolerance.

In this study and also in our previous experiments, we observed two bands (protein kinases) in the range of 38–45 kDa that use MAPKAPK-2 as a substrate in vitro. We investigated the specificity of the reaction for p38-MAPK by immunoprecipitation with a p38-MAPK polyclonal antibody (C-20). The antibody is specific for p38-MAPK and is not cross-reactive with p38-MAPK-beta. The same antibody was used for detection of p38-MAPK content presented in this study (see Fig. 7A). We found that the antibody reacted very strongly with a 38-kDa protein of molecular mass of (p38-MAPK) and when the immunoprecipitate was tested by in-gel phosphorylation

of MAPKAPK-2, we found activity only in the range of 38 kDa. We cannot exclude the possibility that the upper band of 45 kDa represents some isoform of p38-MAPK, but our results show that SB inhibits preferentially the activity of the lower (38-kDa) band. It is known that the p38-MAPK exists in at least six isoforms (two alternative spliced isoforms α and β and isoforms τ and δ). These p38-MAPKs differ in their sensitivity to stimulation, inhibitor sensitivity, and also substrate specificity. We cannot exclude the possibility that more than one isoform of p38-MAPK is activated during myocardial ischemia. However, PC12 cells showed a selective activation of p38-MAPK-α and p38-MAPK-γ by hypoxia (24). Hypoxia had no effect on the activity of the β and δ isoforms. Our results obtained with SB in vitro (phosphorylation step of in-gel assay; Fig. 8A and C) show that SB fully inhibited the ischemia-induced p38-MAPK activity. It has been described that the γ and δ isoforms are resistant to inhibition by SB (25,26). This would suggest that these two p38-MAPK isoforms (γ and δ) are not involved in the effects of SB during ischemia and in mechanisms leading to ischemic death.

In conclusion, we provide detailed information about the detrimental effect of p38-MAPK activation during ischemia, which can be inhibited by SB. We have provided further evidence for our hypothesis that ischemia/reperfusion activates different signaling cascades with opposing effects on survival, of which the ERKs and the SAPK/JNKs favor survival, and the p38-MAPKs accelerate cell death. The development of future treatment strategies for ischemic syndromes may find these observations useful.

REFERENCES

1. Murry CE, Richard VJ, Jennings RB, Reimer KA. Preconditioning with ischemia: is the protective effect mediated by free radical-induced myocardial stunning [Abstract]? *Circulation* 1988;78 (Suppl II):308.
2. Knöll R, Arras M, Zimmermann R, Schaper J, Schaper W. Changes in gene expression following short coronary occlusions studied in porcine hearts with run-on assays. *Cardiovasc Res* 1994; 28:1062–9.
3. Brand T, Sharma HS, Fleischmann KE, et al. Proto-oncogene expression in porcine myocardium subjected to ischemia and reperfusion. *Circ Res* 1992;71:1351–60.
4. Barancik M, Htun P, Maeno Y, Zimmermann R, Schaper W. Differential regulation of distinct protein kinase cascades by ischemia and ischemia/reperfusion in porcine myocardium [Abstract]. *Circulation* 1997;96(Suppl I):1397.
5. Bogoyevitch MA, Ketterman AJ, Sugden PH. Cellular stresses differentially activate c-jun N-terminal protein kinases and extracellular signal-regulated protein kinases in cultured ventricular myocytes. *J Biol Chem* 1995;270:29710–7.
6. Cano E, Hazzalin CA, Mahadevan LC. Anisomycin-activated protein kinases p45 and p55 but not mitogen-activated protein kinases ERK-1 and -2 are implicated in the induction of c-fos and c-jun. *Mol Cell Biol* 1994;14:7352–62.
7. Htun P, Barancik M, Maeno Y, Kilian SAR, Schaper W. Inhibition of the p38 kinase by SB203580 delays ischemic cell death in pig myocardium. *J Mol Cell Cardiol* 1998;30:A16.
8. Podzuweit T, Braun W, Müller A, Schaper W. Arrhythmias and infarction in the ischemic pig heart are not mediated by xanthine oxidase-derived free oxygen radicals [Abstract]. *Circulation* 1986; 74(Suppl II):346.
9. Vogt AM, Htun P, Arras M, Podzuweit T, Schaper W. Intramyocardial infusion of tool drugs for the study of molecular mechanisms in ischemic preconditioning. *Basic Res Cardiol* 1996;91: 389–400.
10. Clerk A, Sudgen PH. The p38-MAPK inhibitor, SB203580, inhibits cardiac stress-activated protein kinases/c-Jun N-terminal kinases (SAPKs/JNKs). *FEBS Lett* 1998;426:93–6.
11. Bogoyevitch MA, Gillespie-Brown J, Ketterman AJ, et al. Stimulation of the stress-activated mitogen-activated protein kinases and c-jun N-terminal kinases are activated by ischemia/reperfusion. *Circ Res* 1996;79:162–73.
12. Knight RJ, Buxton DB. Stimulation of c-jun kinase and mitogen-activated protein kinase by ischemia and reperfusion in the perfused rat hearts. *Biochem Biophys Res Commun* 1996;218:83–8.
13. Weinbrenner C, Liu GS, Cohen MV, Downey JM. Phosphorylation of tyrosine 182 of p38 mitogen-activated protein kinase correlates with the protection of preconditioning in rabbit heart. *J Mol Cell Cardiol* 1997;29:2383–91.
14. Ma XL, Kumar S, Gao F, et al. Inhibition of p38 mitogen-activated protein-kinase decreases cardiomyocyte apoptosis and improves cardiac function after myocardial ischemia and reperfusion. *Circulation* 1999;99:1685–91.
15. Mackay K, Mochly-Rosen D. An inhibitor of p38 mitogen-activated protein kinase protects neonatal cardiac myocytes from ischemia. *J Biol Chem* 1999;274:6272–9.
16. Nagarkatti DS, Sha'afi RI. Role of p38 MAP kinase in myocardial stress. *J Mol Cell Cardiol* 1998;30:1651–64.
17. Strohm CE, Barancik M, Kilian SAR, Schaper W. Inhibition of the ER-kinases by PD098059 counteracts ischemic preconditioning. *J Mol Cell Cardiol* 1999;31:A94.
18. Htun P, Barancik M, Maeno Y, Zimmermann R, Schaper W. Stimulation of stress activated protein kinases by anisomycin protects ischemic myocardium [Abstract]. *Circulation* 1997;96(Suppl I):1399.
19. Barancik M, Htun P, Schaper W. Okadaic acid and anisomycin are protective and stimulate the SAPK/JNK pathway. *J Cardiovasc Pharmacol* 1999;34:182–90.
20. Wang Y, Su B, Sah VP, Brown JH, Han J, Chien KR. Cardiac hypertrophy induced by mitogen-activated protein kinase kinase 7, a specific activator for c-Jun NH_2-terminal kinase in ventricular muscle cells. *J Biol Chem* 1998;273:5423–6.
21. Maulik N, Sato M, Price BD, Das DK. An essential role of NFkappaB in tyrosine kinase signaling of p38 MAP kinase regulation of myocardial adaption to ischemia. *FEBS Lett* 1998;429:365–9.
22. Meldrum DR. Tumor necrosis factor in the heart. *Am J Physiol* 1998;274:R577–95.
23. Meldrum DR, Dinarello CA, Cleveland JC, et al. Hydrogen peroxide induces tumor necrosis factor alpha-mediated cardiac injury by a p38 mitogen-activated protein kinase-dependent mechanism. *Surgery* 1998;124:291–7.
24. Conrad PW, Rust RT, Han J, Millhorn DE, Beitner-Johnson D. Selective activation of p38-alpha and p38-gamma by hypoxia: role in regulation of cyclin D1 by hypoxia in PC12 cells. *J Biol Chem* 1999;274:23570–6.
25. Lazou A, Sugden PH, Clerk A. Activation of mitogen-activated protein kinases (p38-MAPKs, SAPKs/JNKs and ERKs) by the G-protein-coupled receptor agonist phenylephrine in the perfused rat heart. *Biochem J* 1998;332:459–65.
26. Jiang Y, Gram H, Zhao M, et al. Characterization of the structure and function of the fourth member of p38 group mitogen-activated protein kinases, p38-delta. *J Biol Chem* 1997;272:30122–8.

This Page is Inserted by IFW Indexing and Scanning Operations and is not part of the Official Record

BEST AVAILABLE IMAGES

Defective images within this document are accurate representations of the original documents submitted by the applicant.

Defects in the images include but are not limited to the items checked:

- ☐ BLACK BORDERS
- ☑ IMAGE CUT OFF AT TOP, BOTTOM OR SIDES
- ☑ FADED TEXT OR DRAWING
- ☐ BLURRED OR ILLEGIBLE TEXT OR DRAWING
- ☐ SKEWED/SLANTED IMAGES
- ☐ COLOR OR BLACK AND WHITE PHOTOGRAPHS
- ☐ GRAY SCALE DOCUMENTS
- ☑ LINES OR MARKS ON ORIGINAL DOCUMENT
- ☐ REFERENCE(S) OR EXHIBIT(S) SUBMITTED ARE POOR QUALITY
- ☐ OTHER: _____

IMAGES ARE BEST AVAILABLE COPY.
As rescanning these documents will not correct the image problems checked, please do not report these problems to the IFW Image Problem Mailbox.